MENDEL UNIVERSITY IN BRNO
FACULTY OF AGRONOMY

Ph.D. thesis

BRNO 2015 **Ing. IVA BLAŽKOVÁ**

Mendel University in Brno
Faculty of Agronomy
Department of Chemistry and Biochemistry

Nanomaterials as a platform for the doxorubicin transport – Fluorescence imaging

Ph.D. thesis

Branch of study: 4106V017 Agricultural Chemistry

Thesis supervisor:
Doc. RNDr. Vojtěch Adam, Ph.D.

Specialist supervisor:
Mgr. Markéta Vaculovičová, Ph.D.

Candidate:
Ing. Iva Blažková

Brno 2015

Čestné prohlášení

Prohlašuji, že jsem práci „Nanomateriály jako platforma pro transport doxorubicinu - Fluorescenční zobrazování (Nanomaterials as a platform for the doxorubicin transport – Fluorescence imaging“) vypracovala samostatně a veškeré použité prameny a informace uvádím v seznamu použité literatury. Souhlasím, aby moje práce byla zveřejněna v souladu s § 47b zákona č. 111/1998 Sb., o vysokých školách ve znění pozdějších předpisů a v souladu s platnou *Směrnicí o zveřejňování vysokoškolských závěrečných prací.*

Jsem si vědoma, že se na moji práci vztahuje zákon č. 121/2000 Sb., autorský zákon, a že Mendelova univerzita v Brně má právo na uzavření licenční smlouvy a užití této práce jako školního díla podle § 60 odst. 1 autorského zákona.

Dále se zavazuji, že před sepsáním licenční smlouvy o využití díla jinou osobou (subjektem) si vyžádám písemné stanovisko univerzity, že předmětná licenční smlouva není v rozporu s oprávněnými zájmy univerzity, a zavazuji se uhradit případný příspěvek na úhradu nákladů spojených se vznikem díla, a to až do jejich skutečné výše.

V Brně dne: 20. 2. 2015

……

podpis

This work was financially supported by the specific university research through project IGA AF n. IP 22/2013.

This work was realised in CEITEC – Central European Institute of Technology, with research infrastructure supported by the project CZ.1.05/1.1.00/ 02.0068 financed from European Regional Development Fund.

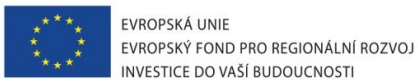

This Ph.D. thesis was financially supported by the project GAČR P301/10/0356 CYTORES.

This work was financially supported by the Ph.D. project PGS 25_2012.

Acknowledgements

I would like to thank to Professor René Kizek for the opportunity to be a member of his group, and for the possibility to get more knowledge and professional experience.

My special gratitude goes to the thesis supervisor Vojtěch Adam for his willingness and help with the designing of experiments and interpretation of the results.

I would like to thank to Markéta Vaculovičová for a valuable advices, help, support and professional guidance in processing of thesis.

I thank the co-authors for preparation of publications, which are the basis of this work. I thank to all my colleagues from Laboratory of Metallomics and Nanotechnologies for their help with experiments. I want to thanks them very much for their kindness and support in every day work.

I am very grateful for the support of my parents and other members of my family.

Annotation

Doxorubicin (DOX) is an important anthracycline antineoplastic drug used to treat a variety of cancers. As well as other antineoplastic agents, DOX has negative side effects; the most serious one is cardiotoxicity. Conjugation of DOX with nanomaterials could help to reduce its adverse effects. The presented thesis entitled „Nanomaterials as a platform for the DOX transport – Fluorescence imaging“ is primarily focused on the study of DOX interaction with biomolecules such as amino acids and albumin. The interaction was analysed by fluorescence spectrometry and by other analytical methods and significant interaction with amino acids as well as with protein albumin was detected. Next work was focused on the utilization of nanoparticles in DOX transport. DOX was conjugated with fullerenes or encapsulated in liposomes and properties of these nanoconstructs, *in vitro* and *in vivo*, were analysed. Both of these nanomaterials seemed to be good nanotransporters for DOX targeted delivery.

Key words: doxorubicin, fluorescence imaging, fullerene, liposome, nanoparticles

Anotace

Doxorubicin (DOX) je významné antracyklinové cytostatikum užívané k léčbě řady nádorových onemocnění. Stejně jako jiná cytostatika má i DOX vedlejší negativní účinky, z nichž nejzávažnější je kardiotoxicita. Vazba DOX s nanomateriály by mohla pomoci snížit jeho nežádoucí účinky. Předkládaná disertační práce „Nanomateriály jako platforma pro transport DOX - Fluorescenční zobrazování“ je primárně zaměřena na studium interakce DOX s biomolekulami jako jsou aminokyseliny a albumin. Interakce byla pozorována pomocí fluorescenční spektrometrie a také dalšími analytickými metodami a byla zaznamenána významná interakce jak s aminokyselinami, tak také s proteinem albuminem. Další část práce byla zaměřena na využití nanočástic v dopravě DOX. DOX byl konjugován s fullereny, nebo uzavřen do lipozomů a následně byly analyzovány vlastnosti takto vytvořených nanostruktur *in vitro* a *in vivo*. Oba z těchto nanomateriálů vykazovaly vhodné vlastnosti pro cílený transport DOX.

Klíčová slova: doxorubicin, fluorescenční zobrazování, fullereny, lipozomy, nanočástice

CONTENT

1 INTRODUCTION

Tumour diseases represent serious health problem in developed as well as in developing countries. The treatment is difficult and when the tumour is detected late, there is a serious threat to die from cancer. Therefore, much attention is paid and a lot of money spent to improve the efficacy of tumour detection and treatment.

The fight against cancer started Paul Ehrlich with the postulate "wir müssen chemisch zielen lernen" ("we have to learn how to aim chemically). His landmark immunological insights were awarded in 1908 with the Nobel Prize for Physiology or Medicine. These immunological achievements evolved into what became Ehrlich's 'magic bullet concept': drugs that go straight to their cell-structural targets. Targeted drugs should attack only the tumour cells without damaging the healthy tissue. His postulate inspired generations of scientists to construct powerful molecular cancer therapeutics.

The beginning of the modern era of cancer chemotherapy is connected with nitrogen mustard studies in 1940–1952. Sidney Farber, who studied the effects of antagonist to folic acid (aminopterin) to leukaemia, is regarded as the father of modern chemotherapy.

A significant influence on the development of cancer drugs had Richard Feynman´s speech entitled "There's Plenty of Room at the Bottom" at an American Physical Society meeting at the California Institute of Technology in 1959. Feynman described a process in which scientists would be able to manipulate and control individual atoms and molecules. One decade later, Professor Norio Taniguchi termed these nanometer size applications as nanotechnology. The application of nanotechnology in management of cancer belongs nowadays to one of the most rapidly developing branches of medicine and is a promising tool for targeting delivery and elimination of negative side effects of drugs.

2 AIMS

- Summarization of the literature information on nanotransporters
- Investigation of apoferritin usage in DOX transport
- The conjugation of DOX with fullerenes and their *in vitro* and *in vivo* study by optical and electrochemical methods
- Study of the DOX encapsulation into the liposomes and determination of the cholesterol effect on the DOX release

3 LITERARY OVERVIEW

3.1 Tumour diseases

Tumour diseases (neoplasms) represent an uncontrolled proliferation of the cells, these cells are invading normal tissues and organs (benign tumours) and eventually spreading throughout the body (malignant tumours, cancer) and form secondary tumours (metastases) (Klener and Klener 2013).

The loss of growth control exhibited by cancer cells is the result of accumulated abnormalities in regulatory systems (Nunney 1999; Cooper 2000). The local microenvironment, or niche, of a cancer cell plays important role in cancer development; the most important is the extracellular matrix (ECM), a complex network of macromolecules with different properties. Abnormal ECM affects cancer progression by directly promoting cellular transformation and metastasis (Lu, Weaver et al. 2012). Underlying these hallmarks are genome instability (Hanahan and Weinberg 2011). Cancer is characterized by sustaining proliferative signalling, evading growth suppressors, resisting cell death, enabling replicative immortality, inducing angiogenesis, and activating invasion and metastasis (Carmeliet and Jain 2000; Narang and Varia 2011). Accompanying phenomenon of cancer progression is angiogenesis (Bray, Binner et al. 2014). The ability of the body to resist the carcinogenesis depends upon genetic and metabolic context, age, state of immunity and inflammatory responses (Hainaut and Plymoth 2013).

3.1.1 Incidence of tumour diseases

Cancer is the main cause of morbidity and mortality worldwide. This life-threatening disease causes nearly 7 million deaths every year worldwide (Sultana, Khan et al. 2013) and presents 25% of death caused in the developed countries (Siegel, Ma et al. 2014). On the other hand, mortality caused by this disease decreases and survival time increases due to an early diagnosis and effective treatment (Siegel, Naishadham et al. 2012). The risk of dying from cancer decreased by 20% between 1991 and 2010 (Siegel, Ma et al. 2014). In the United States, every third woman and every second man is diagnosed with cancer during live (Siegel, DeSantis et al. 2012) and cancer is here the second leading cause of deaths (following accidents) in children (Ward, DeSantis et al. 2014). Cancer mortality in Czech Republic is about 20% (Zaloudik 2007; Ferlay, Steliarova-Foucher et al. 2013). Death rates continue to decline for all 4 major cancer sites (lung, colorectum, breast, and

prostate), with lung cancer accounting for almost 40% of the total decline in men and breast cancer accounting for 34% of the total decline in women (Siegel, Naishadham et al. 2012) . The most often detected is the cancer of the female breast, followed by colorectal, prostate and lung cancer. These four cancers represent half of all detected cancer types in Europe. The most common causes of death are cancers of the lung, followed by colorectal, breast and stomach (Ferlay, Steliarova-Foucher et al. 2013). Early detection of cancer can significantly impact survival of cancer patients, so the regular screening is highly recommended (Carter, Albertsen et al. 2013; Esserman, Thompson et al. 2013).

3.2 Diagnostic of tumour diseases

Early detection of cancer has a significant impact on patients survival, so different diagnostic methods are intensively studied (Wainstein, Algarra et al. 2015). Nowadays, the most often used diagnostic methods are blood tests (Tsay, DeCotiis et al. 2013) and imaging methods (Towbin, Trout et al. 2014), after them often follows biopsy (Berg, Zhang et al. 2012). Biopsy is a procedure that includes taking of a small tissue sample for the histological analysis (Al-Bataineh, Jenne et al. 2012). Biopsy is an important diagnostic tool especially in prostate cancer (Grossfeld and Carroll 2001), colon cancer (Baalbergen, Veenstra et al. 2013) and also cervical cancer (Peng, He et al. 2015) diagnosis.

3.2.1 Biomarkers

The ability to study nonhematologic cancers through a noninvasive sampling of blood is fast developing field in cancer diagnostics (Haber and Velculescu 2014). Blood tests envision haematological and biochemical examinations and tumour biomarkers analysis (Schenone, Culzoni et al. 2013; Crispo, Grimaldi et al. 2015). Blood-based diagnostics can classify tumours into distinct molecular subtypes and monitor disease relapse and response to treatment (Hanash, Baik et al. 2011). Biomarkers can be detected except the blood also in other body fluids (Kelloff and Sigman 2012) foremost in urine (Ploussard and de la Taille 2010). Tumour biomarkers are usually proteins that are usually expressed as a consequence of cancer development and progression (Cramer, Bast et al. ; Kelloff and Sigman 2012).

3.2.2 Imaging methods

Imaging is an important tool used in all stages of cancer care, from disease detection and characterization, to treatment response assessment (Akin, Brennan et al. 2012). Molecular

imaging enable the study of human body inner workings with the visualization of complex biochemical processes involved in normal physiology and also in disease states (James and Gambhir 2012). Imaging methods can be invasive like spectroscopy (colonoscopy, gastroscopy) (Pickhardt, Hassan et al. 2011; Freilich, Mellon et al. 2014; Shin, Kim et al. 2014) or used for noninvasive imaging (Mellon, Springett et al. 2014). Currently used imaging techniques for diagnostics and treatment control are mainly computer tomography (CT), magnetic resonance (MRI), ultrasonography (US), positron emission tomography (PET), single-photon emission computed tomography (SPECT) and optical imaging techniques (Schnall and Rosen 2006; Mura and Couvreur 2012; Key and Leary 2014). The imaging of tumours is based on anatomic differences in density, water content, shape, and size (Farwell, Pryma et al. 2014). Different imaging modalities provide a range of information about the patient. CT scans provide information about the structure and are the most sensitive to electron-dense elements, like those found in bones (Key and Leary 2014). It is a technique that relies on differential levels of X-ray attenuation by tissues within the body to produce images reflecting anatomy (James and Gambhir 2012). CT is used for head and abdomen scans and is the most commonly used method for lung cancer screening (Tsay, DeCotiis et al. 2013; Konecny 2015; Lin, Xiong et al. 2015; Morgensztern, Campo et al. 2015). MRI scans provide information about soft tissues, and are the most sensitive to organs (Key and Leary 2014). MRI uses a powerful magnet and radiofrequency energy to visualize the internal structure and soft tissue morphology of the body (James and Gambhir 2012). This modality is used to scan prostate, breast, colorectal and neurological cancers (Meng, Zaorsky et al. 2013; Tapan, Ozbayrak et al. 2014; Banday, Jeelani et al. 2015; Ohaegbulam, Assal et al. 2015). The resolution of both CT and MRI scans can be highly improved by introduction of contrast agents, which increase the electron density or the relaxation time (Key and Leary 2014).

PET, a radionuclide molecular imaging technique can provide information about metabolic parameters, and is sensitive to detection of high-metabolism tumours and infections (James and Gambhir 2012; Key and Leary 2014). Widely used radiotracer for the staging and restaging of most tumours is 18F-fluorodeoxyglucose (Farwell, Pryma et al. 2014; Choi, Bang et al. 2015). This imaging modality can screen among other lung cancer, colorectal cancer, lymphoma, melanoma, head and neck cancer (Czernin and Phelps 2002). US is less used in cancer diagnosis, but still has a potential in neoplasm detection, for example breast screening (Berg, Zhang et al. 2012) and transrectal ultrasonography (Grossfeld and Carroll 2001). Breast cancer can be detected by diverse imaging methods, but the most often

applied is mammography (Schenone, Culzoni et al. 2013), which is based on low-energy X-rays (Giess, Frost et al. 2012). Potential for use in clinical practice has photoacoustic imaging. It is sensitive to the abnormal angiogenesis deep in the biological tissue, and may be used for scanning of cervical cancer (Peng, He et al. 2015).

With the aim of better analyses, the imaging methods can be used in tandem, which is called multimodal imaging (Staples, Kaneko et al. 2014). Multimodal imaging combines two or more imaging modalities into one system to image more details in clinical diagnostic imaging, such as high spatial resolution, soft tissue contrast, and biological information on the molecular level with high sensitivity (Bucci, Vellecco et al. 2012). Multimodal imaging of cancer is focused on the integration of anatomical and functional characteristics, such as PET-CT and SPECT-CT and also on the multiple quantitative, functional measurements PET-MRI (Saha, Burke et al. 2013; Sabroso and Torres-Suarez 2014; Yankeelov, Abramson et al. 2014).

3.2.3 Fluorescence imaging

Monitoring the behaviour of biologically active compounds in the body is the key to understand their effect (Cheng, Lu et al. 2012; Xu, Liu et al. 2012). Optical imaging technologies are becoming, due to their variability, flexibility, specificity and sensitivity, powerful clinical tools not only for diagnosis, but also guided treatment and monitoring therapies (Wouters, Verveer et al. 2001; Balas 2009; Stemmer, Mehnert et al. 2012). Optical methods are relatively cheap non-ionizing techniques based on the specific optical properties and are an important tool for non-invasive and objective diagnosis with still improving resolution (Blazkova, Vaculovicova et al. 2014). Fluorescence imaging is the optical method based on the usage of fluorophores, the compounds, that can emit light after absorption of the appropriate wavelenght (Frangioni 2003). Organic compounds such as fluorescein or rhodamin are widely used as fluorophores (Chatterjee, Zhang et al. 2010). Biological fluorophores can be represented by green fluorescent protein, which is widely used as universal genetically encoded fluorescent label (Chudakov, Matz et al. 2010). Inorganic compounds are promising imaging tools to be used in medical practise (Minotti, Menna et al. 2004; Andreadou, Sigala et al. 2007). In monitoring of the therapies the inherent fluorescence of some drugs can be exploited (Al-Bataineh, Jenne et al. 2012; Blazkova, Ryvolova et al. 2013). There are several parameters that define the effectiveness of imaging agents *in vivo*, the attention must be paid to excitation and emission wavelengths, fluorophore solubility, photobleaching threshold, biodistribution, target

binding affinity, pharmacokinetics, biocompatibility, photophysics, excitation light delivery and fluorescence light collection (Frangioni 2003; Hilderbrand and Weissleder 2010).

Fluorescence imaging is a good method for preclinical studies of anticancer drug action on cell cultures or in small animals (Hwang, Park et al. 2012; Scheuer, van Dam et al. 2012). Imaging of targeted fluorescent probes offers significant advantages for investigating disease and tissue function (Niedre, de Kleine et al. 2008). The sensitive detection and imaging of deep targets *in vivo* is limited due to the diffusion, absorption and scattering of light by the tissues and due to the emission of autofluorescence from intrinsic chromophores (Bouccara, Sitbon et al. 2015). The signal detected from the same light source will become weaker the deeper it is embedded in tissue, and strongly depends on the optical properties of the surrounding tissue (Gorthi, Schaak et al. 2013).

The setup for imaging generally consists of a charge-coupled device (CCD) camera and a source of filtered light (Scheuer, van Dam et al. 2012). But the use of low-energy photons means that the depth of penetration is limited to only a few centimeters, which makes it virtually impossible to study deep tissues in human subjects (Scheuer, van Dam et al. 2012). From this point of view are interesting fluorophores that emit light in the near infrared region (NIR) of a spectral window (Ntziachristos, Bremer et al. 2003). The use of NIR probes improve photon penetration through tissue and minimizes the tissue autofluorescence (Hilderbrand and Weissleder 2010). Haemoglobin and water absorb minimally in this region so photons can penetrate several centimetres into the tissue (Ntziachristos, Bremer et al. 2003).

The development of NIR fluorophores over the past decade has facilitated the translation of fluorescence imaging from the microscopic (epifluorescence, confocal and multifocal microscopy, and mesoscopic optical projection tomography) to macroscopic imaging (fluorescence reflectance imaging – FRI, fluorescence-mediated molecular tomography - FMT) (Cho, Wang et al. 2008; Hilderbrand and Weissleder 2010; Vavrova, Jansova et al. 2013; Konecna, Nguyen et al. 2014).

Fluorescence microscopy is a powerful tool to study the morphology and function of subcellular compartments, molecular and cellular processes in cell culture and tissue samples or to determine the localization of proteins (Stuker, Ripoll et al. 2011; Eckers and Deponte 2012; Gorthi, Schaak et al. 2013). Fluorescence lifetime imaging microscopy (FLIM) is a great tool for monitoring dynamic changes on microscopic level and is used to study kinetics of anti-cancer drugs that bear fluorescent moieties in cells (Deniset-Besseau,

Miannay et al. 2012; Chen, Wu et al. 2012; Chen, Wu et al. 2012; Wiench, Eichhorn et al. 2012; Konecna, Nguyen et al. 2014). Intravital imaging enables the investigation of physiological processes in the living organism, and provides a complete picture of disease pathology and development (Hilderbrand and Weissleder 2010; Masedunskas, Milberg et al. 2012) and could be used in real-time fluorescence-guided surgery (Key and Leary 2014).

FRI enables imaging of fluorescent probes in tissues. In this case, the source of radiation and detector are at the same side of the object. Connection of laser and sensitive CCD device together with advanced mathematical models allows sensitive detection and evaluation of fluorescence signal intensity (Bremer, Ntziachristos et al. 2003; Ntziachristos, Bremer et al. 2003; Stuker, Ripoll et al. 2011). FMT is a technique that can three-dimensionally map the distribution of a fluorescent probe or image gene expression by resolving fluorescence activation in deep tissues (Ntziachristos, Bremer et al. 2003; Stuker, Ripoll et al. 2011). FMT development is towards 360° whole body animal scanners which allows to freely select one or several regions of interest without need for moving the animal (Stuker, Ripoll et al. 2011).

NIR fluorescence imaging is in some applications already used in the clinic. Indocyanine green (ICG) is NIR fluorophore used in angiography (Mielke, Malinova et al. 2014). ICG is moderately soluble in aqueous buffer, heavily bind to proteins (Frangioni 2003) and is used on almost every aneurysm case. ICG angiography is a noninvasive, quick, relatively inexpensive, and safe method, intraoperative digital subtraction angiography is nowadays rarely used (Abla and Lawton 2014). ICG angiography is applied to map the vascular configuration of cerebral arteriovenous malformations during resection (Zaidi, Abla et al. 2014). ICG have been used in ophthalmology to dye the anterior capsule in cataract operations and to stain epiretinal membranes (Hiebl, Gunther et al. 2005).

3.3 Treatment

The most frequently used approaches in cancer therapy are chemotherapy, radiotherapy and surgery (Meng, Zaorsky et al. 2013; Yang, Diao et al. 2013; Mohammed, Van Buren et al. 2014). Also other methods like stem cell transplant (Staples, Kaneko et al. 2014), hyperthermia (Bucci, Vellecco et al. 2012), hormonal therapy (Shin, Kim et al. 2014), phototherapy (using nontoxic light-sensitive compounds) (Lin, Xiong et al. 2015), immunotherapy (Banday, Jeelani et al. 2015; Ohaegbulam, Assal et al. 2015) and also

personalized and targeted therapies can be applied (Konecny 2015; Morgensztern, Campo et al. 2015).

3.3.1 Cytostatics

The number of patients receiving chemotherapy has considerably increased in the last decades (Mahnik, Lenz et al. 2007; Nussbaumer, Bonnabry et al. 2011). Chemotherapy involves the use of low-molecular-weight drugs, which either inhibit cell growth or directly destroy tumour cells (Thurston 2006). Many of anticancer drugs acts as apoptosis inducers of tumour cells, that are subsequently engulfed by phagocytes, initiating an immune reaction (Inoue, Setoyama et al. 2014). Among the commonly used antineoplastic drugs belong transtuzumab, etoposide, taxans, anthracyclines and platinum-based agents (Gulyaev, Anisimova et al. 1998; Petrakova, Nenutil et al. 2007; Patel and Tannock 2009; Alkilany and Murphy 2010; Du, Du et al. 2011; Buss, Kalayda et al. 2012; Termsarasab, Yoon et al. 2014). The use of chemotherapeutic drugs is limited by high toxicity and drug resistance (Kirtane, Kalscheuer et al. 2013). The combination of two or more therapeutic drugs is beneficial to overcome the limitations (Hua, Liu et al. 2014). Co-delivery strategy enable minimize the amount of each drug and achieve the synergistic effect for cancer therapies (Wang, Zhao et al. 2011). Chemotherapy drugs are also used as adjuvant therapy, to decrease the risk of recurrence (Myhr 2008).

3.3.2 Doxorubicin

Doxorubicin (Adriamycin, DOX) is a widely used broad-spectrum antineoplastic drug (Injac and Strukej 2008). DOX has been first isolated in the early 1960s and belongs to the most effective anticancer drugs ever developed (Takemura and Fujiwara 2007). DOX is a secondary metabolite of *Streptomyces peucetius* var. *caesius*, along with daunorubicin, epirubicin, idarubicin etc. and belongs to the family of anthracyclines (Octavia, Tocchetti et al. 2012; Ma and Mumper 2013). This drug is used for the treatment of a large number of cancers including breast cancer, lymphomas, solid tumours, and sarcomas (Luo, Bernshaw et al. 2002; Dong and Mumper 2010; Henderson, Borders et al. 2014). This drug possess aglyconic and sugar moieties (Fig. 1). The aglycone consists of a tetracyclic ring with quinine-hydroquinone adjacent groups, methoxy substituent short side chain followed by the carbonyl group. The sugar component (also known as daunosamine) is attached to one of the rings by a glycosidic bond (Tacar, Sriamornsak et al. 2013).

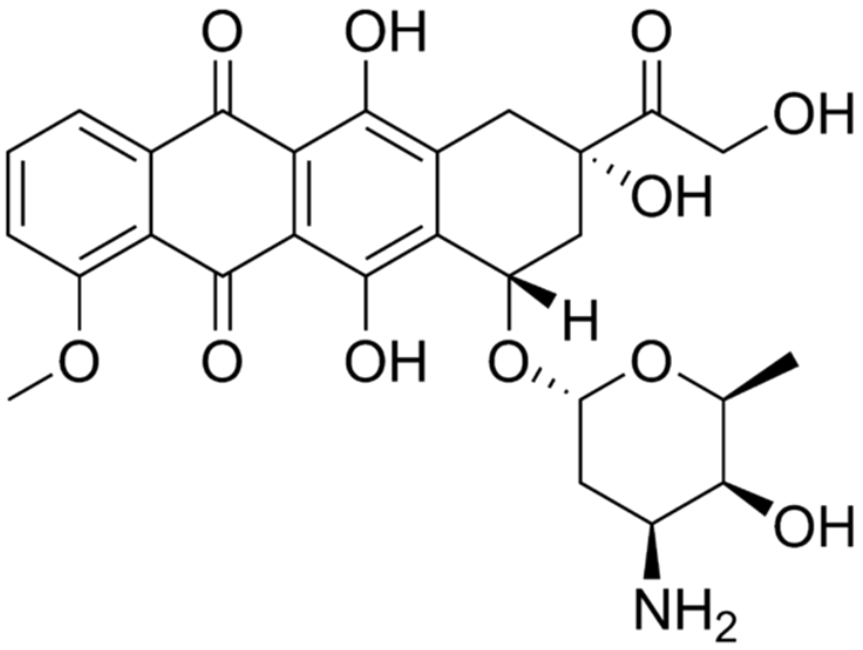

Figure 1. Chemical structure of DOX.

DOX is a red-coloured, naturally fluorescent agent and it's very good fluorescence properties can be used for the study of its action to cells or tissues. DOX fluorescence could be also used to monitor the behaviour of this drug in the living organism. But its detection is limited to small animals because the depth of detection is about 10 mm as shown in Fig. 2 (Primeau, Rendon et al. 2005; Blazkova, Dostalova et al. 2012; Blazkova, Vaculovicova et al. 2014).

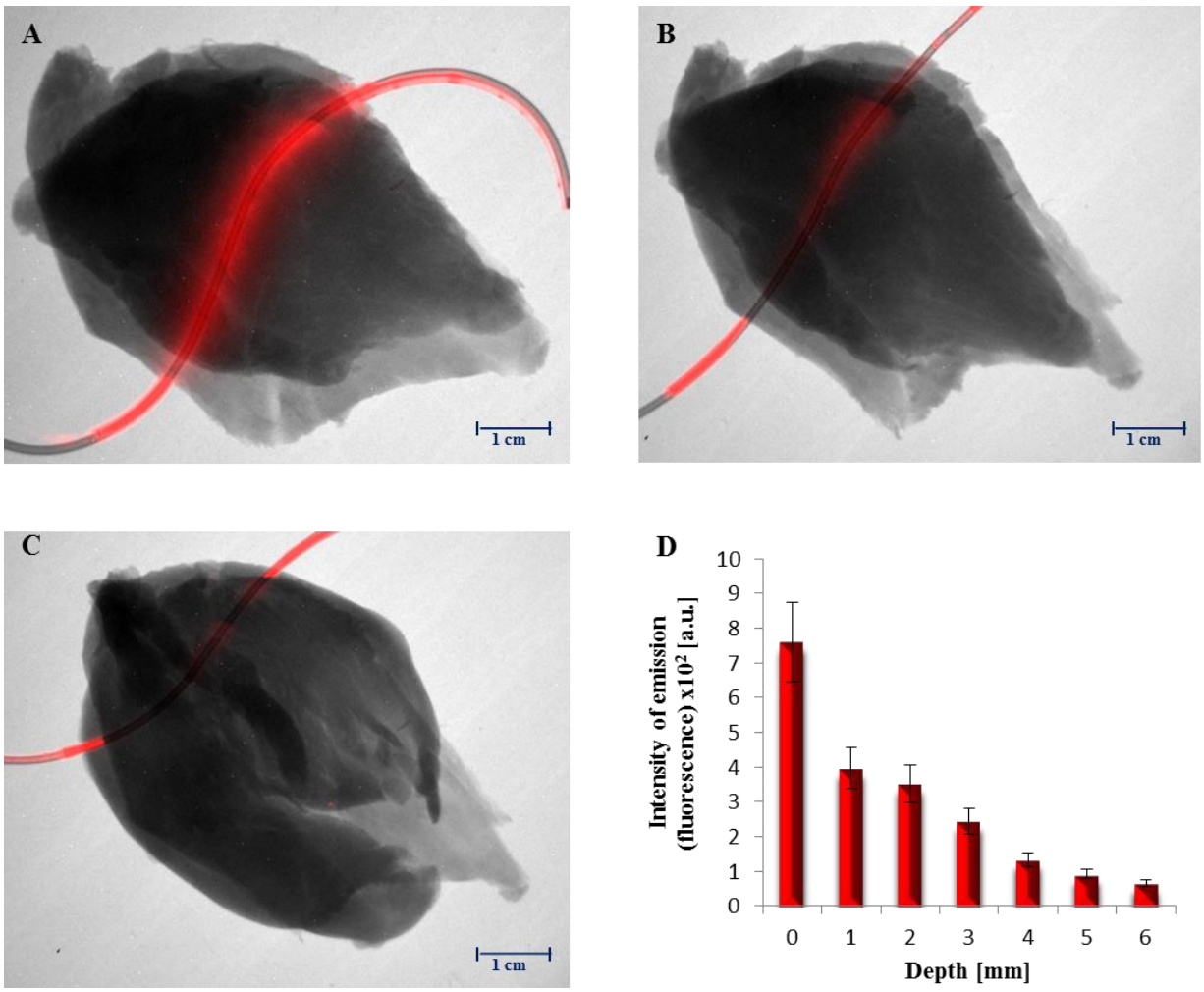

Figure 2. Detection of DOX fluorescence (500 µg/mL in methanol) in the tube (internal diameter of 1 mm) in the different depths of the chicken breast muscle tissue: (A) tube in the depth of 4 mm; (B) tube in the depth of 5 mm; (C) tube in the depth of 6 mm; (D) decreasing DOX fluorescence intensity depending on the tube depth in the tissue (Blazkova, Vaculovicova et al. 2014).

3.3.2.1 Mechanism of the action

Multiple mechanisms are involved in DOX effect (Octavia, Tocchetti et al. 2012), DOX intercalate into the DNA and uncoil the double-stranded helix. The binding to DNA inhibits DNA polymerase and nucleic acid synthesis (De Beer, Bottone et al. 2001; Cutts, Nudelman et al. 2005). For DOX optimal interaction with DNA, unmodified daunosamine amino group is important (Agudelo, Bourassa et al. 2014). DOX interference with the genome is regarded as the primary cause of the anti-tumour action (De Beer, Bottone et al. 2001). Anthracycline compounds have been established to form covalent drug–DNA adducts utilising endogenous and exogenous sources of formaldehyde (Forrest, Swift et al. 2012; Zhu, Myint et al. 2012). For adduct formation DOX must react with cellular formaldehyde to form an activated Schiff base which is then able to form an aminal (N-C-

N) linkage to the exocyclic amino group of guanine residues. The mono-adducts form primarily at G of 5'-GCN-3' sequences where the chromophore of the drug is intercalated between the C and N base pair (Cutts, Nudelman et al. 2005). The intercalation promotes nucleosome turnover around promoters by its effect on DNA topology, with possible implications for mechanisms of cell killing during cancer chemotherapy (Yang, Kemp et al. 2013; Deng, Yan et al. 2014). In tumour cells, these anthracycline-induced perturbations are believed to result in a final common pathway of endonucleolytic DNA fragmentation known as apoptosis (De Beer, Bottone et al. 2001). DOX resulted apoptosis of tumour cells is causes by the activation of various molecular signals like AMPK (AMP-activated protein kinase inducing apoptosis) and the Bcl-2/Bax apoptosis pathway (Cheng, Lu et al. 2012; Tacar, Sriamornsak et al. 2013).

DOX stabilize the cleavable complex between DNA and homodimeric topoisomerase II (TOP2) enzyme subunits, resulting in the formation of protein-linked DNA double strand breaks (De Beer, Bottone et al. 2001). TOP2α is a major target of many commonly used anticancer drugs (Magan, Isaacs et al. 2012). TOP2α is a proliferation cell marker overexpressed in tumours and is considered to be the molecular basis of DOX's anticancer activity (Magan, Isaacs et al. 2012; Zhang, Liu et al. 2012). DOX treatment increases lipid oxidation, catalase activity and production of hydrogen peroxide (Lagoa, Ganan et al. 2014). Anthracyclines are the only group of the drugs that binds to the metal. DOX's α-ketol group interact with Fe(III) with the result of hydroxyl radicals formation. Metal attachment to the α-ketol group is facilitated by the phosphate groups of DNA (Eizaguirre, Yanez et al. 2012). The changes in cellular iron metabolism are connected with drug resistance (Chekhun, Lukyanova et al. 2013).

3.3.2.2 Cardiotoxicity

The use of DOX is confined by toxicities such as hematopoietic suppression, nausea, vomiting, extravasation, alopecia (Octavia, Tocchetti et al. 2012), its usefulness is limited by nephrotoxicity, hepatotoxicity and the most serious is acute and also latent cardiac toxicity (Carvalho, Santos et al. 2009; Zordoky, Anwar-Mohamed et al. 2011; Henderson, Borders et al. 2014). Cardiotoxicity is usually manifested by congestive heart failure. When congestive heart failure develops, mortality is approximately 50% (Chatterjee, Zhang et al. 2010). It is necessary to control the dose of DOX administered to patients. The cumulative dose, which should not be exceeded, is approximately 500 mg/m^2 (Singal, Iliskovic et al. 1997; Batist, Ramakrishnan et al. 2001; Theodoulou and Hudis 2004;

Huska, Adam et al. 2009). Almost 10% of patients treated with DOX or its derivatives will develop cardiac complications up to 10 years after the termination of chemotherapy (Octavia, Tocchetti et al. 2012). Suggested contributors to DOX-induced cardiomyopathy include formation of reactive oxygen species, apoptosis, inhibited expression of cardiomyocyte-specific genes, and altered molecular signalling (Takemura and Fujiwara 2007). The toxic effect of DOX to cardiomyocytes cannot be the result of DNA synthesis inhibition, because these cells do not replicate (Myers 1998), the cardiac cell proliferation stops after 2 months of age (De Beer, Bottone et al. 2001). But low activity of antioxidant enzymes in the cardiomyocytes could have the impact (Xu, Persson et al. 2005).

DOX is believed to cause dose-dependent cardiotoxicity through redox cycling and the generation of reactive oxygen species (ROS) (Strigun, Wahrheit et al. 2012; Zhang, Liu et al. 2012). The free radical-mediated alteration of energy metabolism is probably an important mechanism mediating DOX-induced cardiac injury (Zhao, Miriyala et al. 2014). The cardiotoxicity can be attributed to the damage of mitochondrial DNA (Finkel 2012; Nitiss and Nitiss 2014) and mitochondrial iron accumulation (Ichikawa, Ghanefar et al. 2014). Cardiac mitochondrial dysfunction seem as critical site of gender difference of cardiotoxicity (Moulin, Piquereau et al. 2014). DOX could negatively affect mitochondria by inhibiting respiratory capacity, leading to an increase in H_2O_2-emitting potential (Gilliam, Fisher-Wellman et al. 2013). Oxidative stress has been established as the primary cause of cardiotoxicity. The elevated level of ROS often induces oxidative protein modifications that result in alteration of protein functions and ROS increase formation of lipid peroxidation products (Zhao, Miriyala et al. 2014).

The chronic DOX administration leads to an imbalance between cytochrome P450-mediated cardiotoxic and cardioprotective pathways. The chronic DOX cardiotoxicity significantly induced gene expression of hypertrophic markers, apoptotic markers and soluble epoxide hydrolase (sEH) enzyme (Alsaad, Zordoky et al. 2012). Acute DOX toxicity alters the expression of several CYP and sEH enzymes with a consequent alteration in arachidonic acid metabolism (Zordoky, Anwar-Mohamed et al. 2010).

One of the proposed mechanism for DOX induced cardiotoxicity is the formation of metabolites (Xu, Liu et al. 2012). DOX metabolites are doxorubicinol (DOXol) DOX aglycone, DOXol hydroxyaglycone and DOX hydroxyaglycone (Licata, Saponiero et al. 2000; Bains, Szeitz et al. 2013). Second-generation anthracycline analogues like epirubicin or idarubicin exhibit improvements in their therapeutic index, but the risk of inducing cardiomyopathy is not abated (Minotti, Menna et al. 2004). Epirubicin was developed to

circumvent the cardiotoxic limitations associated with the use of DOX in the clinic. The rate of formation of epirubicin-DNA adducts is slower and production of hydroxyl radicals is lower (Eizaguirre, Yanez et al. 2012; Zhu, Myint et al. 2012). Patients with higher expression of TOP2β in cardiomyocytes are probably more sensitive to DOX induced cardiotoxicity (Zhang, Liu et al. 2012). Catalytic TOP2 inhibitors may directly protect the heart from DOX cardiotoxicity but also potentially sensitise cancer cells to anthracyclines, which in turn may permit anthracyclines dose reduction with secondary reduction of cardiotoxicity risk (Vavrova, Jansova et al. 2013).

3.3.2.3 Cardioprotective compounds

Nowadays, the usage of new DOX analogues and combination of DOX with protective drugs and nutritional supplements to reduce the cardiotoxicity is studied (Pathan, Bhandari et al. 2012; Rajasekaran and Kalaimagal 2012; Bjelogrlic, Lukic et al. 2013; El Boghdady 2013; Lin and Yin 2013; Matouk, Taye et al. 2013). Greatly cardioprotective effect has dexrazoxane (ICRF-187). Regardless of incomplete understanding to its mechanism of action (Jirkovsky, Lencova-Popelova et al. 2013), dexrazoxane is the only clinically approved cardioprotective agent against anthracycline cardiotoxicity (Vavrova, Jansova et al. 2013). Dexrazoxane has an intrinsic antineoplastic activity and significant iron binding properties (Doroshow 2012). The mechanism of action of this is due to its hydrolytic transformation into the iron-chelating metabolite ADR-925 that may act by displacing iron from anthracycline-iron complexes or by chelating free or loosely bound cellular iron. This prevents the iron-catalysed ROS damage (Simunek, Sterba et al. 2009; Sterba, Popelova et al. 2013). Dexrazoxane is as well a catalytic inhibitor of TOP2 and decreases early myocardial injury during anthracycline treatment and early use of dexrazoxane protects against the development of cardiotoxicity in paediatric cancer patients (Kang, Kim et al. 2012). Also other drugs (Amifosfitie, Zofenopril, Mito-Tempol (4), Nicorandil, Rapamycin) (Ahmed and El-Maraghy 2013; Dickey, Gonzalez et al. 2013; Dragojevic-Simic, Dobric et al. 2013; Monti, Terzuoli et al. 2013; Sishi, Loos et al. 2013) or natural products (quercetin oleuropein resveratrol, flavonoids) are tested for their cardioprotective properties (Andreadou, Sigala et al. 2007; Wang, Han et al. 2010; Matouk, Taye et al. 2013; Osman, Al-Harthi et al. 2013). More clinical studies are needed to elucidate the mechanism and develop strategies in prevention against DOX-induced cardiotoxicity (Lin and Yin 2013). Numerous antioxidants and several iron chelators have been tested *in vitro* and *in vivo* with different outcomes. None of these compounds have

matched or even surpassed the effectiveness of dexrazoxane in chronic anthracycline cardiotoxicity settings, regardless of being stronger chelators and/or antioxidants (Sterba, Popelova et al. 2013). Promising tools for the decrease of the DOX cardiotoxicity and effective treatment with fewer side effects are nanoparticles (NPs).

3.4 NPs

Nanotechnology is a field that utilizes NPs in various disciplines of technology and science. As shown in Fig. 3, NPs are particles in the size range of 1–100 nm (in at least one dimension) and are potential candidates for various applications ranging from biosensors to the delivery of genes and therapeutic agents to tissue engineering (Davis, Chen et al. 2008; Choi, Tripathi et al. 2014). The size of NPs gives them unique physical, chemical, and biological properties (Ranganathan, Madanmohan et al. 2012) and enables their utilization in biological systems because of the size smaller than or comparable to the size of cell (10–100 μm), virus (20–450 nm), protein (5–50 nm) and DNA double helix (2 nm in width) (Wu, Ou et al. 2010). The application of nanotechnology in the medical field is defined as nanomedicine. Nanomedicine can greatly affect and improve diagnostics and treatment of life-threatening diseases (Wang, Billone et al. 2013). The most important area of nanomedicine is nanooncology, which utilizes NPs in cancer management (Ranganathan, Madanmohan et al. 2012). NPs have a great potential to become a new class of cancer therapeutics (Gabizon, Bradbury et al. 2015). NPs could solve a number of issues associated with conventional therapeutic agents, including their poor water solubility, lack of targeting capability, nonspecific distribution, systemic toxicity, and low therapeutic index (Sun, Zhang et al. 2014). NPs enable selective targeting of therapeutic drugs into the tumour cells. Selective targeting enhances the concentration of drug in the tumour and decreases the concentration in surrounding healthy tissues with a result of less serious side effects and effective treatment (van 't Veer and Bernards 2008; Sobolev 2013; Sultana, Khan et al. 2013). The drugs can be adsorbed onto the surface, entrapped inside, or dissolved within the matrix of the NPs (Ranganathan, Madanmohan et al. 2012). There are a lot of NPs (liposomes; polymeric micelles, peptide/protein conjugates, magnetic, gold, silica, cyclodextrin NPs, carbon nanotubes), that are widely studied in the cancer treatment (Ma and Mumper 2013). NPs improve the delivery of anticancer agents to the tumour tissue (passive targeting), by incorporation of targeting moieties, more effective drug targeting is enabled (active targeting) (Czernin and Phelps 2002). Several therapeutic NPs have been approved for clinical use. Nevertheless, there are only a few clinically approved

NPs that incorporate molecules to selectively bind and target cancer cells (Peer, Karp et al. 2007; Myhr 2008; Freilich, Mellon et al. 2014). For rapid and effective translation to clinical practise, the NPs should be made from a biocompatible material, to be well characterized, and easily functionalized, exhibit high differential uptake efficiency in the target cells over normal cells (or tissue), be either soluble or colloidal under aqueous conditions for increased effectiveness, have an extended circulating half-life, a low rate of aggregation, and a long stability (Peer, Karp et al. 2007).

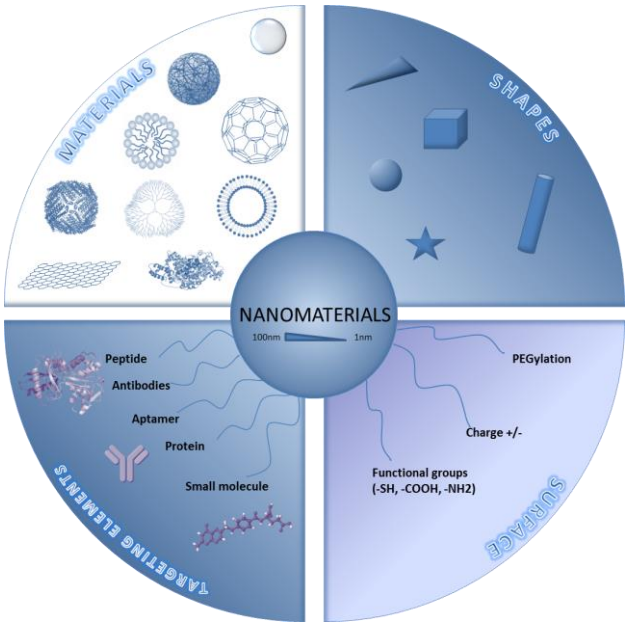

Figure 3. Summary of NPs properties. Efficacy of NPs considerably affects their shape and size. NPs can be synthetized from different materials and coated by differ functional groups and surface ligands. Sometimes are NPs also conjugated with targeting ligands (Li, Lie et al. 2008).

There is an effort to individualize chemotherapeutic interventions on the basis of *ex vivo* and *in vivo* information on patient and on the basis of disease-specific characteristics (Lammers, Rizzo et al. 2012). The tests based on the detection of genes expressed by tumours belong to the field of personalized medicine (van 't Veer and Bernards 2008). This approach could utilize genetic and proteomic profiling and also *in vivo* imaging to analyse the type, the stage, the grade of the disease and predict the response to the treatment (Lammers, Rizzo et al. 2012). This increases the need of diagnostic biomarkers and NPs targeted transporters (Sakamoto, van de Ven et al. 2010; Hanash, Baik et al. 2011). The development in cancer genomics brings the opportunity of targeting cancer cells by directly targeting the culprit genes. Except viral vectors, different NPs can be used to deliver DNA, small interfering RNA, antisense oligonucleotides or microRNA (Schaffert and Wagner 2008; Pissuwan, Niidome et al. 2011; Samal, Dash et al. 2012; Xu, Li et al. 2014). While NPs are usually designed for targeted drug delivery, they can also

simultaneously provide diagnostic information by a variety of *in vivo* imaging methods (Key and Leary 2014). The combination of diagnostic and treatment agent into the one single platform is the purpose of theranostics (therapy and diagnostics) (Janib, Moses et al. 2010; Xie, Lee et al. 2010).

Some inorganic NPs have fluorescent properties that can be exploit to enhance the sensitivity, resolution and imaging depth of fluorescence *in vivo* imaging (Bouccara, Sitbon et al. 2015). Enhanced targeting potential, imaging, and controlled release of drugs or therapeutic molecules could be possible due to multi-functional nanocarriers (Sultana, Khan et al. 2013). These multi-functional carriers share three main design components: carrier platform (NPs), encapsulated payload/biologically active agents (drug, imaging element), and targeting/surface ligand (Jabr-Milane, van Vlerken et al. 2008; Hwang, Park et al. 2012). Also multicomponent NPs that contain two or more imaging elements enabling the use of several imaging techniques and precisely monitoring the events in body are used. NPs of appropriate composition can greatly improve the resolution of each of imaging modalities (Key and Leary 2014).

NPs offer an attractive platform to overcome drug resistance (Kirtane, Kalscheuer et al. 2013). Until now, many anthracycline nano-delivery systems have been developed and reported to effectively circumvent multidrug resistance, and some of these systems have even advanced to clinical trials (Dong and Mumper 2010; Arora, Jensen et al. 2012; Ma and Mumper 2013). The use of NPs in different applications is widely studied, NPs were successfully used as contrast agents (Chanda, Upendran et al. 2014), in photothermal therapy (Chen, Wang et al. 2014), radiofrequency (Gannon, Patra et al. 2008), regenerative medicine (Das, Mohanty et al. 2012) etc.

3.4.1 The journey of the NPs with drug in the body

An increasing number of novel and complex nano-sized carriers are synthetized. But this raise in complexity does not always offer more efficient systems. These carriers are often successfully tested on cells and usually on rodents, but in the preclinical studies are often declared as unfit for reason of pharmacokinetic/biodistribution profiles and/or unacceptable toxicities (Bertrand and Leroux 2012). Nowadays, there is a limited understanding of the link between the physicochemical properties of NPs and their effect on the physiological system (Lee, Choi et al. 2015). The physiochemical characteristics such as size, surface charge, membrane lipid packing, steric stabilization, dose, and route of administration have significant impact (Zamboni 2008). There are questions about NPs

stability in *in vivo* system as flocculation, aggregation, jamming and bridging, and also their adsorption, adhesion and hydrodynamics (Ruenraroengsak, Cook et al. 2010). Particle–particle interactions in physiological media are important determinants for NPs fate and transport (Pyrgiotakis, Blattmann et al. 2013).

Upon intravenous administration, NPs and nano-sized molecules (NMs) enter the vascular system and are distributed to the organs and peripheral tissues of the body (Patel and Tannock 2009). In the vascular compartment NPs encounter blood cells, platelets, coagulation factors, and plasma proteins. In the dependence of the size and charge, NPs and NMs can undergo adsorption or opsonization by serum proteins (Longmire, Choyke et al. 2008). Protein coronas created during the initial reaction with NPs can determine the subsequent immunological cascade. Adsorption of plasma proteins on the surface can led to biochemical activation of defence cascades, and trigger elimination by multiple types of phagocytic cell (Karmali and Simberg 2011). Immunotoxicity can be mitigated or activated depending on the type of NPs and adsorbed plasma protein (Lee, Choi et al. 2015). Adsorption or opsonization of NPs affects the effective size of the NPs and results in a particle diameter referred to as the *in vivo* hydrodynamic diameter (HD) (Longmire, Choyke et al. 2008). The immune recognition of NPs significantly influences drug delivery efficacy and toxicity. Understanding the mechanisms of recognition and stability of NPs in biological system will become an important part of NPs design (Peer, Karp et al. 2007; Karmali and Simberg 2011). The encapsulation of drug into the NPs can result in a bypass of P-glycoprotein-mediated drug efflux (Li, Wang et al. 2012).

Anticancer drugs gain access to solid tumours via the circulatory system, and must penetrate the extravascular space to reach cancer cells at a sufficient concentration to cause lethal toxicity (Primeau, Rendon et al. 2005). NPs with a surface charge either slightly positive or slightly negative should have accessibility to and within disseminated tumours. If the size is correct, these NPs will be restricted from exiting normal vasculature (requires sizes less than 1–2 nm) and if the surface charge becomes larger the scavenging by macrophages increases with subsequent greater clearance by the reticuloendothelial system (Davis, Chen et al. 2008). NPs have been designed to increase circulation time of drugs in the bloodstream (Cho, Wang et al. 2008), this slow-release systems enable effective drug deliver into the tumour tissue (Drummond, Meyer et al. 1999). In the tissue the drug is shuttled into cells by the NPs and released inside cells usually after endocytosis (Wang, Cheng et al. 2011), formed endosome merge with lysosome, which decomposed the complex (Iversen, Skotland et al. 2011). NPs drug delivery to the tumour is impacted by

multiple factors, NPs have to evade clearance by renal filtration and the reticuloendothelial system, extravasate through the enlarged endothelial gaps in tumours, penetrate through dense stroma in the tumour microenvironment to reach the tumour cells, remain in the tumour tissue for a prolonged period of time, and finally release the active agent to induce pharmacological effect (Ernsting, Murakami et al. 2013).

3.4.1.1 Clearance

The most important organs influencing the journey of the drug in the body are kidney, liver and spleen (Bertrand and Leroux 2012). NPs injected into blood are after administration rapidly eliminated and within minutes accumulate in the liver and spleen (Issa, Obaidat et al. 2013). NPs of the size till 100–150 nm in diameter are able to access the liver (Davis, Chen et al. 2008) and their subsequent clearance by kidneys highly influence NPs toxicity. NPs possess rapid clearance by the kidney if they are smaller than ~10 nm in diameter (Choi, Zuckerman et al. 2011). Molecular size, shape, charge and also molecular deformability are the major determinants of solute permeability across the glomerular capillary wall (Venturoli and Rippe 2005), these properties preclude efficient clearance from the body as intact NPs (Longmire, Choyke et al. 2008). Size/HD of NPs is a key factor governing their renal clearance (Liu, Yu et al. 2013). The HD affects blood clearance and therefore blood half-life and whole body half-life. The HD is inversely related to rate of glomerular filtration and is directly related to blood and whole body half-life (Longmire, Choyke et al. 2008). Negatively charged proteins are retarded compared with neutral ones (Venturoli and Rippe 2005).

3.4.2 Targeting of NPs to the tumour tissue

Efficient delivery of therapeutics into tumour cells to increase the intracellular drug concentration is a major challenge. For the passive targeting of NPs to the site of the action, the natural properties of NPs and specific tumour environment are utilized (Ou, Wang et al. 2014).

Solid tumours are complex societies where cells reside within variable microenvironments that can influence their response to chemotherapy (Primeau, Rendon et al. 2005; Lowengrub, Frieboes et al. 2010; Martin Sabroso and Torres-Suarez 2014; Zhang and Kong 2015). Angiogenesis is characteristic for tumour development and this great blood supply enables targeting of drugs and NPs. Hypoxia in the tumour can be also exploited in the targeted therapy (Osinsky, Zavelevich et al. 2009; Wu, Shao et al. 2014). Rapid

development of new, irregular blood vessels causes the discontinuous epithelium (Karathanasis, Chan et al. 2008). Blood vessels in tumour tissue have defective architecture with gaps as large as 200–1000 nm (Hobbs, Monsky et al. 1998; Ranganathan, Madanmohan et al. 2012). These gaps enable the transmission of large molecules and small particles (Torchilin 2011). This permeation of cell wall near the tumour established the phenomenon - EPR effect (enhanced permeability and retention effect) (Maeda 2012; Nichols and Bae 2014). Delivery of NPs by EPR effect to the tumour is influenced by regional blood flow to the tumour, permeability of the tumour vasculature, structural barriers imposed by perivascular tumour cells and extracellular matrix and intratumoural pressure (Kobayashi, Watanabe et al. 2014).

Because of the rapid development also the pH in tumour differs from the normal cells. Extracellular pH of tumour is acidic (6.8-6.9) compare to extracellular pH of normal cells (7.4) (Yan, Robinson et al. 2007; Medeiros, Santos et al. 2011). The increased drug dissociation rate in acidic environment is beneficial for controlled DOX release (Kievit, Wang et al. 2011; Wang, Cheng et al. 2011; Das, Singh et al. 2013; Gautier, Allard-Vannier et al. 2013; Anbarasan, Babu et al. 2015).

Active targeting can be achieved by site-specific delivery or site-specific triggering (Myhr 2008). NPs can be targeted to cancer cells if their surfaces contain different peptides, proteins, antibodies, nucleic acids, sugars and small molecules such as vitamins, that enable specific interaction with tumour cell surface receptors (Marcucci and Lefoulon 2004; Davis, Chen et al. 2008; Kikkeri, Lepenies et al. 2009; Jiang, Chen et al. 2012; Bertrand, Wu et al. 2014; Gallo, Garcia et al. 2014). Multiple functionalities can be incorporated into the design of NPs to enable imaging and triggered intracellular drug release (Yu, Tai et al. 2010).

3.4.3 Inorganic NPs

Different inorganic NPs are for their unique properties broadly studied. In cancer diagnosis and therapy carbon nanostructures, quantum dots (QDs), gold and magnetic particles are highly investigated. These NPs possess unique optical, electrical, magnetic and/or electrochemical properties (Gong, Chen et al. 2012; Yang, Jin et al. 2012).

3.4.3.1 QDs

QDs attracted huge attention over the last decade. Great optical properties of QDs over conventional organic dyes make them interesting labels for a wide range of biomedical

applications (Wang, Hu et al. 2013; Zhu, Hong et al. 2013). They have broad absorption spectrum and a narrow emission spectrum and are photostable (Hong, Wang et al. 2012; Gallo, Garcia et al. 2014). Fluorescence properties of QDs can be successfully exploit for imaging of tumour cells as well as *in situ* investigations of tumour tissue (Hu, Fang et al. 2014; Moulick, Blazkova et al. 2014). QDs of different colours detected within a chicken embryo are shown in Figure 4.

QDs are semiconductor NPs (1 – 20 nm) with very good fluorescence properties, which are usually synthesised from atoms of group II-IV or III-V. The most used QDs are CdTe, CdSe, CdS, ZnSe and ZnS QDs (Cooper, Franco et al. 2011; Gomes, Vieira et al. 2011; Sobhana, Devi et al. 2011; Tmejova, Hynek et al. 2014) and were utilized for labelling and detection of different biomolecules (Ryvolova, Chomoucka et al. 2011; Geszke-Moritz and Moritz 2013; Krejcova, Hynek et al. 2013; Sobrova, Blazkova et al. 2013; Tmejova, Hynek et al. 2014). Because of the content of heavy metals, the toxicity of QDs is discussed (Lin, Ding et al. 2014).

The conjugation of DOX on the surface of AgZnInS QDs enhanced the cytotoxicity of DOX to multidrug-resistant cancer cells (Qu, Deng et al. 2014). The multifunctional QDs are promising vehicles for the delivery of chemotherapeutics such as DOX and for real-time tracking of treatment (Li, Wang et al. 2012). Nanoconjugates of CdSe/CdS/ZnS QDs and DOX enable targeted delivery of drug and DOX released from the QDs-DOX conjugate showed unchanged properties (Chakravarthy, Davidson et al. 2011).

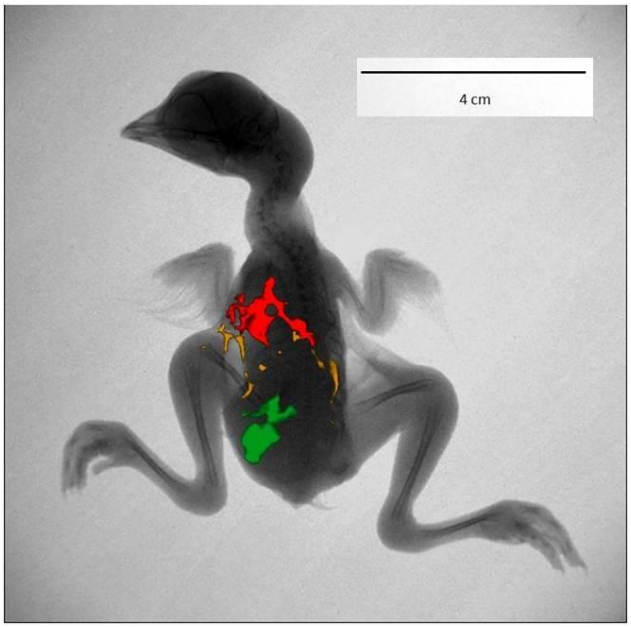

Figure 4. Different CdTe QDs applied into the chicken embryo (18th developmental day) detected by In vivo Xtreme by Carestream (Rochester, NY, USA). The fluorescence of three different QDs detected with excitation filter: 480 nm and emission filter: 535 nm (CdTe green), 600 nm (CdTe yellow) and 700 nm (CdTe red). The fluorescence images were overlaid and combined with x-ray image (Blazkova, Konecna et al. 2014).

3.4.3.2 Carbon nanostructures

Among the numerous types of nanomaterials developed in recent years, research on carbon nanostructures such as carbon nanotubes (CNTs), graphene (GFN), graphene oxide (GO), reduced graphene oxide (rGO), fullerene and other carbon NPs (CNPs) has emerged as a booming area, especially for the development of delivery vehicles for imaging agents and drugs (Chen, Huang et al. 2013). Carbon nanostructures possess sufficient surface-to-volume ratio, thermal conductivity, rigid structural properties capable of post chemical modification and excellent biocompatibility (Lim, Sim et al. 2014). CNTs serve as smart nanomaterials for the development of novel drug delivery systems in cancer theranostics (Levi-Polyachenko, Carroll et al. 2008; Chen, Huang et al. 2013). GFN is one-atom-thick sheet of carbon, which combines different properties, such as extreme mechanical strength, exceptionally high electronic and thermal conductivity (Novoselov, Fal'ko et al. 2012). The scaled-up and reliable production of graphene derivatives, such as GO and rGO offers a wide range of possibilities to synthesize graphene-based functional materials for various applications (Huang, Qi et al. 2012). The utilization of graphene materials in cancer cell imaging, delivery of cytostatics and delivery of genes are discussed at the end of this literature overview in book chapter I. CNTs are made of rolled-up sheets of graphene (Castro Neto, Guinea et al. 2006). These fibre-like materials are usually investigated in the

form of single-walled carbon nanotubes (SWCNTs) or multi-walled carbon nanotubes (MWCNTs) (Moller, Christophersen et al. 2014). The utilization of SWNTs and MWNTs in drug, especially DOX delivery is mentioned in the book chapter II in this thesis.

Fullerenes are wrapped-up graphene molecules that form polyhedral cages (Castro Neto, Guinea et al. 2006; Schwerdtfeger, Wirz et al. 2015). Fullerenes have been applied in MRI and photoacoustic imaging, in photodynamic therapy, photothermal treatment, radiotherapy and chemotherapy (Chaban, Pyatakov et al. 1999; Wrobel and Graja 2006; Brown, Chung et al. 2010; Chen, Ma et al. 2012; Guo, Ding et al. 2014; Shevtsov, Nikolaev et al. 2014; Yin, Wang et al. 2014). Fullerenes can be exploited in theranostics and are important antioxidants (Dellinger, Zhou et al. 2013). Their anti-tumour effect may be associated with the anti-angiogenesis and immunostimulatory activity (Chen, Ma et al. 2012).

Conjugation of DOX with fullerene significantly differ its distribution in cells. DOX is predominantly accumulated in cell nucleus (Wang, Wu et al. 2013), whereas DOX-fullerene conjugate is mostly detected in the cytoplasm (Liu, Cao et al. 2010). Conjugation of DOX with fullerene led to 1.5-2-fold increase in tumour cell toxicity with concurrently life period prolongation by 63% and metastasis inhibition (mice model). Tumour cells were dying due to the superoxide radical production and induction of apoptosis (Prylutska, Grynyuk et al. 2014; Prylutskyy, Evstigneev et al. 2014; Panchuk, Prylutska et al. 2015).

3.4.4 Organic NPs

Developing the drug delivery systems that would be biocompatible and non-toxic is a challenging issue in anticancer drug management (Kilic, Ozlu et al. 2012). Materials that are natural for human body are more acceptable by the organism and thus become an attractive approach in the research (Heger, Skalickova et al. 2014). It is evidenced, that the most of the FDA (Food and Drug Administration) approved marketed nanomedicines are organic-based formulations (Wang, Billone et al. 2013). Different coatings of inorganic NPs or organic NPs are being developed to increase the bioavailability (Chen, Huang et al. 2013). The most commonly used approach is hydrophilic coating by poly(ethylene glycol) (PEG), which is also often referred to as poly(ethylene oxide) (PEO) (Chen, Ehlerding et al. 2014). This polymer is non-toxic, non-immunogenic, non-antigenic, highly soluble in water and FDA approved. The PEG-drug conjugates have several advantages: a prolonged continuance in body, minimised interaction with plasma proteins, decreased degradation by metabolic enzymes and has ability to escape the mononuclear phagocyte system, which

prevents preliminary elimination of NPs from the blood stream (Levi-Polyachenko, Carroll et al. 2008; Larsen, Nielsen et al. 2012; Das, Singh et al. 2013; Chen, Ehlerding et al. 2014). The mechanism is unclear but chain length, chain density, and chain conformation highly influence the interaction with plasma proteins (Wilson, Kerlan et al. 2004). Modification of NPs by the linking of one or more PEG chains is defined as PEGylation (Lim, Sim et al. 2014).

3.4.4.1 Apoferritin

Proteins and peptides have the potential to deliver the anticancer drugs. They can enhance the intratumour concentration of the drug, can prolonged the administration and reduce burden on the body (Hawkins, Soon-Shiong et al. 2008). Approved drug for cancer treatment (metastatic breast cancer) based on the protein is Abraxane. Abraxane is 130 nanometer-size particle formed by drug paclitaxel and albumin. The action is based on the utilization of endogenous albumin pathways to increase intratumour concentrations of the active drug (Dulkeith, Morteani et al. 2002; Dreaden, Alkilany et al. 2012; Wilczewska, Niemirowicz et al. 2012).

Other protein, which is not currently used in treatment, but is studied for its good properties is ferritin (Gumulec, Fojtu et al. 2014). Ferritin is a nano-size spherical protein that naturally occurs in most living organisms. Ferritin function is to store iron that the cells do not require immediately for metabolic processes and thus protects against the toxic effects of free Fe^{2+} (Dominguez-Vera, Fernandez et al. 2010). A lot of applications have demonstrated the possibilities of iron-free ferritins, called apoferritins, serving as platforms for various nanomedical purposes (Bradshaw, Junor et al. 2013; Hwang, Lee et al. 2013; Xie, Zhen et al. 2013; Heger, Skalickova et al. 2014). The encapsulation of drugs inside the apoferritin cavity significantly increases its stability and bioavailability while maintaining its therapeutic properties (Ma-Ham, Wu et al. 2011; Cutrin, Crich et al. 2013). Apoferritin has been exploited to deliver simultaneously therapeutic and imaging agents (loaded into its internal cavity) to hepatocytes as this protein is efficiently taken up from blood via the ferritin transporting route (Cutrin, Crich et al. 2013). Selective anti-tumour activity of apoferritin encapsulated PbS quantum dots (AFt-PbS) was observed on human colorectal carcinoma cell lines. This nanocomposite material stopped the proliferation of the cells and caused the apoptosis due to the generation of ROS. On the contrary AFt-PbS did not affect the growth and cell cycle of normal human endothelial cells (Bradshaw, Junor et al. 2013). Apoferritin was successfully employed to encapsulate anticancer drugs cisplatin,

carboplatin and oxaliplatin (Yang, Wang et al. 2007; Xing, Wang et al. 2009). Drug can be encapsulated by disassembling of the apoferritin structure in low pH and subsequently reassembling it back by pH increase. The apoferritin-DOX complex has been formed by 'opening' and 'closing' the apoferritin sphere in the presence of DOX (Konecna, Nguyen et al. 2014). pH decreasing lower than 4 was sufficient for the opening of apoferritin structure (Tmejova, Hynek et al. 2013). The efficiency of DOX entrapment was detected as five DOX molecules per apoferritin (Simsek and Kilic 2005). DOX is not only encapsulated in the cage, but small amount is also desorbed on the surface (Blazkova, Hoai Viet et al. 2013). Tumour targeting potentiality, relative high loading capacity and good water solubility make apoferritin a promising carrier for anticancer drugs (Xing, Wang et al. 2009).

3.4.4.2 Liposomes

Liposomes are phospholipid membrane vesicles that can act as carriers for targeted drug therapy (Swenson, Perkins et al. 2001). Liposomes were discovered in the 1965 by Alec Bangham and because of their similarity with cell membranes, they are widely used in the anticancer drugs research and treatment (Bangham and Horne 1964; Bangham 1993). Liposomes appear to be suitable carriers of various substances within the inner cavity (Kensova, Blazkova et al. 2013). There are several formulations of these nanocarrier systems in various stages of clinical trials, as well as currently clinically approved liposomal-based drugs (Hofheinz, Gnad-Vogt et al. 2005; Cukierman and Khan 2010).

The main advantage of liposomal drugs is the reduction of the DOX negative side effects due to differences in pharmacokinetics and distribution of the drug in the body (Blazkova, Ryvolova et al. 2013). The major benefit of liposome application is the steric stabilization and remote loading of drugs by pH and ion gradients (Barenholz 2001). Liposomes demonstrated the highest penetration ability and accumulation inside cancer cells compared to linear PEG and dendrimers (Saad, Garbuzenko et al. 2008). The liposomal DOX has an extended circulation half-life in comparison to the free DOX and improved accumulation and retention within tumours (Lowery, Onishko et al. 2011) and liposomal formulation of DOX increases patients survival time and reduced hepatic extraction of DOX (Hosoda, Unezaki et al. 1995; Hilmer, Cogger et al. 2004). Higher toxicity of liposomal DOX for tumour cells and significantly lower toxicity for non-tumour cells was observed (Gumulec, Fojtu et al. 2014). And safe cumulative dose of liposomal

DOX increased (785 mg/m^2) compared to DOX without liposome (Longmuir, Haynes et al. 2009).

DOX liposome form is marketed as non-pegylated liposomal DOX Myocet used especially for treatment of metastatic breast cancer (Leonard, Williams et al. 2009) or as PEGylated liposomal DOX (PLD) Doxil or Caelyx used for the treatment of ovarian cancer, sarcoma and multiple myeloma (Seynhaeve, Dicheva et al. 2013). Doxil has been approved for the treatment of AIDS-related Kaposi's sarcoma. The characteristics of PLD are reduction of the severe side effects of cardiac toxicity and myelosuppression seen with DOX, and a higher anti-tumour effect from the selective high maintenance of the drug concentration in the tumour tissue (Sekiya and Imamura 2008). Doxil, the first FDA-approved nano-drug (1995) is based on prolonged drug circulation time and avoidance of the RES due to the use of PEGylated nano-liposomes and high and stable remote loading of DOX (Safra, Muggia et al. 2000; Barenholz 2012; Barenholz and Peer 2012; Ma and Mumper 2013). Due to the EPR effect, Doxil is "passively targeted" to tumours, where DOX is released and becomes available to tumour cells (Barenholz 2012). Doxil provides comparable efficacy to DOX, with significantly reduction of cardiotoxicity, myelosuppression, vomiting and alopecia (O'Brien, Wigler et al. 2004).

Thermosensitive liposomes are a promising tools for targeting of drugs to the solid tumours and release of drugs by hypertermia (Kneidl, Peller et al. 2014). ThermoDox is approved formulation of DOX which release is significantly increased after heating of the tumour side above 39.5 °C usually 41- 42 °C (Mylonopoulou, Arvanitis et al. 2010; May and Li 2013; Needham 2013).

3.5 Chapter in book I

BLAZKOVA, I; KOPEL, P.; VACULOVICOVA, M.; ADAM, V.; KIZEK, R. Graphene-Like Structures as Cages for Doxorubicin. *Graphene Science Handbook*, accepted.

Participation in the manuscript preparation of the author Blažková, I.: 44%.

Graphene-Like Structures as Cages for Doxorubicin

Iva Blazkova[1], Pavel Kopel[1,2], Marketa Vaculovicova[1,2],Vojtech Adam[1,2] and Rene Kizek[1,2]*

[1]Department of Chemistry and Biochemistry, Faculty of Agronomy, Mendel University in Brno, Zemedelska 1, CZ-613 00 Brno, Czech Republic, European Union

[2]Central European Institute of Technology, Brno University of Technology, Technicka 3058/10, CZ-616 00 Brno, Czech Republic, European Union

***Corresponding author**

Rene Kizek, Department of Chemistry and Biochemistry, Mendel University in Brno, Zemedelska 1, CZ-613 00 Brno, Czech Republic, European Union; E-mail: kizek@sci.muni.cz; phone: +420-5-4513-3350; fax: +420-5-4521-2044

Abstract

Carbon nanomaterials including graphene belong to the most intensively explored in materials science. Extraordinary physicochemical and structural properties and biocompatibility of graphene and graphene oxide predetermine them for many potential applications including photocatalysis, electrochemistry, electronics and optoelectronics. Moreover, two dimensional layer of sp^2 bonded carbon atoms and high specific surface area is very promising platform for biomedical applications. In this chapter we describe recent results on employing graphene and its oxide in diagnosis of tumour diseases and in treatment of these diseases. Various drug delivery systems are discussed. Moreover, we give brief discussion on the challenges and perspectives of these materials for future progress in the field of biomedical applications.

Keywords

Graphene; Tumour Disease; Treatment; Drug Delivery System; Doxorubicin

Table of Content

1. Introduction

Nanotechnology belongs to the most developing branch of science in the first decade of the 21st century. Nanomaterials are interesting because they have specific physicochemical properties and can be applied in many fields of science, electronics, optics and medicine (Wang et al. 2009; Zhang, Nayak, et al. 2012). The most used materials in medicine are quantum dots (Pollinger et al. 2014; Cai et al. 2007), paramagnetic nanoparticles (Gong et al. 2009; Thorek et al. 2006), liposomes (Lim et al. 2014; Burger et al. 2002), microspheres (Haase et al. 2013), polymeric shells (Sciallero et al. 2013; Maeda, Sawa, and Konno 2001; Hirsch et al. 2006), and carbon nanotubes (Lacerda et al. 2006; Pumera 2009; Villegas et al. 2014). Some of the nanomaterials are applied as transporters where cargo can be loaded by different kinds of mechanisms, such as encapsulation, surface absorption and hydrogen bonding. Loading capacity can be improved by very strong π-stacking interactions as it was found in binding of aromatic drug molecules to carbon nanotubes (Liu et al. 2007). The variety of carbon-based nanomaterials with potential of transporting properties is summarized in Fig. 1.

Graphene (GFN), as well as its derivatives graphene oxide (GO), and reduced graphene oxide (rGO), are formed by two-dimensional (2D) structure of sp^2 –hybridized carbon atoms arranged in six-membered rings with high specific surface area (2630 m^2/g). Physicochemical and structural properties of GFN, namely conductivity, high elasticity, mechanical strength, large surface area, and rapid heterogeneous electron transfer, make the material very interesting for many applications (Novoselov et al. 2004; Wei and Qu 2012; Li et al. 2014; Kong and Huang 2014). There are many papers and studies describing the use of GFN for widespread biomedical applications, ranging from biosensors (Song, Wei, and Qu 2011; Shao et al. 2010; Huang et al. 2011; Pandey et al. 2014), drug and gene delivery (Liu et al. 2011; Feng and Liu 2011; Liu et al. 2008; Misra et al. 2012; Zhou and Liang 2014), cell imaging, biological sensing and imaging (Yang et al. 2010; Zhang, Lu, et al. 2012; Zhang, Nayak, et al. 2012; Liu, Gao, et al. 2014; Zhang et al. 2014; Mosaiab, In, and Park 2013; Mao and Li 2013) to biocompatible scaffold for cell culture. The intensive research on the bioapplications of GFN and its derivatives is due to many fascinating properties, such as high specific surface area, electronic and thermal conductivities, biocompatibility, facile biological/chemical functionalization and low cost and scalable production (Jiang 2011; Guo and Dong 2011).

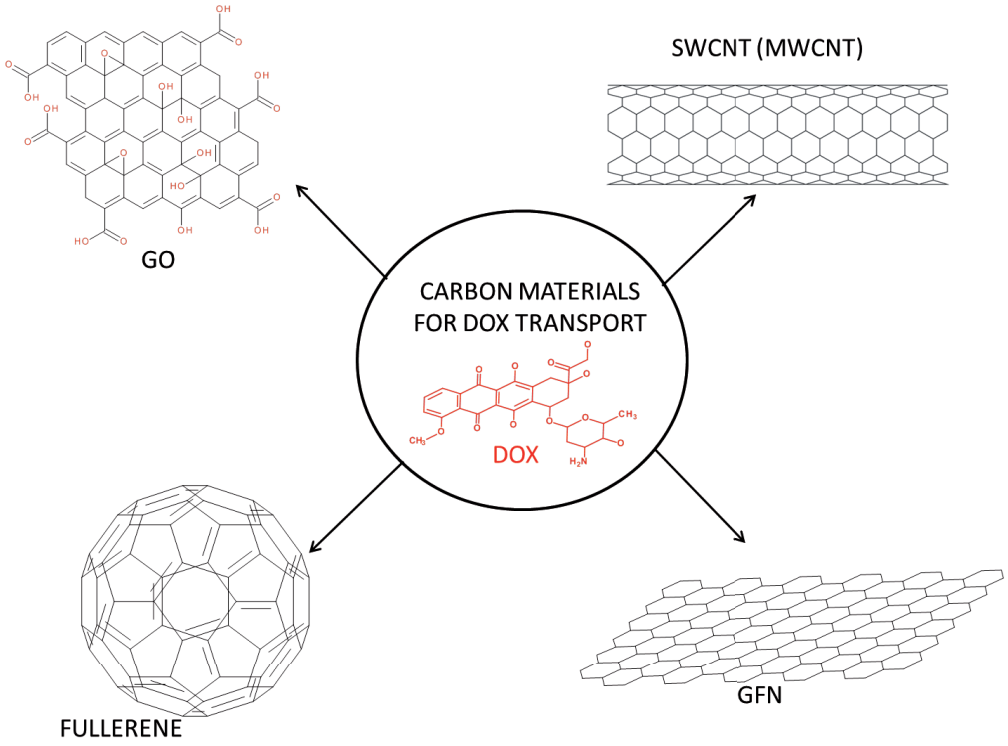

Figure 1. Summary of carbon-based nanocarriers employed for nanomedical applications.

It was a study of Liu et al. (Liu et al. 2008) in 2008 that started interest of use of GO as an efficient nanotransporter for drug delivery. GO, prepared by oxidation of graphite by Hummers method (Hummers and Offeman 1958), is an ideal nanotransporter for efficient drug and gene delivery. GO used for drug delivery is usually composed of 1-3 layers (1-2 nm thick), with size ranging from a few nanometers to several hundred nanometers (Loh et al. 2010; Kovtyukhova et al. 1999; Sun et al. 2008; Shen et al. 2012). Moreover, the presence of reactive COOH and OH groups enable formation of composite materials with polymers (Shan et al. 2009; Cha et al. 2014), biomolecules as DNA (Lei et al. 2011; Liu et al. 2013), protein (Zhang et al. 2010; Lee et al. 2011; Tan et al. 2013), quantum dots (Dong et al. 2010; Markad et al. 2013) and iron oxide nanoparticles (Li et al. 2011; Mendes et al. 2012).

2. Graphene and its Oxide for Tumour Disease Diagnostics

GFN and GO are an increasingly important nanomaterials, which exhibit great promise in the area of bionanotechnology and nanobiomedicine, such as biological imaging, molecular imaging, drug and gene delivery and cancer therapy (Kim et al. 2011; Ku and Park 2013; Li and Yang 2013; Zhang, Peng, et al. 2013) (Fig. 2). However, exploration of GFN with

intracellular monitoring and *in situ* molecular probing is still at an early stage. Thus, graphene appears to be auspicious nanoparticle in medicine and may bring novel opportunities for future disease diagnosis and treatment (Feng and Liu 2011; Wang et al. 2010; Yue et al. 2013). GFN and GO can inhibit the migration and invasion of cancer cells (Zhou et al. 2014). The different inorganic nanoparticles can be attached to the surface of GFN, obtaining functional graphene-based nanocomposites with good optical and magnetic properties useful for multi-modal imaging and imaging guided cancer therapy. GFN materials are used as carriers for antibody, DNA, protein, and drug (Du, Yang, and Lin 2012).

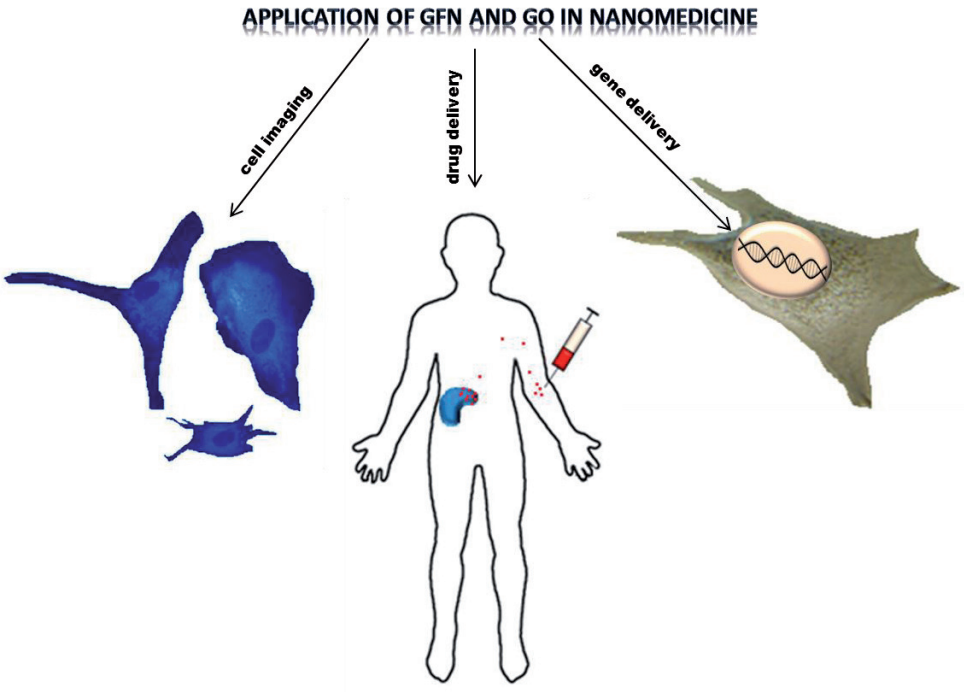

Figure 2. Schematic illustration of application of GFN and GO in nanomedicine.

2.1 Biosensing of Tumour Cells

Molecular biosensing systems can be based on naturally available and artificially designed enzymes, binding proteins and antibodies (Cissell et al. 2008). GFN is great material for biosensing and biological imaging (Du, Yang, and Lin 2012) and is a promising material for ultrasensitive nanomaterial based biosensors. Manipulable multi-functionalized surface chemistry allows realizing sensitive and selective detection of biomolecules (Li and Yang 2013). Because fast cancer diagnosis and effective measurement of cancer cells is a main challenge in early cancer diagnosis, miniature multiplex chip was created for *in situ*

detection of cancer cells by implementing a novel graphene oxide (GO)-based Förster resonance energy transfer (FRET) biosensor strategy (Cao et al. 2012).

GFN can be also used in single-molecule label-free biosensing technologies (Kravets et al. 2013). Highly sensitive and label-free detection of the biomarker carbohydrate antigen 15-3 (CA 15-3) is prospect of the breast cancer diagnosis and the electrochemical immunosensor with a highly conductive GFN (i.e. N-doped graphene sheets)-modified electrode, exhibited considerably increased electron transfer and high sensitivity toward CA 15-3. This strategy is promising for clinical research and diagnostic applications (Li et al. 2013). An electrochemical immunosensor for sensitive detection of cancer biomarker alpha-fetoprotein (AFP) has been also shown. The sensor was based on grapheme sheet platform and functionalized carbon nanospheres (CNSs) labelled with horseradish peroxidase-secondary antibodies (HRP-Ab2). Developed immunosensor showed a 7-fold increase in detection signal in comparison to the immunosensor without GFN modification and CNSs labelling (Du et al. 2010).

The GO might be a promising material for targeted drug delivery to the lungs. Compared with other carbon nanomaterials, GO had long blood circulation time (half-time 5.3 ± 1.2 h), and GO showed good biocompatibility with red blood cells and was predominantly deposited in the lungs. Low uptake of GO was observed in reticuloendothelial system (Zhang et al. 2011) and it was found that nanoparticle vectors can penetrate endothelial barriers to reach tumour sites (Portney and Ozkan 2006).

The novel highly sensitive multiplex electrochemiluminescence (ECL) immunoassay for the simultaneous detection of AFP (Alpha-Fetoprotein, marker for hepatocellular and germ cell carcinoma) and CEA (carcinoembryonic antigen) was developed using QDs as trace tag and GFN as a conducting bridge. This immunosensor is great for simultaneous detection of AFP and CEA with wide linear ranges, low detection limits, good specificity and acceptable accuracy (Guo et al. 2013). Also novel graphene oxide sheets/polyaniline/CdSe quantum dots (GO/PANi/CdSe) nanocomposites were prepared and used for the sensitive ECL biosensing (Hu et al. 2013). The graphene-based cathodic electrogenerated chemiluminescence immunosensor was demonstrated to determine PSA (prostate specific antigen) in human serum samples (Xu et al. 2011). As an alternative, the modification of immunosensor surface led to acceleration of electron transfer and high specificity and sensitivity was demonstrated (Wu et al. 2013). The described immunosensor was prepared by covalent immobilization of antibodies on a chitosan/electrochemically rGO film-modified

glassy carbon electrode. Cells were captured with a sandwich-type immunoreaction and various QD-coated silica nanoparticle tracers were captured on the surface of the cells.

It is necessary to pay the attention to the toxicity of the GO as soon as it is used for biomedical applications (Zhang et al. 2011). The cytotoxicity characteristics, cellular-uptake mechanism, and intracellular metabolic pathway of GFN and its derivatives are still not well-understood (Du, Yang, and Lin 2012; Pumera 2012; Horvath et al. 2013). It was observed that after the exposition of the mice to GO (10 mg/kg body weight) for 14 days, changes including inflammation, cell infiltration, pulmonary edema, and granuloma formation were found. No pathological changes were observed in examined organs when mice were exposed to 1 mg/kg body weight of GO for 14 days (Zhang et al. 2011). When 80 mg/kg was injected intravenously into mice, there was 100% fatality in the GO-treated group, but 100% survival among mice treated with pGO (polyethylene glycol-grafted graphene oxide nanosheets). The pGO nanosheets have superior *in vivo* safety relative to GO (Miao et al. 2013). As the main mechanism involved in the cytotoxicity of the rGO sheets was determined oxidative stress and cell membrane damage (Akhavan, Ghaderi, and Akhavan 2012). GO is found to be more toxic than rGO of same size. GO and rGO induce significant increases in both intercellular reactive oxygen species (ROS) levels and messenger RNA (mRNA) levels of heme oxygenase 1 (HO1) and thioredoxin reductase (TrxR) (Das et al. 2013). Better water solubility and stability of GO caused it's grafting with phosphorylcholine oligomer. Good biocompatibility and incorporation into cells by endocytosis was then observed (Liu, Zhang, et al. 2014). The aspiration of GFN cause only mild oxidation and did not caused inflammation in mice so it probably could be used in tissue engineering (Schinwald et al. 2014). The ability to stimulate myogenic differentiation by GO shows a potential for skeletal tissue engineering applications (Ku and Park 2013). Biocompatibly coated nano-graphene with ultra-small sizes can be cleared out from the organism after systemic administration, without noticeable toxicity to the treated mice (Li and Yang 2013). GO has cytoprotective effect, it enables control over gene transfection through region-selective gene delivery only into GO-untreated cells, and not into the GO-treated cells. GO can protect cells from internalization of toxic hydrophobic molecules, nanoparticles, and nucleic acids such as siRNA and plasmid DNA by interacting with cell surface lipid bilayers without noticeably reducing cell viability (Na et al. 2013).

2.2 Imaging of Tumour Cells

Tumour imaging has become an indispensable tool in the studying of cancer biology and in clinical prognosis and treatment (Condeelis and Weissleder 2010). The backbone of biomolecules and biological structures is carbon-based, thus, it is no doubt to integrate biological systems with nanocarbons and to use graphene-based scaffold for cell culture (Yang, Yao, and Duan 2013). Because of fine biocompatibility and low toxicity strongly fluorescent graphene QDs (GQDs) are demonstrated to be excellent bioimaging agents in cell imaging. The synthesized GQDs showed high solubility, excellent biocompatibility, and excellent optical properties and could be used directly for intracellular imaging without any surface modification (Zhu et al. 2011; Sun et al. 2013). Graphene-based FRET for cellular imaging was also reported (Wang et al. 2010). A multi-component nanosystem based on GFN and containing individual cyclodextrins (hosts for functional units) can be used as imaging agents, for anti-cancer drug delivery, and as tumour-specific ligands. The cyclodextrin-functionalized graphene nanosheet (GNS/-CD) facilitates host-guest chemistry between the nanohybrid and functional payloads (Dong et al. 2013). Moreover, the biocompatible nitrogen-doped GQDs (N-GQDs) may be used as efficient two-photon fluorescent probes for cellular and deep-tissue imaging. N-GQD can achieve a large imaging depth of 1800 μm, significantly exceeding the fundamental two-photon imaging depth limit. The N-GQD is nontoxic to living cells and exhibits great photostability under repeated laser irradiation (Zhang, Lu, et al. 2012). Also, graphene oxide nanoparticles (GONs) have been shown to be good optical probes because of their strong two-photon luminescence (Zhang, Lu, et al. 2012). After the cell labelling by GONs, highly localized and low power/energy therapy can be achieved. They can be functionalized with other targeting molecules, which enable more specific targeting into the different malignant tissues.

3. Graphene and its Oxide for Drug Delivery Systems

3.1 Cytostatics

GFN has been widely explored as novel nano-carriers for drug delivery (Li and Yang 2013). Ultrasmall GO nanosheets (less than 50 nm) could be used as the ideal nanocarriers for drug delivery due to the great biocompatibility, lower cytotoxicity and higher cellular uptake amount compared to the random large GO nanosheets (Zhang, Peng, et al. 2013). A triple functionalized drug delivery system was developed by encapsulation of superparamagnetic GO and doxorubicin (DOX) (Kizek et al. 2012; Stiborova et al. 2012) with folic acid (FA) conjugated chitosan (CHI) (Wang, Zhou, et al. 2013). The release of DOX was

pH sensitive, the lower pH values lead to weaker hydrogen bonds and degradation of CHI, and thus result in a higher release rate of DOX. This system could be used as a dual-targeted drug nanocarrier by combination of biological (active) and magnetic (passive) targeting capabilities. The micrograph of human fibroblast cells exposed to GFN conjugated to DOX is shown in Fig. 3.Also a multi-functional superparamagnetic GO-iron oxide hybrid nanocomposite (GO-IONP) can be synthetized and functionalized by a biocompatible polyethylene glycol (PEG) polymer to achieve high stability in physiological solutions. DOX can be loaded onto GO-IONP-PEG, forming a GO-IONP-PEG-DOX complex, which enables magnetically targeted drug delivery (Ma et al. 2012). The targeting peptide (IP) modified mesoporous silica-coated graphene nanosheet (GSPI) can serve as drug delivery field. Conjugation of DOX with chlorotoxin – GO complex increased the toxicity of DOX to cancer cells (Wang et al. 2014).

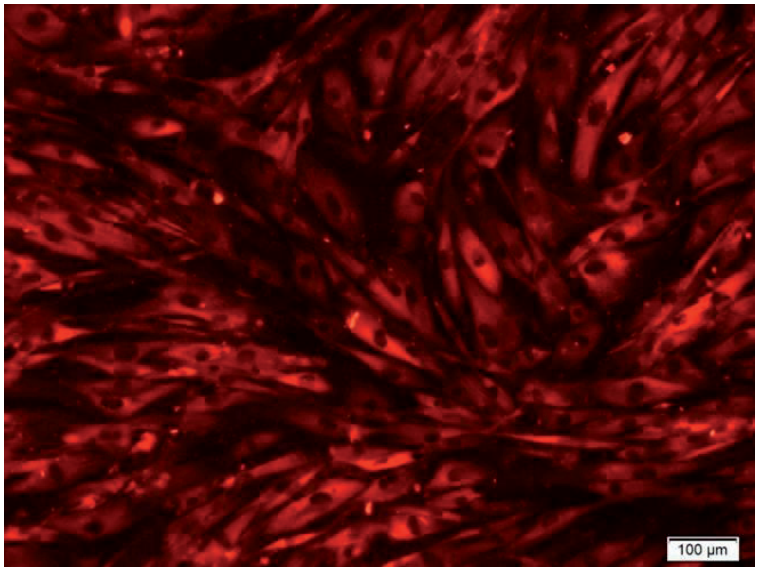

Figure 3. Fluorescent microphotograph of Human foreskin fibroblasts exposed to the DOX-GFN (30 minutes incubation, excitation 520 – 550 nm, emission: 580 nm; exposure time: 104.5 ms, ISO 200, magnification: 100×, temperature: 37°C, atmosphere: 5% CO_2).

Hyaluronic acid-GO conjugate has very low toxicity to cells and after its connection with DOX selectively delivered the drug and inhibited the grow of the tumours in mice (Wu et al. 2014). A DOX-loaded GSPI-based system (GSPID) showed heat-stimulative, pH-responsive, and sustained release properties. Combined therapy, chemotherapy and photothermal therapy was more toxic to glioma cells compared to single chemotherapy or photothermal therapy (Wang, Wang, et al. 2013). Kavitha et al. (Kavitha, Abdi, and Park 2013) presented GO

functionalized covalently with pH-sensitive poly[2-(diethylamino) ethyl methacrylate] (PDEA). Common water-insoluble cancer drug camptothecin (CPT) was loaded on GO-PDEA by simple physisorption by π-π stacking and by hydrophobic interaction. Loaded CPT can be released only at the lower (acidic) pH, which is normally found in a tumour environment but not in basic and neutral pH. GO-PDEA is not toxic to N2a cancer cells but the GO-PDEA-CPT complex exhibited high potency in killing N2a cancer cells *in vitro*. The GO-PDEA nanocargo carrier could be a good material for site-specific anticancer drug delivery and controlled release. Also the interaction of GO, a medicinal drug 10-hydroxy camptothecin (HCPT) and bovine serum albumin (BSA) was studied by Ni et al. (Ni, Zhang, and Kokot 2013). The delivery of HCPT to BSA was improved in the presence of GO. GO enhances the fluorescence response of HCPT to BSA. The low cost fluorescence bio-sensing platform was created for fluorescence-enhanced detection of BSA based on GO. Alternatively, daunorubicin (DNR) loaded graphene-gold nanocomposites inducing apoptosis in drug resistant leukaemia cells (K562/A02; KA) was investigated by Zhang et al. (Zhang, Chang, et al. 2013). The monoclonal P-glycoprotein (P-gp) antibodies and DNR anticancer drug linked to graphene-gold nanocomposites (GGN) was proven to be a good drug delivery vector inducing apoptosis of KA cells and inhibiting tumour growth in KA nude mice. Moreover, enhanced cell death was detected by combination treatment of SWNT/GO and Tx (paclitaxel) indicating a synergistic effect and demonstrated the potential of SWNT/GO as co-therapeutic agents with Tx for the treatment of lung cancer (Arya et al. 2013).In the aim to improve its water solubility and biocompatibility, 6-armed PEG was grafted onto GO via an amidation process. Oridonin, cancer chemotherapy drug, was connected on GO-PEG. The drug loading ratio (105 %) was higher than in other ordinary drug carriers. The GO-PEG/oridoninnanocarrier showed higher cytotoxicity in A549 and MCF-7 cells in comparison to oridonin (Xu et al. 2013). Yang et al. demonstrated that the ^{125}I labelled PEGylated GO, was less adsorbed in intestine after oral uptake (Shi et al. 2013). On the other side after i.p. injection high accumulation of PEGyalted GO derivatives was observed in the reticuloendothelial system including liver and spleen. Although, GO and PEGylated GO derivatives would retain in the mouse body over a long period of time, their toxicity to the treated animals is insignificant.

The rGO can be used for *in vivo* tumour vasculature targeting. The targeting of rGO in a breast cancer model was detected, with ^{64}Cu as the positron emission tomography PET label and TRC105 (TRC105 is proangiogenic and play role in remodelling the vasculature of malignant tumours) as the targeting ligand. CD105 (antigen, transmembrane glycoprotein),

the target of TRC105, is specifically heavily expressed on proliferating tumour endothelial cells of many solid tumour types, it makes it suitable for nanomaterial-based tumour targeting. The rGO conjugates exhibited great stability and high specificity for CD105. ^{64}Cu–NOTA–rGO–TRC105 (NOTA -1,4,7-triazacyclononane-1,4,7-triacetic acid) exhibited little extravasation in the 4T1 cell line, showing that tumour vasculature (instead of tumour cell) targeting is a valid and preferred approach for nanomaterials. The rGO conjugate could serve as a promising theranostic agent (integrates imaging and therapeutic components) (Shi et al. 2013).

3.2 Gene Delivery

As a result of their good solubility and biocompatibility, GNF and GO are promising carriers for gene delivery in non-viral based gene therapy (Du, Yang, and Lin 2012; Feng, Zhang, and Liu 2011). Functionalization of GO by branched polyethylenimine (PEI-GO) proved significantly lower cytotoxicity than PEI 25 kDa. The PEI-GO could effectively deliver plasmid DNA into cells and could be localized in the nucleus (Chen, Liu, Zhang, et al. 2011). The GO/PEI/DNA complex was effective for intracellular gene delivery into the widely used HeLa cell cultures (Feng, Zhang, and Liu 2011). Single stranded DNA is immediately adsorbed onto functionalized GFN forming strong molecular interactions that prevent DNase I from approaching the constrained DNA. Constraining a single-stranded DNA probe on GFN improved the specificity of its response to a target sequence. The features properties of DNA–GFN interactions can be used to construct DNA–GFN nanobiosensors with facile design, excellent sensitivity, selectivity, and biostability. Whereas the low cost of producing GFNs, the use of graphene in both fundamental research and practical applications is promising (Tang et al. 2010).

The positively charged GO-PEI complexes are able to bind with plasmid DNA (pDNA) for intracellular transfection (Feng, Zhang, and Liu 2011). The study on the intracellular uptake of Cy3 labelled pDNA indicated that the supplementation of one of the primary nuclear localized signal peptides called PV7 could effectively assist the GO-PEI to deliver plasmid DNA directly into the nucleus without common aggregations. The cytotoxicity of GO-PEI was much lower than PEI 10 kDa and PEI 25 kDa against both HeLa cells and 293 T cells. This complex can serve as an alternative strategy for a nuclear targeted gene delivery (Ren et al. 2012). Moreover, PEI grafted ultra-small graphene oxide (PEI-g-USGO) has good transfection efficiencies and very low cytotoxicity. The transfection of plasmid DNA into mammalian cell lines was with up to 95% efficiency and 90% viability (Zhou et al.

2012). Low-molecular mass branched polyethylenimine (BPEI) to GO improved the effective molecular weight of BPEI and also improved DNA binding and condensation and transfection efficiency (Kim et al. 2011). An efficient gene delivery system based on graphene oxide chemically-functionalized with a non-toxic linear PEI (LP-GO) was reported. Linear PEI grafted GO conjugates, efficiently condensed pDNA and delivered it to the insides of the cells. LP-GO is able to deliver siRNA efficiently into the cells (Tripathi et al. 2013). The *in vivo* results indicate significant regression in tumour growth and tumour weight after plasmid-based Stat3 siRNA delivered by GO-PEI-PEG treatment and no side effect from GO-PEI-PEG treatment was detected (Yin et al. 2013).

4. Methods for Studying of Graphene Based Biomaterials

Currently GFN, GO and related materials are used as a detection platform for sensitive determination of numerous analytes. The applicability of GFN and GO as a tool for biosensing has been reviewed many times (Gan and Hu 2011; He et al. 2012; Jiang 2011; Liu, Dong, and Chen 2012; Ratinac et al. 2011; Stine et al. 2013; Pumera et al. 2010; Shao et al. 2010; Pumera 2010). Mainly due to the excellent electronic properties of these materials numerous studies developing and utilizing GFN and GO as electrochemical sensors have been presented (Shao et al. 2010; Gan and Hu 2011). Summary of review articles focused on application of graphene is given in table 1. On the other hand, the overviews of methods investigating the GFN and mainly its bioconjugates as analytes are not so common. Generally the reviews are mostly focused on characterization of GFN and GO from the fabrication point of view determining the mechanical (Ferralis 2010), electronic (Gruneis 2013; Craciun et al. 2011; Molitor et al. 2011; Sheng et al. 2012) and optical (Cao et al. 2013; Liu, Zhang, et al. 2012) properties, and/or looking for defects (Banhart, Kotakoski, and Krasheninnikov 2011; Dresselhaus et al. 2010).

A group of basic methods for GFN analysis includes spectroscopic methods such as Raman spectroscopy (Ferrari 2007; Saito et al. 2011; Tang, Hu, and Gao 2010), impedance spectroscopy (Bonanni and Pumera 2013; Loo, Bonanni, and Pumera 2013), X-ray spectroscopy (Ilkiv, Petrovska, Sergiienko, Tomai, et al. 2012; Ilkiv, Petrovska, Sergiienko, and Zaulychnyy 2012; Lee et al. 2012), infrared spectroscopy (Li et al. 2008), and/or UV-Vis spectroscopy (Lai et al. 2012; Mak et al. 2012). Another set of methods comprises microscopic techniques such as transmission electron microscopy (Liu, Wang, et al. 2012; Zan et al. 2011, 2012), scanning tunnelling microscopy (Paredes et al. 2009; Sutter et al. 2009; Andrei, Li, and Du 2012), and/or atomic force microscopy (Paredes et al. 2009; Ahmad

et al. 2011; Ding et al. 2011). The methods used for the grapheme characterization are summarized in Tab. 2.

Table 1. Summary of review articles focused on graphene

Review main topic	Title	First author	Number of pages	Number of references cited	Year	Reference
Diagnostics and delivery	Graphene Based Nanomaterials: Diagnostic Applications	Pandey	26	344	2014	(Pandey et al. 2014)
	Graphene-based nanomaterials for drug delivery and tissue engineering	Goenka	14	165	2014	(Goenka, Sant, and Sant 2014)
Biosensing applications	Fabrication, Optimization, and Use of Graphene Field Effect Sensors	Stine	13	152	2013	(Stine et al. 2013)
	Biological and chemical sensors based on graphene materials	Liu	25	312	2012	(Liu, Dong, and Chen 2012)
	Graphene-based electronic sensors	He	9	106	2012	(He et al. 2012)
	Chemical Preparation of Graphene-Based Nanomaterials and Their Applications in Chemical and Biological Sensors	Jiang	15	125	2011	(Jiang 2011)

	Graphene and Related Materials in Electrochemical Sensing	Ratinac	24	143	2011	(Ratinac et al. 2011)
	Electrochemical sensors based on graphene materials	Gan	19	178	2011	(Gan and Hu 2011)
	Graphene for electrochemical sensing and biosensing	Pumera	12	56	2010	(Pumera et al. 2010)
Material physical properties	Novel graphene-based nanostructures: physicochemical properties and applications	Chernozatonskii	29	285	2014	(Chernozatonskii, Sorokin, and Artukh 2014)
	Synthesis and electronic properties of chemically functionalized graphene on metal surfaces	Gruneis	14	100	2013	(Burger et al. 2002)
	Photoluminescence Properties of Graphene versus Other Carbon Nanomaterials	Cao	10	42	2013	(Cao et al. 2013)
	Electronic and optical properties of semiconductor and graphene quantum dots	Sheng	25	160	2012	(Sheng et al. 2012)

	Tuneable electronic properties in graphene	Craciun	19	121	2011	(Craciun et al. 2011)
	Electronic properties of graphene nanostructures	Molitor	5	74	2011	(Molitor et al. 2011)
	Probing mechanical properties of graphene with Raman spectroscopy	Ferralis	20	103	2010	(Ferralis 2010)

Table 2. Summary of analytical methods used for graphene characterization

	Analytical method	**Reference**
Spectroscopy	Raman spectroscopy	(Tang, Hu, and Gao 2010)
		(Saito et al. 2011)
		(Ferrari 2007)
	Impedance spectroscopy	(Bonanni and Pumera 2013)
		(Loo, Bonanni, and Pumera 2013)
	X-ray spectroscopy	(Ilkiv, Petrovska, Sergiienko, Tomai, et al. 2012)
		(Ilkiv, Petrovska, Sergiienko, and Zaulychnyy 2012)
	IR spectroscopy	(Li et al. 2008)
	UV/Vis spectroscopy	(Lai et al. 2012)
Microscopic techniques	TEM	(Liu, Wang, et al. 2012)
		(Zan et al. 2012)
	scanning tunneling microscopy	(Paredes et al. 2009)
		(Sutter et al. 2009)
		(Andrei, Li, and Du 2012)
	AFM	(Paredes et al. 2009)
		(Ahmad et al. 2011)
		(Ding et al. 2011)

The methods characterizing GFN in terms of its bioconjugation are depending on the nature of the bioconjugate. In case of conjugation with fluorescent partner such as QDs or fluorescently labelled biomolecules the appropriate method is based on fluorescence properties. QDs with GFN can be used for fluorescence imaging of live cells (Chen, Liu, Hu, et al. 2011). Due to fluorescent properties, DOX conjugated with fullerenes can be detected as it is shown in Fig. 4.

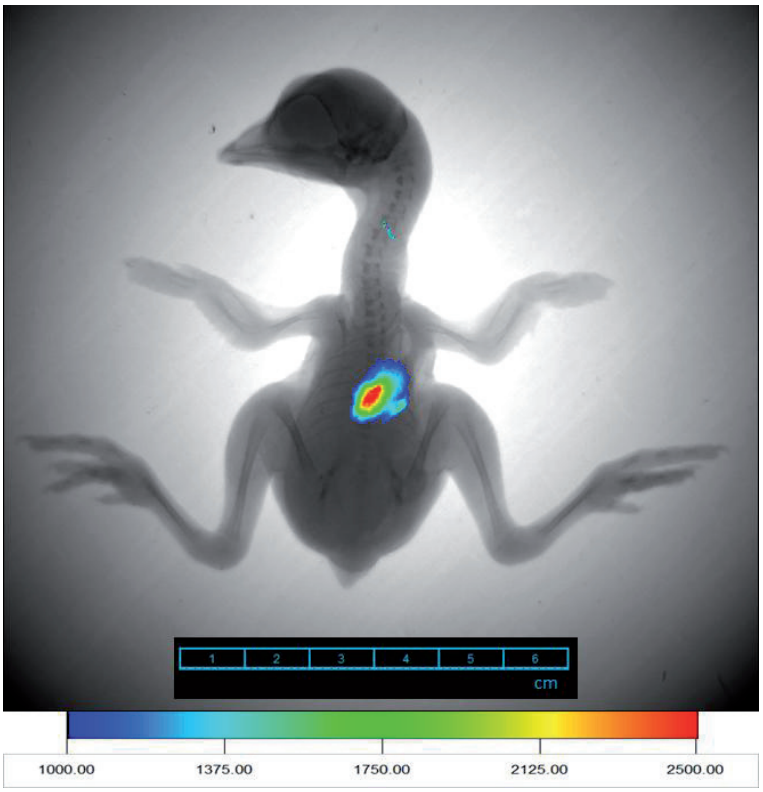

Figure 4. Fluorescence *in vivo* imaging of the DOX in the chicken embryo. X-ray image of the embryo overlaid with fluorescence image of the embryo after the application of fullerenes with DOX into the chicken breast muscle tissue (100 µl fullerene with DOX (500 µg/ml DOX); Parameters: excitation - 480 nm, emission - 600 nm, exposure time - 2 seconds, binning: 2×2 pixels - 2×2, Field of view – 11.5×11.5 cm, f Stop - 1.1.

Conclusions

Due to their unique properties, carbon nanomaterials including fullerenes, nanotubes, graphene and grapheme oxide, have already proven their potential, applicability and benefits in numerous areas of the research. Biochemical analyses as well as biomedical applications have been significantly improved by utilization of these carbon-based nanoparticles. However, despite their promise, both graphene and carbon nanotubes still face considerable challenges such as heterogeneity and in case of GFN separating the layers and keeping them separated, control the number of layers, minimizing folding and bending during processing. One challenges connected to biomedical applications of GFN is thorough and profound understanding of interactions between GFN and cells. Especially the cellular uptake mechanism has to be fully understood. However, given its structural features and exceptional physicochemical properties, design of GFN-based delivery/therapeutic multimodal and multifunctional platform is a new direction to follow. Finally, it has to highlighted, that these aims can only be reached by the combined effort from chemistry, biomedicine, materials sciences, and nanotechnology.

Acknowledgement

Financial support from CYTORES GA CR P301/10/0356 is highly acknowledged.

References

Ahmad, M., S. A. Han, D. H. Tien, J. Jung, and Y. Seo. 2011. Local conductance measurement of graphene layer using conductive atomic force microscopy. *J. Appl. Phys.* 110 (5):1-6.

Akhavan, O., E. Ghaderi, and A. Akhavan. 2012. Size-dependent genotoxicity of graphene nanoplatelets in human stem cells. *Biomaterials* 33 (32):8017-8025.

Andrei, E. Y., G. H. Li, and X. Du. 2012. Electronic properties of graphene: a perspective from scanning tunneling microscopy and magnetotransport. *Rep. Prog. Phys.* 75 (5):1-79.

Arya, N., A. Arora, K. S. Vasu, A. K. Sood, and D. S. Katti. 2013. Combination of single walled carbon nanotubes/graphene oxide with paclitaxel: a reactive oxygen species mediated synergism for treatment of lung cancer. *Nanoscale* 5 (7):2818-2829.

Banhart, F., J. Kotakoski, and A. V. Krasheninnikov. 2011. Structural Defects in Graphene. *ACS Nano* 5 (1):26-41.

Bonanni, A., and M. Pumera. 2013. High-resolution impedance spectroscopy for graphene characterization. *Electrochem. Commun.* 26:52-54.

Burger, K. N. J., R.W.H.M Staffhorst, H. C. de Vijlder, M. J. Velinova, P. H. Bomans, P. M. Frederik, and B. de Kruijff. 2002. Nanocapsules: lipid-coated aggregates of cisplatin with high cytotoxicity. *Nat. Med.* 8 (1):81-84.

Cai, W. B., A. R. Hsu, Z. B. Li, and X. Y. Chen. 2007. Are quantum dots ready for in vivo imaging in human subjects? *Nanoscale Res. Lett.* 2 (6):265-281.

Cao, L. L., L. W. Cheng, Z. Y. Zhang, Y. Wang, X. X. Zhang, H. Chen, B. H. Liu, S. Zhang, and J. L. Kong. 2012. Visual and high-throughput detection of cancer cells using a graphene oxide-based FRET aptasensing microfluidic chip. *Lab Chip* 12 (22):4864-4869.

Cao, L., M. J. Meziani, S. Sahu, and Y. P. Sun. 2013. Photoluminescence Properties of Graphene versus Other Carbon Nanomaterials. *Accounts Chem. Res.* 46 (1):171-180.

Cissell, K. A., S. Shrestha, J. Purdie, D. Kroodsma, and S. K. Deo. 2008. Molecular biosensing system based on intrinsically disordered proteins. *Anal. Bioanal. Chem.* 391 (5):1721-1729.

Condeelis, J., and R. Weissleder. 2010. In Vivo Imaging in Cancer. *Cold Spring Harbor Perspect. Biol.* 2 (12):1-22.

Craciun, M. F., S. Russo, M. Yamamoto, and S. Tarucha. 2011. Tuneable electronic properties in graphene. *Nano Today* 6 (1):42-60.

Das, S., S. Singh, V. Singh, D. Joung, J. M. Dowding, D. Reid, J. Anderson, L. Zhai, S. I. Khondaker, W. T. Self, and S. Seal. 2013. Oxygenated Functional Group Density on Graphene Oxide: Its Effect on Cell Toxicity. *Part. Part. Syst. Charact.* 30 (2):148-157.

Ding, Y. H., P. Zhang, H. M. Ren, Q. Zhuo, Z. M. Yang, X. Jiang, and Y. Jiang. 2011. Surface adhesion properties of graphene and graphene oxide studied by colloid-probe atomic force microscopy. *Appl. Surf. Sci.* 258 (3):1077-1081.

Dong, H. F., W. C. Gao, F. Yan, H. X. Ji, and H. X. Ju. 2010. Fluorescence Resonance Energy Transfer between Quantum Dots and Graphene Oxide for Sensing Biomolecules. *Anal. Chem.* 82 (13):5511-5517.

Dong, H. Q., Y. Y. Li, J. H. Yu, Y. Y. Song, X. J. Cai, J. Q. Liu, J. M. Zhang, R. C. Ewing, and D. L. Shi. 2013. A Versatile Multicomponent Assembly via -cyclodextrin HostGuest Chemistry on Graphene for Biomedical Applications. *Small* 9 (3):446-456.

Dresselhaus, M. S., A. Jorio, A. G. Souza, and R. Saito. 2010. Defect characterization in graphene and carbon nanotubes using Raman spectroscopy. *Philos. Trans. R. Soc. A-Math. Phys. Eng. Sci.* 368 (1932):5355-5377.

Du, D., Y. Q. Yang, and Y. H. Lin. 2012. Graphene-based materials for biosensing and bioimaging. *MRS Bull.* 37 (12):1290-1296.

Du, D., Z. X. Zou, Y. S. Shin, J. Wang, H. Wu, M. H. Engelhard, J. Liu, I. A. Aksay, and Y. H. Lin. 2010. Sensitive Immunosensor for Cancer Biomarker Based on Dual Signal Amplification Strategy of Graphene Sheets and Multienzyme Functionalized Carbon Nanospheres. *Anal. Chem.* 82 (7):2989-2995.

Feng, L. Z., and Z. A. Liu. 2011. Graphene in biomedicine: opportunities and challenges. *Nanomedicine* 6 (2):317-324.

Feng, L. Z., S. A. Zhang, and Z. A. Liu. 2011. Graphene based gene transfection. *Nanoscale* 3 (3):1252-1257.

Ferralis, N. 2010. Probing mechanical properties of graphene with Raman spectroscopy. *J. Mater. Sci.* 45 (19):5135-5149.

Ferrari, A. C. 2007. Raman spectroscopy of graphene and graphite: Disorder, electron-phonon coupling, doping and nonadiabatic effects. *Solid State Commun.* 143 (1-2):47-57.

Gan, T., and S. S. Hu. 2011. Electrochemical sensors based on graphene materials. *Microchim. Acta* 175 (1-2):1-19.

Goenka, S., V. Sant, and S. Sant. 2014. Graphene-based nanomaterials for drug delivery and tissue engineering. *Journal of Controlled Release* 173:75-88.

Gong, Y. Y., N. Pei, Z. Y. Huang, J. B. Ge, W. L. Ma, and W. L. Zheng. 2009. *Deep Capture of Paramagnetic Particle for Targeting Therapeutics*. Edited by R. Shi, W. J. Fu, Y. Q. Wang and H. B. Wang, *Proceedings of the 2009 2nd International Conference on Biomedical Engineering and Informatics, Vols 1-4*. New York: Ieee.

Gruneis, A. 2013. Synthesis and electronic properties of chemically functionalized graphene on metal surfaces. *J. Phys.-Condes. Matter* 25 (4):1-7.

Guo, S. J., and S. J. Dong. 2011. Graphene nanosheet: synthesis, molecular engineering, thin film, hybrids, and energy and analytical applications. *Chem. Soc. Rev.* 40 (5):2644-2672.

Guo, Z. Y., T. T. Hao, S. P. Du, B. B. Chen, Z. B. Wang, X. Li, and S. Wang. 2013. Multiplex electrochemiluminescence immunoassay of two tumor markers using multicolor quantum dots as labels and graphene as conducting bridge. *Biosens. Bioelectron.* 44:101-107.

Haase, M. G., K. Liepe, D. Faulhaber, G. Wunderlich, M. Andreeff, R. Jung, G. B. Baretton, G. Fitze, and J. Kotzerke. 2013. Dose-dependent histological alterations in the rat lung following intravenous application of Re-188-labeled microspheres. *International Journal of Radiation Biology* 89 (10):863-869.

He, Q. Y., S. X. Wu, Z. Y. Yin, and H. Zhang. 2012. Graphene-based electronic sensors. *Chem. Sci.* 3 (6):1764-1772.

Hirsch, L. R., A. M. Gobin, A. R. Lowery, F. Tam, R. A. Drezek, N. J. Halas, and J. L. West. 2006. Metal nanoshells. *Ann. Biomed. Eng.* 34 (1):15-22.

Horvath, L., A. Magrez, M. Burghard, K. Kern, L. Forro, and B. Schwaller. 2013. Evaluation of the toxicity of graphene derivatives on cells of the lung luminal surface. *Carbon* 64:45-60.

Hu, X. W., C. J. Mao, J. M. Song, H. L. Niu, S. Y. Zhang, and H. P. Huang. 2013. Fabrication of GO/PANi/CdSe nanocomposites for sensitive electrochemiluminescence biosensor. *Biosens. Bioelectron.* 41:372-378.

Huang, X., Z. Y. Yin, S. X. Wu, X. Y. Qi, Q. Y. He, Q. C. Zhang, Q. Y. Yan, F. Boey, and H. Zhang. 2011. Graphene-Based Materials: Synthesis, Characterization, Properties, and Applications. *Small* 7 (14):1876-1902.

Hummers, W. S., and R. E. Offeman. 1958. Preparation of graphitic oxide. *J. Am. Chem. Soc.* 80 (6):1339-1339.

Cha, I., Y. Yagi, T. Kawahara, K. Hashimoto, K. Fujiki, S. Tamesue, T. Yamauchi, and N. Tsubokawa. 2014. Grafting of polymers onto graphene oxide by trapping of polymer radicals and ligand-exchange reaction of polymers bearing ferrocene moieties. *Colloids and Surfaces a-Physicochemical and Engineering Aspects* 441:474-480.

Chen, B. A., M. Liu, L. M. Zhang, J. Huang, J. L. Yao, and Z. J. Zhang. 2011. Polyethylenimine-functionalized graphene oxide as an efficient gene delivery vector. *J. Mater. Chem.* 21 (21):7736-7741.

Chen, M. L., J. W. Liu, B. Hu, and J. H. Wang. 2011. Conjugation of quantum dots with graphene for fluorescence imaging of live cells. *Analyst* 136 (20):4277-4283.

Chernozatonskii, L. A., P. B. Sorokin, and A. A. Artukh. 2014. Novel graphene-based nanostructures: physicochemical properties and applications. *Russian Chemical Reviews* 83 (3):251-279.

Ilkiv, B., S. Petrovska, R. Sergiienko, T. Tomai, E. Shibata, T. Nakamura, I. Honma, and Y. Zaulychnyy. 2012. X-Ray Emission Spectra of Graphene Nanosheets. *J. Nanosci. Nanotechnol.* 12 (12):8913-8919.

Ilkiv, B., S. Petrovska, R. Sergiienko, and Y. Zaulychnyy. 2012. X-Ray Spectral Investigation of Graphene Nanosheets Deposited on Silicon Substrate. *Metallofiz. Nov. Tekhnol.-Met. Phys. Adv. Techn.* 34 (11):1487-1493.

Jiang, H. J. 2011. Chemical Preparation of Graphene-Based Nanomaterials and Their Applications in Chemical and Biological Sensors. *Small* 7 (17):2413-2427.

Kavitha, T., S. I. H. Abdi, and S. Y. Park. 2013. pH-Sensitive nanocargo based on smart polymer functionalized graphene oxide for site-specific drug delivery. *Phys. Chem. Chem. Phys.* 15 (14):5176-5185.

Kim, H., R. Namgung, K. Singha, I. K. Oh, and W. J. Kim. 2011. Graphene Oxide-Polyethylenimine Nanoconstruct as a Gene Delivery Vector and Bioimaging Tool. *Bioconjugate Chem.* 22 (12):2558-2567.

Kizek, R., V. Adam, J. Hrabeta, T. Eckschlager, S. Smutny, J. V. Burda, E. Frei, and M. Stiborova. 2012. Anthracyclines and ellipticines as DNA-damaging anticancer drugs: Recent advances. *Pharmacol. Ther.* 133 (1):26-39.

Kong, X. L., and Y. Huang. 2014. Applications of Graphene in Mass Spectrometry. *Journal of Nanoscience and Nanotechnology* 14 (7):4719-4732.

Kovtyukhova, N. I., P. J. Ollivier, B. R. Martin, T. E. Mallouk, S. A. Chizhik, E. V. Buzaneva, and A. D. Gorchinskiy. 1999. Layer-by-layer assembly of ultrathin composite films from micron-sized graphite oxide sheets and polycations. *Chem. Mat.* 11 (3):771-778.

Kravets, V. G., F. Schedin, R. Jalil, L. Britnell, R. V. Gorbachev, D. Ansell, B. Thackray, K. S. Novoselov, A. K. Geim, A. V. Kabashin, and A. N. Grigorenko. 2013. Singular phase nano-optics in plasmonic metamaterials for label-free single-molecule detection. *Nat. Mater.* 12 (4):304-309.

Ku, S. H., and C. B. Park. 2013. Myoblast differentiation on graphene oxide. *Biomaterials* 34 (8):2017-2023.

Lacerda, L., A. Bianco, M. Prato, and K. Kostarelos. 2006. Carbon nanotubes as nanomedicines: From toxicology to pharmacology. *Adv. Drug Deliv. Rev.* 58 (14):1460-1470.

Lai, Q., S. F. Zhu, X. P. Luo, M. Zou, and S. H. Huang. 2012. Ultraviolet-visible spectroscopy of graphene oxides. *AIP Adv.* 2 (3):1-5.

Lee, D. Y., Z. Khatun, J. H. Lee, Y. K. Lee, and I. In. 2011. Blood Compatible Graphene/Heparin Conjugate through Noncovalent Chemistry. *Biomacromolecules* 12 (2):336-341.

Lei, H. Z., L. J. Mi, X. J. Zhou, J. J. Chen, J. Hu, S. W. Guo, and Y. Zhang. 2011. Adsorption of double-stranded DNA to graphene oxide preventing enzymatic digestion. *Nanoscale* 3 (9):3888-3892.

Li, H., J. He, S. J. Li, and A. P. F. Turner. 2013. Electrochemical immunosensor with N-doped graphene-modified electrode for label-free detection of the breast cancer biomarker CA 15-3. *Biosens. Bioelectron.* 43:25-29.

Li, J., and X. Y. Yang. 2013. Applications of Novel Carbon Nanomaterials-Graphene and Its Derivatives in Biosensing. *Prog. Chem.* 25 (2-3):380-396.

Li, Q. F., D. A. P. Tang, J. Tang, B. L. Su, G. N. Chen, and M. D. Wei. 2011. Magneto-controlled electrochemical immunosensor for direct detection of squamous cell carcinoma antigen by using serum as supporting electrolyte. *Biosens. Bioelectron.* 27 (1):153-159.

Li, Z., M. Y. He, D. D. Xu, and Z. H. Liu. 2014. Graphene materials-based energy acceptor systems and sensors. *Journal of Photochemistry and Photobiology C-Photochemistry Reviews* 18:1-17.

Li, Z. Q., E. A. Henriksen, Z. Jiang, Z. Hao, M. C. Martin, P. Kim, H. L. Stormer, and D. N. Basov. 2008. Dirac charge dynamics in graphene by infrared spectroscopy. *Nat. Phys.* 4 (7):532-535.

Lim, S. K., D. H. Shin, M. H. Choi, and J. S. Kim. 2014. Enhanced antitumor efficacy of gemcitabine-loaded temperature-sensitive liposome by hyperthermia in tumor-bearing mice. *Drug Development and Industrial Pharmacy* 40 (4):470-476.

Liu, B. W., Z. Y. Sun, X. Zhang, and J. W. Liu. 2013. Mechanisms of DNA Sensing on Graphene Oxide. *Analytical Chemistry* 85 (16):7987-7993.

Liu, F. Y., Y. L. Gao, H. J. Li, and S. G. Sun. 2014. Interaction of propidium iodide with graphene oxide and its application for live cell staining. *Carbon* 71:190-195.

Liu, X. H., J. W. Wang, Y. Liu, H. Zheng, A. Kushima, S. Huang, T. Zhu, S. X. Mao, J. Li, S. L. Zhang, W. Lu, J. M. Tour, and J. Y. Huang. 2012. In situ transmission electron microscopy of electrochemical lithiation, delithiation and deformation of individual graphene nanoribbons. *Carbon* 50 (10):3836-3844.

Liu, Y. X., X. C. Dong, and P. Chen. 2012. Biological and chemical sensors based on graphene materials. *Chem. Soc. Rev.* 41 (6):2283-2307.

Liu, Y., Y. Zhang, T. Zhang, Y. J. Jiang, and X. F. Liu. 2014. Synthesis, characterization and cytotoxicity of phosphorylcholine oligomer grafted graphene oxide. *Carbon* 71:166-175.

Liu, Z. B., X. L. Zhang, X. Q. Yan, Y. S. Chen, and J. G. Tian. 2012. Nonlinear optical properties of graphene-based materials. *Chin. Sci. Bull.* 57 (23):2971-2982.

Liu, Z., J. T. Robinson, X. M. Sun, and H. J. Dai. 2008. PEGylated nanographene oxide for delivery of water-insoluble cancer drugs. *J. Am. Chem. Soc.* 130 (33):10876-+.

Liu, Z., J. T. Robinson, S. M. Tabakman, K. Yang, and H. J. Dai. 2011. Carbon materials for drug delivery & cancer therapy. *Mater. Today* 14 (7-8):316-323.

Liu, Z., X. M. Sun, N. Nakayama-Ratchford, and H. J. Dai. 2007. Supramolecular chemistry on water-soluble carbon nanotubes for drug loading and delivery. *ACS Nano* 1 (1):50-56.

Loh, K. P., Q. L. Bao, G. Eda, and M. Chhowalla. 2010. Graphene oxide as a chemically tunable platform for optical applications. *Nat. Chem.* 2 (12):1015-1024.

Loo, A. H., A. Bonanni, and M. Pumera. 2013. Soldering DNA to graphene via 0, 1 and 2-point contacts: Electrochemical impedance spectroscopic investigation. *Electrochem. Commun.* 28:83-86.

Ma, X. X., H. Q. Tao, K. Yang, L. Z. Feng, L. Cheng, X. Z. Shi, Y. G. Li, L. Guo, and Z. Liu. 2012. A functionalized graphene oxide-iron oxide nanocomposite for magnetically targeted drug delivery, photothermal therapy, and magnetic resonance imaging. *Nano Res.* 5 (3):199-212.

Maeda, H., T. Sawa, and T. Konno. 2001. Mechanism of tumor-targeted delivery of macromolecular drugs, including the EPR effect in solid tumor and clinical overview of the prototype polymeric drug SMANCS. *J. Control. Release* 74 (1-3):47-61.

Mao, X. W., and H. B. Li. 2013. Chiral imaging in living cells with functionalized graphene oxide. *Journal of Materials Chemistry B* 1 (34):4267-4272.

Markad, G. B., S. Battu, S. Kapoor, and S. K. Haram. 2013. Interaction between Quantum Dots of CdTe and Reduced Graphene Oxide: Investigation through Cyclic Voltammetry and Spectroscopy. *Journal of Physical Chemistry C* 117 (40):20944-20950.

Mendes, R. G., A. Bachmatiuk, A. A. El-Gendy, S. Melkhanova, R. Klingeler, B. Buchner, and M. H. Rummeli. 2012. A Facile Route to Coat Iron Oxide Nanoparticles with Few-Layer Graphene. *Journal of Physical Chemistry C* 116 (44):23749-23756.

Miao, W., G. Shim, S. Lee, Y. S. Choe, and Y. K. Oh. 2013. Safety and tumor tissue accumulation of pegylated graphene oxide nanosheets for co-delivery of anticancer drug and photosensitizer. *Biomaterials* 34 (13):3402-3410.

Misra, S. K., P. Kondaiah, S. Bhattacharya, and C. N. R. Rao. 2012. Graphene as a Nanocarrier for Tamoxifen Induces Apoptosis in Transformed Cancer Cell Lines of Different Origins. *Small* 8 (1):131-143.

Molitor, F., J. Guttinger, C. Stampfer, S. Droscher, A. Jacobsen, T. Ihn, and K. Ensslin. 2011. Electronic properties of graphene nanostructures. *J. Phys.-Condes. Matter* 23 (24):1-5.

Mosaiab, T., I. In, and S. Y. Park. 2013. Temperature and pH-Tunable Fluorescence Nanoplatform with Graphene Oxide and BODIPY-Conjugated Polymer for Cell Imaging and Therapy. *Macromolecular Rapid Communications* 34 (17):1408-1415.

Na, H. K., M. H. Kim, J. Lee, Y. K. Kim, H. Jang, K. E. Lee, H. Park, W. D. Heo, H. Jeon, I. S. Choi, Y. Lee, and D. H. Min. 2013. Cytoprotective effects of graphene oxide for mammalian cells against internalization of exogenous materials. *Nanoscale* 5 (4):1669-1677.

Ni, Y. N., F. Y. Zhang, and S. Kokot. 2013. Graphene oxide as a nanocarrier for loading and delivery of medicinal drugs and as a biosensor for detection of serum albumin. *Anal. Chim. Acta* 769:40-48.

Novoselov, K. S., A. K. Geim, S. V. Morozov, D. Jiang, Y. Zhang, S. V. Dubonos, I. V. Grigorieva, and A. A. Firsov. 2004. Electric field effect in atomically thin carbon films. *Science* 306 (5696):666-669.

Pandey, A. P., K. P. Karande, M. P. More, S. G. Gattani, and P. K. Deshmukh. 2014. Graphene Based Nanomaterials: Diagnostic Applications. *Journal of Biomedical Nanotechnology* 10 (2):179-204.

Paredes, J. I., S. Villar-Rodil, P. Solis-Fernandez, A. Martinez-Alonso, and J. M. D. Tascon. 2009. Atomic Force and Scanning Tunneling Microscopy Imaging of Graphene Nanosheets Derived from Graphite Oxide. *Langmuir* 25 (10):5957-5968.

Pollinger, K., R. Hennig, S. Bauer, M. Breunig, J. Tessmar, A. Buschauer, R. Witzgall, and A. Goepferich. 2014. Biodistribution of Quantum Dots in the Kidney After Intravenous Injection. *Journal of Nanoscience and Nanotechnology* 14 (5):3313-3319.

Portney, N. G., and M. Ozkan. 2006. Nano-oncology: drug delivery, imaging, and sensing. *Anal. Bioanal. Chem.* 384 (3):620-630.

Pumera, M. 2009. The Electrochemistry of Carbon Nanotubes: Fundamentals and Applications. *Chem.-Eur. J.* 15 (20):4970-4978.

Repeated Author. 2010. Graphene-based nanomaterials and their electrochemistry. *Chem. Soc. Rev.* 39 (11):4146-4157.

Repeated Author. 2012. Graphene, Carbon Nanotubes and Nanoparticles in Cell Metabolism. *Curr. Drug Metab.* 13 (3):251-256.

Pumera, M., A. Ambrosi, A. Bonanni, E. L. K. Chng, and H. L. Poh. 2010. Graphene for electrochemical sensing and biosensing. *TRAC-Trends Anal. Chem.* 29 (9):954-965.

Ratinac, K. R., W. R. Yang, J. J. Gooding, P. Thordarson, and F. Braet. 2011. Graphene and Related Materials in Electrochemical Sensing. *Electroanalysis* 23 (4):803-826.

Ren, T. B., L. Li, X. J. Cai, H. Q. Dong, S. M. Liu, and Y. Y. Li. 2012. Engineered polyethylenimine/graphene oxide nanocomposite for nuclear localized gene delivery. *Polym. Chem.* 3 (9):2561-2569.

Saito, R., M. Hofmann, G. Dresselhaus, A. Jorio, and M. S. Dresselhaus. 2011. Raman spectroscopy of graphene and carbon nanotubes. *Adv. Phys.* 60 (3):413-550.

Sciallero, C., D. Grishenkov, Svvn Kothapalli, L. Oddo, and A. Trucco. 2013. Acoustic characterization and contrast imaging of microbubbles encapsulated by polymeric shells coated or filled with magnetic nanoparticles. *Journal of the Acoustical Society of America* 134 (5):3918-3930.

Shan, C. S., H. F. Yang, D. X. Han, Q. X. Zhang, A. Ivaska, and L. Niu. 2009. Water-Soluble Graphene Covalently Functionalized by Biocompatible Poly-L-lysine. *Langmuir* 25 (20):12030-12033.

Shao, Y. Y., J. Wang, H. Wu, J. Liu, I. A. Aksay, and Y. H. Lin. 2010. Graphene Based Electrochemical Sensors and Biosensors: A Review. *Electroanalysis* 22 (10):1027-1036.

Shen, H., L. M. Zhang, M. Liu, and Z. J. Zhang. 2012. Biomedical Applications of Graphene. *Theranostics* 2 (3):283-294.

Sheng, W. D., M. Korkusinski, A. D. Guclu, M. Zielinski, P. Potasz, E. S. Kadantsev, O. Voznyy, and P. Hawrylak. 2012. Electronic and optical properties of semiconductor and graphene quantum dots. *Front. Phys.* 7 (3):328-352.

Shi, S. X., K. Yang, H. Hong, H. F. Valdovinos, T. R. Nayak, Y. Zhang, C. P. Theuer, T. E. Barnhart, Z. Liu, and W. B. Cai. 2013. Tumor vasculature targeting and imaging in living mice with reduced graphene oxide. *Biomaterials* 34 (12):3002-3009.

Schinwald, A., F. Murphy, A. Askounis, V. Koutsos, K. Sefiane, K. Donaldson, and C. J. Campbell. 2014. Minimal oxidation and inflammogenicity of pristine graphene with residence in the lung. *Nanotoxicology* 8 (8):824-832.

Song, Y. J., W. L. Wei, and X. G. Qu. 2011. Colorimetric Biosensing Using Smart Materials. *Adv. Mater.* 23 (37):4215-4236.

Stiborova, M., T. Eckschlager, J. Poljakova, J. Hrabeta, V. Adam, R. Kizek, and E. Frei. 2012. The Synergistic Effects of DNA-Targeted Chemotherapeutics and Histone Deacetylase Inhibitors As Therapeutic Strategies for Cancer Treatment. *Curr. Med. Chem.* 19 (25):4218-4238.

Stine, R., S. P. Mulvaney, J. T. Robinson, C. R. Tamanaha, and P. E. Sheehan. 2013. Fabrication, Optimization, and Use of Graphene Field Effect Sensors. *Anal. Chem.* 85 (2):509-521.

Sun, H. J., L. Wu, N. Gao, J. S. Ren, and X. G. Qu. 2013. Improvement of Photoluminescence of Graphene Quantum Dots with a Biocompatible Photochemical Reduction Pathway and Its Bioimaging Application. *ACS Appl. Mater. Interfaces* 5 (3):1174-1179.

Sun, X. M., Z. Liu, K. Welsher, J. T. Robinson, A. Goodwin, S. Zaric, and H. J. Dai. 2008. Nano-Graphene Oxide for Cellular Imaging and Drug Delivery. *Nano Res.* 1 (3):203-212.

Sutter, E., D. P. Acharya, J. T. Sadowski, and P. Sutter. 2009. Scanning tunneling microscopy on epitaxial bilayer graphene on ruthenium (0001). *Appl. Phys. Lett.* 94 (13):1-3.

Tan, X. F., L. Z. Feng, J. Zhang, K. Yang, S. Zhang, Z. Liu, and R. Peng. 2013. Functionalization of Graphene Oxide Generates a Unique Interface for Selective Serum Protein Interactions. *Acs Applied Materials & Interfaces* 5 (4):1370-1377.

Tang, B., G. X. Hu, and H. Y. Gao. 2010. Raman Spectroscopic Characterization of Graphene. *Appl. Spectrosc. Rev.* 45 (5):369-407.

Tang, Z. W., H. Wu, J. R. Cort, G. W. Buchko, Y. Y. Zhang, Y. Y. Shao, I. A. Aksay, J. Liu, and Y. H. Lin. 2010. Constraint of DNA on Functionalized Graphene Improves its Biostability and Specificity. *Small* 6 (11):1205-1209.

Thorek, D. L. J., A. Chen, J. Czupryna, and A. Tsourkas. 2006. Superparamagnetic iron oxide nanoparticle probes for molecular imaging. *Ann. Biomed. Eng.* 34 (1):23-38.

Tripathi, S. K., R. Goyal, K. C. Gupta, and P. Kumar. 2013. Functionalized graphene oxide mediated nucleic acid delivery. *Carbon* 51:224-235.

Villegas, J. C., L. Alvarez-Montes, L. Rodriguez-Fernandez, J. Gonzalez, R. Valiente, and M. L. Fanarraga. 2014. Multiwalled Carbon Nanotubes Hinder Microglia Function Interfering with Cell Migration and Phagocytosis. *Advanced Healthcare Materials* 3 (3):424-432.

Wang, H., W. Gu, N. Xiao, L. Ye, and Q. Y. Xu. 2014. Chlorotoxin-conjugated graphene oxide for targeted delivery of an anticancer drug. *International Journal of Nanomedicine* 9:1433-1442.

Wang, X., L. H. Liu, O. Ramstrom, and M. D. Yan. 2009. Engineering Nanomaterial Surfaces for Biomedical Applications. *Exp. Biol. Med.* 234 (10):1128-1139.

Wang, Y., Z. H. Li, D. H. Hu, C. T. Lin, J. H. Li, and Y. H. Lin. 2010. Aptamer/Graphene Oxide Nanocomplex for in Situ Molecular Probing in Living Cells. *J. Am. Chem. Soc.* 132 (27):9274-9276.

Wang, Y., K. Y. Wang, J. F. Zhao, X. G. Liu, J. Bu, X. Y. Yan, and R. Q. Huang. 2013. Multifunctional Mesoporous Silica-Coated Graphene Nanosheet Used for Chemo-Photothermal Synergistic Targeted Therapy of Glioma. *J. Am. Chem. Soc.* 135 (12):4799-4804.

Wang, Z. H., C. F. Zhou, J. F. Xia, B. Via, Y. Z. Xia, F. F. Zhang, Y. H. Li, and L. H. Xia. 2013. Fabrication and characterization of a triple functionalization of graphene oxide with Fe3O4, folic acid and doxorubicin as dual-targeted drug nanocarrier. *Colloid Surf. B-Biointerfaces* 106:60-65.

Wei, W. L., and X. G. Qu. 2012. Extraordinary Physical Properties of Functionalized Graphene. *Small* 8 (14):2138-2151.

Wu, H. X., H. L. Shi, Y. P. Wang, X. Q. Jia, C. Z. Tang, J. M. Zhang, and S. P. Yang. 2014. Hyaluronic acid conjugated graphene oxide for targeted drug delivery. *Carbon* 69:379-389.

Wu, Y. F., P. Xue, Y. J. Kang, and K. M. Hui. 2013. Highly Specific and Ultrasensitive Graphene-Enhanced Electrochemical Detection of Low-Abundance Tumor Cells Using Silica

Nanoparticles Coated with Antibody-Conjugated Quantum Dots. *Anal. Chem.* 85 (6):3166-3173.

Xu, S. J., Y. Liu, T. H. Wang, and J. H. Li. 2011. Positive Potential Operation of a Cathodic Electrogenerated Chemiluminescence Immunosensor Based on Luminol and Graphene for Cancer Biomarker Detection. *Anal. Chem.* 83 (10):3817-3823.

Xu, Z. Y., Y. J. Li, P. Shi, B. C. Wang, and X. Y. Huang. 2013. Functionalized Graphene Oxide as a Nanocarrier for Loading and Delivering of Oridonin. *Chin. J. Org. Chem.* 33 (3):573-580.

Yang, K., S. A. Zhang, G. X. Zhang, X. M. Sun, S. T. Lee, and Z. A. Liu. 2010. Graphene in Mice: Ultrahigh In Vivo Tumor Uptake and Efficient Photothermal Therapy. *Nano Lett.* 10 (9):3318-3323.

Yang, M., J. Yao, and Y. X. Duan. 2013. Graphene and its derivatives for cell biotechnology. *Analyst* 138 (1):72-86.

Yin, D., Y. Li, H. Lin, B. F. Guo, Y. W. Du, X. Li, H. J. Jia, X. J. Zhao, J. Tang, and L. Zhang. 2013. Functional graphene oxide as a plasmid-based Stat3 siRNA carrier inhibits mouse malignant melanoma growth in vivo. *Nanotechnology* 24 (10):1-9.

Yue, Z. G., P. P. Lv, H. Yue, Y. J. Gao, D. Ma, W. Wei, and G. H. Ma. 2013. Inducible graphene oxide probe for high-specific tumor diagnosis. *Chemical Communications* 49 (37):3902-3904.

Zan, R., U. Bangert, Q. Ramasse, and K. S. Novoselov. 2012. Interaction of Metals with Suspended Graphene Observed by Transmission Electron Microscopy. *J. Phys. Chem. Lett.* 3 (7):953-958.

Zhang, G., H. C. Chang, C. Amatore, Y. Chen, H. Jiang, and X. M. Wang. 2013. Apoptosis induction and inhibition of drug resistant tumor growth in vivo involving daunorubicin-loaded graphene-gold composites. *J. Mat. Chem. B* 1 (4):493-499.

Zhang, H., C. Peng, J. Z. Yang, M. Lv, R. Liu, D. N. He, C. H. Fan, and Q. Huang. 2013. Uniform Ultrasmall Graphene Oxide Nanosheets with Low Cytotoxicity and High Cellular Uptake. *ACS Appl. Mater. Interfaces* 5 (5):1761-1767.

Zhang, J. L., F. Zhang, H. J. Yang, X. L. Huang, H. Liu, J. Y. Zhang, and S. W. Guo. 2010. Graphene Oxide as a Matrix for Enzyme Immobilization. *Langmuir* 26 (9):6083-6085.

Zhang, L. N., H. H. Deng, F. L. Lin, X. W. Xu, S. H. Weng, A. L. Liu, X. H. Lin, X. H. Xia, and W. Chen. 2014. In Situ Growth of Porous Platinum Nanoparticles on Graphene Oxide for Colorimetric Detection of Cancer Cells. *Analytical Chemistry* 86 (5):2711-2718.

Zhang, T. Y., G. W. Lu, J. Liu, H. M. Shen, P. Perriat, M. Martini, O. Tillement, and Q. H. Gong. 2012. Strong two-photon fluorescence enhanced jointly by dipolar and quadrupolar modes of a single plasmonic nanostructure. *Appl. Phys. Lett.* 101 (5):1-5.

Zhang, X. Y., J. L. Yin, C. Peng, W. Q. Hu, Z. Y. Zhu, W. X. Li, C. H. Fan, and Q. Huang. 2011. Distribution and biocompatibility studies of graphene oxide in mice after intravenous administration. *Carbon* 49 (3):986-995.

Zhang, Y., T. R. Nayak, H. Hong, and W. B. Cai. 2012. Graphene: a versatile nanoplatform for biomedical applications. *Nanoscale* 4 (13):3833-3842.

Zhou, H. J., B. Zhang, J. J. Zheng, M. F. Yu, T. Zhou, K. Zhao, Y. X. Jia, X. F. Gao, C. Y. Chen, and T. T. Wei. 2014. The inhibition of migration and invasion of cancer cells by graphene via the impairment of mitochondrial respiration. *Biomaterials* 35 (5):1597-1607.

Zhou, X. F., and F. Liang. 2014. Application of Graphene/Graphene Oxide in Biomedicine and Biotechnology. *Current Medicinal Chemistry* 21 (7):855-869.

Zhou, X., F. Laroche, G. E. M. Lamers, V. Torraca, P. Voskamp, T. Lu, F. Q. Chu, H. P. Spaink, J. P. Abrahams, and Z. F. Liu. 2012. Ultra-small graphene oxide functionalized with polyethylenimine (PEI) for very efficient gene delivery in cell and zebrafish embryos. *Nano Res.* 5 (10):703-709.

Zhu, S. J., J. H. Zhang, C. Y. Qiao, S. J. Tang, Y. F. Li, W. J. Yuan, B. Li, L. Tian, F. Liu, R. Hu, H. N. Gao, H. T. Wei, H. Zhang, H. C. Sun, and B. Yang. 2011. Strongly green-photoluminescent graphene quantum dots for bioimaging applications. *Chem. Commun.* 47 (24):6858-6860.

3.6 Chapter in book II

KOPEL, P.; BLAZKOVA, I; VACULOVICOVA, M.; ADAM, V.; ECKSCHLAGER, T.; STIBOROVA, M.; KIZEK, R. Characterization of Carbon Nanotubes for Doxorubicin Encapsulation. *Concise Encyclopedia of nanotechnology*, accepted.

Participation in the manuscript preparation of the author Blažková, I.: 33%.

Characterization of Carbon Nanotubes for Doxorubicin Encapsulation

Pavel Kopel[1,2], Iva Blazkova[1], Marketa Vaculovicova[1,2], Vojtech Adam[1,2], Tomas Eckschlager[3], Marie Stiborova[4], Rene Kizek[1,2*]

[1]Department of Chemistry and Biochemistry, Faculty of Agronomy, Mendel University in Brno, Zemedelska 1, CZ-613 00 Brno, Czech Republic, European Union

[2]Central European Institute of Technology, Brno University of Technology, Technicka 3058/10, CZ-616 00 Brno, Czech Republic, European Union

[3]Department of Paediatric Haematology and Oncology, 2nd Medical Faculty and University Hospital Motol, V Úvalu 84, CZ 150 06 Prague, Czech Republic, European Union

[4]Department of Biochemistry, Faculty of Science, Charles University, Albertov 2030, CZ-128 40 Prague 2, Czech Republic, European Union

***Corresponding author**

Rene Kizek, Department of Chemistry and Biochemistry, Mendel University in Brno, Zemedelska 1, CZ-613 00 Brno, Czech Republic, European Union; E-mail: kizek@sci.muni.cz; phone: +420-5-4513-3350; fax: +420-5-4521-2044

Abstract

The pioneering nanomechanical and nanoelectrical engineering have been rapidly overtaken by life sciences including chemistry and biology as well as biophysics and biomedicine. Therefore the opportunity of application of nano-size objects such as nanoparticles of various types and nature as drug carriers and/or tumour detecting agents is of great interest. Physico-chemical properties of carbon nanotubes (CNTs) especially their thermal and chemical stability, tensile strength, perfect transport conductivity and optoelectronic properties are discussed in this review. Besides interesting properties of CNTs, they can be also used as carriers of compounds with the effects on organisms. From these compounds, anticancer drugs are often tested to decrease their toxicity and/or overcome chemoresistance due to encapsulation of them with CNTs. Therefore, drug and gene delivery transporters based on CNTs and their using in thermotherapy is given. The particular attention is paid to cytostatic drug doxorubicin.

1. Introduction

The interest in carbon nanostructures research studies has begun since the discovery of fullerene in 1985. Since then, various carbon nanostructures like carbon nanotubes (CNTs), graphene, graphite oxide and fullerene are the most studied ones as promising materials with applications in different kinds of technologies including in biology and medicine (Roy et al., 2012). Structures of carbon nanomaterials are shown in Fig. 1.

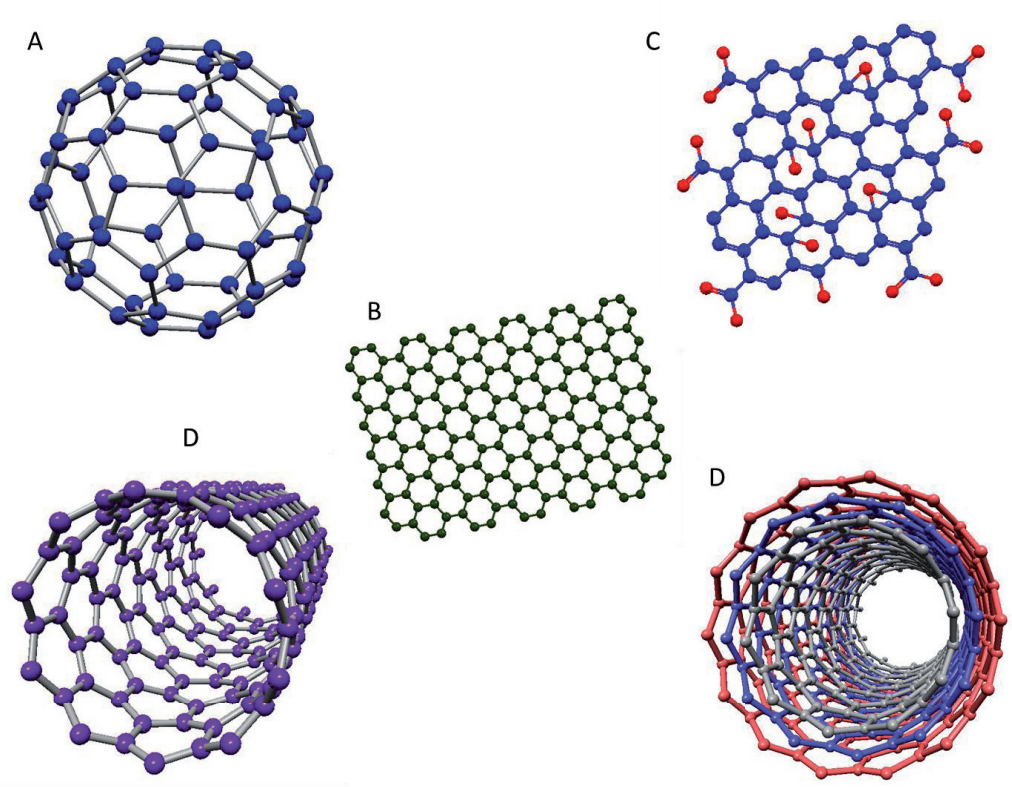

Figure 1. Structures of carbon nanomaterials: A) fullerene, B) graphene, C) oxidized graphene, D) single-wall carbon nanotube, D) multi-wall carbon nanotube

Carbon nanotubes (CNTs) can be described as rolled up graphene sheets with no overlapping edges. Their diameters typically vary from 1 to 100 nm and their lengths can be several orders of magnitude larger, typically micrometer scale lengths. Depending on the number of graphene layers, which are rolled up, the CNTs are categorized as single-walled (SWCNTs), double-walled (DWCNTs) and multi-walled (MWCNTs). MWNTs consist of a coaxial assembly of several SWNTs, separated from one another by ~0.34 nm, which is slightly more than the interlayer distance in single-crystal graphite. DWNTs consist of two graphene layers

only and represent a special form of nanotubes with properties closer to SWCNTs. The properties of CNTs strongly depend on the arrangement of the graphene sheets, the diameter and length of the tubes and the nanostructure.

It was found that CNTs are perfect building blocks for engineering materials, owing to their promising mechanical properties and low density (Yu et al., 2000a; Yu et al., 2000b). SWCNT has a density of about 1.33 – 1.40 g/cm^3, which is just half dense than aluminum, whilst its elastic modulus is comparable to that of diamond (1.2 TPa). The tensile strength for SWCNT bundles is measured as 13–52 GPa and has been calculated as 150 GPa for a single SWCNT. The modulus and strength of a typical SWCNT can reach 640 and 37 GPa, respectively, which is higher than that of steel (2 GPa) (Baughman et al., 2002). It is still a great challenge to retain such mechanical properties when CNTs are assembled into fibres or films.

The electrical conductivity of the SWCNT films is given by the conductivity of individual nanotubes within the network that are associated with the junctions between SWCNTs. There are many factors that influence conductivity, such as doping levels and a ratio of metallic and semiconducting fractions of SWCNT. The conductivity is also given by the density, geometry and distribution of CNT networks (Cao and Rogers, 2009; Hu et al., 2010; Kim et al., 2002; Zhou et al., 2009). Conductive films can be prepared by filtration, but the directly synthesized films have much better electrical and mechanical properties, for example the electrical conductivity can reach 2000 Scm^{-1} and the strength may be up 360 MPa (Ma et al., 2007).

Optical properties are based on the fact that SWCNTs are direct-band gap materials with a gap depending on diameter and chirality. Theoretical and experimental studies have shown that CNTs are strongly nonlinear media, since the delocalization of π electrons has been shown to be a major contribution to the large off resonant third-order optical susceptibility. A CNT is a highly delocalized π -conjugated electron system. The fast nonlinear optical response may be due to the large polarization arising mainly from the $\pi - \pi^*$ virtual transitions (Dresselhaus and Eklund, 2000; Liu et al., 1999; Nemilentsau et al., 2006; Xie and Jiang, 1997).

Semiconducting SWCNTs emit fluorescence at near-infrared (NIR) wavelengths that are characteristic of the specific diameter and the chiral angle (Huang et al., 2011). While providing a convenient method for structural identification of semiconducting SWCNTs, NIR fluorescence of SWCNT also offers a powerful approach for sensor development and *in vivo* or real-time imaging of biological systems. It is always necessary to obtain individually dispersed semiconducting SWCNTs with reasonably good purity, which is a critical step in

acquiring NIR fluorescence spectra. Ultrashort-pulse lasers with spectral tuning capability have widespread applications in fields such as spectroscopy, biomedical research and telecommunications.

2. CNTs in drug delivery

Due to the advances in materials chemistry in recent years, numerous nanomaterials have been developed to be used for a variety of biomedical use, such as diagnostics (Biddlestone-Thorpe et al., 2012; Pandey et al., 2014), imaging (He et al., 2013; Xing et al., 2012), treatment and drug delivery (Drbohlavova et al., 2013; Goenka et al., 2014; Chen et al., 2013b). This family of nanomaterials includes metal particles such as silver and gold nanoparticles as well as quantum dots, organic nanoparticles such as dendrimers, liposomes and micelles, and finally carbon nanomaterials including CNTs. Because of the abovementioned properties of CNTs they seem to be an ideal material for bioapplications such as imaging and/or delivery of compounds.

Two major principles of the molecular transport by nanomaterials can be distinguished: I) encapsulation into the cavity of the nanoparticle and II) adsorption or specific binding onto the surface of the nanomaterial transporter. The large surface area of CNTs, allows multi-conjugation of various molecules on the sidewalls. Molecules containing aromatic groups can be easily bound to CNTs non-covalently by strong π–π interactions (Vashist et al., 2011), amide linkage (Das et al., 2013c), hydrazone bond (Gu et al., 2011) and/or ester linkage (Chen et al., 2012b). Also several works have described the transport of the cargo inside of the CNT cylinder (Li et al., 2012b; Raoof et al., 2013; Tripisciano et al., 2009).

In general, the optimal drug delivery system combines targeted delivery focused to the target cells or tissues with release of the cargo triggered by a specific impact characteristic for the diseased tissue. Moreover, the delivery system should be able to diminish the negative side effects of the transported pharmaceuticals. To direct the transporter to the site of action is taking advantage of the specific affinity between antibody and its antigen and/or receptors overexpressed on the surface of diseased cells specific for certain molecules such as folic acid (FA), hyaluronic acid (HA) as well as epidermal growth factor.

Besides all these requirements for delivery system it is highly beneficial that the size of such complex is in the range of tens of nanometres to prolong its retention in the organism and delay the renal clearance. CNTs are widely tested as carriers for drug delivery due to their facile transport through cellular membranes. CNTs have unique properties, including, high cell membrane penetrability, high drug capacity, pH-dependent releasing, prolonged

circulating time and photothermal activity (Karchemski et al., 2012; Meng et al., 2012). A wide range of biologically active molecules have been conjugated to CNTs for their targeted delivery. The summary of selected cytostatic drugs carried by CNTs is given in Tab. 1.

	drug	**CNT type**	**Interaction type or surface modification**	**Targeting ligand**	
Alkaloids	paclitaxel	SWCNT	lipid-mediated conjugation/ hydrophobic interactions	FA	(Shao et al., 2013)
	paclitaxel	MWCNT	poly(lactide)-poly(ethylene glycol) co-polymer-mediated conjugation	-	(Moore et al., 2013)
	paclitaxel	SWCNT	poly{[2-(dimethylamino)ethyl methacrylate]-co-(methacrylic acid)}	-	(Lee and Geckeler, 2012)
	paclitaxel		PEG	-	(D'Yachkov and D'Yachkov, 2013)
	camptothecin	MWCNT	π–π conjugation /Pluronic P123	-	(Tian et al., 2011)
	7-Ethyl-10-hydroxy-camptothecin	SWCNT	PEG	EGFR antibody C225	(Lee et al., 2013a)
Anthracyclines	paclitaxel, doxorubicin		PEG	-	(Lay et al., 2011)
	docetaxel	SWNT	π–π conjugation and amide linkage	FA	(Zhu et al., 2013)
	doxorubicin	MWCNT	amide linkage	-	(Lee et al., 2013b)
	doxorubicin	MWCNT	amide linkage /dendrimer	FA	(Wen et al., 2013b)

	doxorubicin	MWCNT	PEG linked 17 beta-Estradiol	-	(Das et al., 2013b)
	doxorubicin	MWCNT	cleavable hydrazone bond	FA	(Fan et al., 2013)
	doxorubicin	MWCNT	π–π conjugation/ PEG	FA	(Mehra and Jain, 2013)
	doxorubicin	SWCNT	PEG/ non-covalent	FA	(Niu et al., 2013)
	doxorubicin	SWCNT	AS1411 aptamer	-	(Zhang et al., 2013)
	doxorubicin	MWCNT	polyglycolic acid (PGA)-co-heparin	-	(Tsai et al., 2013)
	doxorubicin	SWCNT	PEG	FA	(Jeyamohan et al., 2013)
	doxorubicin	MWCNT	Dexamethasone	-	(Lodhi et al., 2013)
	doxorubicin	MWCNT	CdTe quantum dots with Fe_3O_4 filled CNTs	-	(Chen et al., 2012c)
	doxorubicin	MWCNT	Gold, PEG	-	(Minati et al., 2012)
	doxorubicin	MWCNT	-	HA	(Datir et al., 2012)
	azalide-azithromycin	SWCNT	-	-	(Darabi et al., 2014)
platinum-based drugs	platinum(IV) complex	MWCNT	-	-	(Li et al., 2012a)
	oxaliplatin	MWCNT	PEG	-	(Wu et al., 2013)
	cisplatin	MWCNT	Gold nanoparticles	-	(Li et al., 2012b)

	carboplatin	MWCNT	-	-	(Haase et al., 2011)
	cisplatin pro-drug	MWCNT	-	mitochondrial-targeting fluorescent rhodamine-110	(Yoong et al., 2014)
topoisomerase inhibitor	etoposide	SWCNT	chitosan	epidermal growth factor	(Chen et al., 2012a)
antifolate	methotrexate	MWCNT	hydrolyzable ester linkage	FA	(Das et al., 2013a)
immunosuppressant and P-gp inhibitor	cyclosporin A	SWCNT	PEG, amide linkage	-	(Hadidi et al., 2013)
Hormonal inhibitor	tamoxifen	SWCNT	aspargine-glycine-arginine peptide- mediated conjugation	-	(Chen et al., 2013a)
nucleoside analog	gemcitabine	MWCNT	amide linkage	FA	(Singh et al., 2013)
immunosuppressant	gliotoxin	SWCNT	-	Lysozyme, p53 and FA	(Bhatnagar et al., 2014)

Table 1. Summary of drugs delivered by CNTs, and the targeting ligands used for delivery.

2.1 CNTs for doxorubicin delivery

Doxorubicin (DOX) is a member of the anthracycline family of cytostatic agents that are used for the treatment of many common human cancers. The generally accepted mechanism of action of DOX is its interaction with DNA (intercalation and topoisomerase II inhibition) blocking the transcription mechanism (Kizek et al., 2012; Masarik et al., 2012; Masarik et al., 2010; Stiborova et al., 2012). However, DOX is highly toxic and can result in severe suppression of haematopoiesis, gastrointestinal and cardiac toxicity (Heger et al., 2013). Nowadays, several approaches, including delivery using liposomes and/or fullerenes have been developed to reduce the toxicity and enhance the clinical utility of this highly active antineoplastic agent (Blazkova et al., 2013a; Blazkova et al., 2014a; Stanisavljevic et al., 2012; Tmejova et al., 2013). Due to the abilities of DOX effectively fight numerous cancer types on one hand and due to its toxic properties on the other hand, DOX is currently the most often utilized anticancer drug tested for delivery by CNTs (Wong et al., 2013). Anthracyclines in nanoparticle formulation have been approved by the US Federal Drug Administration and European Medicines Agency: liposomal DOX (Myocet; Elan Pharmaceuticals, Cedar Knolls, NJ), PEGylated liposomal DOX (Doxil; Ortho Biotech, and Caelyx; ScheringPlough), PEGylated liposomal daunorubicin (DaunoXome; Diatos), and the recently approved albumin-bound paclitaxel loaded NPs (Abraxane; Abraxis Bioscience). The only „nonanthracycline“ approved nanoparticle cytostatic is albumin-bound paclitaxel loaded nanoparticles (Abraxane; Abraxis Bioscience).The summary of nanomaterials suitable for delivery of DOX is given in Fig. 2 and the options of linkage DOX to the carbon nanotubes are highlighted in Fig. 3.

Amide linked DOX on CNTs can induce burst release of DOX in an acidic environment and can reduce the amount of anticancer drug by 10-fold compared to the free drug and thus lower the toxicity of DOX. DOX-MWCNTs (DOX loaded MWCNTs) were transported by endocytosis and subsequently delivered by early and late endosomes to the cancer cells. DOX-MWCNTs were highly stable in the extracellular region and blood. The clearance of accumulated CNTs in the liver was observed after 4 week (Shao et al., 2013). At pH 7.4, the release of drug from CNTs was around 15−20%. Decreased pH 5.5 allowed 45−55% release of drug. Pristine CNTs – DOX entrapment efficiency is around 99% and drug loading content around 33%. The uptake can be elevated by binding with FA or HA (Das et al., 2013c).

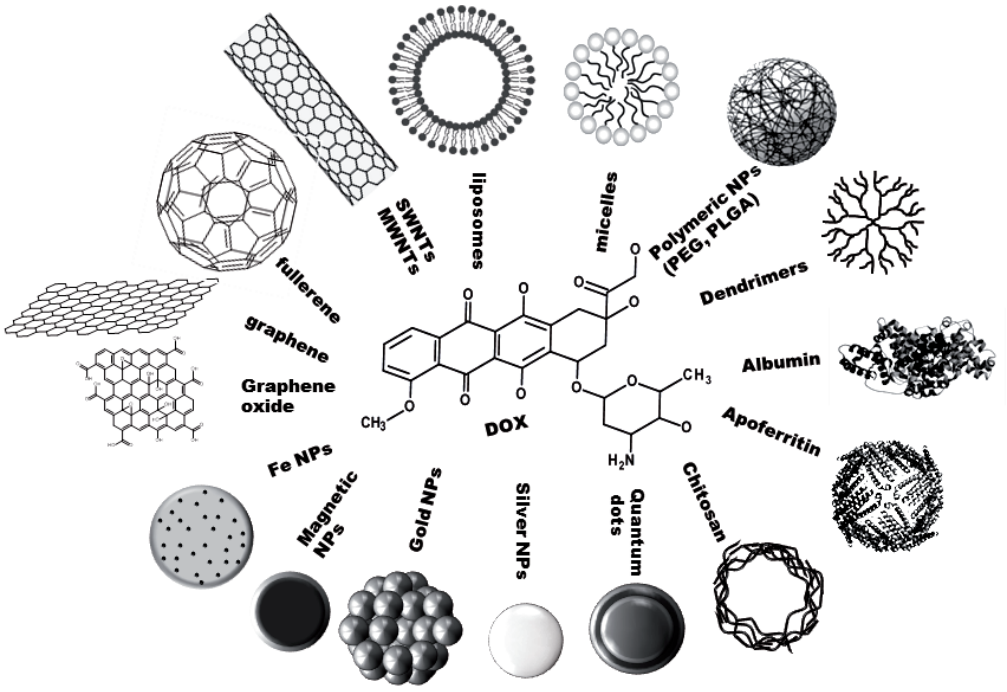

Figure 2. Different types of nanoparticles that may interact with DOX.

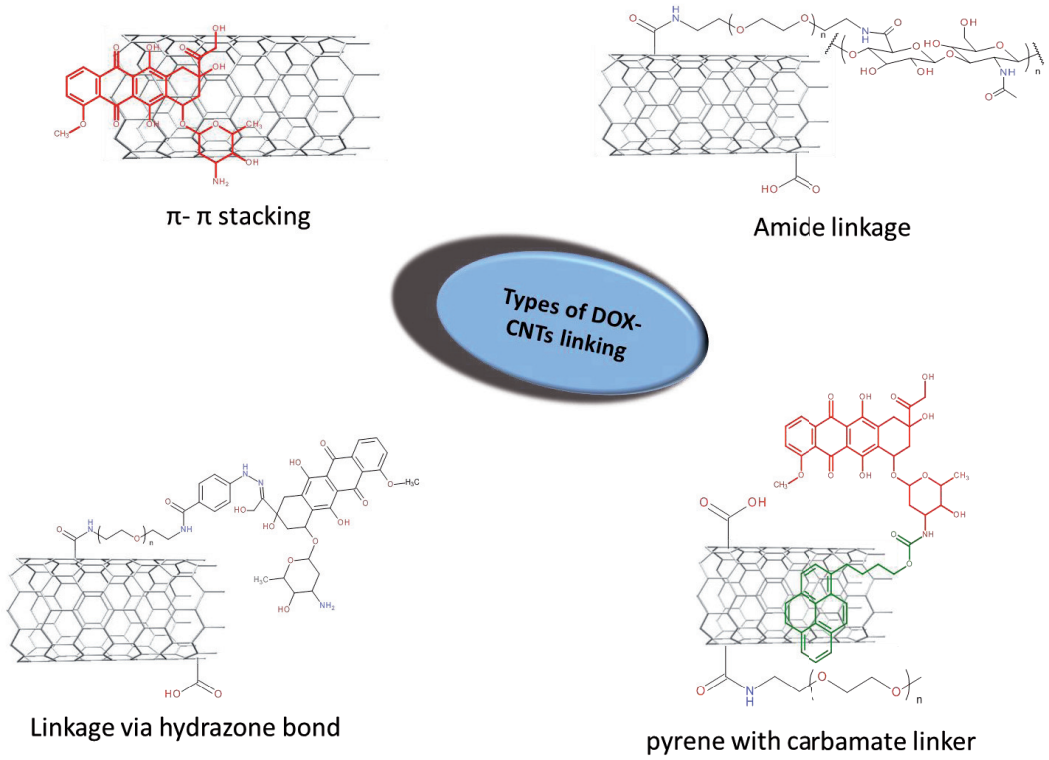

Figure 3. Types of linkage between DOX and CNTs.

The system of DOX loaded via π–π stacking interaction on MWCNTs-HA conjugate can be used for cancer therapy. Covalent functionalization of MWCNTs with HA improved their internalization into human lung adenocarcinoma cells (A549) via hyaluronan receptors (HR) mediated endocytosis. Internalized nanotubes showed lysosomal trafficking, followed by low pH-triggered DOX release under endolysosomal conditions. Consequently, DOX-loaded HA-MWCNTs exhibited 3.2 times higher cytotoxicity and increased apoptotic activity than free DOX. The tumor-growth inhibitory effect of HA-MWCNT-DOX was 5 times higher than free DOX in equivalent concentration. Free DOX is quickly cleared away from the blood. The hydrophilic drug DOX is highly eliminated from the body through urinary excretion. The distribution of DOX in the organs and accumulation in the tumor environment did not depend on the loading of DOX to the CNTs or using free drug, but depended on the functionalization. Functionalized CNTs eased the drug-associated cardiotoxicity. Cardiotoxity, hepatotoxicity, or nephrotoxicity (serious complication of DOX therapy in mice but not in humans) was not observed in case of DOX delivered through HA-MWCNTs in Ehlrich ascites tumor bearing mice (Datir et al., 2012).

Multifunctional dendrimer-modified MWCNTs can be used as a targeted and pH-responsive delivery system for targeting therapy of different types of cancer cells (Wen et al., 2013c). Targeting ligands as well as imaging molecules can be loaded onto the MWCNTs through a one-step dendrimer-mediated reaction. FA-modified MWCNTs can specifically target to cancer cells. MWCNTs with multifunctional poly(amidoamine) (PAMAM) dendrimers can be used for cancer cell targeting and imaging (Shi et al., 2009). Multifunctional dendrimer-modified MWCNTs were used for targeted and pH-responsive delivery of DOX into cancer cells. Amine-terminated generation of 5 poly(amidoamine) (PAMAM) dendrimers modified with fluorescein isothiocyanate (FITC) and FA were covalently connected to acid-treated MWCNTs, than the remaining dendrimer terminal amines were acetylated to neutralize the positive surface potential. The formed multifunctional MWCNTs (MWCNT/G5.NHAc-FI-FA) showed 97.8% loading of the drug. The drug release was very slow in physiological pH, but the release in acidic environment was very fast (Wen et al., 2013a).

FA-derivatized nanoparticles connected with DOX show increase cellular uptake, higher tumor regression contrary to underivatized nanoparticles or the free drug. The adverse side effects as well as *in vitro* and *in vivo* were not detected (Panda et al., 2013). FA-MWCNTs targeted colorectal cancer cells with a 400–500% greater affinity than untargeted MWNTs. Non-specific MWCNTs interaction and a similar MWNTs–FA affinity in a non-cancerous cell line was observed. FA–MWNTs used in photothermal therapy bring out a 50–60%

decrease in colorectal cancer cell viability in contrast to a 4–10% decrease by untargeted MWNTs (Graham et al., 2013).

DOX bonded onto CNTs via a cleavable hydrazone and functionalized with FA can preferably enter folate receptor (FR)-positive cancer cells. After the incubation with the DOX–hydrazone–CNTs–FA, HeLa cells (FR-positive cells) had higher fluorescence and lower viability compared to the FR-negative cells (L929 and A549), indicating that far more DOX–hydrazone–CNTs–FA systems were internalized into these FR-negative cells. In addition, lower viability of HeLa cells was observed. CNTs carrier exhibits photodynamic therapeutic action, under light irradiation. As a result of the photodynamic therapeutic effect afforded by the carrier CNTs, the prodrug system can be used as an effective cancer treatment system (Fan et al., 2013). Water-soluble nano-conjugates of DOX, the FA-PEG and MWCNTs (DOX/FA-PEG-MWCNTs) can be used also for a targeted transport. Contrary to the free DOX, the DOX/FA-PEG-MWCNTs nanoconjugate provides higher effectiveness of tumor growth suppression; it was taken in the cultured MCF-7 cells through caveolae-mediated endocytosis. The treatment of rats by DOX/FA-PEG-MWCNTs prolonged the median survival time, contrary to free DOX. This complex could be used as safe and effective nano-drug (Mehra and Jain, 2013). A highly effective drug carrier is constructed by coating FA-terminated poly(ethylene glycol) (PEG-FA) on SWNTs. PEG-FA was non-covalently linked to SWNTs and DOX was connected to the surface of SWNTs (DOX/PEG-FA/SWNTs). DOX/PEG-FA/SWNTs were stable in blood serum, but it was released in tumor environment and intracellular lysosomes and endosomes (low pH). The complex selectively connected to the cancer cells and entered the lysosomes and endosomes. The DOX migrates into nucleus and there it inhibits transcription and induces cell death. DOX/PEG-FA/SWNTs reduced potential side effects, because it enters to cancer cells and kill them and show low side effects to normal cells (Niu et al., 2013).

Functionalized SWNTs with polymeric poly(ethylene imine) was linked with NGR (Asn-Gly-Arg) tumor-targeting peptide and then DOX was connected. This SWNT-PEI/DOX/NGR delivery system remarkableness inhibited the tumor grow *in vitro* and also *in vivo* and this system can be used in the chemo-photothermal therapy. The SWNT-PEI/DOX/NGR delivery system reduced systemic toxicity and allowed tumor-targeting and pH-dependent release (Wang et al., 2013). *In vivo* imaging of the biodistribution SWNTs is possible by its labeling with recombinant thermo-stable *Luciola cruciate* luciferase (LcL). The DOX was loaded on an LcL-SWNTs carrier with 16% loading efficiency. This drug system was the most distributed to the mesenteric lymphatic system (El-Sayed et al., 2013). A targeting and

photothermal drug delivery system of DOX was developed based on the AS1411 aptamer modified SWNTs. DOX was efficiently loaded onto SWNTs (DOX-AS1411-SWNTs). The loading efficiency of drug was 121% and the drug was released by changing the pH. This drug complex inhibited the growth of EC-109 cells with higher efficacy than pure DOX (Zhang et al., 2013). DOX-loaded Polyoxyl 35 Castor Oil (Cremophor EL, CrEL) noncovalent modified SWNTs (CrEL-SWNTs-DOX) could effectively suppress the tumor growth and enhance DOX level in the tumor in comparison to free DOX. A retention time of CrEL-SWNTs-DOX in tumor was 27.6-fold higher than in case of free DOX. Lower accumulation in other organs, in particular in heart was also detected (Liu et al., 2012). A tocopheryl polyethylene glycol succinate (TPGS) noncovalent modification of SWNTs loading DOX due the physical absorption was developed. DOX was successfully loaded onto the surface of carbon nanotubes (loading amount was 168.7 μg/ml). After intratumoral injection of TPGS-SWNTs-DOX, there was up to 40.2% delay of tumor growth compared with free DOX treatment. TPGS-SWNTs-DOX had the longer retention time in tumor and highest tumor accumulation was detected. TPGS-SWNTs-DOX is a promising strategy for cancer treatment (Tang et al., 2012). The two-dye labeling approach was used for the drug system detection inside the cell. SWNTs were labeled with FITC and the inherent fluorescence of DOX was detected. The unloading of DOX from the vehicle was pH-dependent, DOX detached from SWNTs inside the lysosomes passed into the cytoplasm and finally into the nucleus, whereas SWNTs stayed in the lysosomes (Kang et al., 2012).

Dexamethasone conjugated MWCNTs (DEX-MWCNTs) were developed for controlled delivery of DOX and it was observed that DOX/DEX-MWCNTs were less hemolytic and more cytotoxic than free DOX (evaluated on the A-549 lung epithelial cancer cell line). Good dispersed DEX-MWCNTS could entrap 92.6 +/- 0.5% of DOX (Lodhi et al., 2013). Intrinsically cell penetrable MWCNTs can be used for intranuclear drug delivery. Biocunjugate of PEG, 17 beta-estradiol (E-2) and MWCNT (E-2-PEG-MWCNTs) can be used as a molecular transporter and effective breast cancer treatment enabling nuclear targeting through an estrogen receptor (ER)-mediated pathway and also enhanced anticancer properties *in vivo*. Diblock copolymer polyglycolic acid (PGA)-co-heparin linked to MWCNTs (PGA MWCNTs) efficiently transported the DOX into targeted cell nuclei and caused cell death. PGA MWCNTs labeled by fluorescein isothiocyanate (FITC-PGA MWCNTs) were observed by fluorescence microscopy. Distribution of DOX in the nuclei of HeLa cells was observed as red fluorescence and it was determined that DOX was efficiently released from PGA MWCNTs into the nucleus of HeLa cells. DOX release was very low in

extracellular (pH 7.4) and lysosomal (pH 4.5) environments. After 24 hours, the drug release was around 20% for all simulated environments (Tsai et al., 2013).

Due to the fluorescent properties of DOX, its CNTs conjugates are suitable for fluorescent *in vivo* imaging (Blazkova et al., 2013b; Blazkova et al., 2014b) as demonstrated in Fig. 4, where a chicken embryo was injected by DOX-SWCNTs conjugates and imaged using 480 nm excitation light. The emission was detected at 600 nm.

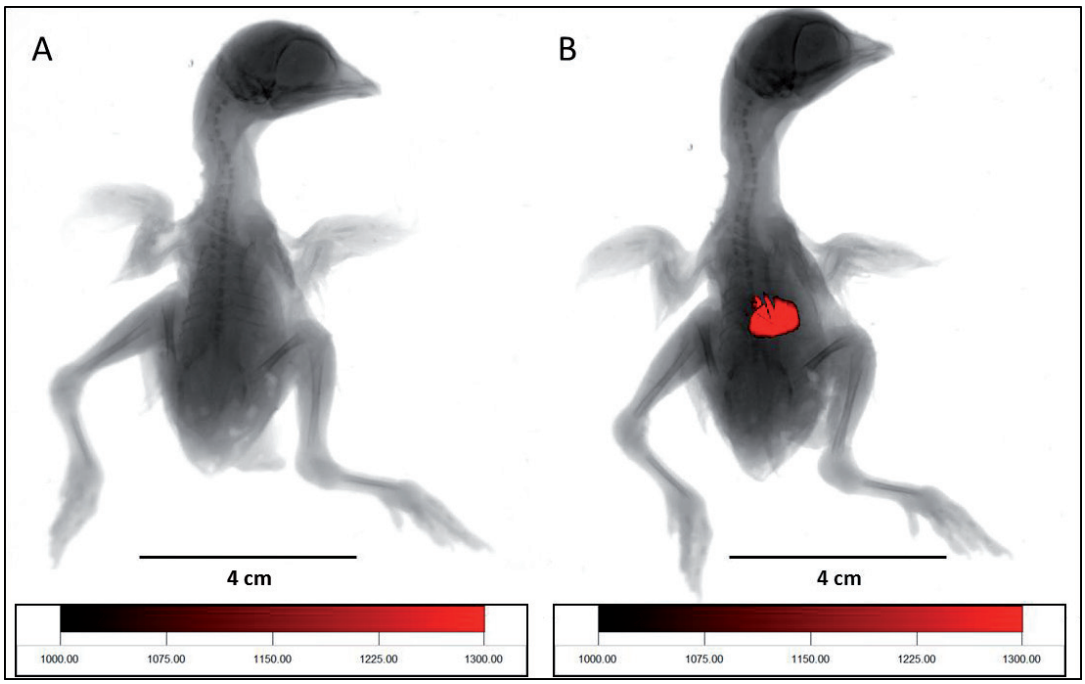

Figure 4. Fluorescence of SWNTs with DOX in chicken embryo of developmental day 18. A) control embryo (without DOX); B) embryo with SWNTs + DOX. Monitoring was performed using an In vivo Xtreme system by Carestream (Rochester, NY, USA). The excitation wavelength was set at 480 nm and the emission was measured at 600 nm. The exposure time was 2 s, binning - 2x2 pixels, fStop - 1.1, field of view – 11.5 x 11.5 cm.

3. Conclusion

It can be concluded that functionalized CNTs can be effectively used for diagnosis and targeted drug therapy. Even though they have been employed for delivery of a wide variety of pharmaceuticals DOX is the most widely employed drug due to significant decrease of its cardiotoxic effects in nano binding DOX.

Acknowledgement

Financial support by CYTORES P301/10/0356, GACR 14-18344S and project for conceptual development of research organization 00064203 are highly acknowledged.

References

Baughman, R.H., Zakhidov, A.A. and de Heer, W.A. "Carbon nanotubes - the route toward applications." *Science* 297 no. 5582 (2002): 787-92.

Bhatnagar, I., Venkatesan, J. and Kim, S.K. "Polymer Functionalized Single Walled Carbon Nanotubes Mediated Drug Delivery of Gliotoxin in Cancer Cells." *Journal of Biomedical Nanotechnology* 10 no. 1 (2014): 120-30.

Biddlestone-Thorpe, L., Marchi, N., Guo, K., Ghosh, C., Janigro, D., Valerie, K. and Yang, H. "Nanomaterial-mediated CNS delivery of diagnostic and therapeutic agents." *Advanced Drug Delivery Reviews* 64 no. 7 (2012): 605-13.

Blazkova, I., Nguyen, H.V., Dostalova, S., Kopel, P., Stanisavljevic, M., Vaculovicova, M., Stiborova, M., Eckschlager, T., Kizek, R. and Adam, V. "Apoferritin Modified Magnetic Particles as Doxorubicin Carriers for Anticancer Drug Delivery." *International Journal of Molecular Sciences* 14 no. 7 (2013a): 13391-402.

Blazkova, I., Nguyen, V.H., Kominkova, M., Konecna, R., Chudobova, D., Krejcova, L., Kopel, P., Hynek, D., Zitka, O., Beklova, M., Adam, V. and Kizek, R. "Fullerene as a transporter for doxorubicin investigated by analytical methods and in vivo imaging." *Electrophoresis* in press no. (2014a).

Blazkova, I., Ryvolova, M., Krizkova, S., Jilkova, E., Kopel, P., Eckschlager, T., Stiborova, M., Adam, V. and Kizek, R. "Modern imaging techniques for anthracycline cytostatics – Review of the Literature." *Klinicka Onkologie* 26 no. 4 (2013b): 239-44.

Blazkova, I., Vaculovicova, M., Eckschlager, T., Stiborova, M., Trnkova, L., Adam, V. and Kizek, R. "Study of fluorescence of doxorubicin in muscle tissue using highly sensitive fluorescence sensing." *Chem. Sensors* in press no. (2014b).

Cao, Q. and Rogers, J.A. "Ultrathin Films of Single-Walled Carbon Nanotubes for Electronics and Sensors: A Review of Fundamental and Applied Aspects." *Advanced Materials* 21 no. 1 (2009): 29-53.

D'Yachkov, E.P. and D'Yachkov, P.N. "Location of Paclitaxel and Poly(ethylene glycol) in Triple Antitumor Complexes with Single-Walled Nanotubes According to the Molecular Docking Method." *Nanoscience and Nanotechnology Letters* 5 no. 11 (2013): 1188-90.

Darabi, H.R., Roozkhosh, A., Tehrani, M.J., Aghapoor, K., Sayahi, H., Balavar, Y. and Mohsenzadeh, F. "Characterization of ester- or thioamide-functionalized single-walled carbon nanotube-azithromycin conjugates." *Applied Surface Science* 288 no. (2014): 122-29.

Das, M., Datir, S.R., Singh, R.P. and Jain, S. "Augmented Anticancer Activity of a Targeted, Intracellularly Activatable, Theranostic Nanomedicine Based on Fluorescent and

Radiolabeled, Methotrexate-Folic Acid-Multiwalled Carbon Nanotube Conjugate." *Molecular Pharmaceutics* 10 no. 7 (2013a): 2543-57.

Das, M., Singh, R.P., Datir, S.R. and Jain, S. "Intranuclear Drug Delivery and Effective in Vivo Cancer Therapy via Estradiol-PEG-Appended Multiwalled Carbon Nanotubes." *Molecular Pharmaceutics* 10 no. 9 (2013b): 3404-16.

Das, M., Singh, R.P., Datir, S.R. and Jain, S. "Surface Chemistry Dependent "Switch" Regulates the Trafficking and Therapeutic Performance of Drug-Loaded Carbon Nanotubes." *Bioconjugate Chemistry* 24 no. 4 (2013c): 626-39.

Datir, S.R., Das, M., Singh, R.P. and Jain, S. "Hyaluronate Tethered, "Smart" Multiwalled Carbon Nanotubes for Tumor-Targeted Delivery of Doxorubicin." *Bioconjugate Chemistry* 23 no. 11 (2012): 2201-13.

Drbohlavova, J., Chomoucka, J., Adam, V., Ryvolova, M., Eckschlager, T., Hubalek, J. and Kizek, R. "Nanocarriers for Anticancer Drugs - New Trends in Nanomedicine." *Current Drug Metabolism* 14 no. 5 (2013): 547-64.

Dresselhaus, M.S. and Eklund, P.C. "Phonons in carbon nanotubes." *Advances in Physics* 49 no. 6 (2000): 705-814.

El-Sayed, R., Eita, M., Barrefelt, A., Ye, F., Jain, H., Fares, M., Lundin, A., Crona, M., Abu-Salah, K., Muhammed, M. and Hassan, M. "Thermostable Luciferase from Luciola cruciate for Imaging of Carbon Nanotubes and Carbon Nanotubes Carrying Doxorubicin Using in Vivo Imaging System." *Nano Letters* 13 no. 4 (2013): 1393-98.

Fan, J.Q., Zeng, F., Xu, J.S. and Wu, S.Z. "Targeted anti-cancer prodrug based on carbon nanotube with photodynamic therapeutic effect and pH-triggered drug release." *Journal of Nanoparticle Research* 15 no. 9 (2013).

Goenka, S., Sant, V. and Sant, S. "Graphene-based nanomaterials for drug delivery and tissue engineering." *Journal of Controlled Release* 173 no. (2014): 75-88.

Graham, E.G., MacNeill, C.M. and Levi-Polyachenko, N.H. "Quantifying folic acid-functionalized multi-walled carbon nanotubes bound to colorectal cancer cells for improved photothermal ablation." *Journal of Nanoparticle Research* 15 no. 5 (2013).

Gu, Y.J., Cheng, J.P., Jin, J.F., Cheng, S.H. and Wong, W.T. "Development and evaluation of pH-responsive single-walled carbon nanotube-doxorubicin complexes in cancer cells." *International Journal of Nanomedicine* 6 no. (2011): 2889-98.

Haase, D., Hampel, S., Kraemer, K., Kunze, D., Taylor, A., Arlt, M., Thomas, J., Oswald, S., Ritschel, M., Klingeler, R., Leonhardt, A. and Buchner, B. (2011) Carbon Nanotubes Filled with Carboplatin: Towards Carbon Nanotube-Supported Delivery of Chemotherapeutic Agents. In Klingeler, R.

and Sim, R.B. (eds.), *Carbon Nanotubes for Biomedical Applications*. Springer-Verlag Berlin, Berlin, pp. 247-58.

Hadidi, N., Kobarfard, F., Nafissi-Varcheh, N. and Aboofazeli, R. "PEGylated Single-Walled Carbon Nanotubes as Nanocarriers for Cyclosporin A Delivery." *Aaps Pharmscitech* 14 no. 2 (2013): 593-600.

He, X., Ma, Y.H., Li, M., Zhang, P., Li, Y.Y. and Zhang, Z.Y. "Quantifying and Imaging Engineered Nanomaterials In Vivo: Challenges and Techniques." *Small* 9 no. 9-10 (2013): 1482-91.

Heger, Z., Cernei, N., Kudr, J., Gumulec, J., Blazkova, I., Zitka, O., Eckschlager, T., Stiborova, M., Adam, V. and Kizek, R. "A novel insight into the cardiotoxicity of antineoplastic drug doxorubicin." *Int. J. Mol. Sci.* 14 no. 11 (2013): 21629-46.

Hu, L.B., Hecht, D.S. and Gruner, G. "Carbon Nanotube Thin Films: Fabrication, Properties, and Applications." *Chemical Reviews* 110 no. 10 (2010): 5790-844.

Huang, H.D., Zou, M.J., Xu, X., Wang, X.Y., Liu, F. and Li, N. "Near-infrared fluorescence spectroscopy of single-walled carbon nanotubes and its applications." *Trac-Trends in Analytical Chemistry* 30 no. 7 (2011): 1109-19.

Chen, C., Xie, X.X., Zhou, Q., Zhang, F.Y., Wang, Q.L., Liu, Y.Q., Zou, Y.N., Tao, Q., Ji, X.M. and Yu, S.Q. "EGF-functionalized single-walled carbon nanotubes for targeting delivery of etoposide." *Nanotechnology* 23 no. 4 (2012a).

Chen, C.Q., Hou, L., Zhang, H.J., Zhu, L., Zhang, H.L., Zhang, C.F., Shi, J.J., Wang, L., Jia, X. and Zhang, Z.Z. "Single-walled carbon nanotubes mediated targeted tamoxifen delivery system using aspargine-glycine-arginine peptide." *Journal of Drug Targeting* 21 no. 9 (2013a): 809-21.

Chen, G., He, Y.F., Wu, X.H., Zhang, Y., Luo, C.L. and Jing, P. "In vitro and in vivo studies of pirarubicin-loaded SWNT for the treatment of bladder cancer." *Brazilian Journal of Medical and Biological Research* 45 no. 8 (2012b): 771-76.

Chen, M.L., He, Y.J., Chen, X.W. and Wang, J.H. "Quantum Dots Conjugated with Fe3O4-Filled Carbon Nanotubes for Cancer-Targeted Imaging and Magnetically Guided Drug Delivery." *Langmuir* 28 no. 47 (2012c): 16469-76.

Chen, Y.C., Huang, X.C., Luo, Y.L., Chang, Y.C., Hsieh, Y.Z. and Hsu, H.Y. "Non-metallic nanomaterials in cancer theranostics: a review of silica- and carbon-based drug delivery systems." *Science and Technology of Advanced Materials* 14 no. 4 (2013b).

Jeyamohan, P., Hasumura, T., Nagaoka, Y., Yoshida, Y., Maekawa, T. and Kumar, D.S. "Accelerated killing of cancer cells using a multifunctional single-walled carbon nanotube-based system for targeted drug delivery in combination with photothermal therapy." *International Journal of Nanomedicine* 8 no. (2013): 2653-67.

Kang, B., Li, J., Chang, S.Q., Dai, M.Z., Ren, C., Dai, Y.D. and Chen, D. "Subcellular Tracking of Drug Release from Carbon Nanotube Vehicles in Living Cells." *Small* 8 no. 5 (2012): 777-82.

Karchemski, F., Zucker, D., Barenholz, Y. and Regev, O. "Carbon nanotubes-liposomes conjugate as a platform for drug delivery into cells." *Journal of Controlled Release* 160 no. 2 (2012): 339-45.

Kim, W., Choi, H.C., Shim, M., Li, Y.M., Wang, D.W. and Dai, H.J. "Synthesis of ultralong and high percentage of semiconducting single-walled carbon nanotubes." *Nano Letters* 2 no. 7 (2002): 703-08.

Kizek, R., Adam, V., Hrabeta, J., Eckschlager, T., Smutny, S., Burda, J.V., Frei, E. and Stiborova, M. "Anthracyclines and ellipticines as DNA-damaging anticancer drugs: Recent advances." *Pharmacology & Therapeutics* 133 no. 1 (2012): 26-39.

Lay, C.L., Liu, J. and Liu, Y. "Functionalized carbon nanotubes for anticancer drug delivery." *Expert Review of Medical Devices* 8 no. 5 (2011): 561-66.

Lee, P.C., Chiou, Y.C., Wong, J.M., Peng, C.L. and Shieh, M.J. "Targeting colorectal cancer cells with single-walled carbon nanotubes conjugated to anticancer agent SN-38 and EGFR antibody." *Biomaterials* 34 no. 34 (2013a): 8756-65.

Lee, Y. and Geckeler, K.E. "Cellular Interactions of a Water-Soluble Supramolecular Polymer Complex of Carbon Nanotubes with Human Epithelial Colorectal Adenocarcinoma Cells." *Macromolecular Bioscience* 12 no. 8 (2012): 1060-67.

Lee, Y.K., Choi, J., Wang, W., Lee, S., Nam, T.H., Choi, W.S., Kim, C.J., Lee, J.K., Kim, S.H., Kang, S.S. and Khang, D. "Nullifying Tumor Efflux by Prolonged Endolysosome Vesicles: Development of Low Dose Anticancer-Carbon Nanotube Drug." *Acs Nano* 7 no. 10 (2013b): 8484-97.

Li, J., Yap, S.Q., Chin, C.F., Tian, Q., Yoong, S.L., Pastorin, G. and Ang, W.H. "Platinum(IV) prodrugs entrapped within multiwalled carbon nanotubes: Selective release by chemical reduction and hydrophobicity reversal." *Chemical Science* 3 no. 6 (2012a): 2083-87.

Li, J., Yap, S.Q., Yoong, S.L., Nayak, T.R., Chandra, G.W., Ang, W.H., Panczyk, T., Ramaprabhu, S., Vashist, S.K., Sheu, F.S., Tan, A. and Pastorin, G. "Carbon nanotube bottles for incorporation, release and enhanced cytotoxic effect of cisplatin." *Carbon* 50 no. 4 (2012b): 1625-34.

Liu, H.Z., Xu, H., Wang, Y., He, Z.G. and Li, S.M. "Effect of intratumoral injection on the biodistribution and therapeutic potential of novel chemophor EL-modified single-walled nanotube loading doxorubicin." *Drug Development and Industrial Pharmacy* 38 no. 9 (2012): 1031-38.

Liu, X.C., Si, J.H., Chang, B.H., Xu, G., Yang, Q.G., Pan, Z.W., Xie, S.S., Ye, P.X., Fan, J.H. and Wan, M.X. "Third-order optical nonlinearity of the carbon nanotubes." *Applied Physics Letters* 74 no. 2 (1999): 164-66.

Lodhi, N., Mehra, N.K. and Jain, N.K. "Development and characterization of dexamethasone mesylate anchored on multi walled carbon nanotubes." *Journal of Drug Targeting* 21 no. 1 (2013): 67-76.

Ma, W.J., Song, L., Yang, R., Zhang, T.H., Zhao, Y.C., Sun, L.F., Ren, Y., Liu, D.F., Liu, L.F., Shen, J., Zhang, Z.X., Xiang, Y.J., Zhou, W.Y. and Xie, S.S. "Directly synthesized strong, highly conducting, transparent single-walled carbon nanotube films." *Nano Letters* 7 no. 8 (2007): 2307-11.

Masarik, M., Krejcova, L., Hynek, D., Adam, V., Stiborova, M., Eckschlager, T. and Kizek, R. "Electrochemical characterization of doxorubicin interaction with DNA." *International Journal of Molecular Medicine* 30 no. (2012): S45-S45.

Masarik, M., Kynclova, H., Huska, D., Hubalek, J., Adam, V., Babula, P., Eckschlager, T., Stiborova, M. and Kizek, R. "DNA-doxorubicin interactions revealed by electrochemistry." *International Journal of Molecular Medicine* 26 no. (2010): S46-S46.

Mehra, N.K. and Jain, N.K. "Development, characterization and cancer targeting potential of surface engineered carbon nanotubes." *Journal of Drug Targeting* 21 no. 8 (2013): 745-58.

Meng, L.J., Zhang, X.K., Lu, Q.H., Fei, Z.F. and Dyson, P.J. "Single walled carbon nanotubes as drug delivery vehicles: Targeting doxorubicin to tumors." *Biomaterials* 33 no. 6 (2012): 1689-98.

Minati, L., Antonini, V., Dalla Serra, M. and Speranza, G. "Multifunctional Branched Gold-Carbon Nanotube Hybrid for Cell Imaging and Drug Delivery." *Langmuir* 28 no. 45 (2012): 15900-06.

Moore, T.L., Pitzer, J.E., Podila, R., Wang, X.J., Lewis, R.L., Grimes, S.W., Wilson, J.R., Skjervold, E., Brown, J.M., Rao, A. and Alexis, F. "Multifunctional Polymer-Coated Carbon Nanotubes for Safe Drug Delivery." *Particle & Particle Systems Characterization* 30 no. 4 (2013): 365-73.

Nemilentsau, A.M., Slepyan, G.Y., Khrutchinskii, A.A. and Maksimenko, S.A. "Third-order optical nonlinearity in single-wall carbon nanotubes." *Carbon* 44 no. 11 (2006): 2246-53.

Niu, L.Y., Meng, L.J. and Lu, Q.H. "Folate-Conjugated PEG on Single Walled Carbon Nanotubes for Targeting Delivery of Doxorubicin to Cancer Cells." *Macromolecular Bioscience* 13 no. 6 (2013): 735-44.

Panda, J.J., Kaul, A., Kumar, S., Alam, S., Mishra, A.K., Kundu, G.C. and Chauhan, V.S. "Modified dipeptide-based nanoparticles: vehicles for targeted tumor drug delivery." *Nanomedicine* 8 no. 12 (2013): 1927-42.

Pandey, A.P., Karande, K.P., More, M.P., Gattani, S.G. and Deshmukh, P.K. "Graphene Based Nanomaterials: Diagnostic Applications." *Journal of Biomedical Nanotechnology* 10 no. 2 (2014): 179-204.

Raoof, M., Cisneros, B.T., Guven, A., Phounsavath, S., Corr, S.J., Wilson, L.J. and Curley, S.A. "Remotely triggered cisplatin release from carbon nanocapsules by radiofrequency fields." *Biomaterials* 34 no. 7 (2013): 1862-69.

Roy, N., Sengupta, R. and Bhowmick, A.K. "Modifications of carbon for polymer composites and nanocomposites." *Progress in Polymer Science* 37 no. 6 (2012): 781-819.

Shao, W., Paul, A., Zhao, B., Lee, C., Rodes, L. and Prakash, S. "Carbon nanotube lipid drug approach for targeted delivery of a chemotherapy drug in a human breast cancer xenograft animal model." *Biomaterials* 34 no. 38 (2013): 10109-19.

Shi, X.Y., Wang, S.H., Shen, M.W., Antwerp, M.E., Chen, X.S., Li, C., Petersen, E.J., Huang, Q.G., Weber, W.J. and Baker, J.R. "Multifunctional Dendrimer-Modified Multiwalled Carbon Nanotubes: Synthesis, Characterization, and In Vitro Cancer Cell Targeting and Imaging." *Biomacromolecules* 10 no. 7 (2009): 1744-50.

Singh, R., Mehra, N.K., Jain, V. and Jain, N.K. "Gemcitabine-loaded smart carbon nanotubes for effective targeting to cancer cells." *Journal of Drug Targeting* 21 no. 6 (2013): 581-92.

Stanisavljevic, M., Ryvolova, M., Kopel, P., Adam, V., Eckschlager, T. and Kizek, R. (2012) *ANALYSIS OF DOXORUBICIN ENCAPSULATION IN APOFERRITIN CAGE BY CAPILLARY ELECTROPHORESIS WITH LASER-INDUCED FLUORESCENCE DETECTION*. Inst Analytical Chemistry Ascr, V V I-Iac, Brno.

Stiborova, M., Poljakova, J., Eckschlager, T., Kizek, R. and Frei, E. "Analysis of covalent ellipticine- and doxorubicin-derived adducts in DNA of neuroblastoma cells by the P-32-postlabeling technique." *Biomedical Papers-Olomouc* 156 no. 2 (2012): 115-21.

Tang, A.C.L., Hwang, G.L., Tsai, S.J., Chang, M.Y., Tang, Z.C.W., Tsai, M.D., Luo, C.Y., Hoffman, A.S. and Hsieh, P.C.H. "Biosafety of Non-Surface Modified Carbon Nanocapsules as a Potential Alternative to Carbon Nanotubes for Drug Delivery Purposes." *Plos One* 7 no. 3 (2012).

Tian, Z., Yin, M., Ma, H.M., Zhu, L.Z., Shen, H.B. and Jia, N.Q. "Supramolecular Assembly and Antitumor Activity of Multiwalled Carbon Nanotube-Camptothecin Complexes." *Journal of Nanoscience and Nanotechnology* 11 no. 2 (2011): 953-58.

Tmejova, K., Hynek, D., Kopel, P., Dostalova, S., Smerkova, K., Stanisavljevic, M., Nguyen, H.V., Nejdl, L., Vaculovicova, M., Krizkova, S., Kizek, R. and Adam, V. "Electrochemical Behaviour of Doxorubicin Encapsulated in Apoferritin." *International Journal of Electrochemical Science* 8 no. 12 (2013): 12658-71.

Tripisciano, C., Kraemer, K., Taylor, A. and Borowiak-Palen, E. "Single-wall carbon nanotubes based anticancer drug delivery system." *Chemical Physics Letters* 478 no. 4-6 (2009): 200-05.

Tsai, H.C., Lin, J.Y., Maryani, F., Huang, C.C. and Imae, T. "Drug-loading capacity and nuclear targeting of multiwalled carbon nanotubes grafted with anionic amphiphilic copolymers." *International Journal of Nanomedicine* 8 no. (2013): 4427-40.

Vashist, S.K., Zheng, D., Pastorin, G., Al-Rubeaan, K., Luong, J.H.T. and Sheu, F.S. "Delivery of drugs and biomolecules using carbon nanotubes." *Carbon* 49 no. 13 (2011): 4077-97.

Wang, L., Shi, J.J., Jia, X., Liu, R.Y., Wang, H.H., Wang, Z.Z., Li, L.L., Zhang, J., Zhang, C.F. and Zhang, Z.Z. "NIR-/pH-Responsive Drug Delivery of Functionalized Single-Walled Carbon Nanotubes for Potential Application in Cancer Chemo-Photothermal Therapy." *Pharmaceutical Research* 30 no. 11 (2013): 2757-71.

Wen, S., Liu, H., Cai, H., Shen, M. and Shi, X. "Targeted and pH-responsive delivery of doxorubicin to cancer cells using multifunctional dendrimer-modified multi-walled carbon nanotubes." *Advanced healthcare materials* 2 no. 9 (2013a): 1267-76.

Wen, S.H., Liu, H., Cai, H.D., Shen, M.W. and Shi, X.Y. "Targeted and pH-Responsive Delivery of Doxorubicin to Cancer Cells Using Multifunctional Dendrimer-Modified Multi-Walled Carbon Nanotubes." *Advanced Healthcare Materials* 2 no. 9 (2013b): 1267-76.

Wen, S.H., Liu, H., Cai, H.D., Shen, M.W. and Shi, X.Y. "Targeted and pH-responsive delivery of doxorubicin to cancer cells using mutifunctional dendrimer-modified multi-walled carbon nanotubes." *Abstracts of Papers of the American Chemical Society* 245 no. (2013c).

Wong, B.S., Yoong, S.L., Jagusiak, A., Panczyk, T., Ho, H.K., Ang, W.H. and Pastorin, G. "Carbon nanotubes for delivery of small molecule drugs." *Advanced Drug Delivery Reviews* 65 no. 15 (2013): 1964-2015.

Wu, L.L., Man, C.J., Wang, H., Lu, X.H., Ma, Q.H., Cai, Y. and Ma, W.S. "PEGylated Multi-Walled Carbon Nanotubes for Encapsulation and Sustained Release of Oxaliplatin." *Pharmaceutical Research* 30 no. 2 (2013): 412-23.

Xie, R.H. and Jiang, J. "Nonlinear optical properties of armchair nanotube." *Applied Physics Letters* 71 no. 8 (1997): 1029-31.

Xing, H., Wong, N.Y., Xiang, Y. and Lu, Y. "DNA aptamer functionalized nanomaterials for intracellular analysis, cancer cell imaging and drug delivery." *Current Opinion in Chemical Biology* 16 no. 3-4 (2012): 429-35.

Yoong, S.L., Wong, B.S., Zhou, Q.L., Chin, C.F., Li, J., Venkatesan, T., Ho, H.K., Yu, V., Ang, W.H. and Pastorin, G. "Enhanced cytotoxicity to cancer cells by mitochondria-targeting MWCNTs containing platinum(IV) prodrug of cisplatin." *Biomaterials* 35 no. 2 (2014): 748-59.

Yu, M.F., Files, B.S., Arepalli, S. and Ruoff, R.S. "Tensile loading of ropes of single wall carbon nanotubes and their mechanical properties." *Physical Review Letters* 84 no. 24 (2000a): 5552-55.

Yu, M.F., Lourie, O., Dyer, M.J., Moloni, K., Kelly, T.F. and Ruoff, R.S. "Strength and breaking mechanism of multiwalled carbon nanotubes under tensile load." *Science* 287 no. 5453 (2000b): 637-40.

Zhang, H.J., Chen, C.Q., Hou, L., Jin, N., Shi, J.J., Wang, Z., Liu, Y., Feng, Q.H. and Zhang, Z.Z. "Targeting and hyperthermia of doxorubicin by the delivery of single-walled carbon nanotubes to EC-109 cells." *Journal of Drug Targeting* 21 no. 3 (2013): 312-19.

Zhou, W.Y., Bai, X.D., Wang, E.G. and Xie, S.S. "Synthesis, Structure, and Properties of Single-Walled Carbon Nanotubes." *Advanced Materials* 21 no. 45 (2009): 4565-83.

Zhu, X.L., Huang, S.N., Xie, Y.X., Zhang, H.J., Hou, L., Zhang, Y.J., Huang, H.Q., Shi, J.J., Wang, L. and Zhang, Z.Z. "Folic acid mediated solid lipid nanocarriers loaded with docetaxel and oxidized single-walled carbon nanotubes." *Journal of Nanoparticle Research* 16 no. 1 (2013).

4 MATERIALS AND METHODS

4.1 Chemicals

All chemicals used in these studies were purchased from Sigma Aldrich (St. Louis, MO, USA) in ACS purity unless noted otherwise. Pipetting was performed by pipettes from Eppendorf (Hamburg, Germany). ACS water (Sigma Aldrich) or high purity deionized water (Milli-Q Millipore 18.2 MΩ/cm, MA, USA) was used.

4.2 Methods

4.2.1 Fluorescence spectrophotometry

The fluorescence of DOX was analysed by fluorescence spectrometer Tecan infinite M200 PRO (Tecan, Grödig, Austria) on the plate NanoQuant plate™ (Tecan, Grödig, Austria) or Costar Corning® microtitration plate (Corning, NY, USA). The absorption scan was measured within the range from 230 to 800 nm per 5 nm steps. For fluorescence spectra measurement an excitation wavelength was set to 480 nm and the fluorescence scan was measured within the range from 510 to 850 nm. The detector gain was set to 100. All measurements were five times repeated. The data were processed by Microplate Reader software i-control™ 1.9 (Tecan, Grödig, Austria).

4.2.2 Fluorescence imaging

Fluorescence monitoring in the organism was performed using an *In vivo* Xtreme system by Carestream Health Inc. (Rochester, NY, USA). This instrument was equipped with a 400 W xenon light source and the emitted light was captured by 4 MP CCD detector. The excitation wavelength was set at 480 nm and the emission was measured at 600 nm. The exposure time was 2 s, binning – 2 x 2 pixels, fStop - 1.1, field of view – 17.5 × 17.5 cm (11.5 x 11.5 cm).

4.2.3 Fluorescence microscopy

The cells of bacterial culture *Staphylococcus aureus* incubated with DOX were pipetted on the microscope slide and covered by cover slip. The sample was placed by coverslip down and the immersion oil was used. The objective (PlanFLN; Mag. 100x; NA 1,3; F.N. 26.5) and the magnification lens 1.6x was used with the total magnification 1600x. The inverted research fluorescence microscope Olympus IX71S8F-3 (Olympus Corporation, Tokyo,

Japan) was used. The images were captured by Olympus Camera DP73 and processed by Olympus Stream Basic 1.7 Software. The images resolution was 4800 x 3600 pixels. The parameters for the ambient light images were following: exposure time – 2.2 ms and ISO 200. Fluorescence of the DOX was detected using excitation filter – 520 - 550 nm and emission filter – 580 nm, exposure time: 530.8 ms and ISO 100.

4.2.4 Microdialysis arrangement

The CMA 4004 Syringe Pump (CMA, Holliston, Massachusetts, USA) with syringe Gastight 1750 (Hamilton Bonaduz AG, Bonaduz, Switzerland) was used for the pulseless dosage of perfusion fluid (1, 2 or 5 μL/min). Different perfusion fluids in this work were tested as follows: ACS water, Ringer´s solution (155 mM NaCl, 2.4 mM $CaCl_2$, and 5.6 mM KCl, pH 7.4 (Song and Lunte 1999)) and Perfusion fluid T1 (Na^+ 147 mmol/L, K^+ 4 mmol/L, Ca^{2+} 2.3 mmol/L, Cl^- 156 mmol/L, pH 6, osmolality: 290 mosm/kg; M Dialysis AB, Solna, Sweden). For the microdialysis the CMA 20 Elite probe (M Dialysis AB, Solna, Sweden) was used (membrane length: 4 mm, membrane diameter: 0.5 mm, material: Polyarylethersulphone, cut-off: 20 kDa). The dialysates (30 μL) were collected in the Refrigerated Fraction Collector CMA 470 (CMA Microdialysis AB, Solna, Sweden) set on 6 °C.

4.2.5 Capillary electrophoresis

Capillary electrophoresis with laser induced fluorescence detection (CE-LIF) was carried out using Beckman P/ACE MDQ capillary electrophoresis system equipped with laser induced detector with excitation wavelength of 488 nm (argon ion laser) and emission wavelength was 600 nm. Separation was carried out in uncoated fused silica capillary with total length of 63.5 cm, effective length of 54.5 cm, internal diameter of 75 μm and outer diameter of 375 μm. 100 mM phosphate buffer of pH 5.0 with 60 μM spermine and 70% of ACN v/v was used as background electrolyte. Separation was carried out at 25 kV with hydrodynamic injection 15 s by 34 mbar. Samples were diluted 100 times prior to the analysis.

5 RESULTS AND DISCUSSION

Results and Discussion part of this Ph.D. thesis is presented as 4 publications in scientific journals and supplemented by the comments of the author. For each work also author contribution on the creation of publication is marked.

5.1 Interaction of DOX with biomolecules

DOX is important antineoplastic drug and also like other drugs has serious side effects. The promising tool for minimizing of these effects is usage of NPs (Du, Du et al. 2011). But up to now, there is little known about the NPs metabolism and mechanism of the action (Li, Lie et al. 2008). For the study of DOX-NPs conjugates behaviour in the body, it is necessary to understand the behaviour of free DOX (Zhang and Kong 2015). In the organism, DOX can interact with different biomolecules. We focused on the interaction with amino acids and proteins. The strength of this interaction and the effect on the DOX associated cardiotoxicity was analysed.

5.1.1 Research article I

HEGER, Z.; CERNEI, N.; KUDR, J.; GUMULEC, J.; **BLAZKOVA, I.**; ZITKA, O.; ECKSCHLAGER, T.; STIBOROVA, M.; ADAM, V.; KIZEK, R. A novel insight into the cardiotoxicity of antineoplastic drug doxorubicin. *International Journal of Molecular Science*, 2013. 14(11): p. 21629-21646. ISSN 1422-0067.

Participation in the manuscript preparation of the author Blažková, I.: 20%.

DOX caused heart failure is often associated with changes in energy metabolism (Tanada, Shioi et al. 2014). Metabolic remodelling is an integral part of the pathogenesis (Huang, Zhou et al. 2011) and in multiple cellular processes amino acids play a key role (Carubelli, Castrini et al. 2015). Amino acids concentration can change in response to disease (Lewis, Littlejohns et al. 2014) and they exert cardioprotective effect in ischemia and other cardiac disorders. Their role in the metabolism of the ischemic heart has to be yet fully elucidated (Drake, Sidorov et al. 2012). Supplementation of amino acids could help to decrease negative effects. Branched-chain amino acids promoted mitochondrial biogenesis in heart, improved survival of rats with heart failure and inhibited body weight loss (Tanada, Shioi et al. 2014). Amino acid taurine dramatically influences the development of ischemia–reperfusion injury. The loss of taurine from the heart may increase the risk of ventricular remodelling and development of heart failure (Schaffer, Jong et al. 2014).

The aim of this work was the *in vitro* study of DOX interaction with major amino acids in the tissue of chicken cardiac muscle by absorbance and fluorescence spectrometry, *in vivo* fluorescence detector and ion-exchange liquid chromatography - IELC (amino acids analyser). Amino acid profile of myocardium have shown the most abundant amino acids in myocardium, such as proline followed by taurine, glutamic acid, arginine, aspartic acid, leucine, glycine, valine, alanine, isoleucine, threonine, lysine and serine in the concentration range 1 μmol/mL for serine to 14 μmol/mL for proline. The interaction of DOX with amino acids was first of all analysed by fluorescence spectrometry and the interaction of some amino acids was detected. The highest binding activity was detected in the case of lysine, β-alanine, serine, valine and arginine. For the detailed analysis IELC was utilized and this method has proven the interaction of DOX with all amino acids. Changes in retention time of proline and glutamic acid point at possible formation of DOX-amino acid complex. The calculation of amino acids breaking point showed the lowest concentration of DOX that causes noticeable effect on amino acid. The lowest had

been determined for serine (1 μg/mL of DOX) and the highest one for glutamic acid (84 μg/mL of DOX). Finally the amino acid profiles in myocardium after exposure to the DOX were determined, in all analysed amino acids significant reduction of all amino acids concentration was observed ($p = 0.05$).

It was found, that DOX, also in low concentrations, directly influences myocardial amino acids and can change their quantitative composition in myocardium. The generated DOX-amino acid complexes could have the effect on cardiotoxicity of DOX.

Int. J. Mol. Sci. **2013**, *14*, 21629-21646; doi:10.3390/ijms141121629

OPEN ACCESS
International Journal of
Molecular Sciences
ISSN 1422-0067
www.mdpi.com/journal/ijms

Article

A Novel Insight into the Cardiotoxicity of Antineoplastic Drug Doxorubicin

Zbynek Heger [1], Natalia Cernei [1,2], Jiri Kudr [1], Jaromir Gumulec [1,2,3], Iva Blazkova [1], Ondrej Zitka [1,2], Tomas Eckschlager [4], Marie Stiborova [5], Vojtech Adam [1,2] and Rene Kizek [1,2,*]

[1] Department of Chemistry and Biochemistry, Faculty of Agronomy, Mendel University in Brno, Zemedelska 1, Brno CZ-613 00, Czech Republic, E-Mails: heger@mendelu.cz (Z.H.); cernei.natalia3@gmail.com (N.C.); george.kudr@centrum.cz (J.K.); j.gumulec@gmail.com (J.G.); iva.blazkova@seznam.cz (I.B.); ZitkaO@seznam.cz (O.Z.); vojtech.adam@mendelu.cz (V.A.)

[2] Central European Institute of Technology, Brno University of Technology, Technicka 3058/10, Brno CZ-616 00, Czech Republic

[3] Department of Pathological Physiology, Faculty of Medicine, Masaryk University, Komenskeho namesti 2, Brno CZ-662 43, Czech Republic

[4] Department of Paediatric Haematology and Oncology, 2nd Faculty of Medicine, Charles University, and University Hospital Motol, V Uvalu 84, Prague 5 CZ-15006, Czech Republic; E-Mail: Tomas.Eckschlager@fnmotol.cz

[5] Department of Biochemistry, Faculty of Science, Charles University, Albertov 2030, Prague 2 CZ-12840, Czech Republic; E-Mail: stiborov@natur.cuni.cz

* Author to whom correspondence should be addressed; E-Mail: kizek@sci.muni.cz; Tel.: +420-545-133-350; Fax: +420-545-212-044.

Received: 29 August 2013; in revised form: 26 September 2013 / Accepted: 9 October 2013 / Published: 31 October 2013

Abstract: Doxorubicin is a commonly used antineoplastic agent in the treatment of many types of cancer. Little is known about the interactions of doxorubicin with cardiac biomolecules. Serious cardiotoxicity including dilated cardiomyopathy often resulting in a fatal congestive heart failure may occur as a consequence of chemotherapy with doxorubicin. The purpose of this study was to determine the effect of exposure to doxorubicin on the changes in major amino acids in tissue of cardiac muscle (proline, taurine, glutamic acid, arginine, aspartic acid, leucine, glycine, valine, alanine, isoleucine, threonine, lysine and serine). An *in vitro* interaction study was performed as a comparison of amino acid profiles in heart tissue before and after application of doxorubicin. We found that doxorubicin directly influences myocardial amino acid representation even at low

concentrations. In addition, we performed an interaction study that resulted in the determination of breaking points for each of analyzed amino acids. Lysine, arginine, β-alanine, valine and serine were determined as the most sensitive amino acids. Additionally we compared amino acid profiles of myocardium before and after exposure to doxorubicin. The amount of amino acids after interaction with doxorubicin was significantly reduced (p = 0.05). This fact points at an ability of doxorubicin to induce changes in quantitative composition of amino acids in myocardium. Moreover, this confirms that the interactions between doxorubicin and amino acids may act as another factor most likely responsible for adverse effects of doxorubicin on myocardium.

Keywords: myocardium; cardiomyopathy; interaction; amide bond; spectrophotometry; ion-exchange liquid chromatography

---

Abbreviations: 4E-BP, 4E-binding protein; AA, Amino acids; BCAAs, Branched-chain amino acids; DNR, Daunorubicin; DOX, Doxorubicin; IELC, Ion-exchange liquid chromatography; mPTPs, Mitochondrial permeability transition pores; mTOR, Mammalian target of rapamycin; ROS, Reactive oxygen species; S6K, S6 kinase; SREBP, Sterol response element binding protein.

1. Introduction

Doxorubicin, an anthracycline antibiotic, is widely used to treat a number of cancers [1–3], including as breast and lung cancers [4–6]. The first anthracyclines were isolated from the pigment-producing *Streptomyces peucetius* var. *caesius* in the 1960s and named doxorubicin (DOX) and daunorubicin (DNR) [7]. They still remain one of the most effective chemotherapeutic antitumor agents [8], which effect is based on intercalation into DNA helix [9]. In addition, they inhibit the activity of enzyme topoisomerase II that prevents DNA repairing [10–12]. Doxorubicin (DOX) also acts by stabilizing a reaction, in which DNA strands are cut and covalently connected to the tyrosine residues of topoisomerase II, eventually impeding DNA resealing. Topoisomerase II-induced DNA damage is followed by a growth arrest in the G_1 and G_2 phases and apoptosis [13]. Anthracyclines exert their cytotoxic effect also by generating reactive oxygen species (ROS) [14], such as H_2O_2 and superoxide anion radical [15]. These pro-oxidant properties of DOX have a potential to induce cell death through an oxidative damage of mitochondria [16].

On the other hand, doxorubicin may cause several side effects [17,18], which are mainly evidenced by serious deteriorations of the cardiac muscle including dilated cardiomyopathy [19–21], congestive heart failure [22,23], arrhythmias [24] and also myelotoxicity [7]. All these effects significantly limit clinical use of DOX. Despite the extensive studies of the cardiotoxicity of DOX at cellular, biochemical, molecular, and genetic levels, it has not satisfactorily been elucidated yet [7,11]. Most likely, it is a multifactorial process where alterations in cellular structure [25], formation of ROS that attack the non-target structures [26,27], and induction of apoptosis [20,28] play the important roles. Therefore, new strategies for decreasing the cardiotoxicity of DOX are looking for.

Amino acids exert a cardioprotective effect in ischemia and other cardiac disorders. They play a crucial role in the cardiac metabolism as a source of acetyl-CoA, and contribute to the production of NADH and $FADH_2$ and conversion of glutamine and glutamate to free radical scavengers [29,30]. However, the relevance of amino acid metabolism in the general population suffering from heart diseases remains still poorly elucidated [31].

The *in vitro* ion-exchange liquid chromatographic (IELC) and spectrophotometric studies of interactions between fundamental amino acids contained in myocardium with major representative of the anthracycline cytostatics doxorubicin and comparison of content and representation of amino acids in myocardium before and after exposure to doxorubicin were the most important aims of this study. We also determined the breaking points, the critical amount of DOX that is sufficient for formation of mutual complexes for each amino acid.

2. Results and Discussion

2.1. Amino Acid Profile of Chicken Myocardium

The purpose of the study was to investigate the influence of DOX on major amino acids present in myocardium. Proline, taurine, glutamic acid, arginine, aspartic acid, leucine, glycine, valine, alanine, isoleucine, threonine, lysine and serine in the downward trend were determined as the most common amino acids in the amino acid profile obtained by IELC. Their concentrations ranged from 1 μmol mL^{-1} for serine to 14 μmol mL^{-1} for proline (Figure 1), where values of concentrations were obtained as the averages from ten independent measurements. These values ranged in amounts similar to values of some amino acids that were determined in human heart in the study by Weitzel *et al.* [32]. All these amino acids were subsequently used for monitoring possible interactions with DOX.

Figure 1. Average content of amino acids in chicken hearts (average of measurements of 10 samples). Measurements were carried out using ion-exchange liquid chromatography (IELC) with postcolumn derivatization with ninhydrin.

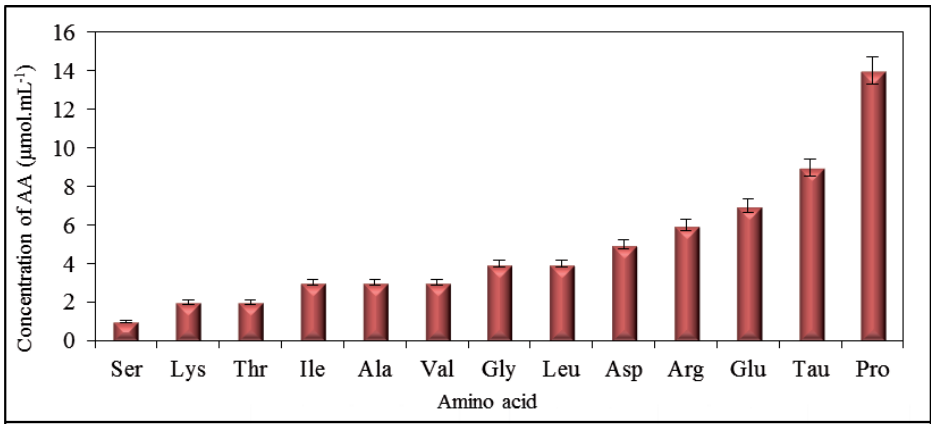

Amino acids	Ser	Lys	Thr	Ile	Ala	Val	Gly	Leu	Asp	Arg	Glu	Taur	Pro
Average (μmol.mL-1)	1	2	2	3	3	3	4	4	5	6	7	9	14

2.2. Spectrophotometric Analysis of Amino Acids-Doxorubicin Interactions

To investigate DOX-induced interactions with amino acids, we primarily used an UV-VIS spectrophotometric method. Marked interactions of lysine, β-alanine, valine, and arginine respectively were evident from the obtained spectra. The spectra of interactions of DOX with other amino acids pointed at no interactions at the constant concentration of doxorubicin when compared different concentrations of AA (Figures 2 and 3). Doxorubicin exhibited the maximum at $\lambda = 480$ nm, which corresponds to findings published in several studies [33–35]. Lysine (Figure 2A), whose amino group is highly reactive and often participates in enzymatic reactions [29], β-alanine (Figure 2E), serine (Figure 3G), valine (Figure 3I) and arginine (Figure 3M) showed significantly stronger interaction with DOX with the increasing concentration (in a concentration dependent manner; highest effects observed at the concentration of 1000 μg mL^{-1}) and thus indicated the highest binding affinity for the formation of complex with DOX. This phenomenon was monitored up to the concentration of 3 μmol mL^{-1} (serine), and 12 μmol mL^{-1} (lysine, arginine, β-alanine, valine and aspartic acid). Other amino acids showed interactions with DOX in much higher concentrations applied as it is apparent from doxorubicin peaks. Trends confirming the above mentioned facts can be seen in insets (a) in Figures 2 and 3, which indicate relations between the concentration of amino acid interacting with DOX and its subsequent effect on absorbance of DOX. Decreasing trend in the series serine, lysine, β-alanine, valine, and arginine points at higher interaction rates and at a higher content of individual amino acids. The insert curves showed no significant changes in the case of all other amino acids.

In addition, we also processed differential spectra of DOX-AA interactions. These results show real forms of interaction output and its real wavelength (insets (a) in Figures 2 and 3). When doxorubicin subjected to interaction with serine, lysine, arginine, β-alanine, valine and aspartic acid, shifts of maximum wavelengths within the range from 464 to 465 nm were observed. Similar wavelength shift was observed also in the case of proline that changed wavelength of doxorubicin to $\lambda = 462$ nm. Other amino acids exhibited relatively small shifts of DOX wavelength, but the differences were present at all of them. These changes mention the amendment to structural changes of molecule of DOX, which is capable to form a complex with amino acid. Curves in insets (a) in Figures 2 and 3 point at weak interaction between DOX, proline and glycine. This interaction is not influenced by concentrations of these amino acids. Low effects of AA concentrations were also observed in the case of leucine, isoleucine, and threonine. Interestingly, among these amino acids the smallest wavelength changes of doxorubicin were also observed. These amino acids were shown as the least accessible for the interaction with DOX. Using the spectrophotometric method we proved that doxorubicin may interact with some amino acids, the basic stones of all myocardial proteins, substrates for the synthesis of proteins, and products of their degradation. Some connections with these products were also found by Taetrneyer *et al.* [36].

Figure 2. Interactions of amino acids (1; 2; 3; 6; 12; 25; 50; 100 µmol mL^{-1}) with doxorubicin (100 µg mL^{-1}) monitored with spectrophotometry. DOX interaction with: (**A**) lysine; (**B**) proline; (**C**) glycine; (**D**) taurine; (**E**) β-alanine, (**F**) threonine; where (**a**) stays for 100 µmol mL^{-1}; (**b**) 50 µmol mL^{-1}; (**c**) 25 µmol mL^{-1}; (**d**) 12 µmol mL^{-1}; (**e**) 6 µmol mL^{-1}; (**f**) 3 µmol mL^{-1}; (**g**) 2 µmol mL^{-1}; (**h**) 1 µmol mL^{-1}; (**i**) 0 µmol mL^{-1} and (**j**) for control (AA without DOX). The dependence of the DOX absorbance at 480 nm on the different concentrations of amino acids is shown in insets marked with lowercase letter a. Insets marked with lowercase letter b express the differences obtained from differential spectra gained as a readout of DOX spectrum from DOX-AA complex spectrum with observed wavelength maximum changes.

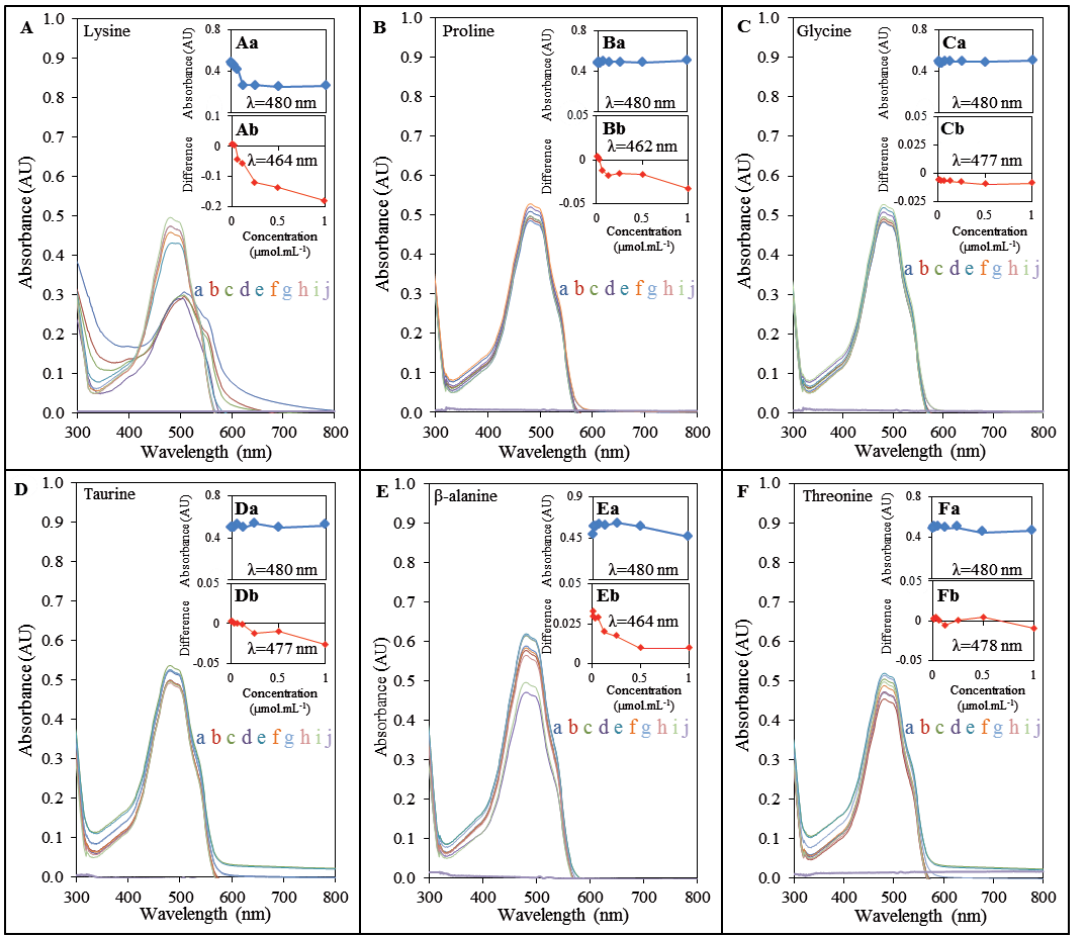

Figure 3. Interactions of amino acids (1; 2; 3; 6; 12; 25; 50; 100 µmol mL^{-1}) with doxorubicin (100 µg mL^{-1}) monitored with spectrophotometry. DOX interaction with: (**G**) serine; (**H**) aspartic acid; (**I**) valine; (**J**) glutamic acid; (**K**) isoleucine; (**L**) leucine; (**M**) arginine, where (**a**) stays for 100 µmol mL^{-1}; (**b**) for 50 µmol mL^{-1}; (**c**) 25 µmol mL^{-1}; (**d**) 12 µmol mL^{-1}; (**e**) 6 µmol mL^{-1}; (**f**) 3 µmol mL^{-1}; (**g**) 2 µmol mL^{-1}; (**h**) 1 µmol mL^{-1}; (**i**) 0 µmol mL^{-1} and (**j**) for control (AA without DOX). The dependence of the absorbance at 480 nm on the different concentrations of amino acids can be observed in insets marked with lowercase letter a. Insets marked with lowercase letter b express the differences obtained from differential spectra gained as readout of DOX spectrum from DOX-AA complex spectrum with observed wavelength changes.

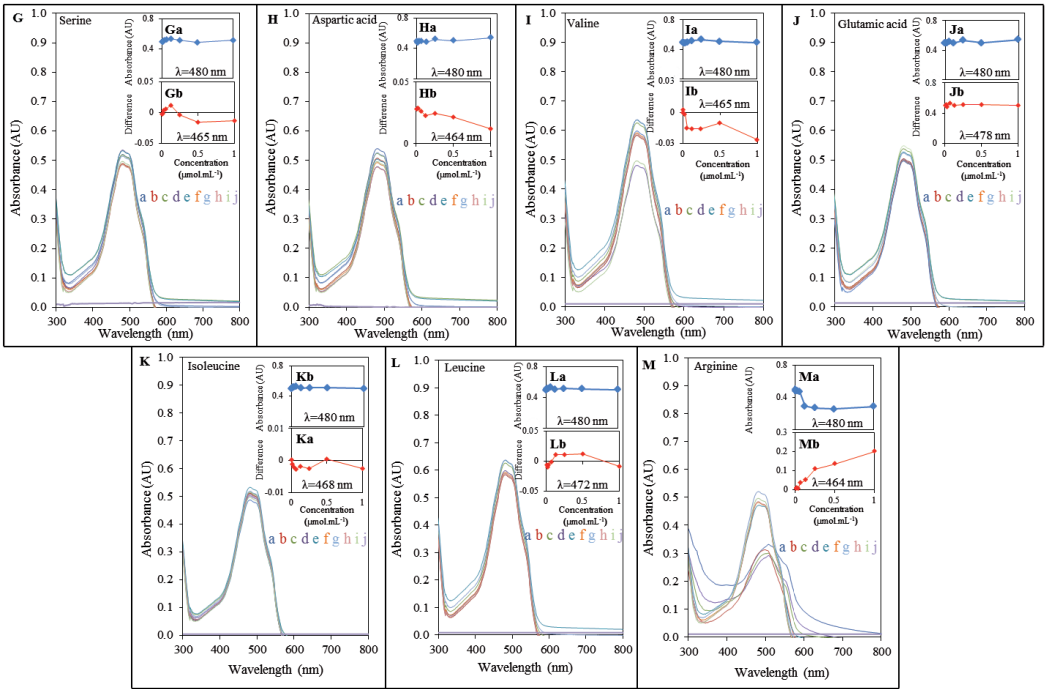

2.3. Analysis of Amino Acids-Doxorubicin Interactions by IELC

To gain more detailed insight into the mechanisms, in terms of how doxorubicin interacts with the amino acids, we carried out IELC analysis. For this purpose, different concentrations of DOX were subjected to interaction with the constant concentration of each AA. As illustrated in Figures 4 and 5, we similarly observed apparent effect of DOX on amino acids serine, lysine, β-alanine, valine, and arginine respectively. Surprisingly, we also observed its effect on other amino acids, *i.e.*, proline, glycine, taurine, threonine, aspartic acid, glutamic acid, isoleucine, and leucine. This effect was manifested even at relatively low concentrations of doxorubicin in the range between 1 µmol mL^{-1} for serine and 84 µmol mL^{-1} for glutamic acid (see Chapter *Breaking points of amino acids*). Amino acids may act as important signaling molecules [31], especially BCAAs are effective activators of the mammalian target of rapamycin (mTOR) signalling cascade [37], which is directly involved in cardiac

hypertrophy in pathways of regulation of proteosynthesis [38,39]. The main function of mTOR is the stimulation of cell growth and anabolism through increasing protein and lipid synthesis via activation of S6K (S6 kinase), 4E-BP (4E-binding protein), and SREBP (sterol response element binding protein) [40,41]. The limited availability of myocardial proteins and the potential to lose the function may induce structural alterations resulting in the formation of free radicals or in changes in antioxidant status [42–44]. Accumulation of free radicals may play a crucial role in depletion of adenosine triphosphate and subsequent opening of the non-specific mitochondrial permeability transition pores (mPTPs) [45] allowing molecules smaller than 1.5 kDa to penetrate through the mitochondrial pores and change mitochondrial membrane potential. All these effects, especially the loss of mitochondrial membrane potential, leads to the release of molecules with pro-apoptotic potential (e.g., cytochrome c) into cytosol [46,47], which results in the degradation of mitochondria, loss of myofilaments and progressive atrophy of myofibrils [48].

Figure 4. Interaction of amino acids (100 µmol mL^{-1}) with doxorubicin (8; 16; 32; 64; 125; 250; 500; 1000 µg mL^{-1}) monitored with IELC. DOX interaction with: (**A**) lysine; (**B**) proline; (**C**) glycine; (**D**) taurine; (**E**) β-alanine; (**F**) threonine. ▲ Expression of retention time changes (min); × real curve of a sample and—calculated overlay expressing amino acids breaking points.

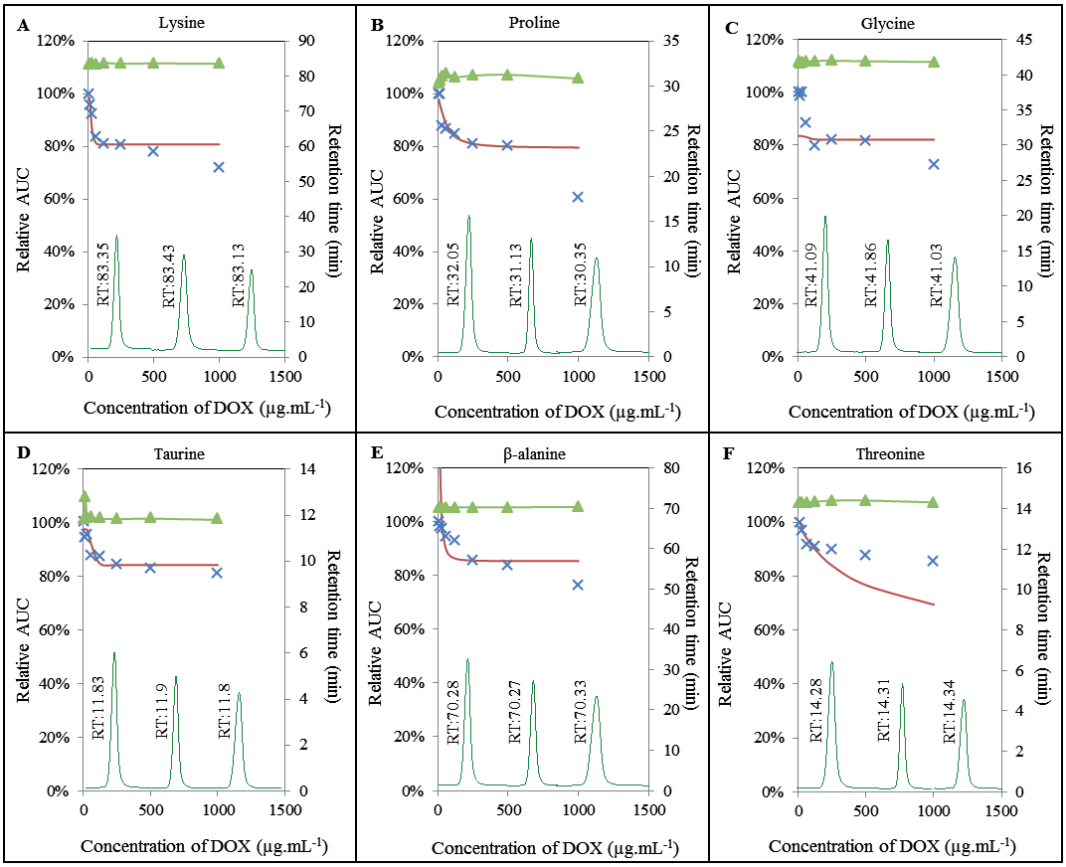

Figure 5. Interaction of amino acids (100 µmol mL^{-1}) with doxorubicin (8; 16; 32; 62; 125; 250; 500; 1000 µg mL^{-1}) monitored with IELC. DOX interaction with: (**J**) serine; (**K**) aspartic acid; (**L**) valine; (**M**) glutamic acid; (**N**) isoleucine; (**O**) leucine; (**P**) arginine. ▲ Expression of retention time changes (min); × real curve of a sample and—calculated overlay expressing amino acids breaking points.

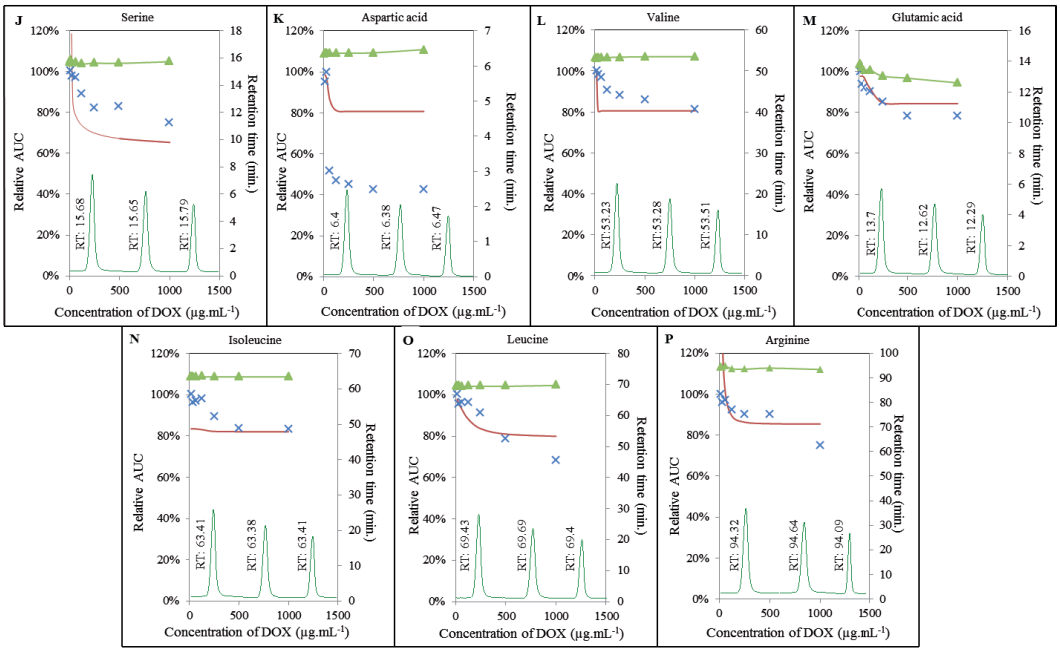

Additionally, we also investigated retention times of individual amino acids. Whereas most of the amino acids analyzed maintained their retention time under the influence of doxorubicin without significant changes, retention time of proline was significantly influenced by DOX in the concentration-dependent manner (Figure 4B). Retention time of proline without DOX added was established at 32.05 min. The highest concentration of doxorubicin (1000 µg mL^{-1}) led to a shortening of retention time to 30.35 min. Similar changes in retention time were observed in the case of glutamic acid, where the signal was observed after 13.7 min without DOX and after 12.29 min after adding of 1000 µg mL^{-1} of doxorubicin (Figure 5M). Changes in retention time point at a possible formation of certain AA-DOX complex that has very similar properties as corresponding amino acid, but slightly shifted its retention time.

2.4. Effect of Doxorubicin on Breaking Points of Amino Acids

Results of IELC analysis showed that doxorubicin interacts with amino acids, especially at low concentrations. Due to this fact, we carried out mathematical analysis of the breaking points for individual amino acids to determine the lowest concentration of DOX that causes noticeable effect on AA (Figure 6A), expressed as the lowest concentration of DOX required for formation of the complex with AA. The lowest breaking point has been determined for serine at the concentration of 1 µg mL^{-1}

of doxorubicin. The highest one has been shown for glutamic acid (84 μg mL^{-1}). The breaking points of all analyzed amino acids are shown in Table 1. As it is clear from Table 1, doxorubicin possesses the ability to interact with amino acids in concentrations lower than we expected. Predictive value of breaking points according to cardiotoxicity is considerable, but it is important to reveal the real amino acids composition of heart. This information may be further applied as a simple mathematical calculation revealing how much of doxorubicin has potential to influence the major amino acids—especially the most vulnerable ones. When compared with spectrophotometric analysis, serine showed the lowest breaking point, however, amino acids serine, lysine, arginine, β-alanine, and valine have very low values of breaking point; thus, these amino acids are the most accessible for interaction with DOX. Valine belongs to the important group of BCAAs that act as the activators of mTOR signalling pathway [49,50]. The depletion of these amino acids may result in the alterations in the function of mTOR with subsequent influencing of synthesis of proteins.

Figure 6. (**A**) Expression of DOX influence on amino acids via breaking points representing the lowest concentration of DOX showing a noticeable effect on amino acids. Results were obtained using IELC with postcolumn derivatization; (**B**) Expression of the effect of amino acids concentrations on DOX spectra carried out on UV/VIS spectrophotometry. There are shown amino acids concentrations, at which DOX spectra showed first observable differences.

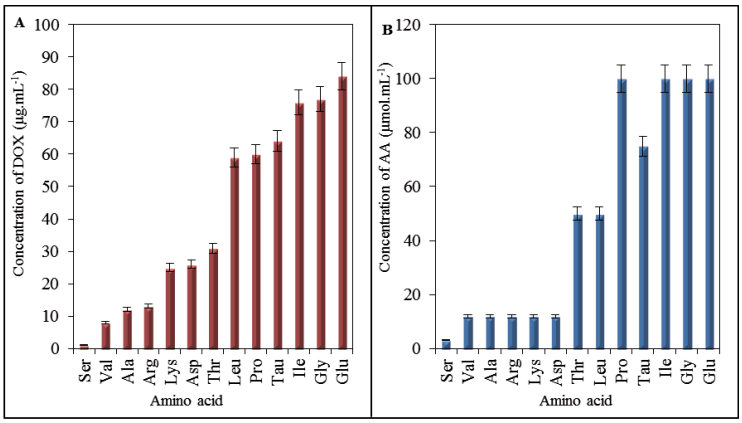

In addition, we assembled the summarizing output from UV/VIS spectrophotometric analysis (Figure 6B). These results are similar to the breaking points shown in Figure 6A regarding to a willingness of amino acids to interact (form a complex) with DOX. When comparing these two outputs coming from different analyses, in the case of the amino acids, which are influenced by the lowest DOX concentration simultaneously, it is valid that a low concentration of amino acid is sufficient to be influenced by the constant concentration of DOX. Serine at the concentration of 3 μmol mL^{-1} exhibited noticeable effect of DOX. At valine, lysine, arginine, β-alanine and aspartic acid sufficient concentration for the same effect was detected to 12 μmol mL^{-1}. Threonine and leucine were influenced by DOX at the concentrations of 50 μmol mL^{-1}, taurine at 75 μmol mL^{-1} and proline, glycine, isoleucine and glutamic acid at 100 μmol mL^{-1}. The concentrations are indicative

for verifying of the interaction trends and are based on the initial concentrations used for UV/VIS spectrophotometric analysis.

Table 1. Overview of the breaking points expressing the lowest concentration of doxorubicin that influences noticeably the amino acids analysed. Ser—serine, Val—valine, Ala—β-alanine, Lys—lysine, Asp—aspartic acid, Thr—threonine, Leu—leucine, Pro—proline, Tau—taurine, Ile—isoleucine, Gly—glycine, Glu—glutamic acid, BP—breaking point.

Amino acid	Ser	Val	Ala	Arg	Lys	Asp	Thr	Leu	Pro	Tau	Ile	Gly	Glu
BP (μg mL^{-1} of DOX)	1	8	12	13	25	26	31	59	60	64	76	77	84

2.5. Impact of Doxorubicin on Amino Acids

According to Manocha and Margaritis, and Yoo and Park [35,51], DOX is a positively charged amphoteric molecule, containing in its sugar moiety (daunosamine) a protonable amino group and in its aglycone part, two deprotonable phenolic groups (Figure 7). At physiological pH or in deionized distilled water, the amino group gets protonated (as NH_3^+) and provides positive charge to the DOX molecule [35]. Hence, it is most likely that electrostatic interactions are established between positively charged DOX and negatively charged amino acids, which results in formation of the DOX-AA complexes in dependence on binding affinity of AA. The ability of doxorubicin to form a linkage through the amide bond has been already described in several studies [52–54]. Therefore, we hypothesize that DOX-AA complexes are formed in the physiological environment found in the human body and this fact affects non-target cytotoxicity of doxorubicin.

Figure 7. Scheme of the interaction between amino acid and doxorubicin resulting in a complex formation, where * stands for protonable functional group; ** stands for deprotonable group.

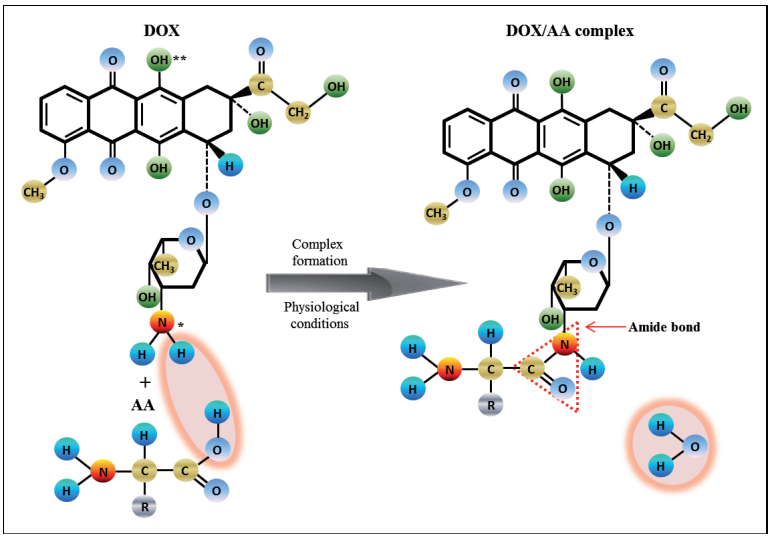

2.6. Comparison of Amino Acid Profile of Myocardium before and after Application of Doxorubicin

We carried out scans of both hearts, untreated and treated with DOX, to confirm its presence in myocardium (Figure 8A,B). Distribution of DOX (red highlighting) mainly in heart apex and estuary of aorta is well evident (red highlighting) in Figure 8B. Compared with control, reduced levels of amino acids occurring in myocardium after exposure to doxorubicin were observed. Proline (19.94% disparity), taurine (19.03%), and glutamic acid (32.54%) were the least affected amino acids by DOX. On the other hand, serine (85.18%) and lysine (83.16%) followed by valine (78.51%) and β-alanine (77.02%) were the most affected amino acids in myocardium (Figure 8C). These data support our findings from previous measurements about increased reactivity of above mentioned amino acids and their ability to interact easily with doxorubicin.

Figure 8. Comparison of chicken myocardium before and after application of 1000 μg mL^{-1} of doxorubicin dissolved in physiological saline solution. (**A**) Chicken cardiac muscle tissue without doxorubicin applied (X-ray image with overlaid fluorescence image); (**B**) Chicken cardiac muscle tissue with 50 μL of doxorubicin applied (X-ray image with overlaid fluorescence image). The fluorescence of doxorubicin was detected by Carestream *In Vivo* Xtreme Imaging System; (**C**) Expression of IELC results of myocardium amino acids content analysis. Both, control and heart, after application of doxorubicin were obtained as the averages from ten measurements. In inset it can be seen the percentage expression of differences between AA concentrations of amino acids in myocardium between and after application of DOX. * refer the differences between amino acid contents as statistically significant (at the $p = 0.05$ level).

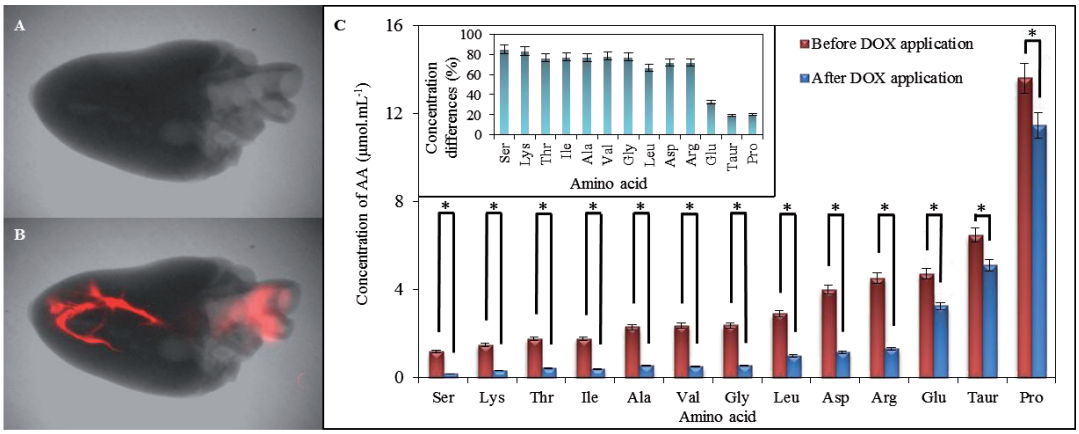

3. Experimental Section

3.1. Chemicals and pH Measurement

Working solutions as buffers or standard solutions of amino acids and DOX were prepared daily by a diluting the stock solutions. Amino acids, DOX standards and others were purchased from Sigma Aldrich (St. Louis, MO, USA) in ACS purity, unless noted otherwise. All solutions were prepared in

deionized water obtained using a reverse osmosis equipment Aqual 25 (Aqual s.r.o., Brno, Czech Republic). The deionized water was further purified by using an apparatus Direct-Q 3 UV Water Purification System equipped with an UV lamp from Millipore (Billerica, MA, USA). The resistance was established to 18 MΩ cm^{-1}. The pH was measured using a pH meter WTW inoLab (Weilheim, Germany).

3.2. Preparation of Myocardium Samples and DOX Fluorescence Detection

For acquisition of the profiles of amino acids, ten chicken hearts were obtained (Diema s.r.o., Frydek-Mistek, Czech Republic). From each heart (n = 10), 10 mg of tissue was equally removed, weighed and added to 0.5 mL of 6 M HCl. Sample was subsequently subjected to digestion in a microwave reaction system Anton Paar (Anton Paar GmbH, Graz, Austria) using the following conditions: power-80, Ramp 15 min, Hold 90 min, Max 120 °C, Max pressure 25 bar, Rotor-XF-100-6. Thereafter, the digested sample was diluted 10 times with dilution buffer composed of thiodiglycol 5 mL L^{-1}, citric acid 14 g L^{-1}, sodium chloride 11.5 g mL^{-1} and centrifuged using a Microcentrifuge 5417R (Eppendorf AG, Hamburg, Germany) under 25,000 g at 4 °C for 10 min. The samples prepared like this were diluted with a neutralizing solution (6 M NaOH in a dilution buffer) again in ratio 1:1 and analyzed on an analyzer of amino acids (Model AAA-400, Ingos, Prague, Czech Republic). Ten chicken hearts were thereafter injected with 50 μL doxorubicin dissolved in physiological saline solution to the final concentration of 1000 μg mL^{-1}. For confirmation of the presence of DOX in the myocardium, a Carestream *In Vivo* Xtreme Imaging System (Carestream Health, Inc., Rochester, NY, USA) was used to detect the fluorescence of doxorubicin after one hour-lasting exposure. Parameters were set as it follows: excitation wavelength—480 nm, emission wavelength—600 nm, exposure time—2 s, binning—2 × 2, *f*-stop—1.1, field of view—7.2 × 7.2 cm. For analysis of amino acids profile in myocardium, samples were prepared in the same way as was described above in this chapter. Analysis was then carried out at on an analyzer of amino acids (Model AAA-400, Ingos, Prague, Czech Republic) using conditions described in chapter "*Determination of content of amino acids in myocardium and analysis of interactions using IELC*". To compare content of amino acids before and after application of DOX, the differences were expressed as percentage disparities.

3.3. Preparation of Amino Acid-Doxorubicin Sample for Interaction Study

The results showing the most abundant amino acids in chicken hearts were further used to monitor interactions with DOX. The stock solutions of amino acids (AA) and doxorubicin were prepared daily in the concentration of 1 mg mL^{-1} by diluting with ACS water. The final concentrations of AA and DOX were prepared by diluting with ACS water from the stock solutions unless noted otherwise. The concentrations of DOX of 8; 16; 32; 64; 125; 250; 500 and 1000 μg mL^{-1} interacting with the constant concentration of amino acids of 100 μg mL^{-1} were used for IELC evaluation of AA-DOX interactions. The concentrations of individual amino acids of 1; 2; 3; 6; 12; 25; 50 and 100 μmol mL^{-1} were used to obtain absorption spectra of AA-DOX interactions. The absorption spectra were obtained after 24 h of interaction at 25 °C with doxorubicin in concentration of 250 μg mL^{-1}.

3.4. Determination of Content of Amino Acids in Myocardium and Analysis of Interactions Using IELC

Firstly, IELC was used to determine AA content in myocardium before and after DOX application. An ion-exchange liquid chromatography (Model AAA-400, Ingos, Prague, Czech Republic) with post column derivatization by ninhydrin and an absorbance detector in the visible light range (VIS) was used. A glass column with inner diameter of 3.7 mm and 350 mm length was filled manually with strong cation exchanger in the sodium cycle LG ANB with approximately 12 μm particles and 8% porosity. The column was tempered on the 60 °C. The double channel VIS detector with an inner cell of 5 μL volume was set to two wavelengths: 440 and 570 nm. Solution of ninhydrin was prepared in 75% *v*/*v* methylcelosolve (Ingos, Prague, Czech Republic) and in 2% *v*/*v* 4 M acetic buffer (pH 5.5). Tin chloride ($SnCl_2$) was used as a reducing agent. Prepared solution of ninhydrin was stored under inert atmosphere (N_2) in dark at 4 °C. Elution of amino acid was done by a buffer containing 10.0 g of citric acid, 5.6 g of sodium citrate, and 8.36 g of NaCl per liter of solution and pH was 3.0. Flow rate was 0.25 mL min^{-1}. Reactor temperature was set on 120 °C. For dilution of samples, a dilution buffer was used (composition: thiodiglycol 5 mL L^{-1}, citric acid 14 g L^{-1}, sodium chloride 11.5 g mL^{-1}). For monitoring of AA-DOX interactions the same parameters of analysis were used instead of the time of analysis, which depended on amino acid determined.

3.5. Spectrophotometric Analysis

Absorption spectra of interactions between amino acids and doxorubicin were carried out on a spectrophotometer SPECORD 210 (Analytik Jena AG, Jena, Germany) within the range from 220 to 800 nm with 1 nm step. For analysis, an UV semi-micro plastic cuvette with 1 cm optical path (Brand GMBH, Wertheim, Germany) was used. Cell compartment was thermostated to 25 °C by a thermostat Julabo (Labortechnik, Wasserburg, Germany). Absorption spectra were recorded after 24 h of the interaction and evaluated by the program WinASPECT version 2.2.7.0 (Analytik Jena AG, Jena, Germany). Finally, differential spectra of DOX-AA interactions were processed according to the formula:

$$\text{spectrum}_{\text{DOX-AA}} - \text{spectrum}_{\text{DOX}} \quad (1)$$

3.6. Determination of Breaking Points of Amino Acids

For the function calculating the breaking points of amino acids, following variables were defined: *a* for absorbance (*y*-axis), *l* for lowest point on *y*-axis, *u* for uppermost point on *y*-axis, *k* for slope of curve, *i* for log breakpoint position and *c* for concentration of doxorubicin. Using these variables, the relation of doxorubicin concentration and absorbance can be expressed as it follows:

$$a = l - \frac{u - l}{1 + 10^{k(i-c)}} \quad (2)$$

To fit the curve, variables *l*, *u*, *k* and *i* were calculated using the least squares method. Consequently, breakpoint (*b*) was subsequently calculated according to:

$$b = 10^{i} \quad (3)$$

Macro in Microsoft Excel using a solver tool was used to create the fit of the curve and to calculate the breaking points of individual amino acids.

3.7. Descriptive Statistics

Mathematical analyses of the experimental data and their graphical interpretation were realized by the Microsoft Office tools (MS Excel®, MS Word®, and MS PowerPoint®). All results were expressed as a mean ± standard deviation (S.D.) unless noted otherwise. The detection limits (3 signal/noise, S/N) were calculated according to Long and Winefordner [55], whereas N was expressed as a standard deviation of noise determined in the signal domain unless stated otherwise. Differences with $p < 0.05$ were considered significant and were determined by using of one way ANOVA test (particularly Scheffe test), which was applied for means comparison.

4. Conclusions

In our study, we determined that doxorubicin induces formation of complexes with amino acids in myocardium. This fact supports the well-known knowledge about the cardiotoxicity of doxorubicin. Despite the fact that some hypotheses about the mechanism of the anthracycline-induced cardiotoxicity have been established, it has not yet been sufficiently explained. An effect of doxorubicin on amino acids may be an important factor involved in this multifactorial and very complicated process. Possible formations of complexes may play important role in the adverse effects of doxorubicin; however, this phenomenon must be further investigated. We also carried out comparison of the quantitative representation of amino acids in myocardium before and after application of doxorubicin. We observed significant reduction of levels of all amino acids in myocardium after exposure to doxorubicin. These findings lead us to knowledge that amino acids play an important role in the cardiotoxicity of doxorubicin in a dose-dependent manner. Initial amino acid composition of heart may hypothetically play an essential role in resistance of heart to doxorubicin. Nevertheless, sensitive BCAAs are very much needed for mTOR managed proteosynthesis. The solution might be found in nutrition supplements providing branched chain amino acids, and thus protecting the proper function of protein synthesis, but their effectiveness would have to be tested. It is important to reveal if DOX induced damage leads to alterations of contractility or cardiac conduction and if there is any chance how to recognize the progressive and reversible damage. From these purposes we have the future plans to carry out *in vivo* experiments, further uncovering this phenomenon. Understanding the pathophysiology of cardiac dysfunction associated with anthracyclines is important for prediction, treatment, and prevention of these adverse side effects of chemotherapy.

Acknowledgments

Financial support from CYTORES GACR P301/10/0356, CEITEC CZ.1.05/1.1.00/02.0068, by MH CZ-DRO, University Hospital Motol, Prague, Czech Republic 00064203 and Liga proti rakovine LPR 2014 is highly acknowledged.

Conflicts of Interest

The authors declare no conflict of interest.

References

1. Das, J.; Ghosh, J.; Manna, P.; Sil, P.C. Taurine protects rat testes against doxorubicin-induced oxidative stress as well as p53, Fas and caspase 12-mediated apoptosis. *Amino Acids* **2012**, *42*, 1839–1855.
2. Holley, A.K.; Dhar, S.K.; Xu, Y.; St Clair, D.K. Manganese superoxide dismutase: Beyond life and death. *Amino Acids* **2012**, *42*, 139–158.
3. Hossain, S.; Yamamoto, H.; Chowdhury, E.H.; Wu, X.; Hirose, H.; Haque, A.; Doki, Y.; Mori, M.; Akaike, T. Fabrication and intracellular delivery of doxorubicin/carbonate apatite nanocomposites: Effect on growth retardation of established colon tumor. *PLoS One* **2013**, *8*, 1–11.
4. Farolfi, A.; Melegari, E.; Aquilina, M.; Scarpi, E.; Ibrahim, T.; Maltoni, R.; Sarti, S.; Cecconetto, L.; Pietri, E.; Ferrario, C.; *et al.* Trastuzumab-induced cardiotoxicity in early breast cancer patients: A retrospective study of possible risk and protective factors. *Heart* **2013**, *99*, 634–639.
5. Li, M.Q.; Song, W.T.; Tang, Z.H.; Lv, S.X.; Lin, L.; Sun, H.; Li, Q.S.; Yang, Y.; Hong, H.; Chen, X.S. Nanoscaled poly(L-glutamic acid)/doxorubicin-amphiphile complex as pH-responsive drug delivery system for effective treatment of nonsmall cell lung cancer. *ACS Appl. Mater. Interfaces* **2013**, *5*, 1781–1792.
6. Nissen, M.J.; Tsai, M.L.; Blaes, A.H.; Swenson, K.K.; Koering, S. Effectiveness of treatment summaries in increasing breast and colorectal cancer survivors' knowledge about their diagnosis and treatment. *J. Cancer Surviv.* **2013**, *7*, 211–218.
7. Minotti, G.; Menna, P.; Salvatorelli, E.; Cairo, G.; Gianni, L. Anthracyclines: Molecular advances and pharmacologic developments in antitumor activity and cardiotoxicity. *Pharmacol. Rev.* **2004**, *56*, 185–229.
8. Yuan, A.; Wu, J.H.; Song, C.C.; Tang, X.L.; Qiao, Q.; Zhao, L.L.; Gong, G.M.; Hu, Y.Q. A novel self-assembly albumin nanocarrier for reducing doxorubicin-mediated cardiotoxicity. *J. Pharm. Sci.* **2013**, *102*, 1626–1635.
9. Box, V.G.S. The intercalation of DNA double helices with doxorubicin and nagalomycin. *J. Mol. Gr. Model.* **2007**, *26*, 14–19.
10. Swift, L.P.; Rephaeli, A.; Nudelman, A.; Phillips, D.R.; Cutts, S.M. Doxorubicin-DNA adducts induce a non-topoisomerase II-mediated form of cell death. *Cancer Res.* **2006**, *66*, 4863–4871.
11. Schwartz, R.G.; Jain, D.; Storozynsky, E. Traditional and novel methods to assess and prevent chemotherapy-related cardiac dysfunction noninvasively. *J. Nuclear Cardiol.* **2013**, *20*, 443–464.
12. Kizek, R.; Adam, V.; Hrabeta, J.; Eckschlager, T.; Smutny, S.; Burda, J.V.; Frei, E.; Stiborova, M. Anthracyclines and ellipticines as DNA-damaging anticancer drugs: Recent advances. *Pharmacol. Ther.* **2012**, *133*, 26–39.
13. Perego, P.; Corna, E.; de Cesare, M.; Gatti, L.; Polizzi, D.; Pratesi, G.; Supino, R.; Zunino, F. Role of apoptosis and apoptosis-related genes in cellular response and antitumor efficacy of anthracyclines. *Curr. Med. Chem.* **2001**, *8*, 31–37.

14. Yang, E.S.; Huh, Y.J.; Park, J.W. RNA interference targeting sensitive-to-apoptosis gene potentiates doxorubicin- and staurosporine-induced apoptosis of PC3 cells. *Anticancer Res.* **2013**, *33*, 847–855.
15. Wallace, K.B. Doxorubicin-induced cardiac mitochondrionopathy. *Pharm. Toxicol.* **2003**, *93*, 105–115.
16. Sardao, V.A.; Oliveira, P.J.; Holy, J.; Oliveira, C.R.; Wallace, K.B. Doxorubicin-induced mitochondrial dysfunction is secondary to nuclear p53 activation in H9c2 cardiomyoblasts. *Cancer Chemother. Pharm.* **2009**, *64*, 811–827.
17. Toldo, S.; Goehe, R.W.; Lotrionte, M.; Mezzaroma, E.; Sumner, E.T.; Biondi-Zoccai, G.G.L.; Seropian, I.M.; van Tassell, B.W.; Loperfido, F.; Palazzoni, G.; *et al.* Comparative cardiac toxicity of anthracyclines *in vitro* and *in vivo* in the mouse. *PLoS One* **2013**, *8*, 1–8.
18. Fong, M.Y.; Jin, S.Y.; Rane, M.; Singh, R.K.; Gupta, R.; Kakar, S.S. Withaferin a synergizes the therapeutic effect of doxorubicin through ROS-mediated autophagy in ovarian cancer. *PLoS One* **2012**, *7*, 1–16.
19. Gharanei, M.; Hussain, A.; Janneh, O.; Maddock, H.L. Doxorubicin induced myocardial injury is exacerbated following ischaemic stress via opening of the mitochondrial permeability transition pore. *Toxicol. Appl. Pharm.* **2013**, *268*, 149–156.
20. Yang, J.Q.; Maity, B.; Huang, J.; Gao, Z.; Stewart, A.; Weiss, R.M.; Anderson, M.E.; Fisher, R.A. G-protein inactivator RGS6 mediates myocardial cell apoptosis and cardiomyopathy caused by doxorubicin. *Cancer Res.* **2013**, *73*, 1662–1667.
21. Yao, Z.W.; Hu, W.; Yin, S.; Huang, Z.; Zhu, Q.; Chen, J.N.; Zang, Y.H.; Dong, L.; Zhang, J.F. 3,3'-Diindolymethane ameliorates adriamycin-induced cardiac fibrosis via activation of a BRCA1-dependent anti-oxidant pathway. *Pharm. Res.* **2013**, *70*, 139–146.
22. Zeng, Q.B.; Wen, H.B.; Wen, Q.; Chen, X.H.; Wang, Y.G.; Xuan, W.L.; Liang, J.S.; Wan, S.H. Cucumber mosaic virus as drug delivery vehicle for doxorubicin. *Biomaterials* **2013**, *34*, 4632–4642.
23. Eckman, D.M.; Stacey, R.B.; Rowe, R.; D'Agostino, R.; Kock, N.D.; Sane, D.C.; Torti, F.M.; Yeboah, J.; Workman, S.; Lane, K.S.; *et al.* Weekly doxorubicin increases coronary arteriolar wall and adventitial thickness. *PLoS One* **2013**, *8*, 1–6.
24. Pereira Neto, G.B.; Andrade, J.N.B.; Sousa, M.G.; Camacho, A.A. Holter electrocardiography in dogs showing doxorubicin-induced dilated cardiomyopathy. *Arq. Bras. Med. Vet. Zootec.* **2006**, *58*, 1037–1042.
25. Lim, C.C.; Zuppinger, C.; Guo, X.X.; Kuster, G.M.; Helmes, M.; Eppenberger, H.M.; Suter, T.M.; Liao, R.L.; Sawyer, D.B. Anthracyclines induce calpain-dependent titin proteolysis and necrosis in cardiomyocytes. *J. Biol. Chem.* **2004**, *279*, 8290–8299.
26. Liu, T.C.K.; Ismail, S.; Brennan, O.; Hastings, C.; Duffy, G.P. Encapsulation of cardiac stem cells in superoxide dismutase-loaded alginate prevents doxorubicin-mediated toxicity. *J. Tissue Eng. Regen. Med.* **2013**, *7*, 302–311.
27. Masarik, M.; Kynclova, H.; Huska, D.; Hubalek, J.; Adam, V.; Babula, P.; Eckschlager, T.; Stiborova, M.; Kizek, R. DNA-doxorubicin interactions revealed by electrochemistry. *Int. J. Mol. Med.* **2010**, *26*, 46.

28. Feridooni, T.; Hotchkiss, A.; Remley-Carr, S.; Saga, Y.; Pasumarthi, K.B.S. Cardiomyocyte specific ablation of p53 is not sufficient to block doxorubicin induced cardiac fibrosis and associated cytoskeletal changes. *PLoS One* **2011**, *6*, 1–12.
29. Drake, K.J.; Sidorov, V.Y.; McGuinness, O.P.; Wasserman, D.H.; Wikswo, J.P. Amino acids as metabolic substrates during cardiac ischemia. *Exp. Biol. Med.* **2012**, *237*, 1369–1378.
30. Nejdl, L.; Sochor, J.; Zitka, O.; Cernei, N.; Ruttkay-Nedecky, B.; Kopel, P.; Babula, P.; Adam, V.; Hubalek, J.; Kizek, R. Spectrometric and chromatographic study of reactive oxidants hypochlorous and hypobromous acids and their interactions with taurine. *Chromatographia* **2013**, *76*, 363–373.
31. Huang, Y.; Zhou, M.Y.; Sun, H.P.; Wang, Y.B. Branched-chain amino acid metabolism in heart disease: An epiphenomenon or a real culprit? *Cardiovasc. Res.* **2011**, *90*, 220–223.
32. Weitzel, L.B.; Ambardekar, A.V.; Brieke, A.; Cleveland, J.C.; Serkova, N.J.; Wischmeyer, P.E.; Lowes, B.D. Left ventricular assist device effects on metabolic substrates in the failing heart. *PLoS One* **2013**, *8*, 1–6.
33. Tazina, E.V.; Ignatieva, E.V.; Polozkova, A.P.; Oborotova, N.A. Qualitative and quantitative analysis of thermosensitive liposomes loaded with doxorubicin. *Pharm. Chem. J.* **2012**, *46*, 54–59.
34. Albright, C.F.; Graciani, N.; Han, W.; Yue, E.; Stein, R.; Lai, Z.H.; Diamond, M.; Dowling, R.; Grimminger, L.; Zhang, S.Y.; *et al.* Matrix metalloproteinase-activated doxorubicin prodrugs inhibit HT1080 xenograft growth doxorubicin with less toxicity. *Mol. Cancer Ther.* **2005**, *4*, 751–760.
35. Manocha, B.; Margaritis, A. Controlled release of doxorubicin from doxorubicin/γ-polyglutamic acid ionic complex. *J. Nanomater.* **2010**, *2010*, 1–9.
36. Taetrneyer, H.; Harinstein, M.E.; Gheorghiade, M. More than bricks and mortar: Comments on protein and amino acid metabolism in the heart. *Am. J. Cardiol.* **2008**, *101*, 3E–7E.
37. Proud, C.G. Regulation of mammalian translation factors by nutrients. *Eur. J. Biochem.* **2002**, *269*, 5338–5349.
38. Zhang, D.H.; Contu, R.; Latronico, M.V.G.; Zhang, J.A.L.; Rizzi, R.; Catalucci, D.; Miyamoto, S.; Huang, K.; Ceci, M.; Gu, Y.S.; *et al.* MTORC1 regulates cardiac function and myocyte survival through 4E-BP1 inhibition in mice. *J. Clin. Investig.* **2010**, *120*, 2805–2816.
39. Katta, A.; Kundla, S.; Kakarla, S.K.; Wu, M.Z.; Fannin, J.; Paturi, S.; Liu, H.; Addagarla, H.S.; Blough, E.R. Impaired overload-induced hypertrophy is associated with diminished mTOR signaling in insulin-resistant skeletal muscle of the obese Zucker rat. *Am. J. Physiol. Regul. Integr. Comp. Physiol.* **2010**, *299*, R1666–R1675.
40. Wullschleger, S.; Loewith, R.; Hall, M.N. TOR signaling in growth and metabolism. *Cell* **2006**, *124*, 471–484.
41. Porstmann, T.; Santos, C.R.; Griffiths, B.; Cully, M.; Wu, M.; Leevers, S.; Griffiths, J.R.; Chung, Y.L.; Schulze, A. SREBP activity is regulated by mTORC1 and contributes to Akt-dependent cell growth. *Cell Metab.* **2008**, *8*, 224–236.
42. Zima, T.; Tesar, V.; Mantle, D.; Koll, M.; Patel, V.; Richardson, P.J.; Preedy, V.R. Acute doxorubicin (adriamycin) dosage does not reduce cardiac protein synthesis *in vivo*, but decreases diaminopeptidase I and proline endopeptidase activities. *Exp. Mol. Pathol.* **2001**, *70*, 154–161.
43. Takemura, G.; Fujiwara, H. Doxorubicin-induccd cardiomyopathy from the cardiotoxic mechanisms to management. *Prog. Cardiovasc. Dis.* **2007**, *49*, 330–352.

44. Gianni, L.; Herman, E.H.; Lipshultz, S.E.; Minotti, G.; Sarvazyan, N.; Sawyer, D.B. Anthracycline cardiotoxicity: From bench to bedside. *J. Clin. Oncol.* **2008**, *26*, 3777–3784.
45. Yellon, D.M.; Hausenloy, D.J. Mechanisms of disease: Myocardial reperfusion injury. *N. Engl. J. Med.* **2007**, *357*, 1121–1135.
46. Halestrap, A.P. What is the mitochondrial permeability transition pore? *J. Mol. Cell. Cardiol.* **2009**, *46*, 821–831.
47. Halestrap, A.P.; Pasdois, P. The role of the mitochondrial permeability transition pore in heart disease. *Biochim. Biophys. Acta* **2009**, *1787*, 1402–1415.
48. Gava, F.N.; Zacche, E.; Ortiz, E.M.G.; Champion, T.; Bandarra, M.B.; Vasconcelos, R.O.; Barbosa, J.C.; Camacho, A.A. Doxorubicin induced dilated cardiomyopathy in a rabbit model: An update. *Res. Vet. Sci.* **2013**, *94*, 115–121.
49. She, P.X.; Olson, K.C.; Kadota, Y.; Inukai, A.; Shimomura, Y.; Hoppel, C.L.; Adams, S.H.; Kawamata, Y.; Matsumoto, H.; Sakai, R.; *et al.* Leucine and protein metabolism in obese zucker rats. *PLoS One* **2013**, *8*, 1–19.
50. Wilkinson, D.J.; Hossain, T.; Hill, D.S.; Phillips, B.E.; Crossland, H.; Williams, J.; Loughna, P.; Churchward-Venne, T.A.; Breen, L.; Phillips, S.M.; *et al.* Effects of leucine and its metabolite β-hydroxy-β-methylbutyrate on human skeletal muscle protein metabolism. *J. Physiol.* **2013**, *591*, 2911–2923.
51. Yoo, H.S.; Park, T.G. Folate-receptor-targeted delivery of doxorubicin nano-aggregates stabilized by doxorubicin-PEG-folate conjugate. *J. Control. Release* **2004**, *100*, 247–256.
52. Ryppa, C.; Mann-Steinberg, H.; Fichtner, I.; Weber, H.; Satchi-Fainaro, R.; Biniossek, M.L.; Kratz, F. *In vitro* and *in vivo* evaluation of doxorubicin conjugates with the divalent peptide E-[c(RGDfK)$_2$] that targets integrin $\alpha_v\beta_3$. *Bioconjug. Chem.* **2008**, *19*, 1414–1422.
53. King, H.D.; Dubowchik, G.M.; Mastalerz, H.; Willner, D.; Hofstead, S.J.; Firestone, R.A.; Lasch, S.J.; Trail, P.A. Monoclonal antibody conjugates of doxorubicin prepared with branched peptide linkers: Inhibition of aggregation by methoxytriethyleneglycol chains. *J. Med. Chem.* **2002**, *45*, 4336–4343.
54. Agudelo, D.; Bourassa, P.; Bruneau, J.; Berube, G.; Asselin, E.; Tajmir-Riahi, H.A. Probing the binding sites of antibiotic drugs doxorubicin and *N*-(trifluoroacetyl) doxorubicin with human and bovine serum albumins. *PLoS One* **2012**, *7*, 1–13.
55. Long, G.L.; Winefordner, J.D. Limit of detection. *Anal. Chem.* **1983**, *55*, A712–A724.

5.1.2 Research article II

BLAZKOVA, I; SMERKOVA, K.; BLAZKOVA, L.; VACULOVICOVA, M.; STIBOROVA, M.; ECKSCHLAGER, T.; BEKLOVA, M.; ADAM, V.; KIZEK, R. Doxorubicin interactions with bovine serum albumin revealed by microdialysis with on-line laser-induced fluorescence detection at sub-picogram level. *Electrophoresis*, ISSN 0173-0835, in press.

Participation in the manuscript preparation of the author Blažková, I.: 52%.

DOX enters the body by injection into the blood vessels, where it meets the blood elements and biomolecules (Sardi, la Marca et al. 2013; Termsarasab, Yoon et al. 2014). The most abundant protein in blood is albumin, which is presented in blood serum in the concentration of 40 g/L (Sartorius, Spasevska et al. 2012). The DOX interaction with albumin can be studied by different methods. The separation technique, that can be used in *in vitro* and also *in vivo* experiments for the separation of different size molecules and can be used for DOX isolation is microdialysis (Clough 2005; Whitaker and Lunte 2010; Buitrago, Otamendi et al. 2011). Microdialysis is modern sampling technique, which can be used for the monitoring of local concentration of drugs and metabolites or also for delivery of drugs to the tissue or bloodstream (Abrahamsson 2013; Bossers, de Boer et al. 2013). The size of microdialyzed molecules depends on the probe membrane cut off, usually 5 – 100 kDa (Hutchinson, O'Connell et al. 2005; Dahlin, Wetterhall et al. 2010).

The aim of this work was the study of DOX interaction with bovine serum albumin. For the analysis fluorescence spectrophotometer was utilized, or the microdialysis setting was on-line connected with laser-induced fluorescence detector. First step was the optimization of the microdialysis process. We analysed the influence of perfusion fluid composition on the DOX recovery; the best results were obtained with pure water. The recovery was calculated as a ratio of DOX mass extracted and DOX mass in dialyzed solution. The flow rate of perfusion fluid was optimized to 1 μL/min; higher flow rates caused decrease in recovery. The concentration of DOX has also an influence on the recovery; higher DOX concentration (60 μg/mL) means higher recovery (55%). Next step was the study of the DOX-BSA interaction in different DOX and BSA ratio. The probe used in this experiment (20 kDa cut off) enabled microdialysis only of free DOX and was impermeable for BSA (66 kDa). Therefore the DOX detected in microdialysates was the unbound DOX. The more BSA was applied to the solution, the less DOX was microdialyzed. Finally the

microdialysis setting was connected on-line with laser-induced fluorescence detector in the flow injection analysis mode and the changes of DOX concentration were detected in real time. This setting enabled observation of temperature and shaking effect on microdialyzed DOX concentration. Modification of the process conditions caused increase of fluorescence signal for 130%. On-line system was also utilized for the real time monitoring of DOX in the chicken liver tissue.

It can be concluded that the interaction of DOX with BSA caused significant decrease in the amount of DOX extracted by microdialysis. The excess of the protein in the mixture led to higher decrease in DOX extracted concentration. The DOX-BSA interaction occurs in less than thirty minutes and a long-term incubation of DOX with BSA (24 hours) does not have significant effect on the DOX microdialyzed concentration.

Doxorubicin interactions with bovine serum albumin revealed by microdialysis with on-line laser-induced fluorescence detection at sub-picogram level

Iva Blazkova[1], Kristyna Smerkova[1], Lucie Blazkova[1], Marketa Vaculovicova[1,2], Marie Stiborova [3], Tomas Eckschlager [4], Miroslava Beklova[5], Vojtech Adam[1,2], Rene Kizek[1,2*]

[1]*Department of Chemistry and Biochemistry, Laboratory of Metallomics and Nanotechnology, Mendel University in Brno, Zemedelska 1, CZ-613 00 Brno, Czech Republic, European Union*

[2]*Central European Institute of Technology, Brno University of Technology, Technicka 3058/10, CZ-616 00 Brno, Czech Republic, European Union*

[3]*Department of Biochemistry, Faculty of Science, Charles University, Albertov 2030, Prague 2 CZ-128 40, Czech Republic, European Union*

[4]*Department of Paediatric Haematology and Oncology, 2nd Faculty of Medicine and University Hospital Motol, Charles University, V Uvalu 84, Prague 5 CZ-150 06, Czech Republic, European Union*

[5]*Department of Ecology and Diseases of Game, Fish and Bees, Faculty of Veterinary Hygiene and Ecology, University of Veterinary and Pharmaceutical Sciences, Palackeho 1–3, CZ-612 42 Brno, Czech Republic, European Union*

***Corresponding author**

Rene Kizek, Department of Chemistry and Biochemistry, Mendel University in Brno, Zemedelska 1, CZ-613 00 Brno, Czech Republic, European Union; E-mail: kizek@sci.muni.cz; phone: +420-5-4513-3350; fax: +420-5-4521-2044

Abstract

Doxorubicin (DOX) is an effective anti-tumor drug employed for treatment of a wide range of cancers types such as neuroblastoma, osteosarcoma, breast and esophageal carcinomas. On the other hand, the cumulative dose is restricted (300-550 mg/m^2) and its amount administered to a patient has to be closely controlled due to its cardiotoxicity. To understand the mechanisms of the DOX side effects as well as to reveal the ways how to reduce its adverse impact on cardiomyocytes, the interactions with particular components of the blood and tissues have to be studied in greater details. In this work, microdialysis technique was optimized to extract DOX from samples and, subsequently monitor its interaction with bovine serum albumin (BSA). Finally, the microdialysis probe was on-line connected to the laser-induced fluorescence detector to ensure the real-time detection. The best flow rate was 1 μL/min and after 120 min of microdialysis 28% of the doxorubicin was dialyzed out from the sample. The results from investigation of the DOX-BSA interaction indicate that the interaction occurs in less than thirty minutes causing marked decrease in the amount of DOX extracted by microdialysis.

Keywords: anti-tumor drug; bovine serum albumin; capillary electrophoresis; doxorubicin; microdialysis

Introduction

Doxorubicin (Adriamycin, DOX), a water-soluble anthracenedione isolated from *Streptomyces peucetius* var. *caesius,* has been used in the cancer therapy for few decades [1]. It is employed to treat neuroblastoma, breast, thyroid, small cell lung, liver, and esophageal carcinomas, osteosarcoma, Kaposi's sarcoma, and soft-tissue sarcomas, Hodgkin's and non-Hodgkin's lymphomas, and acute lymphoblastic and myeloid leukemia [2, 3]. However, severe cardiotoxic effects of this antineoplastic drug significantly limit its application. Due to the planar structure of the anthracycline ring, DOX is able to 1) intercalate into the DNA double helix and interfere with the amplification process, and 2) form sequence-specific DNA adducts that are highly susceptible to cleavage by topoisomerase II [4]. Besides DOX antitumor activity, it is able to create reactive oxygen species leading to the oxidative stress which negatively affects the heart muscle tissue [5].

Due to the intravenous administration of the drug its interaction with blood components (blood cells, plasma proteins, proteins of the complement) is one of the most extensively studied topics during the pharmacokinetic characterization [6, 7]. Numerous studies have been carried out studying the interaction between DOX and bovine or human serum albumin [8-10]. Albumin is the most abundant protein in serum (40 g/L) that reversibly binds most of the drugs including DOX [11-13]. Subsequently, it provides a drug reservoir that is depleted when an unbound drug is metabolized in liver or excreted by glomerulal filtration in kidneys. Binding to albumin has also physiological significance in the transport, modulation and inactivation of metabolites and drug activities [12]. The main binding forces are hydrophobic and ion–ion interactions. Due to the fact, that albumin is an intrinsic element of the blood, its properties as perfect solubility, stability under the pH range of 4–9, preferential uptake in tumor and inflamed tissue, biodegradability, low toxicity, and immunogenicity make it an ideal candidate for drug delivery applications [14-16]. A number of nanocarriers, including albumin nanoparticles, has been utilized [17-20] to eliminate undesirable side effects of DOX, and also the protective effect of various substances including metalothionein against DOX cardiomyopathy has been found [21].

For all above-mentioned reasons, the attention is paid to the understanding of the drug-protein interactions. A number of methods including fluorescence spectrometry [8, 22],

circular dichroism [23, 24], and UV-Vis and infrared spectroscopy [23] have been utilized for investigation of DOX-albumin interactions. Separation techniques such as ultracentrifugation [25], ultrafiltration [10] and/or equilibrium dialysis, have been employed, too. The application of microdialysis for analysis of DOX has been also investigated [26-28], however the off-line detection has been employed. Microdialysis sampling was combined with flow-injection analysis (FIA) to investigate the streptomycin sulfate-albumin interaction using electrochemical [29] and chemiluminescence [30] detection.

In this work, the DOX-albumin interaction was investigated using microdialysis, fluorescence spectrometry and FIA with laser-induced fluorescence (LIF) detection. The interaction of DOX with bovine serum albumin (BSA) was studied taking advantage from fluorescence properties of DOX. Then, the microdialysis probe was on-line connected to the LIF detector to ensure the real-time detection and enabling low-sample volume analysis.

The proposed approach might be employed for online monitoring of the DOX level in the investigated tissue/blood. We believe that the free drug is responsible for the undesirable damage caused on the cardiomyocytes and, thus, the real-time monitoring of the free drug amount might serve as an indicator of the ability of the organism to metabolize it. The evaluation of this parameter individually for each patient might be helpful to determine the appropriate intervals between chemotherapeutic doses to avoid excessive exhaustion of the patient's organism and therefore to personalize the therapy specifically to the particular patient. Once this hypothesis is verified, the connection of the system to the miniaturized LIF detection system may be foreseen.

Material and Methods

Microdialysis arrangement

The CMA 4004 Syringe Pump (CMA, Holliston, Massachusetts, USA) with syringe Gastight 1750 (Hamilton Bonaduz AG, Bonaduz, Switzerland) was used for the pulseless dosage of perfusion fluid (1, 2 or 5 μL/min). Different perfusion fluids in this work were tested as follows: ACS water, Ringer´s solution (155 mM NaCl, 2.4 mM $CaCl_2$, and 5.6 mM KCl, pH 7.4 [31]) and Perfusion fluid T1 (Na^+ 147 mmol/L, K^+

4 mmol/L, Ca^{2+} 2.3 mmol/L, Cl^- 156 mmol/L, pH 6, osmolality: 290 mosm/kg; M Dialysis AB, Solna, Sweden). For the microdialysis the CMA 20 Elite probe (M Dialysis AB, Solna, Sweden) was used (membrane length: 4 mm, membrane diameter: 0.5 mm, material: Polyarylethersulphone, cut-off: 20 kDa). The dialysates (30 μL) were collected in the Refrigerated Fraction Collector CMA 470 (CMA Microdialysis AB, Solna, Sweden) set on 6 °C.

Fluorescence spectrometry detection

The concentration of DOX in dialysates was analyzed by fluorescence spectrometer Tecan infinite M200 PRO (Tecan, Grödig, Austria) on the NanoQuant plate™ (Tecan, Grödig, Austria). The sample of 2 μL was applied on the plate and fluorescence was determined using excitation filter: 480 nm and emission filter 600 nm. All measurement were five times repeated. The data were processed by Microplate Reader software i-control™ 1.9 (Tecan, Grödig, Austria).

On-line FIA-LIF detection of DOX

The outlet tube of the microdialysis probe was connected with an uncoated fused silica capillary (ID 75 μm) situated in an capillary electrophoretic instrument (Agilent technologies, Waldbronn, Germany) which allowed on-line FIA-LIF detection (ZetaLIF, Picometrics, Toulouse, France) of DOX in the sample (excitation wavelength 488 nm). The volume of the sample flowing through detection point as certain time is at the level of units of nanoliters. The temperature (25 °C or 37 °C) and shaking (300 rpm) was controlled by Thermomixer® comfort (Eppendorf, Germany). The interaction of DOX (125 μg/mL) with BSA (5 mg/mL; 15 mg/mL or 25 mg/mL) in volume ratio 1:1 was investigated. The final molar ratio of DOX and BSA was 2:1, 1:1 or 1:2.

Microdialysis of DOX from the chicken embryo

The fertilized eggs of Lankenfeld roosters and ISA Brown hens (Integra, a.s., Czech Republic) were incubated in the incubator RCom 50 MAX (Gyeongman, Korea) with temperature (37.5 °C) and humidity control (45% rH). After the 17 days of the incubation, the embryos. Subsequently, the embryo was taken out of the shell and the microdialysis probe was inserted into the liver tissue. The fluorescence signal of the

liver tissue was detected on-line by LIF detection. The recovery of DOX from the liver tissue was analyzed after its application (60 μg/mL, 100 μL) into the liver tissue.

Ethics Committee of Mendel University approved animal experiment according to resident governmental legislation. Reference number of accreditation is 5789012012-MZE-I7214. To minimize the distress, an opening into the air cell of the egg was made and the egg was placed into a chamber with inhaled anaesthetics for 20 minutes.

Statistical evaluation

Data were processed by using MICROSOFT EXCEL® (USA) and STATISTICA.CZ Version 8.0 (Czech Republic). Results are expressed as an average ± standard deviation (S.D.) unless noted otherwise (EXCEL®).

Results and Discussion

Microdialysis optimization

The microdialysis technique offers several advantages including low invasiveness and real-time *in vivo* monitoring of analyte presence in a target tissue/blood. However, several disadvantages including time-consuming analysis, a low sample volume and low analyte concentration limiting its application have to be mentioned [32, 33]. Several key parameters play a crucial role in the reliable and reproducible utilization of this method. In this work, the perfusion solution composition was tested to obtain the optimal DOX fluorescence signal. Three solutions such as Ringer´s solution, perfusion solution T1 and ultra-pure water were tested (Fig. 1A). Based on the results obtained, it can be concluded that employing of the ultra-pure water led to the significantly higher signals especially during longer dialysis times compared to the solutions containing high amount of ions. Perfusion solution T1 caused a 27% decrease in fluorescence signal and Ringer´s solution caused a 30% decrease compared to water. For this reason, all experiments were carried out using ultra-pure water as the perfusion solution.

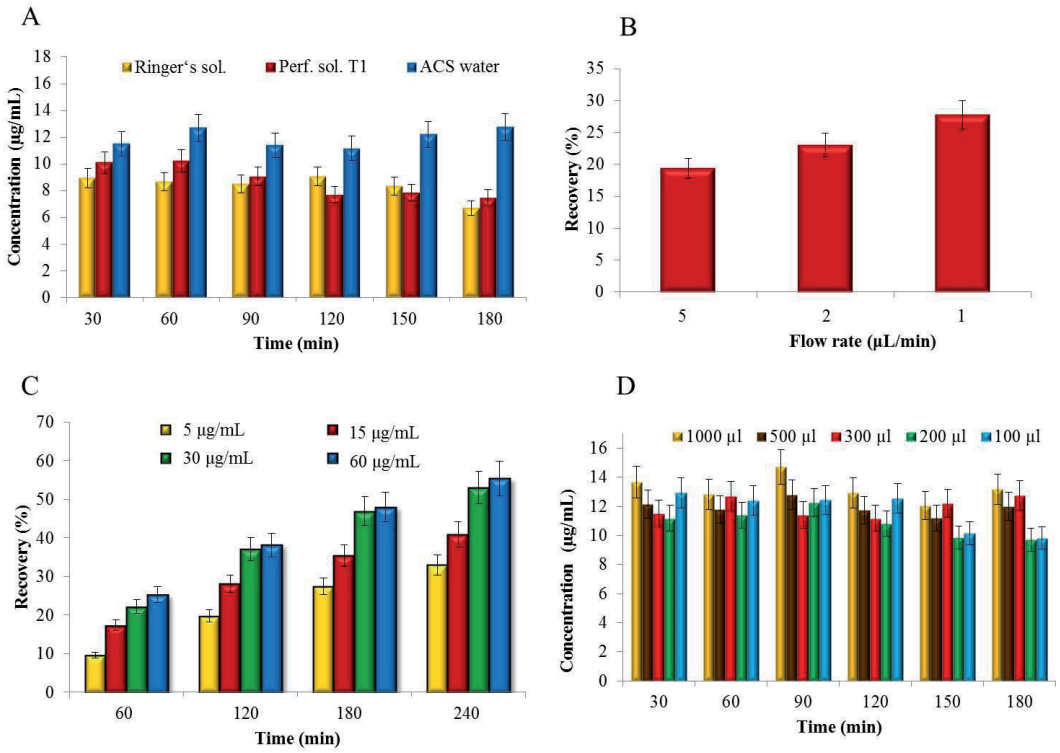

Figure 1. Optimization of the DOX microdialysis: A) Fluorescence intensity of the DOX in dialysates after the 30 – 180 minutes of the dialysis using different perfusion fluids. The efficacy of Ringer´s solution, perfusion solution T1 and ultra-pure water (ACS) were compared (flow rate: 1 µL/min, one fraction: 30 µL, sample volume: 500 µL, DOX concentration: 65 µg/mL); B) Recovery of DOX with different flow rates (1, 2, 5 µL/min) of perfusion fluid (perfusion fluid: ultra-pure water, total dialysis time: 120 minutes, sample volume: 50 µL, DOX concentration: 65 µg/mL). The recovery was calculated as a ratio of DOX mass extracted to original DOX mass in sample; C) Recovery of different DOX concentrations (5; 15; 30; 60 µg/mL). The recovery was calculated after 60 – 240 minutes (perfusion fluid: ultra-pure water, flow rate: 1 µL/min, sample volume: 50 µl, DOX concentration: 62.5 µg/mL); D) Fluorescence intensity of DOX in individual dialysates using different sample volume (100, 200, 300, 500 and 1000 µg/mL). The perfusion fluid ultra-pure water was used (flow rate: 1 µL/min, one fraction: 30 µL, DOX concentration: 65 µg/mL).

The second parameter, which has to be optimized, is the fluid flow rate. The recovery was calculated as a ratio of DOX mass extracted and DOX mass in microdialyzed solution (the solution used as a sample). As it is shown in Fig. 1B, the recovery of the analyte is inversely proportionate to the flow rate. This finding is in agreement with the previously published results by de Lange *et al*. [32]. The highest DOX recovery was

obtained using the flow rate of 1 μL/min. After 120 minutes of dialysis, the recovery of 28%, 23% and 19% of DOX was reached using flow rate of 1 μL/min, 2 μL/min and 5 μL/min, respectively.

Subsequently, the recovery of DOX from solutions with five different concentrations (5, 15, 30 and 60 μg/mL) was determined (Fig. 1C). As expected, the increasing DOX concentration led to the higher recovery rates. The recovery of 33% and 41% (after 240 minutes of microdialysis process) was reached for 5 and 15 μg/mL, respectively. The recovery over 50% was reached for 30 μg/mL (53%) and 60 μg/mL (55%). The concentration of 60 μg/mL was chosen for all further experiments.

In our experiments, we also found out that the volume of the sample (microdialyzed solution) played a significant role. The comparison of microdialysis from different volumes of DOX solution (60 μg/mL) is shown in Fig. 1D. The tested volumes were 100, 200, 300, 500 and 1000 μL. As it is shown, in the case of 100 and 200 μL, after 180 min of dialysis, the signal decreased for 20% compared to 1000 μL. For these reasons, further experiments were carried out using the sample volume of 500 μL. This volume exhibited significantly more stable concentrations in terms of long-term (180 min) microdialysis process.

DOX-BSA interaction

Due to the fact that majority of drugs is administered intravenously; their interaction with blood components is a key factor for their distribution in organisms. Human serum albumin (HSA) and BSA are the most studied serum albumin proteins from the point of views of their interaction with drug. These proteins are homologous from 76% and a repeating pattern of disulfides in their molecules is conserved. The major difference between these proteins is in the number and position of tryptophan residues in their structure. HSA has only one tryptophan at position 214 equivalent to tryptophan located at position 212 for BSA, which is hidden in a hydrophobic pocket at subdomain IIA. BSA has one more additional tryptophan at position 134, which is more exposed to solvent. According to Finlay *et al*. [9], HSA binds DOX approximately twice as strongly as BSA. The data from the literature show that the number of drug molecules bound to the molecule of BSA is 1.5 [23]. Therefore, to investigate the DOX-BSA interaction, mixtures of DOX and protein in different molar ratios were prepared. DOX

solution (125 µg/mL) was mixed with BSA solution (5 mg/mL; 15 mg/mL or 25 mg/mL) in a volume ratio of 1:1, the final molar ratio of DOX and BSA was 2:1, 1:1 or 1:2. One aliquot of each solution underwent the microdialysis process and the second was left to interact for 24 hours at 25 °C and subsequently microdialyzed. The results are summarized in Fig. 2. As expected, a substantial portion of DOX interacted with BSA and even after immediate microdialysis a significant decrease in detected signal was observed. These results indicate that the interaction occurs in less than thirty minutes. In the case of DOX+BSA 2:1 the signal decrease in the first 30 minutes (dark orange column) was 70%. Similarly, the decrease in 78% and 81% were in the case of DOX+BSA 1:1 (dark purple) and DOX+BSA 1:2 (dark green), respectively.

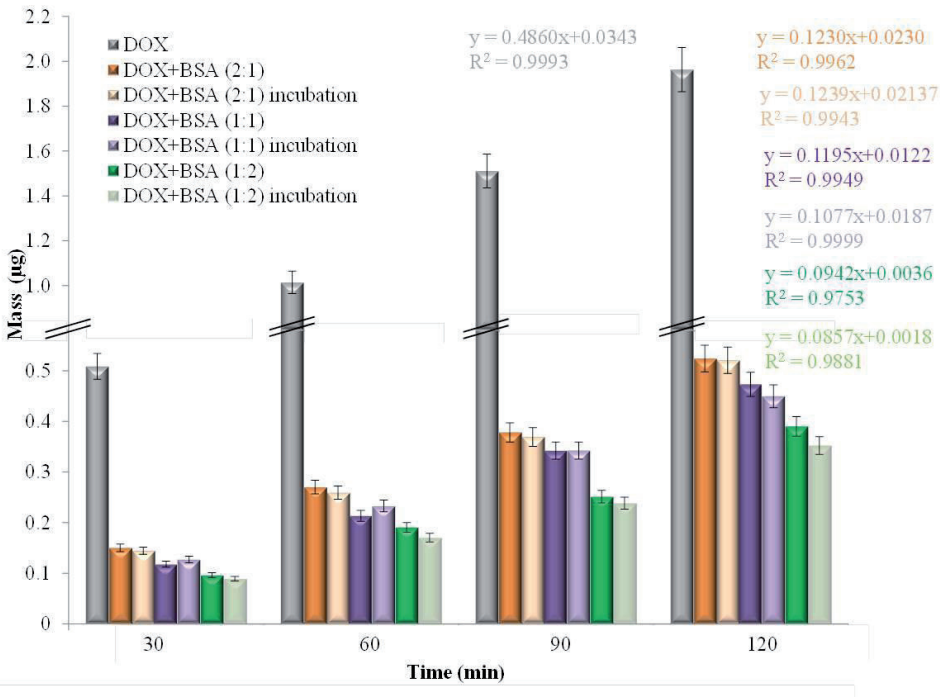

Figure 2. The mass of DOX dialyzed after its interaction with BSA (0 and 24 hours). DOX at a concentration of 125 µg/mL was incubated with BSA (5 mg/mL; 15 mg/mL or 25 mg/mL) in a volume ratio of1:1, the final molar ratio of DOX to BSA was 2:1, 1:1 or 1:2. Total microdialyzed mass of DOX was calculated after 30 – 120 minutes of dialysis (flow rate: 1 µL/min, perfusion fluid: ultra-pure water). Other experimental details see in Fig. 1.

A long-term incubation of DOX with BSA (24 hours) had no significant effect on the fluorescence signal (lighter columns compared to darker columns). In addition, it is shown that the excess of the protein in the mixture (green columns) led to higher

decrease compared to the case of excess of DOX (orange columns). As expected, the higher amount of the protein present in the mixture, the more DOX molecules interact and are unable to pass through the membrane. However, it has to be noted that the effect of adsorption of BSA molecules on the membrane surface may play a role, too.

On-line coupling of microdialysis with laser-induced fluorescence detection

In *in vivo* experiments employing the microdialysis technique, the detection method with high sensitivity and very low sample consumption is required. Furthermore, the real-time detection is valuable for analyses of rapid processes with fast kinetics. The combination of all these benefits was found in application of the laser-induced fluorescence detection in capillary format. The detector conventionally used for capillary electrophoresis (CE) with LIF detection was utilized in a FIA mode. The conventional capillary with internal diameter of 75 μm was connected to the outlet tubing of the microdialysis probe. The coupling device was optimized to prevent leaking of the perfusate and ensure the quantitative transfer of the fluid. The scheme of the whole system is shown in Fig. 3A. The capillary passed the detection point in a similar way as in standard capillary electrophoretic analysis and continued to the outlet vial, which can be utilized either as a waste container or as a fraction collector for subsequent analysis of the sample. The DOX analysis using this system was demonstrated by standard DOX solution with a concentration of 60 μg/mL. Fig. 3B shows a typical record of the real-time FIA-LIF. The flow rate was kept at 5 μL/min because the sensitivity of the detection was sufficient for monitoring of the functionality of the system. The DOX solution was microdialysed using ultra-pure water and after the signal stabilization, the temperature of the sample was increased from 25 °C to 37 °C. The trace is demonstrating not only the fact that microdialysis process is strongly dependent on temperature but also the benefits of the real-time mode of the analysis. The increase in the temperature by 12 °C caused the signal increase for 85%. Moreover, it was found that shaking of the sample vial during the dialysis process led to even a higher increase in the signal due to the enhanced ion exchange on the microdialysis probe surface (Fig. 3C). It can be concluded that the combination of elevated temperature and shaking caused the total increase of the fluorescent signal for 130%.

Under optimized conditions LOD of 70±8 ng/mL of DOX was determined. When the volume of the sample passing the detection window (nanoliters) is taken into account, the sub-picogram amount of DOX is detected.

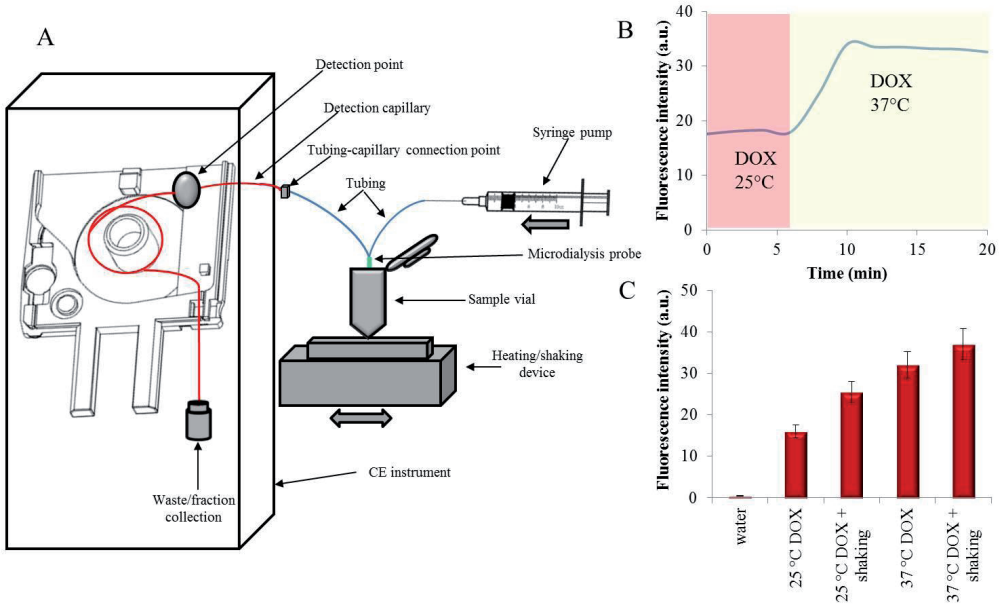

Figure 3. A) The scheme of the on-line DOX fluorescence detection (flow rate: 5 µL/min, perfusion fluid: ultra-pure water, temperature: 25 or 37 °C, DOX concentration: 65 µg/mL); B) On-line detection of DOX in the sample tempered to 25 or 37 °C; C) Fluorescence of DOX in the samples after its dialysis in different conditions (temperature: 25 or 37 °C, rest or shaking the solution). Other experimental details see in Fig. 2

As the next step, the microdialysis-FIA-LIF system was tested on *ex vivo* model – chicken embryo. The microdialysis probe was directly inserted into the liver tissue of the embryo and a real-time FIA-LIF signal was monitored (Fig. 4A). The detected trace is shown in Fig. 4B. After washing the probe in water (red area of the plot) the probe was inserted into the liver tissue (yellow area of the plot). The increase in the signal is caused by molecules microdialyzed from the liver tissue passing through the dialysis membrane (cut-off: 20 kDa), which exhibit fluorescent properties after excitation with 488 nm such as riboflavin. After stabilization of the signal, the tissue in the near proximity of the probe was spiked by 100 µL of standard solution of DOX (65 µg/mL) (blue area of the plot). The increase of the LIF signal is caused by the dialyzed DOX. This experiment was designed as a proof of concept and therefore the microdialysis was carried out using animal *post mortem* and the DOX standard solution was injected

straight into the liver tissue. The results proved that the detection is sensitive enough and sufficiently stable for this type of experiments and the work can be moved forward to the *in vivo* analyses.

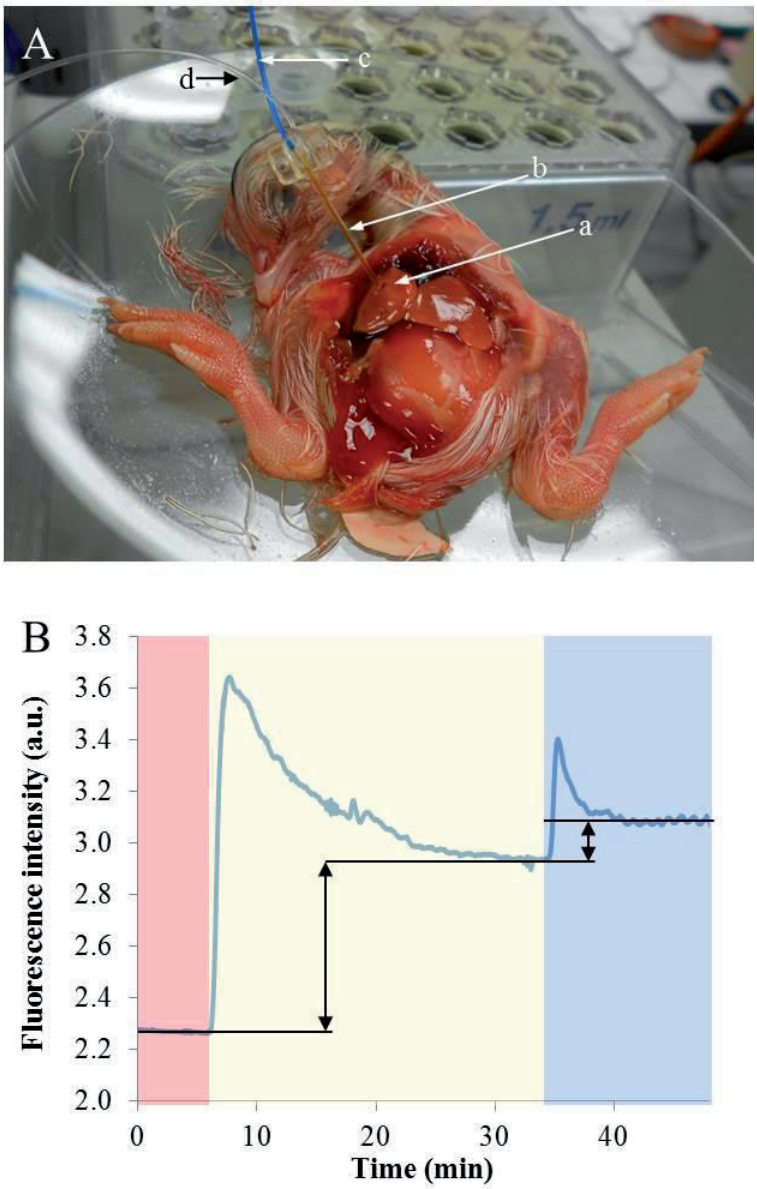

Figure 4. Dialysis of DOX from chicken embryo liver tissue: A) Image of chicken embryo with introduced microdialysis probe into the right lobe of liver (a – liver tissue, b – microdialysis probe, c – perfusate inlet, d – perfusate outlet; B) On-line record of fluorescence intensity detected after washing the probe by water (red area of the plot) and fluorescence intensity after the probe was inserted into the right lobe of liver (yellow area of the plot). After stabilization of the signal the tissue in the near proximity of the probe was spiked by 100 µL of standard solution of DOX (65 µg/mL) (blue area of the plot). Microdialysis set up was as follows - flow rate: 5 µL/min, perfusion fluid: ultra-pure water.

Conclusions

The microdialysis technique is beneficial for *in vivo* applications and in a combination with sensitive real-time detection by laser-induced fluorescence in low-volume format, this method provides high potential for analysis of a number of fluorescent analytes such as other anthracyclines, ellipticine or VP16. This feature may increase the number of options for investigation of interactions of these compounds with biological fluids as well as their distribution in specific tissues during pharmacokinetic studies.
Finally, the analysis of the amount of the free (unbound) drug level in real-time and individually for each patient may help to personalize the therapy.

Acknowledgement

The financial support from Grant agency of Czech Republic (CYTORES P301/10/0356), FR 940/2013/Aa and by the Ministry of Health of the Czech Republic for conceptual development of research organization 00064203 (University Hospital Motol, Prague, Czech Republic) is highly acknowledged. Author would like to acknowledge the assistance of Mr. Petr Kriz.

Conflict of interest

Authors declare no conflict of interest.

References

[1] Kizek, R., Adam, V., Hrabeta, J., Eckschlager, T., Smutny, S., Burda, J. V., Frei, E., Stiborova, M., *Pharmacol. Ther.* 2012, *133*, 26-39.

[2] Singal, P. K., Iliskovic, N., *N. Engl. J. Med.* 1998, *339*, 900-905.

[3] Poljakova, J., Eckschlager, T., Hrebackova, J., Hrabeta, J., Stiborova, M., *Interdiscip Toxicol* 2008, *1*, 186-189.

[4] Stiborova, M., Poljakova, J., Eckschlager, T., Kizek, R., Frei, E., *Biomed. Pap.* 2012, *156*, 115-121.

[5] Sarvazyan, N., *Am. J. Physiol.-Heart Circul. Physiol.* 1996, *271*, H2079-H2085.

[6] Bertrand, N., Leroux, J. C., *J. Control. Release* 2012, *161*, 152-163.

[7] Karmali, P. P., Simberg, D., *Expert Opin. Drug Deliv.* 2011, *8*, 343-357.

[8] TryndaLemiesz, L., Kozlowski, H., *Bioorg. Med. Chem.* 1996, *4*, 1709-1713.

[9] Finlay, G. J., Baguley, B. C., *Cancer Chemother. Pharmacol.* 2000, *45*, 417-422.

[10] Chassany, O., Urien, S., Claudepierre, P., Bastian, G., Tillement, J. P., *Cancer Chemother. Pharmacol.* 1996, *38*, 571-573.

[11] Mehrotra, R., Duong, U., Jiwakanon, S., Kovesdy, C. P., Moran, J., Kopple, J. D., Kalantar-Zadeh, K., *Am. J. Kidney Dis.* 2011, *58*, 418-428.

[12] Day, Y. S. N., Myszka, D. G., *J. Pharm. Sci.* 2003, *92*, 333-343.

[13] Wang, Z. M., Ho, J. X., Ruble, J. R., Rose, J., Ruker, F., Ellenburg, M., Murphy, R., Click, J., Soistman, E., Wilkerson, L., Carter, D. C., *Biochim. Biophys. Acta-Gen. Subj.* 2013, *1830*, 5356-5374.

[14] Kratz, F., *J. Control. Release* 2008, *132*, 171-183.

[15] Lohcharoenkal, W., Wang, L. Y., Chen, Y. C., Rojanasakul, Y., *Biomed Res. Int.* 2014, 1-13.

[16] Jahanshahi, M., Babaei, Z., *Afr. J. Biotechnol.* 2008, *7*, 4926-4934.

[17] Blazkova, I., Nguyen, V. H., Dostalova, S., Kopel, P., Stanisavljevic, M., Vaculovicova, M., Stiborova, M., Eckschlager, T., Kizek, R., Adam, V., *Int. J. Mol. Sci.* 2013, *14*, 13391-13402.

[18] Blazkova, I., Nguyen, V. H., Kominkova, M., Konecna, R., Chudobova, D., Krejcova, L., Kopel, P., Hynek, D., Zitka, O., Beklova, M., Adam, V., Kizek, R., *Electrophoresis* 2014, *35*, 1040-1049.

[19] Konecna, R., Nguyen, V. H., Stanisavljevic, M., Blazkova, I., Krizkova, S., Vaculovicova, M., Stiborova, M., Eckschlager, T., Zitka, O., Adam, V., Kizek, R., *Chromatographia* 2014, *77*, 1469-1476.

[20] Tmejova, K., Hynek, D., Kopel, P., Dostalova, S., Smerkova, K., Stanisavljevic, M., Nguyen, V. H., Nejdl, L., Vaculovicova, M., Krizkova, S., Kizek, R., Adam, V., *Int. J. Electrochem. Sci.* 2013, *8*, 12658-12671.

[21] Li, Y., Chen, Z. W., Gu, N., *Chin. Sci. Bull.* 2012, *57*, 3972-3978.

[22] Bi, S. Y., Sun, Y. T., Qiao, C. Y., Zhang, H. Q., Liu, C. M., *J. Lumines.* 2009, *129*, 541-547.

[23] Agudelo, D., Bourassa, P., Bruneau, J., Berube, G., Asselin, E., Tajmir-Riahi, H. A., *PLoS One* 2012, *7*, 1-13.

[24] Zsila, F., *Mol. Pharm.* 2013, *10*, 1668-1682.

[25] Demant, E. J. F., Jensen, P. B., Sehested, M., *BBA Protein Proteom* 1991, *1118*, 83-90.

[26] Whitaker, G., Lunte, C. E., *J. Pharm. Biomed. Anal.* 2010, *53*, 490-496.

[27] Buitrago, E. F., Otamendi, E., Opezzo, J., Hocht, C., Bramuglia, G., *Ther. Drug Monit.* 2011, *33*, 550-550.

[28] Kitazawa, H., Sato, H., Adachi, I., Masuko, Y., Horikoshi, I., *Biol. Pharm. Bull.* 1997, *20*, 278-281.

[29] Shi, G. Y., Xu, F., Zhou, H. G., Mao, L. Q., Jin, L. T., *Anal. Chim. Acta* 1999, *386*, 123-127.

[30] Huang, Y. M., Zhang, Z. J., Zhang, D. J., Lv, J. G., *Talanta* 2001, *53*, 835-841.

[31] Song, Y., Lunte, C. E., *Anal. Chim. Acta* 1999, *379*, 251-262.

[32] de Lange, E. C. M., de Boer, A. G., Breimer, D. D., *Adv. Drug Deliv. Rev.* 2000, *45*, 125-148.

[33] Dahlin, A. P., Wetterhall, M., Caldwell, K. D., Larsson, A., Bergquist, J., Hillered, L., Hjort, K., *Anal. Chem.* 2010, *82*, 4376-4385.

5.2 The utilization of NPs in DOX transport

The next step of the study was the conjugation of DOX with NPs and the investigation of properties and behaviour of these nanoconstructs in *in vitro* and *in vivo* system. We focused our attention to the only approved nanotransporters for DOX application in the clinics – liposomes. Promising materials, which could be possibly used in medical practise, are carbon nanostructures. Hence we targeted on spherical materials enabling the cage up of drugs – fullerene.

5.2.1 Research article III

KOMINKOVA, M.; GURAN, R.; MERLOS, M.A.R.; KOPEL, P.; **BLAZKOVA, I.**; CHUDOBOVA, D.; NEJDL, L.; HEGER, Z.; RUTTKAY-NEDECKY, B.; ZITKA, O.; ADAM, V.; KIZEK, R. Study of Functional Qualities of Different Types of Tailored Liposomes with Encapsulated Doxorubicin using Electrochemical and Optical Methods. *International Journal of Electrochemical Science*, 2014. 9(6): p. 2993 – 3007. ISSN 1452-3981.

Participation in the manuscript preparation of the author Blažková, I.: 20%.

In order to reduce undesirable side effects of cytostatics, different nanomaterials are intensively studied. But till the date only a few of them pass the clinical trials (Martin Sabroso and Torres-Suarez 2014). In clinical practise are used liposomes, albumin-bond NPs, polymeric micellar NPs, PEGylated liposome and asparaginase and poly(styrene-co-maleic acid)-conjugated neocarzinostatin (Sun, Zhang et al. 2014). Liposomes are the only NPs approved for the use in combination with DOX. Their big advantage is the biocompatibility and the similarity with biological membranes (Barenholz and Peer 2012), the extended circulation half-life (Lowery, Onishko et al. 2011) and decrease in cardiotoxicity while keeping its antiproliferative effect (Batist, Ramakrishnan et al. 2001; Gyoengyoesi, Maurer et al. 2014).

The aim of this work was to study of the liposomes properties. The liposomes were synthetized with different content of cholesterol in the lipid bilayer and the effect of sodium dodecyl sulphate (SDS) on DOX release was assessed in this work. The toxicity, electrochemical properties and fluorescence of nanoconstruct were characterized. Different concentrations of DOX (0, 25, 50 and 100 μg/ml) were encapsulated into the liposomes with different concentration of cholesterol. Liposome 8 contained 100 mg of cholesterol, liposome 9 contained 50 mg of cholesterol and liposome 10 did not contain cholesterol. The encapsulation of DOX into the liposome was confirmed by matrix-assisted laser desorption/ionization time of flight mass spectrometry, high performance liquid chromatography with electrochemical detection and fluorescence microscopy. The characterization of DOX encapsulated in liposomes toxicity consisted of growth curves determination with the utilization of bacterial culture *Staphylococcus aureus* and specification of half maximal inhibitory concentration (IC50). IC50 represents the concentration of a drug that is required for 50% inhibition of bacterial culture. Liposome

10 showed the highest toxicity for bacterial cells (IC50: 2.5 to 3.3 μM). Cholesterol remarkably protected bacterial culture of *Staphylococcus aureus* from DOX toxicity. For DOX determination, flow injection analysis with electrochemical detection was optimized. Cholesterol probably has a role in the improvement of electrochemical detection of encapsulated DOX, but this improvement has a limitation factor in concentration of cholesterol. After opening of liposomes cages by SDS, the highest fluorescence intensity of DOX was detected in the liposome 10. Cholesterol decreases the fluorescence signal of DOX and can significantly affect the properties of liposomes and transport of these NPs in the body.

Int. J. Electrochem. Sci., 9 **(2014)** 2993 - 3007

International Journal of
ELECTROCHEMICAL
SCIENCE
www.electrochemsci.org

Study of Functional Qualities of Different Types of Tailored Liposomes with Encapsulated Doxorubicin using Electrochemical and Optical Methods

Marketa Kominkova[1], Roman Guran[1], Miguel Angel Merlos Rodrigo[1], Pavel Kopel[1,2], Iva Blazkova[1], Dagmar Chudobova[1], Lukas Nejdl[1], Zbynek Heger[1], Branislav Ruttkay-Nedecky[2], Ondrej Zitka[1,2], Vojtech Adam[1,2], Rene Kizek[1,2]*

[1] Department of Chemistry and Biochemistry, Faculty of Agronomy, Mendel University in Brno, Zemedelska 1, CZ-613 00 Brno, Czech Republic, European Union
[2] Central European Institute of Technology, Brno University of Technology, Technicka 3058/10, CZ-616 00 Brno, Czech Republic, European Union
[*]E-mail: kizek@sci.muni.cz

Received: 3 January 2014 / *Accepted:* 31 January 2014 / *Published:* 23 March 2014

This study points to changes in the properties of liposomes and its functional qualities in task of release of encapsulated drug doxorubicin according to the content of cholesterol in the phospholipid bilayer. The influence of sodium dodecyl sulphate (SDS) addition to liposomal variants was also evaluated too. Three variants of liposomes differing in various concentrations of cholesterol were assessed. Firstly, we focused on the toxicity of all liposomal variants to *Staphyloccocus aureus* and it was found that the content of cholesterol increases the IC_{50} values of encapsulated doxorubicin in liposome with higher concentration of cholesterol than in liposome without cholesterol even four times. Further, the new approach to comparing the influence of various liposomes on detection of encapsulated doxorubicin using the electrochemical detection with construction of differential hydrodynamic voltammograms was used. Finally, the fluorescence detection was used to confirm the release of encapsulated doxorubicin from liposomes after the addition of detergent SDS. In this work we demonstrated the suitability of number of methods including electrochemistry for studying of effect of substances such substance as SDS and cholesterol on the lipid functional qualities.

Keywords: Liposome; Cholesterol; Doxorubicin; Sodium Dodecyl Sulphate; Drug Delivery; Drug Encapsulation;

1. INTRODUCTION

Since liposomes were discovered in the 1960s [1], these phospholipidic structures have been studied intensively for their potential to serve as the vehicles for drug transportation. Liposomes are

particles with lipid bilayer enclosing a vesicular space wearing a range of attractive properties including the ability to encapsulate aqueous solutions within the liposome core, sequester lipophilic compounds within the bilayer, and support tailored surface chemistries of the liposomes for targeted delivery [2], however, the most common drug carriers are currently pegylated liposomes which have an immobilised polyethylene glycol on their surface [3,4]. When using liposomes, particularly the pegylated ones, it is possible to achieve prolonged persistence of the drug in the body and to reduce the degradation of drug in the liver, which leads to reduction of the negative effects on the organism while the antitumor efficacy is maintained [5]. For using of liposomes as transporters in anticancer therapy, their ability to aggregate, open and release the drug at the place of interest is necessary. However, this has not been completely resolved yet [3,6].

The release of drug from the liposomes is based on the fusion with its membrane, but the newly appearing option, e.g. sonication, through which the drug is released, can be also used [4,7,8]. Pharmacokinetic properties of the liposomes are given by their physicochemical properties [9,10]. These attributes can be significantly affected by the change of the composition of the lipid bilayer and by the addition of other substances to this structure. The predominant ingredients used in their preparation are glycerophospholipids, sphingolipids and cholesterol [11]. These components give the liposomes a similarity to natural cell membranes [11]. The cholesterol present in the structure of liposomes supports their stability and enables the control of permeability and solubility of the liposome membrane [12,13]. Amphiphilic ends of cholesterol in the lipid bilayer are oriented as parallel with the carbon chains of lipids and carboxyl groups of the aqueous phase [14]. Besides medical applications liposomes can also be used for analytical purposes. Recently, a number of methods based on liposomes have been developed including immobilised liposome chromatography (ILC) [15,16], liposome capillary electrophoresis (LCE) [17,18], biosensors [19] and liposome immunosorbent assay (LISA) [20-22].

In this article we focused our attention on studying of properties of synthesized liposomes, which differed in the content of cholesterol in the lipid bilayer, and on the possibilities of opening these liposomes after addition of sodium dodecyl sulphate (SDS).

2. EXPERIMENTAL PART

2.1. Chemicals and pH measurement

Cholesterol, 1,2-dioleoyl-sn-glycero-3-phospho-rac-(1-glycerol) sodium salt, chloroform, doxorubicin·HCl, sodium dodecyl sulphate (SDS) and water were purchased from Sigma-Aldrich (St. Louis, MO, USA) in ACS purity. Hydrogenated phosphatidylcholine from soybean was obtained from Lipoid GMBH (Ludwigshafen, Germany). The deionised water was prepared using reverse osmosis equipment Aqual 25 (Aqual s.r.o., Brno, Czech Republic). The deionised water was further purified by using MiliQ Direct QUV apparatus equipped with the UV lamp from Millipore (Billerica, MA, USA). The output resistance was 18 MΩ. The pH was measured using pH meter WTW inoLab (Weilheim, Germany).

2.2. Liposomes

2.2.1. Preparation of liposomes

Liposome 8: cholesterol (100 mg), 1,2-dioleoyl-sn-glycero-3-phospho-rac-(1-glycerol) sodium salt (100 mg) and phosphatidylcholine (100 mg) were dissolved in chloroform (4.5 ml). A lipid film was obtained by rotary evaporation of solvent and residual chloroform was blown out by nitrogen.

Liposome 9: cholesterol (50 mg), 1,2-dioleoyl-sn-glycero-3-phospho-rac-(1-glycerol) sodium salt (100 mg) and phosphatidylcholine (100 mg) were dissolved in chloroform (3.75 ml). A lipid film was obtained by rotary evaporation of solvent and residual chloroform was blown out by nitrogen.

Liposome 10: 1,2-dioleoyl-sn-glycero-3-phospho-rac-(1-glycerol) sodium salt (100 mg) and phosphatidylcholine (100 mg) were dissolved in chloroform (3.75 ml). A lipid film was obtained by rotary evaporation of solvent and residual chloroform was blown out by nitrogen.

2.2.2. Preparation of encapsulated doxorubicin

Solutions containing 0, 6.25, 12.5 and 25 µl of doxorubicin·HCl (2 $mg.ml^{-1}$) in 0.5 ml of water were added to liposomes (10 mg). Samples were homogenized in ultrasonic bath Sonorex Digital 10P (Bandelin, Berlin, Germany) for 15 min. The homogenized mixtures were then heated and shaken for 15 min at 60 ºC at Thermomixer Comfort (Eppendorf). The samples were then washed several times with Britton-Robinson buffer (pH = 10) on Amicon 3k (Millipore). Final volume of samples was 0.5 ml.

2.2.3. The analysis of cholesterol amount in liposomes

200 µl of reagent R1 (Greiner, Germany, 0.3 mM 4-aminoantipyrine, 5 mM phenol, peroxidase 3.0 $kU.l^{-1}$, cholesterol esterase 200 $U.l^{-1}$, cholesterol oxidase 100 $U.l^{-1}$ in 50 mM Good's buffer, pH 6.7) were pipetted into the cuvette, then 2 µl of measured sample were added. The three samples of liposomes (8, 9 and 10) with concentration of encapsulated doxorubicin 0, 25, 50 and 100 $\mu g.ml^{-1}$ were used for measurement. Absorbance was measured for 6 minutes at 505 nm. To calculate the absorbance of sample the absorbance values of reagent R1 and absorbance values after 6 minutes of incubation with the sample were used.

2.3. Fluorescence photography

Fluorescence monitoring was performed using an In vivo Xtreme system by Carestream Health Inc. (Rochester, NY, USA). This instrument was equipped with a 400 W xenon light source. Emitted light was captured by 4 MP CCD detector. The excitation wavelength was set at 480 nm and the emission was measured at 600 nm. The exposure time was 2 s, binning – 2 x 2 pixels, fStop - 1.1, field of view – 17.5 × 17.5 cm. Samples (100 µl) were placed in a Nunc MaxiSorp® flat-bottom 96 well plate (Thermo Fisher Scientific, Roskilde Denmark).

2.4. Fluorescence microscopy

Bacterial culture of *Staphylococcus aureus* was observed, after the incubation with doxorubicin in liposome, by fluorescence microscope. The bacterial culture (250 µl) was incubated with 50 µl of doxorubicin (100 $\mu g.ml^{-1}$) in liposome (liposome 8, 9 and 10). After the incubation (24 hours, 37 °C), the culture was washed with PBS buffer (0.24 $g.l^{-1}$ KH_2PO_4, 1.44 $g.l^{-1}$ $Na_2HPO_4.2H_2O$, 8 $g.l^{-1}$ NaCl, 0.2 $g.l^{-1}$ KCl) two times. The culture was stirred with 1 ml of PBS buffer and centrifuged (20 °C, 6000 g, 10 min). Supernatant was removed and procedure was repeated. Finally the cells were stirred in 100 µl of PBS.

The cells obtained were pipetted (5 µl) on the microscope slide and covered by cover slip. The sample was placed by coverslip down and the immersion oil was used. The objective (PlanFLN; Mag. 100x; NA 1,3; F.N. 26.5) and the magnification lens 1.6x was used, and the total magnification was 1600x. The inverted research fluorescence microscope Olympus IX71S8F-3 (Olympus Corporation, Tokyo, Japan) was used. The images were captured by Olympus Camera DP73 and processed by Olympus Stream Basic 1.7 Software. The images resolution was 4800 x 3600 pixels. The parameters for the ambient light images were following: exposure time – 2.2 ms and ISO 200. Fluorescence of the doxorubicin was detected using excitation filter – 520 - 550 nm and emission filter – 580 nm; exposure time: 530.8 ms, ISO 100.

2.5. Matrix-assisted laser desorption/ionization time of flight mass spectrometry

Matrix-assisted laser desorption/ionization time of flight mass spectrometric (MALDI-TOF MS) experiments were performed on a MALDI-TOF/TOF mass spectrometer Bruker ultrafleXtreme (Bruker Daltonik GmbH, Germany) equipped with a laser operating at wavelength of 355 nm with an accelerating voltage of 25 kV, cooled with nitrogen and a maximum energy of 43.2 µJ with repetition rate 2000 Hz in linear and positive mode, and with software for data acquisition and processing of mass spectra flexControl version 3.4 and flexAnalysis version 2.2. The matrix used in the MALDI method was 2,5-dihydroxybenzoic acid (DHB) (Sigma-Aldrich, USA). The saturated matrix solution was prepared in 50% methanol and 0.1% trifluoroacetic acid (TFA). Mixture was thoroughly vortexed and ultrasonicated using Bandelin 152 Sonorex Digital 10P ultrasonic bath (Bandelin electronic GmbH, Germany) for two minutes at 50% of intensity at room temperature. Sample preparation crystallization method for MALDI-TOF was dried-droplet method (DD) as the sample solutions for analysis were mixed with matrix solution in volume ratio of 1:1. After obtaining a homogeneous solution, 2 µl was applied on the MTP 384 polished steel target plate (Bruker) and dried under atmospheric pressure at room temperature. A mixture of peptide calibration standards (Bruker) was used to externally calibrate the instrument. The preparation yielded relatively large crystals on the target surface as well as regions without matrix or analyte. All measurements were performed in the reflector positive mode in the m/z range 0-1200 Da. The MS spectra were typically acquired by averaging 500 sub spectra from a total of 500 shots of the laser (Smartbeam 2. Version: 1_0_38.5) with laser power of 60-75 %.

2.6. Growth curves of Staphylococcus aureus treated with doxorubicin in liposomes

To determine the antimicrobial activity of doxorubicin encapsulated in liposomes and doxorubicin released from liposomes after the addition of SDS, the evaluation of antimicrobial effect of tested compounds on bacterial culture of *Staphylococcus aureus* was performed on Multiskan EX (Thermo Fisher Scientific, Germany). 24-hour grown bacterial culture was diluted with Luria Bertani medium (10 g/l tryptone, 5 g/l yeast extract, 5 g/l NaCl; Sigma-Aldrich, St. Louis, MO, USA) in spectrophotometer Specord 210 (Analytik Jena, Germany) and the absorbance was measured at a wavelength of 600 nm to absorbance 0.1. This diluted culture was pipetted into the microplate in various combinations with tested samples or separately as a control measurement. The ratio of bacterial culture to tested sample was 5:1 (250 µl of bacterial culture and 50 µl of sample). The total volume in the microplate wells in microplate was therefore always 300 µl. Measurements were carried out at starting time 0, then at each half-hour intervals for 24 hours, at 37 °C and at wavelength of 600 nm. The achieved values were evaluated in a graphic form of growth curves for each variant individually.

Software STATISTICA (data analysis software system), version 10.0 (Tulsa, Oklahoma, USA) was used for data processing. Half-maximal concentrations (IC_{50}) were calculated from logarithmic regression of sigmoidal dose-response curve. General regression model was used to analyze differences between the combinations of compounds.

2.7. High performance liquid chromatography with electrochemical detection for determination of doxorubicin

The samples were analyzed using high performance liquid chromatography with electrochemical detection (HPLC-ED). HPLC system consisted of two solvent delivery pumps operating in the range of 0.001-9.999 $ml.min^{-1}$ (Model 582 ESA and Model 584 ESA; ESA Inc., Chelmsford, MA), with reversed-phase chromatographic colony Zorbax eclipse AAA C18 (150 × 4.6; 3.5 nm particles, Agilent Technologies, USA) and a Coulochem electrochemical detector. The electrochemical detector includes one low volume flow-through analytical cell (Model 5040, ESA, USA), which is consisted of glassy carbon working electrode, hydrogen-palladium electrode as reference electrode and auxiliary electrode, and Coulochem III as a control module. Both the detector and the reaction coil/column were thermostated.

The sample (20 µl) was injected using autosampler (Model 542 HPLC, ESA, USA). Samples were kept in the carousel at 8 °C during the analysis. The column was thermostated at 30 °C. The flow rate was 1 $ml.min^{-1}$. Mobile phase consisted of: (A) aqueous solution of 0.05 M Na_2HPO_4 with 0.05 % triethylamine (pH 4.6 was adjusted by citric acid) and (B) acetonitrile. Analysis time was 20 minutes. Samples were diluted 10 times prior to the analysis.

2.8. Releasing of doxorubicin from liposomes

All three variants of liposomes prepared according to the procedure above were divided into aliquots and used for preparing variants of opened liposomes. These were prepared by adding 30 mM SDS to the liposomes in volume ratio 1:1 and vortexed for several seconds.

2.8.1. Absorption and fluorescence spectra of doxorubicin in liposomes

Absorption and fluorescence spectra were measured by multifunctional microplate reader Tecan Infinite 200 PRO (TECAN, Switzerland). The absorption scan was measured within the range from 230 to 800 nm per 5 nm steps. The detector gain was set to 100. For fluorescence spectra measurement, 480 nm was used as an excitation wavelength and the fluorescence scan was measured within the range from 510 to 850 nm. The detector gain was set to 100, too.

Two sets of liposomes 8, 9 and 10 with concentration of doxorubicin 0, 25, 50 and 100 $\mu g.ml^{-1}$ were used. The first set contained liposomes with addition of ACS water in volume ratio 1:1, and the second set contained liposomes with addition of 30 mM SDS in volume ratio 1:1. Both tested sets were placed in UV-transparent 96 well microplate with flat bottom by CoStar (Corning, USA). To each well 50 µl of sample was pipetted. All measurements were performed at 30 °C controlled by Tecan Infinite 200 PRO (TECAN, Switzerland).

2.8.2. Flow injection analysis with electrochemical detection

Flow injection analysis system consisted of a chromatographic pump Model 584 ESA (ESA Inc., Chelmsford, MA) (working range 0.001-9.999 $ml.min^{-1}$) and of an electrochemical detector Coulochem (ESA, USA), to which the amperometric cell (model 5040, ESA, USA) was connected. The cell contained a working electrode made from glassy carbon. The 20 µl of sample was injected automatically by an autosampler (Model 542, ESA, USA). During the analysis the samples were stored in the carousel. Flow rate of a mobile phase was 1 $ml.min^{-1}$. Other conditions were optimized.

2.9. Descriptive statistics

Data were processed using MICROSOFT EXCEL® (USA) and STATISTICA.CZ Version 8.0 (Czech Republic). Results are expressed as mean ± standard deviation (S.D.) unless noted otherwise (EXCEL®). Statistical significances of the differences were determined using STATISTICA.CZ. Differences with $p < 0.05$ were considered significant and were determined by using of one way ANOVA test (particularly Scheffe test), which was applied for means comparison.

3. RESULTS AND DISCUSSION

We focused this study on comparing the properties of differently prepared liposomes with encapsulated doxorubicin. These liposomes differ in the amount of cholesterol contained in phospholipid bilayer (0, 50 and 100 mg of cholesterol used during the preparation) and this fact has a significant influence on physicochemical properties of liposomes [11]. Schemes of prepared liposomes are shown in Fig. 1A-C. Verification of different cholesterol concentrations in liposomes were determined spectrophotometrically with utilization of R1 reagent. In this way the applied amount of cholesterol was confirmed for all liposomes with each concentration of encapsulated doxorubicin (Fig. 1D).

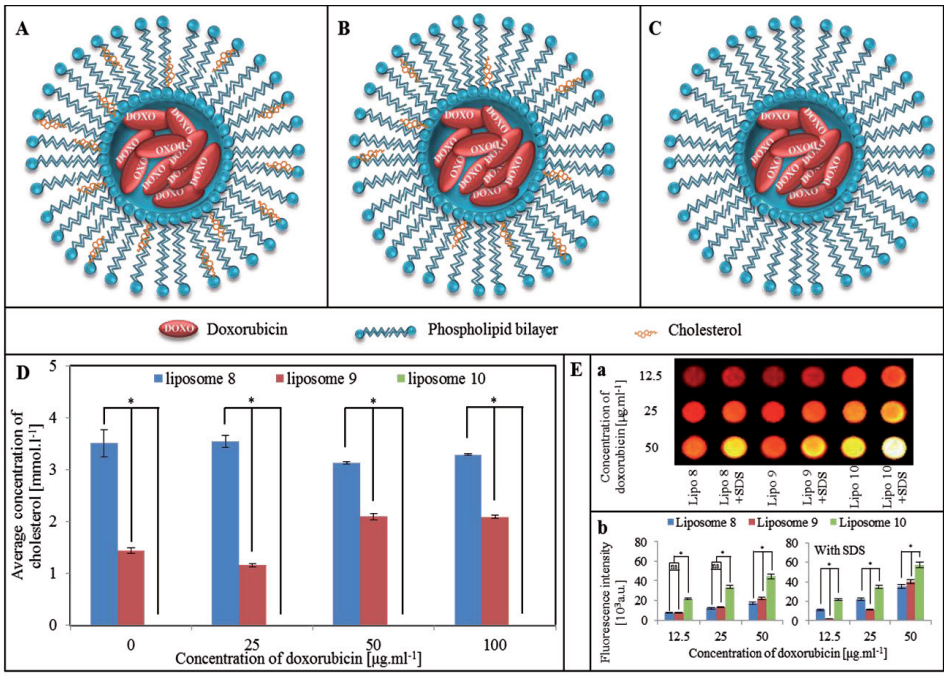

Figure 1. Schemes of studied liposomes, determination of cholesterol in liposomes on BS-400 device and measurements of doxorubicin's fluorescence in liposomes using In-vivo Xtreme device. Absorbance of cholesterol was measured for 6 minutes at 505 nm. For calculation of cholesterol concentration the absorbance values of R1 reagent and of the solution after 6 minutes incubation with sample were used. (**A**) Liposome 8; it contains 100 mg of cholesterol. (**B**) Liposome 9; it contains 50 mg of cholesterol. (**C**) Liposome 10; it doesn't contain cholesterol. (**D**) Concentrations of cholesterol determined in liposomes 8, 9 and 10 with different concentrations of encapsulated doxorubicin (0, 25, 50 and 100 μg.ml-1). (**E**) Fluorescence of liposomes with concentrations of doxorubicin diluted twice. 200 microliters of sample and water (or SDS 30 mM) at volume ratio 1:1 was pipetted on NuncTM 96-well microplate so final concentrations of doxorubicin were 12.5, 25 and 50 $\mu g.ml^{-1}$. Wavelength of excitation radiation was 600 nm. The fluorescence of liposomes without doxorubicin was within the range from 38 to 57 a.u. and so was insignificant. (*) Differences between measured values are statistically significant (at the significance level $\alpha = 0.05$). (ns) Not significant differences between measured values are statistically insignificant (at the significance level $\alpha = 0.05$).

The fluorescence intensity of doxorubicin encapsulated in liposomes was evaluated in terms of characterization of the liposome influence on the detection of doxorubicin. Fluorescence photographs (Fig. 1Ea) and dependence plotted in the graph (Fig. 1Eb) indicate an increased fluorescence of doxorubicin when using the liposome that doesn't contain a cholesterol. This suggests that cholesterol contained in phospholipid bilayer of liposomes reduces the fluorescent properties of doxorubicin. Same effect was also observed for doxorubicin released from liposome by addition of sodium dodecyl sulphate (SDS), when the doxorubicin from liposome 10 (doesn't contain cholesterol) still provided the highest fluorescence. This applies to all used concentrations of doxorubicin.

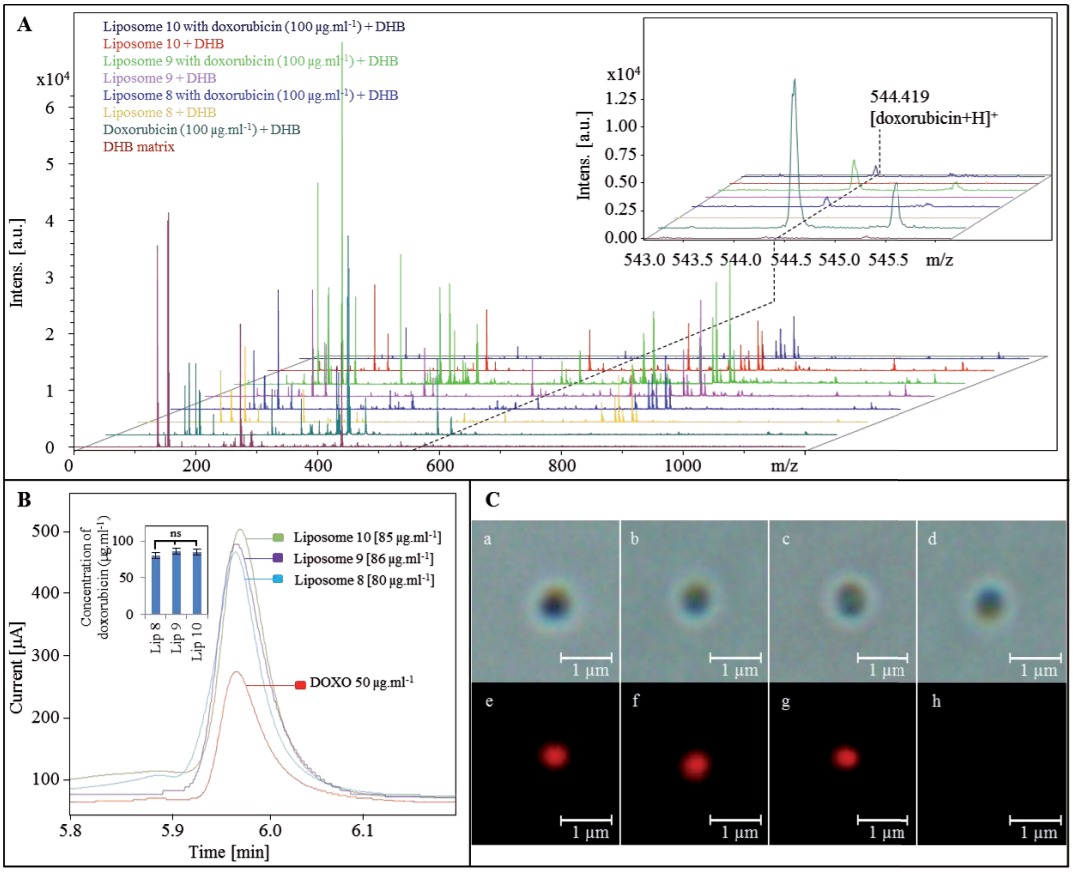

Figure 2. Liposomes with the highest loaded concentration of doxorubicin (100 µg.ml^{-1}) were analysed by mass spectrometry. (**A**) MALDI-TOF mass spectra of liposomes with and without encapsulated doxorubicin, and control spectra of free doxorubicin and DHB matrix. The detail of [doxorubicin+H]$^+$ peak of doxorubicin is presented in inset. (**B**) The total content of encapsulated doxorubicin was determined by HPLC-ED. The comparison of determined concentration of doxorubicin is shown in inset. (C) Microscopic photos of *Staphylococcus aureus* after the incubation of doxorubicin encapsulated in liposomes (Olympus IX71, Tokyo, Japan): **a, b, c, d**: ambient light; **e, f, g, h**: fluorescence photos (excitation: 520 -550 nm; emission: 580 nm); **a**, **e**: Liposome 8; **b**, **f**: Liposome 9; **c**, **g**: Liposome 10; **d**, **h**: *Staphylococcus aureus* without liposome (control sample).

For ensuring that doxorubicin is really encapsulated in liposomes we used several methods as matrix-assisted laser desorption/ionization time of flight mass spectrometry (MALDI-TOF), high performance liquid chromatography with electrochemical detection (HPLC-ED) and fluorescence microscopy. It is obvious from the obtained mass spectra (Fig. 2A) that the presence of doxorubicin was confirmed. Furthermore, there are obvious changes between mass spectra of liposomes with or without cholesterol (386.6 Da). Spectra of liposomes 8 and 9 most likely contain fragments and adducts of cholesterol – peaks with m/z 352.9, 398.9 and 420.9 – which weren't observed in spectra of

liposome 10. After the confirmation of doxorubicin presence, the concentration of doxorubicin was determined by HPLC-ED (Fig. 2B), which was done for all variants of encapsulated doxorubicin with maximal loaded concentration 100 $\mu g.ml^{-1}$. Due to lower recovery, which is probably due to destruction of liposome capsules when it comes to the chromatography system using reverse phase column and high pressure, it provides the determined concentrations within the range of 80 - 86 $\mu g.ml^{-1}$ without significant differences between applied concentrations of cholesterol. Besides the quantitative ability of liposomes to encapsulate applied substance was shown, the visual confirmation of the ability of all three different liposomes to carry the target substance into cells was verified by fluorescence microscopy (Fig. 2C). The results show that all applied liposomes were able to carry encapsulated doxorubicin into cells.

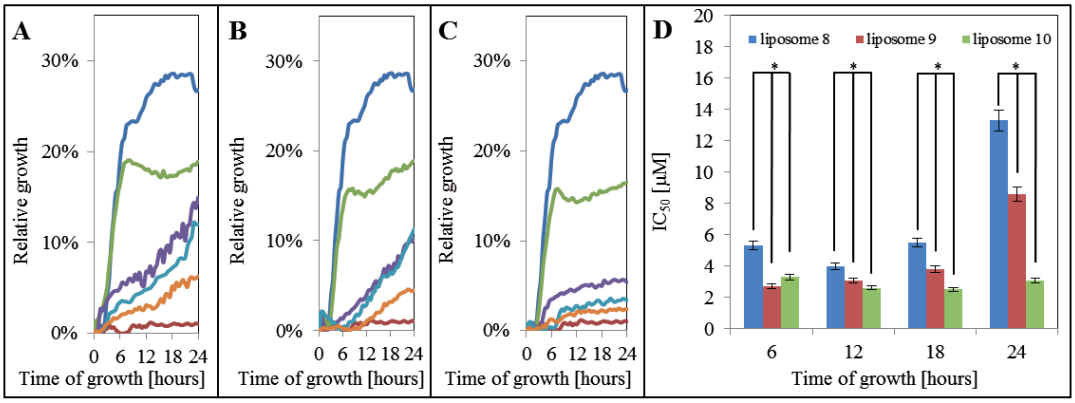

Figure 3. Growth curves, evaluation of antimicrobial effect of doxorubicin encapsulated in liposomes. The effect of substance was tested on bacterial culture of *Staphylococcus aureus* (S.a.) using Multiskan EX device. Measurements were carried out at 30 minutes intervals at 37 °C and at 620 nm. All graphs contain growth curves for doxorubicin (100 $\mu g.ml^{-1}$, red curve) and *S.a.* (dark blue curve). (**A**) Growth curves of bacterial culture treated with doxorubicin encapsulated in liposome 8. (**B**) Growth curves of bacterial culture treated with doxorubicin encapsulated in liposome 9. (**C**) Growth curves of bacterial culture treated with doxorubicin in liposome 10. (**D**) IC_{50} values (µM) for doxorubicin encapsulated in liposomes. Concentrations of doxorubicin in samples were 0 (olive green curve), 12.5 (purple curve), 25 (azure curve) and 50 (orange curve) $\mu g.ml^{-1}$ – it's 0, 23, 46 and 92 µM after conversion. (*) Differences between measured values are statistically significant (at the significance level $\alpha = 0.05$).

Characterization of doxorubicin encapsulated in liposome also included determination of growth curves with utilization of *Staphylococcus aureus* culture and determination of half maximal inhibitory concentration IC_{50} (represents the concentration of a drug that is required for 50% inhibition of *Staphylococcus aureus in vitro*) (Fig. 3). The influence of doxorubicin on the growth of *Staphylococcus aureus* was assessed only for liposomal doxorubicin and for doxorubicin itself because 15 mM concentration of SDS after addition to liposomes was inhibitory for the used bacterial culture. The highest toxicity for bacterial cells showed liposome 10 in the case of all evaluated times (6, 12, 18

and 24 hours) and the IC_{50} was within the range from 2.5 to 3.3 µM. It means that the concentration of encapsulated doxorubicin didn't have a big impact on IC_{50}. In contrast, both variants of liposomes with cholesterol showed dependence of toxicity on the concentration of cholesterol. For liposome 8 the IC_{50} was 13.3 µM at 24 hours and for liposome 9 it was 8.6 µM. This is in correlation with behaviour of cholesterol in phospholipid bilayer, in which it was described that cholesterol strengthens the bilayer and decreases bilayer's permeability [11]. The increased IC_{50} can also be explained by the positive influence of cholesterol on the growth of *Staphylococcus aureus*. Stimulation effect of lower cholesterol concentrations on microorganisms was also previously published [23,24].

3.1. Optimization of FIA-ED conditions for detection of doxorubicin releasing

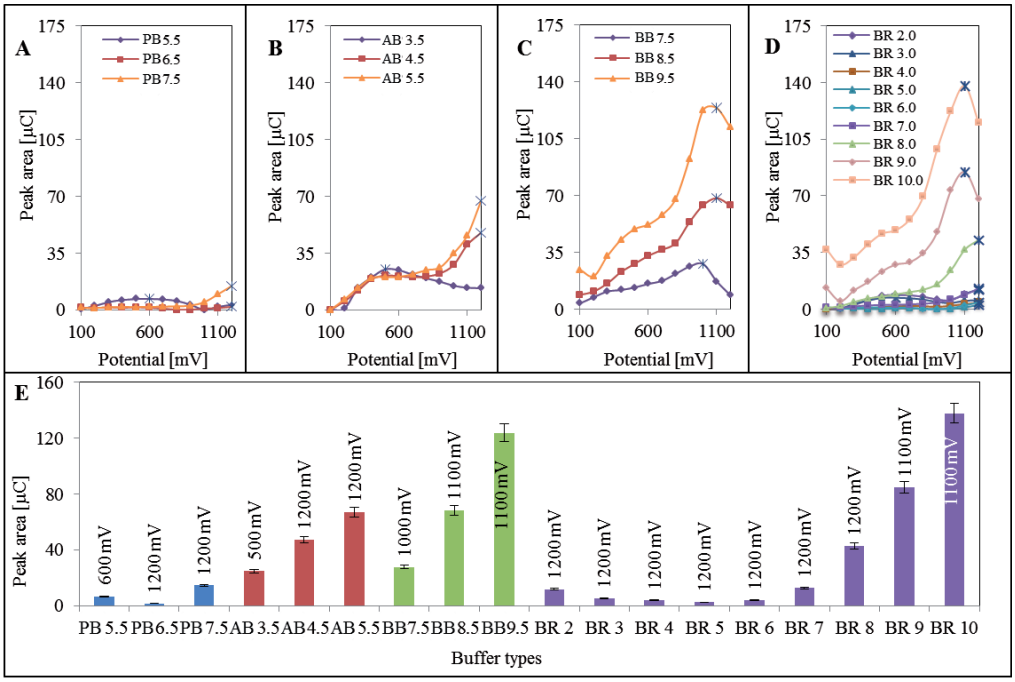

Figure 4. Analysis of doxorubicin (50 $mg.ml^{-1}$) in different buffers by FIA-ED. The buffer, which was used for dilution of doxorubicin aliquot, was used also as the mobile phase. The potential range was from 100 to 1200 mV with 100 mV step. Blue marks in graphs represent maximal measured values. (**A**) Phosphate buffer (PB) with pH 5.5, 6.5 and 7.5. (**B**) Acetate buffer (AB) with pH 3.5, 4.5 and 5.5. (**C**) Borate buffer (BB) with pH 7.5, 8.5 and 9.5. (**D**) Britton-Robinson buffer (BR) with pH 2.0, 3.0, 4.0, 5.0, 6.0, 7.0, 8.0, 9.0 and 10.0. (**E**) The highest detector responses considering different buffers and applied potential.

After that we found the negative effect of all three prepared liposomes on the target bacterial culture, we decided to study way how to open doxorubicin externally. For doxorubicin determination, flow injection analysis (FIA-ED) with electrochemical detection was optimized. Before that we made necessary optimization of different buffers used for doxorubicin detection because it is crucial for this

type of detection [25]. Standard solution of doxorubicin was always diluted to 50 $\mu g.ml^{-1}$ with a buffer, which was also used as mobile phase in FIA-ED. Each buffer was used in its natural buffering range: Britton-Robinson buffer (pH 2, 3, 4, 5, 6, 7, 8, 9, 10), acetate buffer (pH 3.5, 4.5, 5.5), phosphate buffer (pH 5.5, 6.5, 7.5) and borate buffer (pH 7.5, 8.5, 9.5). In each buffer with each pH the hydrodynamic voltammograms (HDVs) were measured with a 100 mV step within the potential range from 100 to 1200 mV (Figs. 4A, B, C, and D).

The largest peak area was achieved using Britton-Robinson buffer at pH 10. With decreasing pH the peak area of doxorubicin measured by FIA-ED was also decreasing. This effect of pH was surprising because with other types of electrochemical detection the low pH is preferably used [26-29]. For similar types of detection in HPLC the lower pH is used as well. Often a phosphate buffer with addition of triethylamine is used at pH lower than 5 [29-31]. These conditions are mainly used for separation but the signal of detector is distinctly lower than with use of our optimized conditions of Britton-Robinson buffer at pH 10 (Fig. 4E).

3.2. Electrochemical monitoring of doxorubicin releasing

According to the results obtained above the electrochemical characterization of all liposomes was performed on glassy carbon electrode under the optimized conditions. Differential HDVs of all samples, including samples with added 30 mM SDS, are shown in Fig. 5. Measurements were performed within the potential range from 100 to 1000 mV with a 100 mV step. Differential HDV's curves were obtained by subtracting the peak area of blank samples (liposomes without doxorubicin) from the peak area of doxorubicin encapsulated in liposomes and are shown in Figs. 5A, B and C for tested liposomes with doxorubicin only and in Figs. 5E, F and G for liposomes with doxorubicin affected by SDS.

In Figs. 5D and H there are shown the maximal differences of peak area at 900 mV potential, which provided the highest response of detector. The statistically significant differences were acquired between individual liposomes with the same concentration of doxorubicin, including those liposomes with addition of SDS. The biggest difference showed liposome 9 with all concentrations of doxorubicin. It is interesting that liposome 8 with higher concentration of cholesterol showed smaller difference of peak areas than liposome 9. Cholesterol probably has a role in the improvement of electrochemical detection of encapsulated doxorubicin, but this improvement has a limitation factor in concentration of cholesterol (critical concentration). It is possible that cholesterol enhances the electron transfer at the applied conditions, but further experiments are necessary to prove it. In Figs. 5E, F, G and H the electrochemical detection was influenced by the addition of SDS in the way that increased differences were obtained in the case of the highest applied concentration of doxorubicin. A significant increase from 13.2 to 29.4 μCin maximal difference of peak areas was determined at liposome 10. In contrast, liposomes with cholesterol provided decreased differences of peak areas and thus the detection was deteriorated. Decreasing trend is in correlation with a concentration of cholesterol in phospholipid bilayer of liposomes.

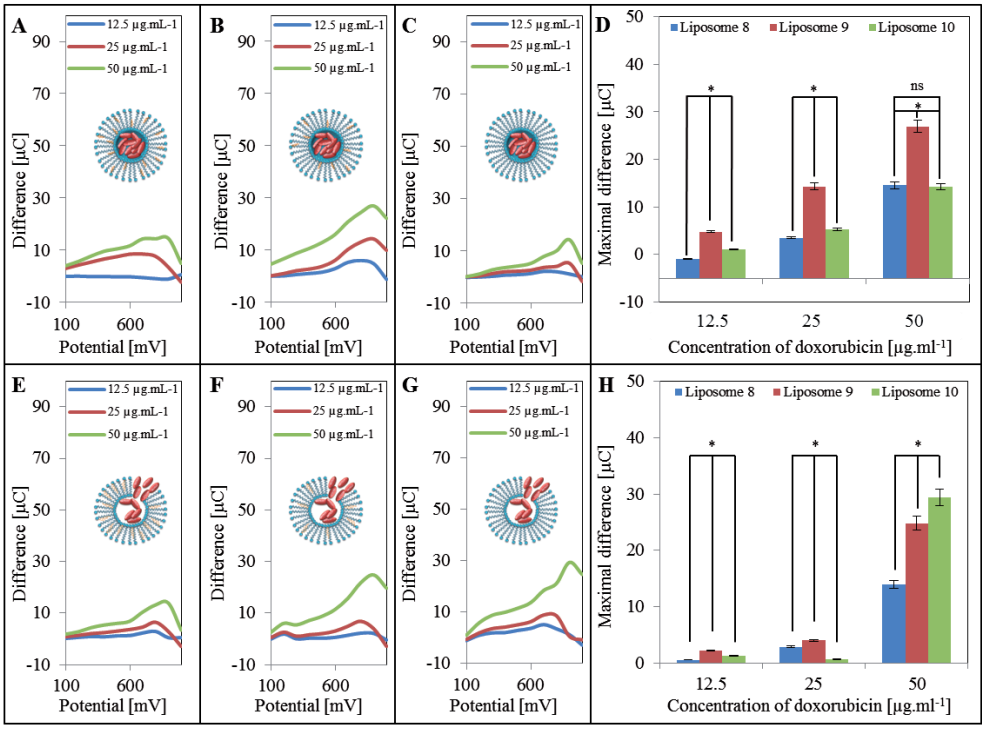

Figure 5. Differential hydrodynamic voltammograms (HDV) of doxorubicin encapsulated in liposomes and of doxorubicin encapsulated in liposomes after the addition of SDS. Differential curves were obtained by subtracting the values of blank samples from the values of samples with doxorubicin. The analysis was performed with FIA-ED. All measurements were done within the range from 100 to 1000 mV with 100 mV step. Samples were prepared in Britton-Robinson buffer with pH 10.0. (**A**)-(**D**) Concentrations of doxorubicin in liposomes were 12.5, 25 and 50 µg.ml^{-1}. (**E**)-(**H**) 30 mM SDS was added to the liposomes with doxorubicin in volume ratio 1:1, thus the final concentrations were 12.5, 25 and 50 µg.ml^{-1}. (**A**), (**E**) Liposome 8. (**B**), (**F**) Liposome 9. (**C**), (**G**) Liposome 10. (**D**), (**H**) The comparison of maximal differences from differential HDVs. (*) Differences between measured values are statistically significant (at the significance level $\alpha = 0.05$). (ns) Not significant differences between measured values are statistically insignificant (at the significance level $\alpha = 0.05$).

3.3. Fluorescence monitoring of doxorubicin releasing

In another part of our study we focused on the effect of liposomes on optical properties of doxorubicin. Firstly, the absorption spectra were determined (insets in Fig. 6A, B, C, E, F and G). It clearly follows from the results obtained that absorption spectra of doxorubicin encapsulated in liposomes were minimally affected. In contrast, the fluorescence spectra (λ_{ex} = 480 nm) show that with the increasing concentration of doxorubicin the fluorescence of each liposome was also increasing (Fig. 6D).

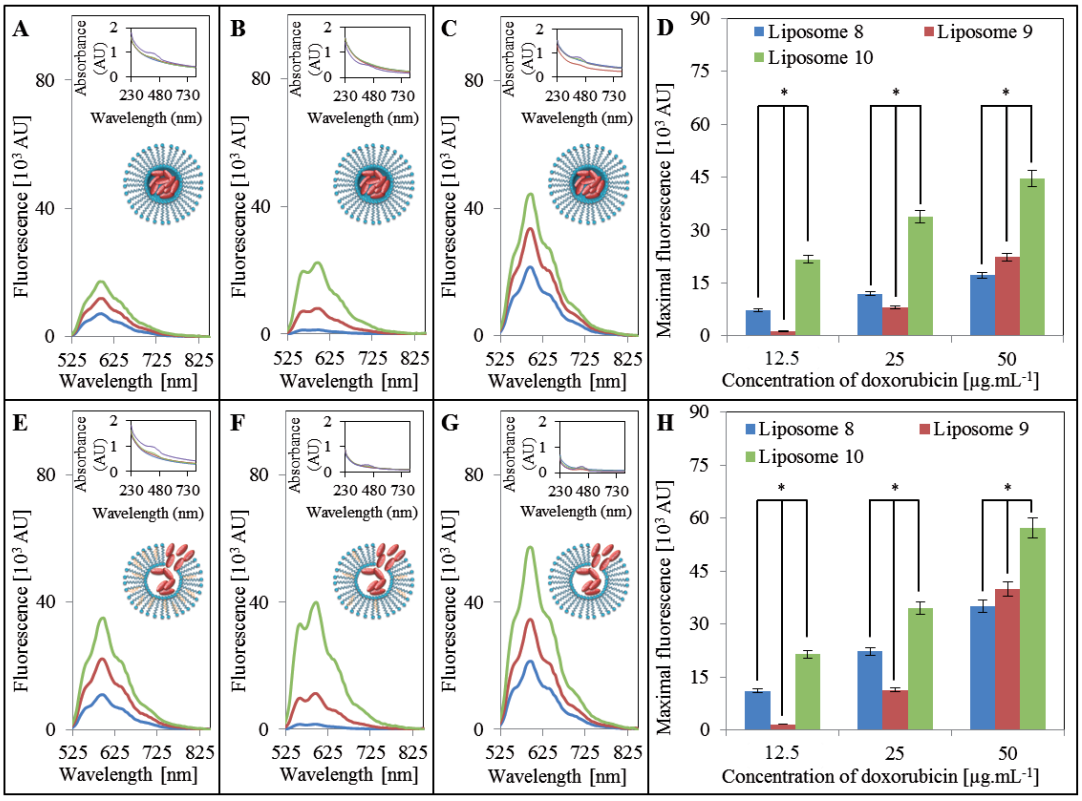

Figure 6. Differential fluorescence spectra (λ_{ex} = 480 nm) and absorption spectra (inserted graphs) of liposomes 8, 9 and 10 with doxorubicin measured on Tecan Infinite 200 PRO. Differential spectra were obtained by subtracting the values of blank samples from the values of samples with doxorubicin. Samples were pipetted into the UV-transparent 96-well plate with a flat bottom (CoStar; Corning, USA). 50 µl of sample was always pipetted. Fluorescence spectra were measured within the range of 510-850 nm with 5 nm steps. Absorption spectra were measured in the range of 230-800 nm. (**A**)-(**D**) The samples of liposomes were diluted with ACS water in volume ratio 1:1. (**E**)-(**H**) 30 mM SDS was added to the samples of liposomes in volume ratio 1:1 in order to unfold liposomes. (**A**), (**E**) Liposome 8. (**B**), (**F**) Liposome 9. (**C**), (**G**) Liposome 10. Concentrations of doxorubicin in the samples after the dilution were 12.5 (blue curve), 25 (red curve) and 50 (olive green curve) µg.ml^{-1}. (**D**), (**H**) Graphs show a maximal fluorescence for the samples after the subtraction of blank samples. (*) Differences between measured values are statistically significant (at the significance level α = 0.05).

The increased fluorescence of all liposomes with addition of 30 mM SDS confirms that liposomes were opened and doxorubicin was released into the solution. It confirms the function of SDS as the substance that is commonly used for releasing encapsulated substance from liposome [11,32,33]. The highest fluorescence from all liposomes was observed in liposome 10 either with encapsulated doxorubicin or with doxorubicin released into the solution (Fig. 6H). Liposomes themselves show negligible fluorescence, thus, it is obvious that these results show changes of

fluorescence on the basis of a composition of phospholipid bilayer, especially on the concentration of cholesterol, eventually of its distraction.

4. CONCLUSIONS

The composition of phospholipid bilayer significantly affects the physicochemical properties of a liposome and allows the use of liposomes for therapeutic purposes as for analytical purposes. One of the most used components of phospholipid bilayer is cholesterol; especially its concentration can significantly affect the properties of liposomes. In this study, we attempted to characterize the toxicity, electrochemical properties and fluorescence of doxorubicin encapsulated in liposomes with different concentrations of cholesterol in phospholipid bilayer. We also studied the influence of sodium dodecyl sulphate (SDS) addition to the liposomes, because SDS served to open liposomes and release the drug into the solution and found that various composition of liposome strongly influenced the releasing of doxorubicin, which is of high importance for further drug delivery studies.

ACKNOWLEDGEMENTS
Financial support from CEITEC CZ.1.05/1.1.00/02.0068 and Liga proti rakovine LPR 2014 is highly acknowledged.

References

1. A. D. Bangham and R. W. Horne, *J. Mol. Biol.*, 8 (1964) 660.
2. R. R. Hood, C. R. Shao, D. M. Omiatek, W. N. Vreeland and D. L. DeVoe, *Pharm. Res.*, 30 (2013) 1597.
3. K. Maruyama, *Adv. Drug Deliv. Rev.*, 63 (2011) 161.
4. K. Hayashi, T. Tatsui, T. Shimanouchi and H. Umakoshi, *Colloid Surf. B-Biointerfaces*, 106 (2013) 258.
5. T. Nguyen, J. Ostergaard, S. Sturup and B. Gammelgaard, *Int. J. Pharm.*, 449 (2013) 95.
6. T. L. Andresen, S. S. Jensen and K. Jorgensen, *Prog. Lipid Res.*, 44 (2005) 68.
7. Y. Komizu, Y. Matsumoto and R. Ueoka, *Bioorg. Med. Chem. Lett.*, 16 (2006) 6131.
8. T. J. Evjen, S. Hupfeld, S. Barnert, S. Fossheim, R. Schubert and M. Brandl, *J. Pharm. Biomed. Anal.*, 78-79 (2013) 118.
9. Y. Omokawa, T. Miyazaki, P. Walde, K. Akiyama, T. Sugahara, S. Masuda, A. Inada, Y. Ohnishi, T. Saeki and K. Kato, *Int. J. Pharm.*, 389 (2010) 157.
10. T. M. Allen and C. Hansen, *Biochim. Biophys. Acta*, 1068 (1991) 133.
11. H. Ohvo-Rekila, B. Ramstedt, P. Leppimaki and J. P. Slotte, *Prog. Lipid Res.*, 41 (2002) 66.
12. Y. Kuang, J. Liu, Z. L. Liu and R. X. Zhuo, *Biomaterials*, 33 (2012) 1596.
13. L. Y. Qiu, M. F. Yao, M. H. Gao and Q. H. Zhao, *J. Liposome Res.*, 22 (2012) 245.
14. L. Hosta-Rigau, Y. Zhang, B. M. Teo, A. Postma and B. Stadler, *Nanoscale*, 5 (2013) 89.
15. C. Zhang, J. Li, L. Xu and Z. G. Shi, *J. Chromatogr. A*, 1233 (2012) 78.
16. S. W. Wang, C. Wang, X. Zhao, S. L. Mao, Y. T. Wu and G. R. Fan, *Anal. Chim. Acta*, 713 (2012) 121.
17. J. Mei, Y. P. Tian, W. He, Y. X. Xiao, J. A. Wei and Y. Q. Feng, *J. Chromatogr. A*, 1217 (2010) 6979.
18. D. Corradini, G. Mancini and C. Bello, *Chromatographia*, 60 (2004) S125.

19. K. P. McNamara and Z. Rosenzweig, *Anal. Chem.*, 70 (1998) 4853.
20. A. Gomez-Hens and J. M. Fernandez-Romero, *TRAC-Trends Anal. Chem.*, 24 (2005)
21. Y. Kumada, K. Tomioka and S. Katoh, *Kag. Kog. Ronbunshu*, 28 (2002) 77.
22. Y. Kumada, K. Tomioka and S. Katoh, *J. Chem. Eng. Jpn.*, 34 (2001) 943.
23. W. E. Shine, R. Silvany and J. P. McCulley, *Invest. Ophthalmol. Vis. Sci.*, 34 (1993)
24. D. T. Clark and M. Soory, *Steroids*, 71 (2006) 352.
25. M. A. M. Rodrigo, O. Zitka, M. Kominkova, V. Adam, M. Beklova and R. Kizek, *Int Electrochem. Sci.*, 8 (2013) 4409.
26. D. Hynek, L. Krejcova, O. Zitka, V. Adam, L. Trnkova, J. Sochor, M. Stiborova, T. E Hubalek and R. Kizek, *Int. J. Electrochem. Sci.*, 7 (2012) 13.
27. Y. J. Guo, Y. H. Chen, Q. Zhao, S. M. Shuang and C. Dong, *Electroanalysis*, 23 (201
28. D. Nieciecka and P. Krysinski, *Langmuir*, 27 (2011) 1100.
29. Z. Jemelkova, J. Zima and J. Barek, *Collect. Czech. Chem. Commun.*, 74 (2009) 1503
30. P. M. Loadman and C. R. Calabrese, *J. Chromatogr. B*, 764 (2001) 193.
31. G. Nicholls, B. J. Clark and J. E. Brown, *J. Pharm. Biomed. Anal.*, 10 (1992) 949.
32. M. Cocera, O. Lopez, L. Coderch, J. L. Parra and A. de la Maza, *Colloid Surf. A-Phys Eng. Asp.*, 221 (2003) 9.
33. A. M. Tan, A. Ziegler, B. Steinbauer and J. Seelig, *Biophys. J.*, 83 (2002) 1547.

5.2.2 Research article IV

BLAZKOVA, I; NGUYEN, H.V.; KOMINKOVA, M.; KONECNA, R.; CHUDOBOVA, D.; KREJCOVA, L.; KOPEL, P.; HYNEK, D.; ZITKA, O.; BEKLOVA, M.; ADAM, V.; KIZEK, R. Fullerene as a transporter for doxorubicin investigated by analytical methods and *in vivo* imaging. *Electrophoresis*, 2014. 35(7): p. 1040-1049. ISSN 0173-0835.

Participation in the manuscript preparation of the author Blažková, I.: 48%.

Fullerenes can improve the delivery of the drug into the tumour cells and as free radicals scavengers are proven to have protective properties against the DOX associated toxicity (An and Jin 2015; Panchuk, Prylutska et al. 2015). The preclinical experiment with different NPs are usually carried out on cell cultures and then on animal models (Guo, Chen et al. 2015). Embryo models represent the transition between the studies on cells and on the animal models (Rashidi and Sottile 2009). The experiments on mammalian animal models are costly and generate ethical issue. Using of non-mammalian vertebrate embryos is possible without any licence and is reproducible with high throughput (Mortell, Giles et al. 2003; Vargas, Zeisser-Labouebe et al. 2007; Zamboni 2008; Ruyra, Yazdi et al. 2015). The experiments on embryos are possible till they are able of independent feeding, it means their whole development (21 days) (Giannaccini, Cuschieri et al. 2014).

The aim of this work was DOX conjugation with fullerenes and characterization of conjugates by spectral and electrochemical methods. The toxicity of the conjugates was evaluated using bacterial culture of *Staphylococcus aureus* and the behaviour of conjugates in *in vivo* system was determined.

In this study, significant protective effect of fullerenes against DOX toxicity was detected and its effect *in vitro* was analysed. Because of decreased toxicity of DOX by its conjugation with fullerenes, the conjugates were applied to the chicken embryos and their distribution in the body was observed. The amount of DOX was analysed within the individual organs and as expected higher concentration was detected in embryos who received fullerenes with higher concentration of DOX. The concentration of DOX differed between the organs and the highest DOX concentration was determined in the intestine followed by heart and liver.

Electrophoresis 2014, *35*, 1040–1049

Iva Blazkova[1]
Hoai Viet Nguyen[1]
Marketa Kominkova[1]
Romana Konecna[1]
Dagmar Chudobova[1]
Ludmila Krejcova[1,2]
Pavel Kopel[1,2]
David Hynek[1,2]
Ondrej Zitka[1,2,3]
Miroslava Beklova[2,3]
Vojtech Adam[1,2]
Rene Kizek[1,2]

[1]Faculty of Agronomy, Department of Chemistry and Biochemistry, Mendel University in Brno, Brno, Czech Republic
[2]Central European Institute of Technology, Brno University of Technology, Brno, Czech Republic
[3]Faculty of Veterinary Hygiene and Ecology, Department of Veterinary Ecology and Environmental Protection, University of Veterinary and Pharmaceutical Sciences, Brno, Czech Republic

Received August 15, 2013
Revised November 5, 2013
Accepted November 5, 2013

Research Article

Fullerene as a transporter for doxorubicin investigated by analytical methods and in vivo imaging

Carbon nanomaterials, including fullerenes, exhibit not only unique structure and electronic properties but also a significant potential to serve as radical scavengers and/or anti-oxidants. Their conjugation with anticancer drugs such as doxorubicin (DOX) may help to balance severe negative side effects of these cytostatics and also improve the delivery of the drug taking advantage of the enhanced cellular uptake, selectivity to cancer cells, and pH regulated release. In this study, the fullerene (C60) surface was oxidized by concentrated nitric acid, which enabled simple DOX–fullerene conjugation based on π–π stacking and hydrophilic interactions with carboxylic groups. The strength of this noncovalent binding is pH dependent. At a low pH, the amino group of DOX is protonated, however at a higher pH, the amino group is deprotonated, resulting in stronger hydrophobic interactions with the fullerene walls. CE and HPLC were employed for characterization of resulting complexes. The cell toxicity of the conjugates was evaluated using *Staphylococcus aureus* and finally they were administered into the chicken embryo to assess the applicability for in vivo imaging.

Keywords:
Clinical analysis / Doxorubicin / Drug delivery / Embryo / Fullerene / Nanomedicine
DOI 10.1002/elps.201300393

1 Introduction

Nanomaterials are nowadays attracting enormous attention in almost all research areas. Hence there is no wonder that their application in medicine is so widely explored. Both, diagnostic as well as therapeutic utilization of various types of nanoparticles have been investigated [1–4]. Metal or semiconductor nanoparticles are employed for imaging applications and visualization, and magnetic particles are utilized for hyperthermia therapy, and variety of other types of nanomaterials are used for drug delivering. Prominent position among nanomaterials used in medicine belongs to carbon nanomaterials such as nanotubes, fullerenes, and/or graphene due to their unique physical and chemical properties [1–3, 5–7]. The π–π stacking effect can be utilized for conjugation of aromatic molecules onto the polyaromatic surface of all carbon nanomaterials. Moreover, fullerenes and their derivatives were studied for their efficient quenching of various free radicals and reactive oxygen species, thus potentially serving as radical scavengers and/or anti-oxidants in biological systems protecting from the oxidative stress and toxicity caused by cytostatic drugs [8–11]. The combination of the protective properties of fullerenes and their ability of drug delivery make them very attractive for anticancer therapy [12,13]. For the clinically highly effective anticancer drug paclitaxel, it was shown that covalent conjugate with C60 for a lipophilic slow-release system enhanced the therapeutic efficacy [14]. Doxorubicin (DOX), another highly effective cytostatic drug in antitumor therapy [15], was also conjugated with fullerenes and carbon nanotubes aiming at mitigating DOX-induced toxic side effects [8, 16, 17] and/or improving the drug delivery [18–21]. Moreover, the optical properties of DOX provide opportunities to track the molecules and conjugates by using fluorescence-based techniques, such as assessing nanocarrier of DOX in cells without any other fluorescence labels [22]. Generally, the coupling between DOX and fullerene surface can be assured by covalent linkage [13, 23], or by nonspecific interaction after activation of the surface by acidic oxidation [18].

In this study, the simple method of DOX–fullerene (C60) conjugation is utilized and the characterization of conjugates by spectral methods, electrochemical analysis, CE, and LC is

Correspondence: Dr. Rene Kizek, Department of Chemistry and Biochemistry, Mendel University in Brno, Zemedelska 1, CZ-613 00 Brno, Czech Republic
E-mail: kizek@sci.muni.cz
Fax: +420-5-4521-2044

Abbreviation: DOX, doxorubicin; **ED**, electrochemical detection; **IC_{50}**, half maximal inhibitory concentration

Colour Online: See the article online to view Figs. 1–6 in colour.

demonstrated. Finally, the monitoring of the effect of prepared conjugates on the bacterial cells as well as in vivo imaging on the chicken embryo is presented.

2 Materials and methods

2.1 Chemicals and pH measurement

HPLC-grade ACN (>99.9%; v/v) from Merck (Darmstadt, Germany) was used. Chemicals used in this study were purchased from Sigma-Aldrich® (St. Louis, MO, USA) in ACS purity unless noted otherwise. Washing solutions were prepared in MilliQ water obtained using reverse osmosis equipment Aqual 25 (Aqual, Brno, Czech Republic). The DI water was further purified by using apparatus Direct-Q 3 UV Water Purification System equipped with the UV lamp from Millipore (Billerica, MA, USA). The resistance was established to 18 MΩ/cm. The pH was measured using pH meter WTW inoLab (Weilheim, Germany).

2.2 Synthesis of the fullerenes with DOX

2.2.1 Conjugates with constant concentration of fullerenes and varying concentration of DOX

The Buckminster Fullerenes C60 (5 mg; Sigma-Aldrich®) were purified with concentrated HNO_3 (70% in ACS water, 1 mL) for 15 min in ultrasonic bath and shaken (1400 rpm, 90°C, 15 min, Thermomixer® comfort, Eppendorf, Germany). The solution was centrifuged (25 000 × *g*, 20°C, 15 min; Centrifuge 5417R, Eppendorf) and the acid was removed. The fullerenes were washed with 1 mL of ACS water (seven times) until the neutral pH was reached and finally resuspended in 1 mL of ACS water. Fifty microliters of the fullerene solution was mixed with 500 μL of the DOX (1000, 500, 250, 125, and 63 μg/ml in ACS water). The solution was sonicated in the ultrasonic bath for 15 min, after 5 min of sonication, 1 mL of the sodium phosphate buffer (pH 7.5) was added. The solution was vortexed for 24 h and subsequently centrifuged using Amicon 3 K (4500 × *g*, 20°C, 15 min; centrifugal filters for sample purification and concentration; EMD Millipore). The solution was subsequently washed with sodium phosphate buffer (pH 7.5) and centrifugation was repeated. Finally the solution of fullerenes and DOX was filled up to 1 mL by ACS water.

2.2.2 Conjugates with constant concentration of DOX and varying concentration of fullerenes

The different concentrations of fullerenes with DOX were prepared in the same way as previous method (Section 2.2.1). There were different fullerenes weight (2.5, 5, 7.5, 10, 12.5 mg) prepared and the one concentration of DOX as 500 μg/mL was used.

2.3 Antimicrobial effect

The procedure for the evaluation of the antimicrobial effect of the fullerenes, DOX, and DOX–fullerene conjugates was based on measuring the absorbance using the apparatus Multiskan EX (Thermo Fisher Scientific, Germany) and subsequent analysis in the form of growth curves. The bacterial culture of *Staphylococcus aureus* cultivated in LB medium (meat peptone 5 g/L, NaCl 5 g/L, bovine extract 1.5 g/L, yeast extract 1.5 g/L HIMEDIA, Mumbai, India; sterilized MilliQ water with 18 MΩ) was diluted with LB medium to absorbance 0.1 at a wavelength of 600 nm, measured using Specord spectrophotometer 210 (Analytik, Jena, Germany). The culture (250 μL) was mixed with different concentrations (1, 2, 4, 8, 16, 31, 63, 125, 250, or 500 μg/mL) of DOX in ACS water, fullerene, or fullerene with DOX. Measurements were carried out at time 0, then every 30 min for 24 h at 37°C and the wavelength of 600 nm.

2.4 Spectrometric characterization of DOX–fullerene conjugates

The absorbance and fluorescence scans of all solutions were acquired using a microtitration plate reader Tecan infinite M200 PRO (Grödig, Austria). A volume of 50 μL of the solution was analyzed in the Costar® microtitration plate (UV plate, 96 well; Corning, NY, USA). The absorbance scan was measured within the range from 230 to 800 nm. The fluorescence spectrum was measured using excitation wavelength 480 nm and emission range of 520–850 nm (emission wavelength step size: 5 nm; gain: 100; number of flashes: 5).

2.5 Electrochemical analysis

Determination of DOX and fullerene interaction by square wave voltammetry (SWV) was performed using a 663 VA Stand (Metrohm, Herisau, Switzerland), equipped with standard electrochemical cell and three electrodes. The three-electrode system consisted of a hanging mercury drop electrode (HMDE) with a drop area of 0.4 mm^2 as the working electrode, an Ag/AgCl/3M KCl reference electrode and a platinum electrode acting as the auxiliary electrode. GPES 4.9 software was employed for data processing. The analyzed samples were deoxygenated prior to measurements by purging with argon (99.999%). Acetate buffer (0.2 M CH_3COONa and CH_3COOH, pH 5.0) was used as a supporting electrolyte. The supporting electrolyte was replaced prior to each analysis. The parameters of the measurement were as follows: purging time 120 s; deposition potential 0.0 V; time of accumulation 120 s; equilibration time 2 s; initial potential 0.0 V; end potential −1.7 V; step potential 0.005 V; modulation amplitude 0.0250 V; volume of measurement cell 1 mL (5 μL of sample; 995 μL acetate buffer).

2.6 Ex vivo imaging

The DOX and the DOX with fullerenes were applied by injection into the chicken embryo breast muscle tissue. The fluorescence was detected by Carestream In-Vivo Xtreme Imaging System (Carestream Health, Rochester, USA). This instrument is equipped with a 400 W xenon light source. Emitted light was captured by a 4MP CCD camera. The excitation wavelength was set at 480 nm and the emission was measured at 600 nm. Other parameters were set as follows: exposure time 2 s; binning 2×2; *f*-stop 1.1; field of view 11.5 × 11.5 cm. The images were processed by Carestream molecular imaging software.

2.7 In vivo experiment

The in vivo distribution of the DOX with fullerene within a body was studied in the chicken embryos. The eggs (ISA Brown) were incubated in RCom 50 MAX incubator (Gyeongnam, Korea) at temperature (37.5°C) and humidity (45% rH) control and automatic egg rolling (every 2 h). There was 250 μL of the fullerene (5 mg/mL) with DOX (31, 63, 125, 250, 500 μg/mL) injected into egg yolk of five eggs with chicken embryo (17 days old). The eggs were incubated for 4 h at 37.5°C. After the incubation the eggshell was removed and the organs were sampled, homogenized, and analyzed by HPLC with electrochemical detection (HPLC-ED) according to the protocol described in the following sections.

2.8 HPLC analyses

2.8.1 Sample preparation

A tissue samples were ground in a mortar using liquid nitrogen with PBS. Samples were further disrupted using an ultrasonic needle. Subsequently, the samples were vortexed (5 min) and centrifuged (25 000 × *g*, 4°C, 20 min). TFA (5%, v/v) was added and the centrifugation was repeated at the same condition. The supernatant was used for the analysis of DOX using HPLC-ED.

2.8.2 HPLC analyses

The samples were analyzed using HPLC with electrochemical and UV-VIS detection (HPLC-ED or HPLC-UV). HPLC system consisted of two solvent delivery pumps operating in the range of 0.001–9.999 mL/min (Model 582 ESA and Model 584 ESA; ESA, Chelmsford, MA), with RP chromatographic colony Zorbax eclipse AAA C18 (150 × 4.6; 3.5 nm particles, Agilent Technologies, USA) and a Coulochem electrochemical detector. The electrochemical detector includes one low volume flow-through analytical cell (Model 5040, ESA, USA), which is consisted of glassy carbon working electrode, hydrogen–palladium electrode as reference electrode and auxiliary electrode, and Coulochem III as a control module. Both the detector and the reaction coil/column were thermostated. The absorbance detector LaChrom Elite L – 2420 with a single wavelength (485 nm) by Hitachi (Berkshire, United Kingdom) was employed.

The sample (20 μL) was injected using autosampler (Model 542 HPLC, ESA, USA). Samples were kept in the carousel at 8°C during the analysis. The column was thermostated at 30°C. The flow rate was 1 mL/min. Mobile phase consisted of: (i) aqueous solution of 0.05 M Na_2HPO_4 with 0.05% triethylamine (pH 4.6 was adjusted by citric acid) and (ii) ACN. The detection of the separated compounds was carried out at 400 mV. Analysis time was 20 min. Samples were diluted ten times prior to the analysis.

2.9 CE-LIF

Measurements were done by Beckman P/ACE MDQ CE (USA) with LIF detection (λ_{ex} = 488 nm, λ_{em} = 600 nm). Uncoated fused silica capillary (l_{tot} = 63.5 cm, l_{eff} = 54.5 cm, and id = 75 μm) was used. BGE was 100 mM phosphate buffer of pH 5.0 with 60 μM spermine and 70% of ACN v/v. Separation was carried out at 25 kV with hydrodynamic injection 15 s by 34 mbar. Samples were diluted 100 times prior to the analysis.

3 Results and discussion

Fullerenes and fullerenols have recently proved their suitability for transport of selected compound with therapeutic properties. The size of fullerenes improves the retention of the conjugated pharmaceutical drug in the organism and therefore prolongs the therapeutic activity of the drug. Previous studies have presented conjugation of fullerene and DOX via covalent bond to the specific linker, however nonspecific interactions between DOX and carbon nanotubes were described in the work by Heister et al. [18] taking advantage from the oxidation of the carbon material by nitric acid. Based on these results we subjected fullerenes to the same procedure (Fig. 1) and obtained product was characterized.

A set of solutions of (i) pure DOX in various concentrations, (ii) fullerenes in different concentrations, (iii) DOX–fullerene conjugates prepared using constant concentration of fullerenes and varying concentration of DOX, and (iv) DOX–fullerene conjugates using constant concentration of DOX and varying concentration of fullerenes was prepared.

3.1 The antimicrobial activity of DOX–fullerene conjugates

At first, the influence of all compounds on bacterial cells of *S. aureus* was observed to establish their suitability for biological application. The results expressed as growth curves can be seen in Fig. 2. One of the methods: how to demonstrate the antimicrobial activity of the studied compound is a

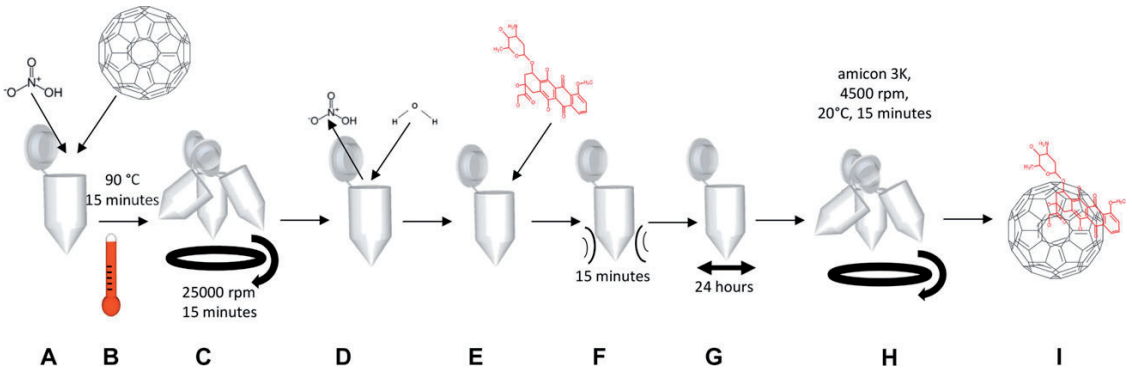

Figure 1. Scheme of preparation of DOX–fullerene conjugates. (A) Mixture of fullerenes and nitric acid, (B) heating for 15 min at 90°C, (C) centrifugation at 25 000 × *g* for 15 min, (D) replacing of nitric acid by water, (E) addition of DOX, (F) sonication for 15 min, (G) vortexing for 24 h, and (H) filtration using centrifugation filters (size 3 K, 4500 × *g* 15 min).

method of growth curves [24–26]. Using these curves and statistical methods it is possible to determine the IC_{50} value (half maximal inhibitory concentration) expressing the concentration required for 50% growth inhibition [27]. The growth of the culture exposed to the eleven concentrations of DOX (0, 1, 2, 4, 8, 16, 31, 63, 125, 250, and 500 μg/mL) is shown in Fig. 2A. Partial and total growth inhibition was observed when the concentrations of 4 and 31 μg/mL, respectively, were used. Application of the fullerene solutions to the *S. aureus* culture did not influence the cell growth as shown in Fig. 2B. In the case of exposure of the cell culture to the solutions of DOX–fullerene conjugates prepared by constant concentration of fullerenes and varying concentration of DOX, the total growth inhibition was not observed under any tested concentration (Fig. 2C). Even though the decrease of the growth curves was obvious it can be concluded that the antimicrobial effect of DOX is slightly suppressed by the presence of fullerenes. The largest influence of all tested solutions on the *S. aureus* culture was observed when solutions of DOX–fullerene conjugates prepared by constant concentration of DOX and varying concentration of fullerenes were applied (Fig. 2D). In this case, even the lowest fullerene concentration (2.5 mg/mL) caused the growth inhibition; however, the impact was not as lethal as in case of exposure to the pure DOX at the same concentration. The obtained results were verified by statistical calculations of IC_{50} values when the lowest value—2500 μg/mL (fullerene concentration) was determined for the last tested variant (Fig. 2D). Based on these results it can be concluded that fullerenes have a significant protective effect against DOX toxicity because for pure DOX solution the IC_{50} is only 15.1 μg/mL.

3.2 Spectroscopic properties of DOX–fullerene conjugates

The promising results obtained using *S. aureus* cultures were encouraging for further investigation of the properties of the DOX–fullerene conjugates. Spectroscopic characterization is shown in Fig. 3. The absorption spectra of conjugates prepared using constant concentration of fullerenes and increasing concentration of DOX exhibit strong signal in the ultraviolet range, and a band with the maximum at 480 nm was observed (Fig. 3A). These signals belong to the DOX molecules adsorbed on the fullerene molecules. Due to the fluorescence properties of DOX, also DOX–fullerene conjugates can be analyzed by fluorescence spectrometry. The intensive maximum of fluorescence emission of the conjugates was detected at 600 nm (Fig. 3B), which is the same wavelength as the emission maximum of DOX solution. Significant quenching of fluorescence was observed depending on the increasing concentration of DOX utilized for preparation of DOX–fullerene conjugates. The fluorescence intensities at 600 nm depending on DOX concentration are plotted in the inset in Fig. 3B. The comparison of the fluorescence intensity of DOX solution and solutions of DOX–fullerene conjugates in the linear range revealed that 47.8% of DOX employed for conjugate preparation was retained and adsorbed to surface of the fullerene molecules.

3.3 Electrochemical properties of DOX–fullerene conjugates

Besides optical, also electrochemical characterization of prepared conjugates was performed (Fig. 3C and D). Using square wave voltammetry, it was observed that DOX solution provided one peak at the potential of −0.47 V (data not shown but correspond to the literature [28–32]), however, when DOX–fullerene conjugates were prepared, the signal changed significantly. Two peaks were observed with maxima at potentials of −0.47 V and −0.51 V. The voltammograms for DOX–fullerenes prepared using constant concentration of fullerenes and varying concentration of DOX (8, 16, 31, 63, 125, 250, and 500 μg/mL) are shown in Fig. 3C. In three lowest concentrations of DOX (8, 16, and 31 μg/mL) the signal was below LOD of the method. For the remaining DOX concentrations (63, 125, 250, and 500 μg/mL), the sum peak area was plotted versus DOX concentration applied for the

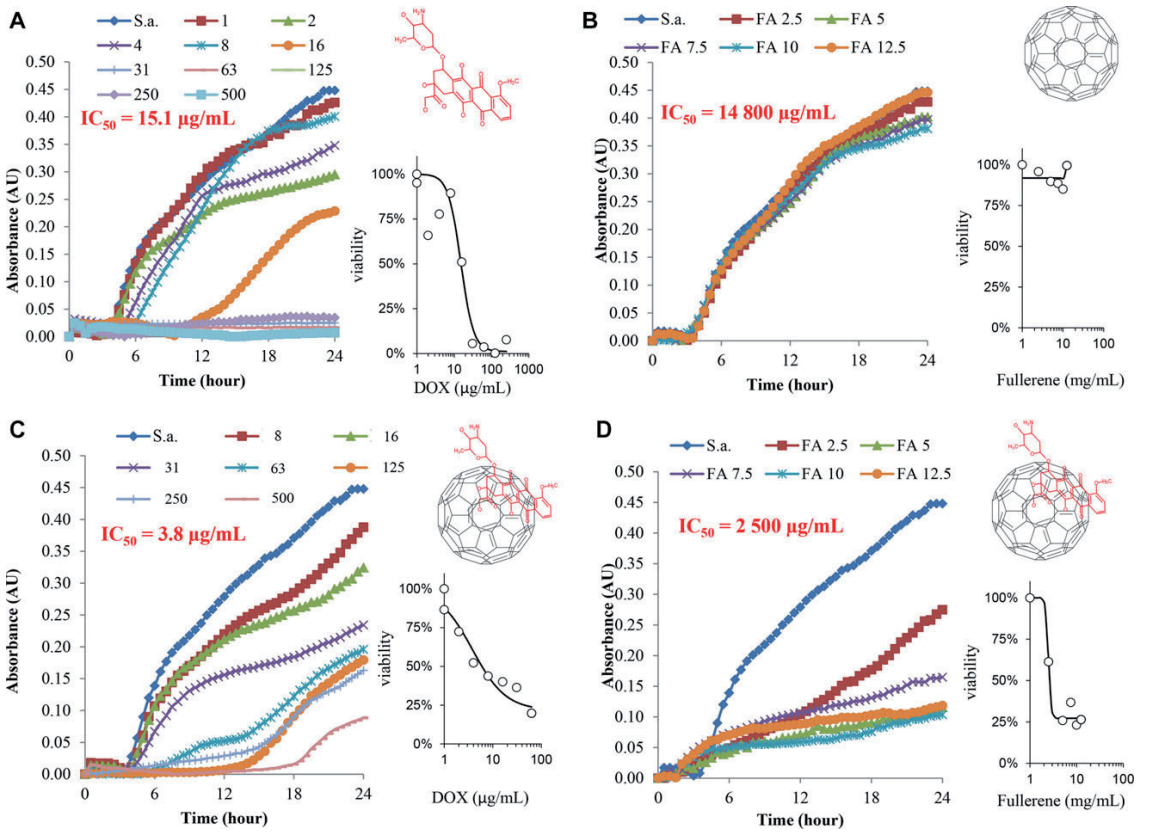

Figure 2. Growth curves of *S. aureus* cultivated in the presence of (A) DOX (0, 1, 2, 4, 8, 16, 31, 63, 125, 250, and 500 µg/mL), (B) fullerenes (0, 2.5, 5, 7.5, 10, and 12.5 mg/mL), (C) conjugates prepared using constant concentration of fullerenes (5 mg/mL) and varying concentration of DOX (0, 8, 16, 31, 63, 125, 250, and 500 µg/mL), and (D) solution prepared using constant concentration of DOX (500 µg/mL) and varying concentration of fullerenes (0, 2.5, 5, 7.5, 10, 12.5 mg/mL). The IC_{50} values were determined for 24 h of influence.

preparation process and a linear trend was observed as shown in the inset in Fig. 3C. The sum peak area was evaluated because it is the most general and suitable method for quantification of such record. The peak height of individual peaks is changing with the changing DOX concentration. The peak 1 height grows with increasing DOX concentration unlike the decreasing peak 2 height.

In the case of the DOX–fullerene conjugates prepared using the constant concentration of DOX and varying concentration of fullerenes the opposite trend was observed, even though the pure fullerene solution is electrochemically inactive and does not provide any peak at the observed potential range. In this place it is necessary to note that electrochemical inactivation of fullerene is connected with the detection method presented here. On the contrary, application of fullerene in the electrochemical research is very widespread [33–36]. The conjugation of DOX with fullerenes caused of the significant decrease of both peaks depending on the increasing amount of fullerene used for the DOX–fullerene conjugation process. The voltammograms are shown in Fig. 3D and as shown in the inset of this figure, the sum peak area is linearly dependent on the concentration of employed fullerenes. This behavior can be explained by the fact that the increasing amount of fullerenes in the solution act as the electronic insulator and prevent the transport of electrons between electrode and DOX molecules.

3.4 HPLC and CE characterization of DOX–fullerene conjugates

The adsorption of DOX molecules on the fullerene molecules leads to the formation of numerous complexes with various stechiometries, which cannot be revealed by stationary analyses and therefore separation techniques including HPLC and CE were employed.

To gain more information about properties of prepared conjugates three different detection techniques were utilized: HPLC-UV, HPLC-ED, and CE-LIF. The results for the set of conjugates prepared using constant concentration of fullerenes and increasing concentration of DOX are shown in Fig. 4. It was found that the retention time of DOX was

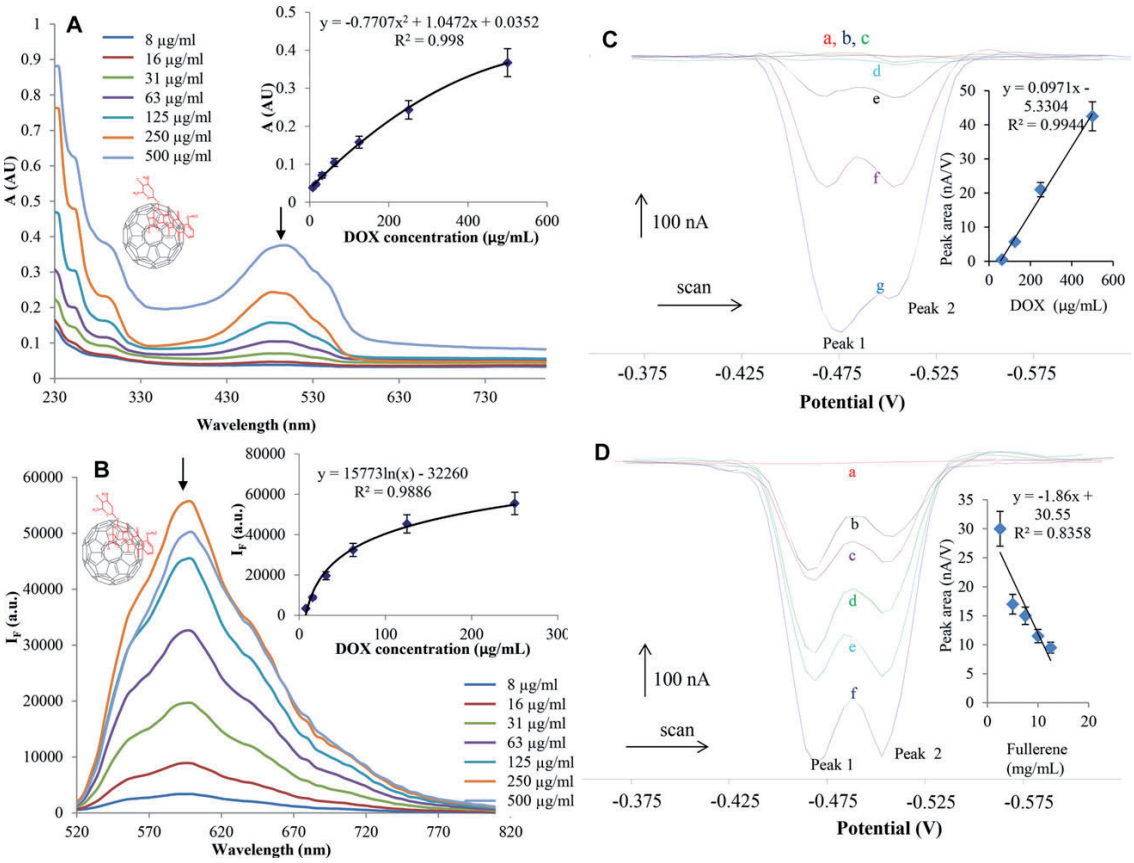

Figure 3. Optical characterization of the prepared conjugates. (A) Absorption spectra of conjugates prepared using constant concentration of fullerenes (5 mg/mL) and varying concentration of DOX (8, 16, 31, 63, 125, 250, and 500 μg/mL), inset: dependence of absorbance on DOX concentration measured at 480 nm. (B) Fluorescence emission spectra of conjugates prepared using constant concentration of fullerenes (5 mg/mL) and varying concentration of DOX (8, 16, 31, 63, 125, 250, and 500 μg/mL), inset: dependence of fluorescence intensity on DOX concentration measured at 600 nm. Electrochemical characterization of the prepared conjugates. (C) Voltammograms of conjugates prepared using constant concentration of fullerenes (5 mg/mL) and varying concentration of DOX (8-a, 16-b, 31-c, 63-d, 125-e, 250-f, and 500-g μg/mL), inset: dependence of the peak area (potential −0.5 V) on DOX concentration. (D) Voltammograms of pure solution of fullerenes (5 mg/mL, a) and conjugates prepared using constant concentration of DOX (500 μg/mL) and varying concentration of fullerenes (2.5-f, 5-e, 7.5-d, 10-c, and 12.5-b mg/mL), inset: dependence of the peak area (potential −0.5 V) on fullerene concentration. All measurements were carried out by square wave voltammetry, parameters were as follows: purging time 120 s; initial potential 0 V; end potential –1.7 V; deposition potential 0.0 V; equilibration time 2 s; time of accumulation 120 s; frequency 150 Hz; step potential 0.005 V; modulation amplitude 0.025 V.

5.9 min under the used HPLC conditions (data not shown). The fact that the signal of pure fullerene solution was not observed under used HPLC conditions using reverse phase and also in the literature the fullerenes are analyzed using different types of separation interactions [37] suggests that the fullerene is retained in the column. Moreover the retention time of DOX and DOX–fullerene conjugates are the same, which supports the hypothesis that the presence of organics in the mobile phase is causing the decomposition of the conjugate and the observed signal belonged to the DOX released from the conjugate. It can be concluded from the results showed in Fig. 4A that the increasing amount of applied DOX led to the increase of the peak height with the retention time of 5.9 min. In the inset of Fig. 5A the dependence of the peak height on the concentration of applied DOX is shown for both electrochemical as well as absorbance detection of HPLC. Both dependences exhibit linear trend with coefficient of determination R^2 of 0.9927 and 0.995, respectively.

On the other hand, analysis by CE-LIF revealed the formation of various complexes of fullerene and DOX (Fig. 4B). Because the fact that the fullerenes do not exhibit fluorescence after the excitation by 488 nm, only conjugates are visualized by this method. The major peak present in the electropherograms is the most abundant complex; however, the formation of other complexes is proved by the presence

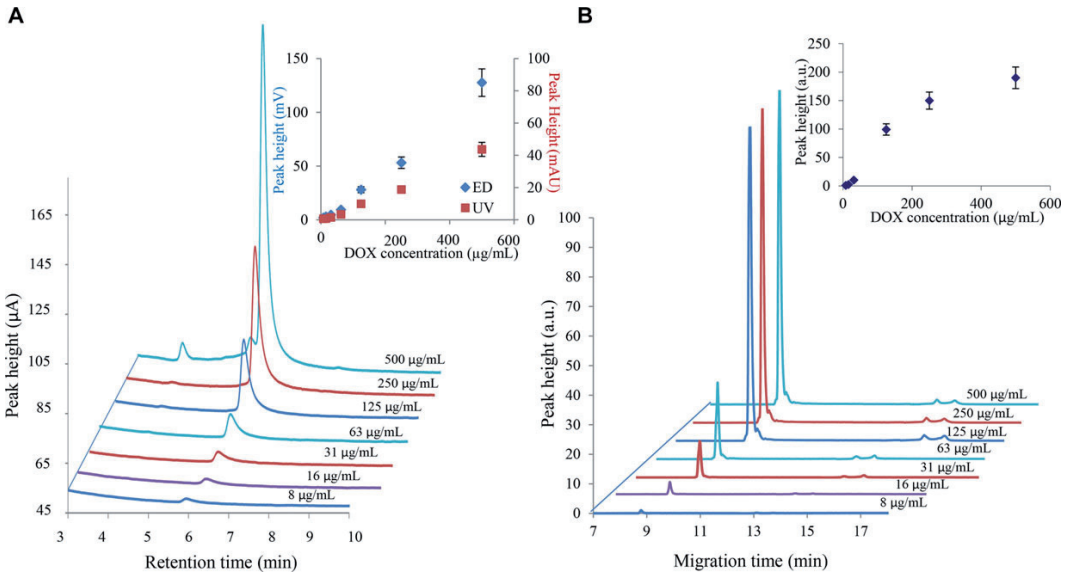

Figure 4. Characterization of DOX–fullerene conjugates by separation techniques. (A) HPLC-ED chromatograms of conjugates prepared using constant concentration of fullerenes (5 mg/mL) and varying concentration of DOX (8, 16, 31, 63, 125, 250, and 500 μg/mL), inset: dependence of the peak height on DOX concentration measured by ED and/or UV detection. (B) Electropherograms measured by CE-LIF of conjugates prepared using constant concentration of fullerenes (5 mg/mL) and varying concentration of DOX (8, 16, 31, 63, 125, 250, and 500 μg/mL); inset: dependence of the peak height on the applied DOX concentration.

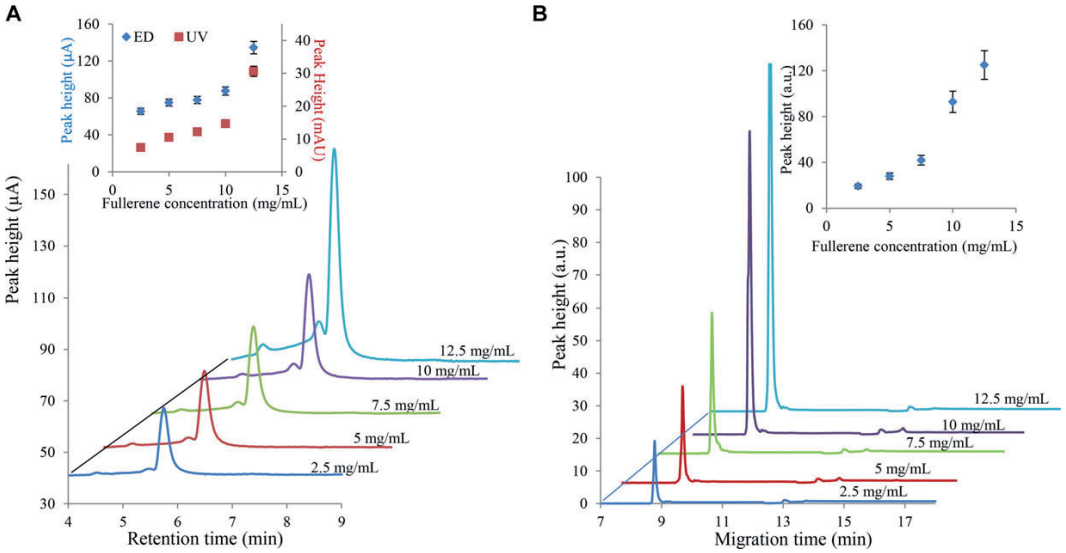

Figure 5. Characterization of DOX–fullerene conjugates by separation techniques. (A) HPLC-ED chromatograms of conjugates prepared using constant concentration of DOX (500 μg/mL) and varying concentration of fullerenes (2.5, 5, 7.5, 10, and 12.5 mg/mL), inset: dependence of the peak height on fullerene concentration measured by ED and UV detection. (B) CE-LIF electropherograms of conjugates prepared using constant concentration of DOX (500 μg/mL) and varying concentration of fullerenes (2.5, 5, 7.5, 10, and 12.5 mg/mL).

of other peaks in the range of 15–17 min with the increasing intensities depending on applied DOX concentration. The dependence of the peak height (major peak) on the concentration of applied DOX is shown in the inset in Fig. 4B. The obtained dependence can be expressed by polynomial equation characterizing the increasing trend of the signal according to concentration of DOX.

Results obtained for the set of solutions prepared using constant concentration of DOX and varying concentration of fullerenes are shown in Fig. 5. Using HPLC an increasing

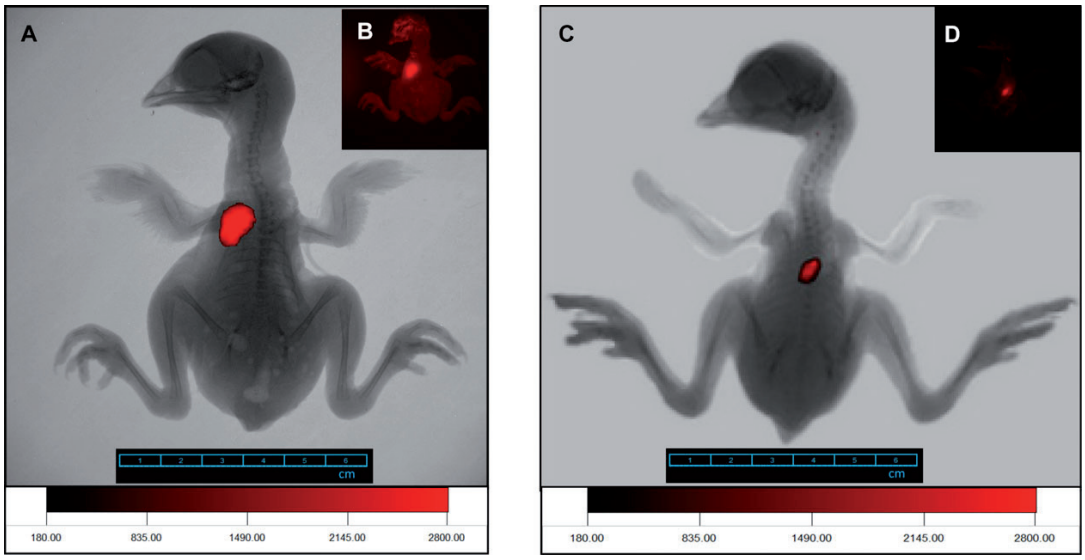

Figure 6. The detection of the DOX in the chicken embryo. Fluorescence monitoring was performed using an In vivo Xtreme system by Carestream. The excitation wavelength was set at 480 nm and the emission was measured at 600 nm. The exposure time 2 s; Binning 2×2 pixels; fStop 1.1; field of view 11.5 × 11.5 cm. (A) Image of chicken embryo (20 days old) administered by DOX–fullerene conjugate (100 μL), overlay of X-ray and fluorescence image, autofluorescence subtracted. (B) Image of chicken embryo administered by DOX–fullerene conjugate, fluorescence image without the subtraction of the autofluorescence. (C) Image of chicken embryo (19 days old) administered by DOX (100 μL), overlay of X-ray and fluorescence image, autofluorescence subtracted. (D) Image of chicken embryo administered by DOX, fluorescence image without the subtraction of the autofluorescence.

trend depending on the increasing the amount of fullerenes is observed (Fig. 5A). As noted previously, the DOX molecules are adsorbed on the fullerene molecules and in the HPLC the DOX is released. This is in agreement with the idea that the increasing amount of fullerenes adsorbs an increasing amount of DOX, which is subsequently released and detected in HPLC. Therefore, the signal of DOX enhanced with the increased concentration of fullerenes as it is shown in the inset in Fig. 5A. The peaks present in chromatograms besides the main peak with migration time of 5.9 min are caused due to the impurities in DOX.

The results for the set of samples prepared using the constant DOX concentration and varying fullerene concentration analyzed by CE-LIF are shown in Fig. 5B. The major peak with migration time of 8.5 min exhibits an increasing signal depending on the increasing concentration of fullerenes. Similarly, the minor peaks with migration time 13–15 min exhibit higher signal in the case of 12.5 mg/mL of fullerenes than in the case of lower concentrations as shown in the inset of the Fig. 5B.

3.5 In vivo sensing of DOX–fullerene conjugates

Finally, behavior of the DOX–fullerene conjugates in the living organism was investigated to verify their great potential for transport and targeted delivery of the cytostatic drugs. Due to the excellent fluorescent properties of DOX, in vivo imaging observation is possible [22]. Moreover, as mentioned, fullerenes exhibit protective properties against the toxic effect of the DOX. The chicken embryo was taken out of the eggshell and the DOX or DOX–fullerene conjugate was applied into the breast muscle tissue, the feather was removed and the autofluorescence of muscle tissue was eliminated by software. Due to the good fluorescence properties of the DOX, it was possible to observe the distribution of DOX–fullerenes in muscle tissues. Fluorescence detected in the chicken using pure DOX solution (100 μL, 500 μg/mL) injected into the 5 mm under the skin is shown in Fig. 6A. The mean fluorescence intensity of DOX was 6549 a.u. The fluorescence image is shown in Fig. 6B—showing besides the signal of DOX also the autofluorescence of the muscle tissue. In Fig. 6C, the chicken embryo administered by the DOX–fullerene conjugates (100 μL, 500 μg/mL DOX, and 5 mg/mL fullerenes) is shown to demonstrate the possibility of the conjugates to be detected by the in vivo system. The mean fluorescence intensity of the conjugates was 5849 a.u. The fluorescence intensity of conjugates was lower compared to pure DOX due to the incomplete conjugation onto the fullerene surface.

Furthermore, the DOX–fullerenes conjugates (250 μL) prepared by the constant concentration of fullerenes (5 mg/mL) and varying concentration of DOX (31, 63, 125, 250, and 500 μg/mL) were administered into the egg yolk of the five specimens of 17 day-old chicken embryos and incubated for 4 h to enable the distribution of the DOX–fullerene conjugates into the embryo. After the desired time the embryos were extracted and the discrete organs (heart, brain, liver, and intestine) were analyzed using HPLC to determine

Table 1. Quantification of DOX supplied in the form of DOX–fullerene conjugates (with varying DOX concentration) accumulated in particular organ of the chicken embryo

		DOX–fullerene		
		Concentration (μg/g)	Sum (μg/g)	Average (μg/g)
500 μg/mL	Brain	1.1	32.2	8.05
	Heart	5.5		
	Liver	3.6		
	Intestine	22.0		
250 μg/mL	Brain	0.5	7.3	1.8
	Heart	3.5		
	Liver	1.1		
	Intestine	2.2		
125 μg/mL	Brain	0.5	2.7	0.7
	Heart	0.8		
	Liver	0.6		
	Intestine	0.8		
63 μg/mL	Brain	0.3	2.7	0.7
	Heart	0.7		
	Liver	1.1		
	Intestine	0.6		
31 μg/mL	Brain	0.4	1.3	0.3
	Heart	0.9		
	Liver	ND		
	Intestine	ND		

the DOX amount. The DOX amount in the organs, the average and total (sum) amount determined per each chicken is summarized in Table 1. As expected the total (sum) and average DOX amount is decreasing depending on the concentration of DOX applied to the preparation process of conjugates. However, within one chicken the DOX amount varied depending on the analyzed organ. Generally, in all studied chicken embryos the highest DOX concentration was determined in the intestine followed by heart and liver.

4 Concluding remarks

The DOX is effective cytostatics, however, exhibiting severe side effect, which can be eliminated by number of approaches [38]. One of them is the conjugation with fullerenes, which have proven to have protective properties against the DOX toxicity. Concurrently, fullerenes increase the size of the DOX molecule and therefore the time before the drug is eliminated from the organism is prolonged. In this study, we demonstrated the conjugation procedure for formation of the DOX–fullerene complexes and their characterization by optical and electrochemical method. Finally, in vivo monitoring of the conjugates in the chicken embryos was performed investigating their distribution in the particular organs of the chicken embryo.

Financial support from CYTORES GA CR P301/10/0356 (EA 14) and CEITEC CZ.1.05/1.1.00/02.0068 is highly acknowledged.

The authors have declared no conflict of interest.

5 References

[1] Dunk, P. W., Kaiser, N. K., Hendrickson, C. L., Quinn, J. P., Ewels, C. P., Nakanishi, Y., Sasaki, Y., Shinohara, H., Marshall, A. G., Kroto, H. W., *Nat. Commun.* 2012, *3*, 855.

[2] Rogers, J. A., Lagally, M. G., Nuzzo, R. G., *Nature* 2011, *477*, 45–53.

[3] Guo, F. W., Yang, B., Yuan, Y. B., Xiao, Z. G., Dong, Q. F., Bi, Y., Huang, J. S., *Nat. Nanotechnol.* 2012, *7*, 798–802.

[4] Popov, A. A., Yang, S. F., Dunsch, L., *Chem. Rev.* 2013, *113*, 5989–6113.

[5] Ji, S. R., Liu, C., Zhang, B., Yang, F., Xu, J., Long, J. A., Jin, C., Fu, D. L., Ni, Q. X., Yu, X. J., *Biochim. Biophys. Acta-Rev. Cancer* 2010, *1806*, 29–35.

[6] Pumera, M., *Curr. Drug Metab.* 2012, *13*, 251–256.

[7] Chen, Z. Y., Mao, R. Q., Liu, Y., *Curr. Drug Metab.* 2012, *13*, 1035–1045.

[8] Injac, R., Perse, M., Boskovic, M., Djordjevic-Milic, V., Djordjevic, A., Hvala, A., Cerar, A., Strukej, B., *Technol. Cancer Res. Treat.* 2008, *7*, 15–25.

[9] Jacevic, V., Djordjevic-Milic, V., Dragojevic-Simic, V., Radic, N., Govedarica, B., Dobric, S., Srdjenovic, B., Injac, R., Djordjevic, A., Vasovic, V., *Toxicol. Lett.* 2007, *172*, S146–S146.

[10] Milic, V. D., Djordjevic, A., Dobric, S., Injac, R., Vuckovic, D., Stankov, K., Simic, V. D., Suvajdzic, L., in: Uskokovic, D. P., Milonjic, S. K., Rakovic, D. I. (Eds.), *Recent Developments in Advanced Materials and Processes*, Trans Tech Publications Ltd, Zurich-Uetikon 2006, pp. 525–529.

[11] Icevic, I. D., Vukmirovic, S. N., Srdenovic, B. U., Sudji, J. J., Djordjevic, A. N., Injac, R. M., Vasovic, V. M., *Hem. Ind.* 2011, *65*, 329–337.

[12] Li, X. H., Zhang, C., Le Guyader, L., Chen, C. Y., *Sci. China-Chem.* 2010, *53*, 2241–2249.

[13] Liu, J. H., Cao, L., Luo, P. J. G., Yang, S. T., Lu, F. S., Wang, H. F., Meziani, M. J., Haque, S. A., Liu, Y. F., Lacher, S., Sun, Y. P., *ACS Appl. Mater. Interfaces* 2010, *2*, 1384–1389.

[14] Zakharian, T. Y., Seryshev, A., Sitharaman, B., Gilbert, B. E., Knight, V., Wilson, L. J., *J. Am. Chem. Soc.* 2005, *127*, 12508–12509.

[15] Kizek, R., Adam, V., Hrabeta, J., Eckschlager, T., Smutny, S., Burda, J. V., Frei, E., Stiborova, M., *Pharmacol. Ther.* 2012, *133*, 26–39.

[16] Bogdanovic, G., Kojic, V., Dordevic, A., Canadanovic-Brunet, J., Vojinovic-Miloradov, M., Baltic, V. V., *Toxicol. Vitro* 2004, *18*, 629–637.

[17] Injac, R., Perse, M., Cerne, M., Potocnik, N., Radic, N., Govedarica, B., Djordjevic, A., Cerar, A., Strukelj, B., *Biomaterials* 2009, *30*, 1184–1196.

[18] Heister, E., Neves, V., Tilmaciu, C., Lipert, K., Beltran, V. S., Coley, H. M., Silva, S. R. P., McFadden, J., *Carbon* 2009, *47*, 2152–2160.

[19] Ali-Boucetta, H., Al-Jamal, K. T., McCarthy, D., Prato, M., Bianco, A., Kostarelos, K., *Chem. Commun.* 2008, *2008*, 459–461.

[20] Chaudhuri, P., Paraskar, A., Soni, S., Mashelkar, R. A., Sengupta, S., *ACS Nano* 2009, *3*, 2505–2514.

[21] Liu, Z., Sun, X. M., Nakayama-Ratchford, N., Dai, H. J., *ACS Nano* 2007, *1*, 50–56.

[22] Blazkova, I., Vaculovicova, M., Eckschlager, T., Stiborova, M., Trnkova, L., Adam, V., Kizek, R., *Chem. Sensors* 2014, *4*, 9.

[23] Lu, F. S., Haque, S. A., Yang, S. T., Luo, P. G., Gu, L. R., Kitaygorodskiy, A., Li, H. P., Lacher, S., Sun, Y. P., *J. Phys. Chem. C* 2009, *113*, 17768–17773.

[24] Fernandez-Saiz, P., Soler, C., Lagaron, J. M., Ocio, M. J., *Int. J. Food Microbiol.* 2010, *137*, 287–294.

[25] Borneman, D. L., Ingham, S. C., Ane, C., *J. Food Prot.* 2009, *72*, 1190–1200.

[26] Rufian-Henares, J. A., Morales, F. J., *Food Chem.* 2008, *111*, 1069–1074.

[27] Hevia, D., Rodriguez-Garcia, A., Cimadevilla, H. M., Mayo, J. C., *Eur. J. Cancer* 2012, *48*, S246–S246.

[28] Huska, D., Adam, V., Babula, P., Hrabeta, J., Stiborova, M., Eckschlager, T., Trnkova, L., Kizek, R., *Electroanalysis* 2009, *21*, 487–494.

[29] Huska, D., Adam, V., Burda, J., Hrabeta, J., Eckschlager, T., Babula, P., Opatrilova, R., Trnkova, L., Stiborova, M., Kizek, R., *Febs J.* 2009, *276*, 109–109.

[30] Hynek, D., Krejcova, L., Zitka, O., Adam, V., Trnkova, L., Sochor, J., Stiborova, M., Eckschlager, T., Hubalek, J., Kizek, R., *Int. J. Electrochem. Sci.* 2012, *7*, 13–33.

[31] Hynek, D., Krejcova, L., Zitka, O., Adam, V., Trnkova, L., Sochor, J., Stiborova, M., Eckschlager, T., Hubalek, J., Kizek, R., *Int. J. Electrochem. Sci.* 2012, *7*, 34–49.

[32] Masarik, M., Krejcova, L., Hynek, D., Adam, V., Stiborova, M., Eckschlager, T., Kizek, R., *Int. J. Mol. Med.* 2012, *30*, S45–S45.

[33] Morita, T., Lindsay, S., *J. Phys. Chem. B* 2008, *112*, 10563–10572.

[34] Park, B. K., Lee, G., Kim, K. H., Kang, H., Lee, C. Y., Miah, M. A., Jung, J., Han, Y. K., Park, J. T., *J. Am. Chem. Soc.* 2006, *128*, 11160–11172.

[35] Winkler, K., Balch, A. L., Kutner, W., *J. Solid State Electrochem.* 2006, *10*, 761–784.

[36] Winkler, K., Costa, D. A., Balch, A. L., *Pol. J. Chem.* 2000, *74*, 1–37.

[37] Coutant, D. E., Clarke, S. A., Francis, A. H., Meyerhoff, M. E., *J. Chromatogr. A* 1998, *824*, 147–157.

[38] Blazkova, I., Nguyen, V. H., Dostalova, S., Kopel, P., Stanisavljevic, M., Vaculovicova, M., Stiborova, M., Eckschlager, T., Kizek, R., Adam, V., *Int. J. Mol. Sci.* 2013, *14*, 13391–13402.

6 CONCLUSION

The research in tumour disease treatment moved from nonspecific cytotoxic chemotherapy to targeting cancer-associated pathways. NPs have emerged as the novel cancer therapeutics, which could target the drug to the tumour and to overcome some limitations of conventional treatment. Drug conjugation with NPs can highly influence their therapeutic index. NPs can enhance the solubility, prolong the circulation in the bloodstream and selectively deliver the drug to the side of the action. NPs with the optimal particle sizes and surface properties, can passively target drugs into the tumour tissues via the EPR effect or can be conjugated with targeting ligands and be actively delivered to the tumour. Although, the nanotechnologies are widely studied till the date there are only few NPs based drugs used in clinical practise. Despite a number of positive effects, there are also some negative impacts. The toxicity and pharmacokinetic of NPs is widely discussed. The mechanism of NPs action and influence of their usage to human organism is still in the shadows of the unknown and undiscovered. One of the fundamental difficulties in cancer therapy is the great genetic diversification in cancers and also diverse response of patients to the treatment. The future of nanomedicine could yield innovative platforms for tumour treatment and the focus to the personalised medicine is expected.

In this work, one of the most effective and one of the most used anthracycline drugs DOX was studied. DOX is a molecule with very good fluorescence properties and these properties were utilized for its detection. It can be concluded that strong DOX interaction with amino acids as well as with protein albumin was detected. DOX interaction with myocardium caused the decrease of all analysed amino acids and this decrease could be connected to the DOX associated toxicity. The interaction with blood protein albumin is very fast and low concentration of free drug was detected in the solution. The toxicological studies showed decrease toxicity of DOX conjugated with fullerenes compared to the free DOX. Properties of DOX encapsulated in the liposomes are considerably influenced by the concentration of cholesterol in the lipid bilayer and can significantly influence transport of DOX in the body. The concentration of DOX in organs was directly proportional to the applied dose of DOX-fullerene conjugates and the highest concentration of DOX differed among the organs, the highest DOX concentration was determined in the intestine followed by heart and liver. Nanotransporters, such as

liposomes and fullerenes, have positive effect on the DOX toxicity and behaviour and seem to be good tools for the targeted drug delivery.

7 LITERATURE

Abla, A. A. and M. T. Lawton (2014). "Indocyanine green angiography for cerebral aneurysm surgery: advantages, limitations, and neurosurgeon intuition." World Neurosurgery **82**(5): E585-E586.

Abrahamsson, P. B. (2013). Method and device for microdialysis sampling, MD Biomedical AB.

Agudelo, D., P. Bourassa, et al. (2014). "Intercalation of antitumor drug doxorubicin and its analogue by DNA duplex: Structural features and biological implications." International Journal of Biological Macromolecules **66**: 144-150.

Ahmed, L. A. and S. A. El-Maraghy (2013). "Nicorandil ameliorates mitochondrial dysfunction in doxorubicin-induced heart failure in rats: Possible mechanism of cardioprotection." Biochemical Pharmacology **86**(9): 1301-1310.

Akin, O., S. B. Brennan, et al. (2012). "Advances in oncologic imaging update on 5 common cancers." Ca-a Cancer Journal for Clinicians **62**(6): 364-393.

Al-Bataineh, O., J. Jenne, et al. (2012). "Clinical and future applications of high intensity focused ultrasound in cancer." Cancer Treatment Reviews **38**(5): 346-353.

Alkilany, A. M. and C. J. Murphy (2010). "Toxicity and cellular uptake of gold nanoparticles: what we have learned so far?" Journal of Nanoparticle Research **12**(7): 2313-2333.

Alsaad, A. M. S., B. N. M. Zordoky, et al. (2012). "Chronic doxorubicin cardiotoxicity modulates cardiac cytochrome P450-mediated arachidonic acid metabolism in rats." Drug Metabolism and Disposition **40**(11): 2126-2135.

An, H. J. and B. Jin (2015). "Fullerenols and fullerene alter cell growth and metabolisms of Escherichia coli." Journal of Biomedical Nanotechnology **11**(7): 1261-1268.

Anbarasan, B., S. V. Babu, et al. (2015). "pH responsive release of doxorubicin to the cancer cells by functionalized multi-walled carbon nanotubes." Journal of Nanoscience and Nanotechnology **15**(7): 4799-4805.

Andreadou, I., F. Sigala, et al. (2007). "Acute doxorubicin cardiotoxicity is successfully treated with the phytochemical oleuropein through suppression of oxidative and nitrosative stress." Journal of Molecular and Cellular Cardiology **42**(3): 549-558.

Arora, H. C., M. P. Jensen, et al. (2012). "Nanocarriers enhance doxorubicin uptake in drug-resistant ovarian cancer cells." Cancer Research **72**(3): 769-778.

Baalbergen, A., Y. Veenstra, et al. (2013). "Primary surgery versus primary radiotherapy with or without chemotherapy for early adenocarcinoma of the uterine cervix." The Cochrane database of systematic reviews **1**: CD006248.

Bains, O. S., A. Szeitz, et al. (2013). "A Correlation between Cytotoxicity and Reductase-Mediated Metabolism in Cell Lines Treated with Doxorubicin and Daunorubicin." Journal of Pharmacology and Experimental Therapeutics **347**(2): 375-387.

Balas, C. (2009). "Review of biomedical optical imaging-a powerful, non-invasive, non-ionizing technology for improving in vivo diagnosis." Measurement Science & Technology **20**(10): 1-12.

Banday, A. H., S. Jeelani, et al. (2015). "Cancer vaccine adjuvants - recent clinical progress and future perspectives." Immunopharmacology and Immunotoxicology **37**(1): 1-11.

Bangham, A. D. (1993). "Liposomes - the babraham connection." Chemistry and Physics of Lipids **64**(1-3): 275-285.

Bangham, A. D. and R. W. Horne (1964). "Negative staining of phospholipids + their structural modification by-surface active agents as observed in electron microscope." Journal of Molecular Biology **8**(5): 660-&.

Barenholz, Y. (2001). "Liposome application: problems and prospects." Current Opinion in Colloid & Interface Science **6**(1): 66-77.

Barenholz, Y. (2012). "Doxil (R) - The first FDA-approved nano-drug: Lessons learned." Journal of Controlled Release **160**(2): 117-134.

Barenholz, Y. and D. Peer (2012). "Liposomes and other assemblies as drugs and nano-drugs: From basic and translational research to the clinics preface." Journal of Controlled Release **160**(2): 115-116.

Batist, G., G. Ramakrishnan, et al. (2001). "Reduced cardiotoxicity and preserved antitumor efficacy of liposome-encapsulated doxorubicin and cyclophosphamide compared with conventional doxorubicin and cyclophosphamide in a randomized, multicenter trial of metastatic breast cancer." Journal of Clinical Oncology **19**(5): 1444-1454.

Berg, W. A., Z. Zhang, et al. (2012). "Detection of breast cancer with addition of annual screening ultrasound or a single screening mri to mammography in women with elevated breast cancer risk." Jama-Journal of the American Medical Association **307**(13): 1394-1404.

Bertrand, N. and J. C. Leroux (2012). "The journey of a drug-carrier in the body: An anatomo-physiological perspective." Journal of Controlled Release **161**(2): 152-163.

Bertrand, N., J. Wu, et al. (2014). "Cancer nanotechnology: The impact of passive and active targeting in the era of modern cancer biology." Advanced Drug Delivery Reviews **66**: 2-25.

Bjelogrlic, S. K., S. T. Lukic, et al. (2013). "Activity of dexrazoxane and amifostine against late cardiotoxicity induced by the combination of doxorubicin and cyclophosphamide in vivo." Basic & Clinical Pharmacology & Toxicology **113**(4): 228-238.

Blazkova, I., S. Dostalova, et al. (2012). "Protinadorove lecivo doxorubicin a jeho in vivo analyza fluorescencni mikroskopii." CHEMagazín **22**(5): 8-10.

Blazkova, I., N. Hoai Viet, et al. (2013). "Apoferritin modified magnetic particles as doxorubicin carriers for anticancer drug delivery." International Journal of Molecular Sciences **14**(7): 13391-13402.

Blazkova, I., M. Konecna, et al. (2014). "Application of quantum dots into chicken embryos." Journal of Metallomics and Nanotechnologies **1**(3): 26-28.

Blazkova, I., M. Ryvolova, et al. (2013). "Modern imaging techniques for anthracycline cytostatics – Review of the Literature." Klinicka Onkologie **26**(4): 239-244.

Blazkova, I., M. Vaculovicova, et al. (2014). "Study of fluorescence of doxorubicin in muscle tissue using highly sensitive fluorescence sensing." Chem. Sensors **4**(9): 1-6.

Blazkova, I., M. Vaculovicova, et al. (2014). "Study of fluorescence of doxorubicin in muscle tissue using highly sensitive fluorescence sensing." Chem. Sensors **in press**.

Bossers, S. M., R. D. H. de Boer, et al. (2013). "The diagnostic accuracy of brain microdialysis during surgery: a qualitative systematic review." Acta Neurochirurgica **155**(2): 345-353.

Bouccara, S., G. Sitbon, et al. (2015). "Enhancing fluorescence in vivo imaging using inorganic nanoprobes." Current Opinion in Biotechnology **34**: 65-72.

Bradshaw, T. D., M. Junor, et al. (2013). "Apoferritin-encapsulated PbS quantum dots significantly inhibit growth of colorectal carcinoma cells." Journal of Materials Chemistry B **1**(45): 6254-6260.

Bray, L. J., M. Binner, et al. (2014). "Three dimensional in vitro models for studying cancer angiogenesis." Anticancer Research **34**(10): 5849-5849.

Bremer, C., V. Ntziachristos, et al. (2003). "Optical-based molecular imaging: contrast agents and potential medical applications." European Radiology **13**(2): 231-243.

Brown, A. P., E. J. Chung, et al. (2010). "Evaluation of the fullerene compound DF-1 as a radiation protector." Radiation Oncology **5**.

Bucci, M., V. Vellecco, et al. (2012). "Hydrogen sulphide is involved in human malignant hypertermia." Nitric Oxide-Biology and Chemistry **27**: S27-S28.

Buitrago, E. F., E. Otamendi, et al. (2011). "Therapeutic drug monitoring of a pegylated liposomal doxorubicin formulation in ovarian cancer patients using a microdialysis technique." Therapeutic Drug Monitoring **33**(4): 550-550.

Buss, I., G. V. Kalayda, et al. (2012). "Effect of reactivity on cellular accumulation and cytotoxicity of oxaliplatin analogues." Journal of Biological Inorganic Chemistry **17**(5): 699-708.

Carmeliet, P. and R. K. Jain (2000). "Angiogenesis in cancer and other diseases." Nature **407**(6801): 249-257.

Carter, H. B., P. C. Albertsen, et al. (2013). "Early detection of prostate cancer: AUA guideline." Journal of Urology **190**(2): 419-426.

Carubelli, V., A. I. Castrini, et al. (2015). "Amino acids and derivatives, a new treatment of chronic heart failure?" Heart Failure Reviews **20**(1): 39-51.

Carvalho, C., R. X. Santos, et al. (2009). "Doxorubicin: The good, the bad and the ugly effect." Current Medicinal Chemistry **16**(25): 3267-3285.

Castro Neto, A. H., F. Guinea, et al. (2006). "Drawing conclusions from graphene." Physics World **19**(11): 33-37.

Clough, G. F. (2005). "Microdialysis of large molecules." Aaps Journal **7**(3): E686-E692.

Cooper, G. M. (2000). The cell: A molecular approach. Sunderland (MA), Sinauer Associates.

Cooper, J. K., A. M. Franco, et al. (2011). "Characterization of primary amine capped CdSe, ZnSe, and ZnS Quantum Dots by FT-IR: Determination of surface bonding interaction and identification of selective desorption." Langmuir **27**(13): 8486-8493.

Cramer, D. W., R. C. Bast, et al. (2011). "Ovarian cancer biomarker performance in prostate, lung, colorectal, and ovarian cancer screening trial specimens." Cancer Prevention Research **4**(3): 365-374.

Crispo, A., M. Grimaldi, et al. (2015). "BMI and breast cancer prognosis benefit: Mammography screening reveals differences between normal weight and overweight women." Breast **24**(1): 86-89.

Cukierman, E. and D. R. Khan (2010). "The benefits and challenges associated with the use of drug delivery systems in cancer therapy." Biochemical Pharmacology **80**(5): 762-770.

Cutrin, J. C., S. G. Crich, et al. (2013). "Curcumin/gd loaded apoferritin: a novel "theranostic" agent to prevent hepatocellular damage in toxic induced acute hepatitis." Molecular Pharmaceutics **10**(5): 2079-2085.

Cutts, S. M., A. Nudelman, et al. (2005). "The power and potential of doxorubicin-DNA adducts." Iubmb Life **57**(2): 73-81.

Czernin, J. and M. E. Phelps (2002). "Positron emission tomography scanning: Current and future applications." Annual Review of Medicine **53**: 89-112.

Dahlin, A. P., M. Wetterhall, et al. (2010). "Methodological aspects on microdialysis protein sampling and quantification in biological fluids: an in vitro study on human ventricular CSF." Analytical Chemistry **82**(11): 4376-4385.

Das, M., C. Mohanty, et al. (2012). "Nanotechnology for regenerative medicine." Nanotechnology in Health Care: 297-319.

Das, M., R. P. Singh, et al. (2013). "Intranuclear drug delivery and effective in vivo cancer therapy via estradiol-peg-appended multiwalled carbon nanotubes." Molecular Pharmaceutics **10**(9): 3404-3416.

Das, M., R. P. Singh, et al. (2013). "Surface chemistry dependent "switch" regulates the trafficking and therapeutic performance of drug-loaded carbon nanotubes." Bioconjugate Chemistry **24**(4): 626-639.

Davis, M. E., Z. Chen, et al. (2008). "Nanoparticle therapeutics: an emerging treatment modality for cancer." Nature Reviews Drug Discovery **7**(9): 771-782.

De Beer, E. L., A. E. Bottone, et al. (2001). "Doxorubicin and mechanical performance of cardiac trabeculae after acute and chronic treatment: a review." European Journal of Pharmacology **415**(1): 1-11.

Dellinger, A., Z. G. Zhou, et al. (2013). "Application of fullerenes in nanomedicine: an update." Nanomedicine **8**(7): 1191-1208.

Deng, S. W., T. D. Yan, et al. (2014). "Dexrazoxane may prevent doxorubicin-induced DNA damage via depleting both Topoisomerase II isoforms." Bmc Cancer **14**.

Deniset-Besseau, A., F.-A. Miannay, et al. (2012). "A fluorescence-based assay for monitoring clinical drug resistance." Journal of Clinical Pathology **65**(11): 1003-1007.

Dickey, J. S., Y. Gonzalez, et al. (2013). "Mito-tempol and dexrazoxane exhibit cardioprotective and chemotherapeutic effects through specific protein oxidation and autophagy in a syngeneic breast tumor preclinical model." Plos One **8**(8).

Dominguez-Vera, J. M., B. Fernandez, et al. (2010). "Native and synthetic ferritins for nanobiomedical applications: recent advances and new perspectives." Future Medicinal Chemistry **2**(4): 609-618.

Dong, X. and R. J. Mumper (2010). "Nanomedicinal strategies to treat multidrug-resistant tumors: current progress." Nanomedicine **5**(4): 597-615.

Doroshow, J. H. (2012). "Dexrazoxane for the prevention of cardiac toxicity and treatment of extravasation injury from the anthracycline antibiotics." Current Pharmaceutical Biotechnology **13**(10): 1949-1956.

Dragojevic-Simic, V., S. Dobric, et al. (2013). "Efficacy of amifostine in protection against doxorubicin-induced acute cardiotoxic effects in rats." Vojnosanitetski Pregled **70**(1): 38-45.

Drake, K. J., V. Y. Sidorov, et al. (2012). "Amino acids as metabolic substrates during cardiac ischemia." Experimental Biology and Medicine **237**(12): 1369-1378.

Dreaden, E. C., A. M. Alkilany, et al. (2012). "The golden age: gold nanoparticles for biomedicine." Chemical Society Reviews **41**(7): 2740-2779.

Drummond, D. C., O. Meyer, et al. (1999). "Optimizing liposomes for delivery of chemotherapeutic agents to solid tumors." Pharmacological Reviews **51**(4): 691-743.

Du, J.-Z., X.-J. Du, et al. (2011). "Tailor-made dual pH-sensitive polymer-doxorubicin nanoparticles for efficient anticancer drug delivery." Journal of the American Chemical Society **133**(44): 17560-17563.

Dulkeith, E., A. C. Morteani, et al. (2002). "Fluorescence quenching of dye molecules near gold nanoparticles: Radiative and nonradiative effects." Physical Review Letters **89**(20).

Eckers, E. and M. Deponte (2012). "No need for labels: The autofluorescence of Leishmania tarentolae mitochondria and the necessity of negative controls." Plos One **7**(10).

Eizaguirre, A., M. Yanez, et al. (2012). "Stability and iron coordination in DNA adducts of anthracycline based anti-cancer drugs." Physical Chemistry Chemical Physics **14**(36): 12505-12514.

El Boghdady, N. A. (2013). "Antioxidant and antiapoptotic effects of proanthocyanidin and ginkgo biloba extract against doxorubicin-induced cardiac injury in rats." Cell Biochemistry and Function **31**(4): 344-351.

Ernsting, M. J., M. Murakami, et al. (2013). "Factors controlling the pharmacokinetics, biodistribution and intratumoral penetration of nanoparticles." Journal of Controlled Release **172**(3): 782-794.

Esserman, L. J., I. M. Thompson, et al. (2013). "Overdiagnosis and overtreatment in cancer an opportunity for improvement." Jama-Journal of the American Medical Association **310**(8): 797-798.

Farwell, M. D., D. A. Pryma, et al. (2014). "PET/CT imaging in cancer: Current applications and future directions." Cancer **120**(22): 3433-3445.

Ferlay, J., E. Steliarova-Foucher, et al. (2013). "Cancer incidence and mortality patterns in Europe: Estimates for 40 countries in 2012." European Journal of Cancer **49**(6): 1374-1403.

Finkel, T. (2012). "Signal tansduction by mitochondrial oxidants." Journal of Biological Chemistry **287**(7): 4434-4440.

Forrest, R. A., L. P. Swift, et al. (2012). "Activation of DNA damage response pathways as a consequence of anthracycline-DNA adduct formation." Biochemical Pharmacology **83**(12): 1602-1612.

Frangioni, J. V. (2003). "In vivo near-infrared fluorescence imaging." Current Opinion in Chemical Biology **7**(5): 626-634.

Freilich, J., E. A. Mellon, et al. (2014). "Outcomes of adjuvant radiotherapy and lymph node dissection in elderly patients with pancreatic cancer treated with surgery and chemotherapy." Journal of Clinical Oncology **32**(3).

Gabizon, A., M. Bradbury, et al. (2015). "Cancer nanomedicines: closing the translational gap." Lancet **384**(9961): 2175-2176.

Gallo, J., I. Garcia, et al. (2014). "CdTe-Based QDs: preparation, cytotoxicity, and tumor cell death by targeting transferrin receptor." Particle & Particle Systems Characterization **31**(1): 126-133.

Gannon, C. J., C. R. Patra, et al. (2008). "Intracellular gold nanoparticles enhance non-invasive radiofrequency thermal destruction of human gastrointestinal cancer cells." Journal of Nanobiotechnology **6**: 2-Article No.: 2.

Gautier, J., E. Allard-Vannier, et al. (2013). "Recent advances in theranostic nanocarriers of doxorubicin based on iron oxide and gold nanoparticles." Journal of Controlled Release **169**(1-2): 48-61.

Geszke-Moritz, M. and M. Moritz (2013). "Quantum dots as versatile probes in medical sciences: Synthesis, modification and properties." Materials Science & Engineering C-Materials for Biological Applications **33**(3): 1008-1021.

Giannaccini, M., A. Cuschieri, et al. (2014). "Non-mammalian vertebrate embryos as models in nanomedicine." Nanomedicine-Nanotechnology Biology and Medicine **10**(4): 703-719.

Giess, C. S., E. P. Frost, et al. (2012). "Difficulties and errors in diagnosis of breast neoplasms." Seminars in Ultrasound Ct and Mri **33**(4): 288-299.

Gilliam, L. A. A., K. H. Fisher-Wellman, et al. (2013). "The anticancer agent doxorubicin disrupts mitochondrial energy metabolism and redox balance in skeletal muscle." Free Radical Biology and Medicine **65**: 988-996.

Gomes, S. A. O., C. S. Vieira, et al. (2011). "CdTe and CdSe quantum dots cytotoxicity: A comparative study on microorganisms." Sensors **11**(12): 11664-11678.

Gong, J., M. Chen, et al. (2012). "Polymeric micelles drug delivery system in oncology." Journal of Controlled Release **159**(3): 312-323.
Gorthi, S. S., D. Schaak, et al. (2013). "Fluorescence imaging of flowing cells using a temporally coded excitation." Optics Express **21**(4): 5164-5170.
Grossfeld, G. D. and P. R. Carroll (2001). "Prostate cancer early detection: a clinical perspective." Epidemiologic Reviews **23**(1): 173-180.
Gulyaev, A. E., E. V. Anisimova, et al. (1998). "Antibacterial effect of antibiotics modified by their interaction with antitumor preparations on the cellular level." Pharmaceutical Chemistry Journal **32**(4): 17 - 19.
Gumulec, J., M. Fojtu, et al. (2014). "Modulation of induced cytotoxicity of doxorubicin by using apoferritin and liposomal cages." International Journal of Molecular Sciences **15**(12): 22960-22977.
Guo, L. T., B. A. Chen, et al. (2015). "Biocompatibility Assessment of Polyethylene Glycol-Poly L-Lysine-Poly Lactic-Co-Glycolic Acid Nanoparticles In Vitro and In Vivo." Journal of Nanoscience and Nanotechnology **15**(5): 3710-3719.
Guo, X., R. Ding, et al. (2014). "Dual Role of Photosensitizer and Carrier Material of Fullerene in Micelles for Chemo-Photodynamic Therapy of Cancer." Journal of Pharmaceutical Sciences **103**(10): 3225-3234.
Gyoengyoesi, M., G. Maurer, et al. (2014). "Comparison of the cardiotoxic effect of doxorubicin and liposome-encapsulation of doxorubicin under experimental condition." Annals of Oncology **25**.
Haber, D. A. and V. E. Velculescu (2014). "Blood-based analyses of cancer: circulating tumor cells and circulating tumor dna." Cancer Discovery **4**(6): 650-661.
Hainaut, P. and A. Plymoth (2013). "Targeting the hallmarks of cancer: towards a rational approach to next-generation cancer therapy." Current Opinion in Oncology **25**(1): 50-51.
Hanahan, D. and R. A. Weinberg (2011). "Hallmarks of Cancer: The Next Generation." Cell **144**(5): 646-674.
Hanash, S. M., C. S. Baik, et al. (2011). "Emerging molecular biomarkers-blood-based strategies to detect and monitor cancer." Nature Reviews Clinical Oncology **8**(3): 142-150.
Hawkins, M. J., P. Soon-Shiong, et al. (2008). "Protein nanoparticles as drug carriers in clinical medicine." Advanced Drug Delivery Reviews **60**(8): 876-885.
Heger, Z., S. Skalickova, et al. (2014). "Apoferritin applications in nanomedicine." Nanomedicine **9**(14): 2233-2245.
Henderson, K. A., R. B. Borders, et al. (2014). "Acute effects of doxorubicin and its primary metabolite doxorubicin-ol on the isolated heart." Journal of Pharmacological and Toxicological Methods **70**(3): 331-331.
Hiebl, W., B. Gunther, et al. (2005). "Substances for staining biological tissues: Use of dyes in ophthalmology." Klinische Monatsblatter Fur Augenheilkunde **222**(4): 309-311.
Hilderbrand, S. A. and R. Weissleder (2010). "Near-infrared fluorescence: application to in vivo molecular imaging." Current Opinion in Chemical Biology **14**(1): 71-79.
Hilmer, S. N., V. C. Cogger, et al. (2004). "The hepatic pharmacokinetics of doxorubicin and liposomal doxorubicin." Drug Metabolism and Disposition **32**(8): 794-799.
Hobbs, S. K., W. L. Monsky, et al. (1998). "Regulation of transport pathways in tumor vessels: Role of tumor type and microenvironment." Proceedings of the National Academy of Sciences of the United States of America **95**(8): 4607-4612.
Hofheinz, R. D., S. U. Gnad-Vogt, et al. (2005). "Liposomal encapsulated anti-cancer drugs." Anti-Cancer Drugs **16**(7): 691-707.

Hong, L., Z. Wang, et al. (2012). "Subcellular distribution of CdSe quantum Dots (QDs) in breast cancer cells." Journal of Nanoscience and Nanotechnology **12**(1): 365-367.
Hosoda, J., S. Unezaki, et al. (1995). "Antitumor-activity of doxorubicin encapsulated in poly(ethylene glycol)-coated liposomes." Biological & Pharmaceutical Bulletin **18**(9): 1234-1237.
Hu, W. Q., M. Fang, et al. (2014). "Tumor invasion unit in gastric cancer revealed by QDs-based in situ molecular imaging and multispectral analysis." Biomaterials **35**(13): 4125-4132.
Hua, G. J., Y. P. Liu, et al. (2014). "Targeting glucose metabolism in chondrosarcoma cells enhances the sensitivity to doxorubicin through the inhibition of lactate dehydrogenase-A." Oncology Reports **31**(6): 2727-2734.
Huang, X., X. Y. Qi, et al. (2012). "Graphene-based composites." Chemical Society Reviews **41**(2): 666-686.
Huang, Y., M. Y. Zhou, et al. (2011). "Branched-chain amino acid metabolism in heart disease: an epiphenomenon or a real culprit?" Cardiovascular Research **90**(2): 220-223.
Huska, D., V. Adam, et al. (2009). "Square-wave voltammetry as a tool for investigation of doxorubicin Interactions with DNA isolated from neuroblastoma cells." Electroanalysis **21**(3-5): 487-494.
Hutchinson, P. J., M. T. O'Connell, et al. (2005). "Cerebral microdialysis methodology - evaluation of 20 kDa and 100 kDa catheters." Physiological Measurement **26**(4): 423-428.
Hwang, J. Y., J. Park, et al. (2012). "Multimodality imaging in vivo for preclinical assessment of tumor-targeted doxorubicin nanoparticles." Plos One **7**(4).
Hwang, J. Y., J. Park, et al. (2012). "Multimodality imaging in vivo for preclinical assessment of tumor-targeted doxorubicin nanoparticles." Plos One **7**(4): 1-9.
Hwang, M. P., J.-W. Lee, et al. (2013). "Think modular: a simple apoferritin-based platform for the multifaceted detection of pancreatic cancer." Acs Nano **7**(9): 8167-8174.
Chaban, A. A., P. A. Pyatakov, et al. (1999). "Photoacoustic phenomena in the layered structure photorefractive crystal-fullerene-photoconductor." Ferroelectrics Letters Section **25**(5-6): 135-140.
Chakravarthy, K. V., B. A. Davidson, et al. (2011). "Doxorubicin-conjugated quantum dots to target alveolar macrophages and inflammation." Nanomedicine-Nanotechnology Biology and Medicine **7**(1): 88-96.
Chanda, N., A. Upendran, et al. (2014). "Gold nanoparticle based x-ray contrast agent for tumor imaging in mice and dog: a potential nano-platform for computer tomography theranostics." Journal of Biomedical Nanotechnology **10**(3): 383-392.
Chatterjee, K., J. Q. Zhang, et al. (2010). "Doxorubicin cardiomyopathy." Cardiology **115**(2): 155-162.
Chekhun, V. F., N. Y. Lukyanova, et al. (2013). "Iron metabolism disturbances in the MCF-7 human breast cancer cells with acquired resistance to doxorubicin and cisplatin." International Journal of Oncology **43**(5): 1481-1486.
Chen, F., E. B. Ehlerding, et al. (2014). "Theranostic nanoparticles." Journal of Nuclear Medicine **55**(12): 1919-1922.
Chen, N.-T., C.-Y. Wu, et al. (2012). "Probing the dynamics of doxorubicin-DNA Intercalation during the Initial activation of apoptosis by fluorescence lifetime imaging microscopy (FLIM)." Plos One **7**(9).
Chen, N. T., C. Y. Wu, et al. (2012). "Probing the dynamics of doxorubicin-DNA Intercalation during the Initial activation of apoptosis by fluorescence lifetime imaging microscopy (FLIM)." Plos One **7**(9).

Chen, Q., C. Wang, et al. (2014). "Near-infrared dye bound albumin with separated imaging and therapy wavelength channels for imaging-guided photothermal therapy." Biomaterials **35**(28): 8206-8214.
Chen, Y.-C., X.-C. Huang, et al. (2013). "Non-metallic nanomaterials in cancer theranostics: a review of silica- and carbon-based drug delivery systems." Science and Technology of Advanced Materials **14**(4).
Chen, Z., L. Ma, et al. (2012). "Applications of functionalized fullerenes in tumor theranostics." Theranostics **2**(3): 238-250.
Cheng, Q., L. Lu, et al. (2012). "Combining C-11 -AnxA5 PET Imaging with Serum Biomarkers for Improved Detection in Live Mice of Modest Cell Death in Human Solid Tumor Xenografts." Plos One **7**(8).
Cho, K. J., X. Wang, et al. (2008). "Therapeutic nanoparticles for drug delivery in cancer." Clinical Cancer Research **14**(5): 1310-1316.
Choi, H., J.-I. Bang, et al. (2015). "18F-Fluorodeoxyglucose and 11C-methionine positron emission tomography in relation to methyl-guanine methyltransferase promoter methylation in high-grade gliomas." Nuclear medicine communications **36**(3): 211-218.
Choi, C. H. J., J. E. Zuckerman, et al. (2011). "Targeting kidney mesangium by nanoparticles of defined size." Proceedings of the National Academy of Sciences of the United States of America **108**(16): 6656-6661.
Choi, S., A. Tripathi, et al. (2014). "Smart nanomaterials for biomedics." Journal of Biomedical Nanotechnology **10**(10): 3162-3188.
Chudakov, D. M., M. V. Matz, et al. (2010). "Fluorescent proteins and their applications in imaging living cells and tissues." Physiological Reviews **90**(3): 1103-1163.
Ichikawa, Y., M. Ghanefar, et al. (2014). "Cardiotoxicity of doxorubicin is mediated through mitochondrial iron accumulation." Journal of Clinical Investigation **124**(2): 617-630.
Injac, R. and B. Strukej (2008). "Recent advances in protection against doxorubicin-induced toxicity." Technology in Cancer Research & Treatment **7**(6): 497-516.
Inoue, S., Y. Setoyama, et al. (2014). "Doxorubicin treatment induces tumor cell death followed by immunomodulation in a murine neuroblastoma model." Experimental and Therapeutic Medicine **7**(3): 703-708.
Issa, B., I. M. Obaidat, et al. (2013). "Magnetic nanoparticles: surface effects and properties related to biomedicine applications." International Journal of Molecular Sciences **14**(11): 21266-21305.
Iversen, T.-G., T. Skotland, et al. (2011). "Endocytosis and intracellular transport of nanoparticles: Present knowledge and need for future studies." Nano Today **6**(2): 176-185.
Jabr-Milane, L., L. van Vlerken, et al. (2008). "Multi-functional nanocarriers for targeted delivery of drugs and genes." Journal of Controlled Release **130**(2): 121-128.
James, M. L. and S. S. Gambhir (2012). "A molecular imaging primer: modalities, imaging agents, and applications " Physiological Reviews **92**(2): 897-965.
Janib, S. M., A. S. Moses, et al. (2010). "Imaging and drug delivery using theranostic nanoparticles." Advanced Drug Delivery Reviews **62**(11): 1052-1063.
Jiang, M. X., Y. Chen, et al. (2012). "Preparation of CdSe QDs-carbohydrate conjugation and its application for HepG2 cells labeling." Bulletin of the Korean Chemical Society **33**(2): 571-574.
Jirkovsky, E., O. Lencova-Popelova, et al. (2013). "Early and delayed cardioprotective intervention with dexrazoxane each show different potential for prevention of chronic anthracycline cardiotoxicity in rabbits." Toxicology **311**(3): 191-204.

Kang, M., K. I. Kim, et al. (2012). "Cardioprotective effect of early dexrazoxane use in anthracycline treated pediatric patients." Journal of Chemotherapy **24**(5): 292-296.
Karathanasis, E., L. Chan, et al. (2008). "Multifunctional nanocarriers for mammographic quantification of tumor dosing and prognosis of breast cancer therapy." Biomaterials **29**(36): 4815-4822.
Karmali, P. P. and D. Simberg (2011). "Interactions of nanoparticles with plasma proteins: implication on clearance and toxicity of drug delivery systems." Expert Opinion on Drug Delivery **8**(3): 343-357.
Kelloff, G. J. and C. C. Sigman (2012). "Cancer biomarkers: selecting the right drug for the right patient." Nature Reviews Drug Discovery **11**(3): 201-214.
Kensova, R., I. Blazkova, et al. (2013). "Lead ions encapsulated in liposomes and their effect on Staphylococcus aureus." Int. J. Environ. Res. Pub. Health **10**(12): 6687-6700.
Key, J. and J. F. Leary (2014). "Nanoparticles for multimodal in vivo imaging in nanomedicine." International Journal of Nanomedicine **9**: 711-726.
Kievit, F. M., F. Y. Wang, et al. (2011). "Doxorubicin loaded iron oxide nanoparticles overcome multidrug resistance in cancer in vitro." Journal of Controlled Release **152**(1): 76-83.
Kikkeri, R., B. Lepenies, et al. (2009). "In vitro imaging and in vivo liver targeting with carbohydrate capped quantum dots." Journal of the American Chemical Society **131**(6): 2110-+.
Kilic, M. A., E. Ozlu, et al. (2012). "A novel protein-based anticancer drug encapsulating nanosphere: apoferritin-doxorubicin complex." Journal of Biomedical Nanotechnology **8**(3): 508-514.
Kirtane, A. R., S. M. Kalscheuer, et al. (2013). "Exploiting nanotechnology to overcome tumor drug resistance: Challenges and opportunities." Advanced Drug Delivery Reviews **65**(13-14): 1731-1747.
Klener, P. and P. Klener (2013). Principy systemove protinadorove lecby. Prague, Grada Publishing, a.s.
Kneidl, B., M. Peller, et al. (2014). "Thermosensitive liposomal drug delivery systems: state of the art review." International Journal of Nanomedicine **9**: 4387-4398.
Kobayashi, H., R. Watanabe, et al. (2014). "Improving conventional enhanced permeability and retention (EPR) effects; what is the appropriate target?" Theranostics **4**(1): 81-89.
Konecna, R., H. V. Nguyen, et al. (2014). "Doxorubicin encapsulation investigated by capillary electrophoresis with laser-induced fluorescence detection." Chromatographia **77**(21-22): 1469-1476.
Konecny, G. E. (2015). "The path to personalized medicine in women's cancers: challenges and recent advances." Current Opinion in Obstetrics & Gynecology **27**(1): 45-47.
Krejcova, L., D. Hynek, et al. (2013). "Quantum dots for electrochemical labelling of neuramidinase genes of H5N1, H1N1 and H3N2 influenza." Int. J. Electrochem. Sci. **8**(4): 4457-4471.
Lagoa, R., C. Ganan, et al. (2014). "The decrease of NAD(P)H:quinone oxidoreductase 1 activity and increase of ROS production by NADPH oxidases are early biomarkers in doxorubicin cardiotoxicity." Biomarkers **19**(2): 142-153.
Lammers, T., L. Y. Rizzo, et al. (2012). "Personalized nanomedicine." Clinical Cancer Research **18**(18): 4889-4894.
Larsen, E. K. U., T. Nielsen, et al. (2012). "Accumulation of magnetic iron oxide nanoparticles coated with variably sized polyethylene glycol in murine tumors." Nanoscale **4**(7): 2352-2361.

Lee, Y. K., E. J. Choi, et al. (2015). "Effect of the protein corona on nanoparticles for modulating cytotoxicity and immunotoxicity." International Journal of Nanomedicine **10**: 97-112.

Leonard, R. C. F., S. Williams, et al. (2009). "Improving the therapeutic index of anthracycline chemotherapy: Focus on liposomal doxorubicin (Myocet (TM))." Breast **18**(4): 218-224.

Levi-Polyachenko, N. H., D. L. Carroll, et al. (2008). Applications of Carbon-Based Nanomaterials for Drug Delivery in Oncology. Dordrecht, Springer.

Lewis, M., B. Littlejohns, et al. (2014). "Cardiac taurine and principal amino acids in right and left ventricles of patients with either aortic valve stenosis or coronary artery disease: the importance of diabetes and gender." SpringerPlus **3**: 523-523.

Li, J. M., Y. Y. Wang, et al. (2012). "Multifunctional QD-based co-delivery of siRNA and doxorubicin to HeLa cells for reversal of multidrug resistance and real-time tracking." Biomaterials **33**(9): 2780-2790.

Li, X., R. Lie, et al. (2008). "Superior antitumor efficiency of cisplatin-loaded nanoparticles by intratumoral delivery with decreased tumor metabolism rate." European Journal of Pharmaceutics and Biopharmaceutics **70**(3): 726-734.

Licata, S., A. Saponiero, et al. (2000). "Doxorubicin metabolism and toxicity in human myocardium: Role of cytoplasmic deglycosidation and carbonyl reduction." Chemical Research in Toxicology **13**(5): 414-420.

Lim, D. J., M. Sim, et al. (2014). "Carbon-based drug delivery carriers for cancer therapy." Archives of Pharmacal Research **37**(1): 43-52.

Lin, G. M., Z. C. Ding, et al. (2014). "Cytotoxicity and immune response of CdSe/ZnS Quantum dots towards a murine macrophage cell line." Rsc Advances **4**(11): 5792-5797.

Lin, L., L. Xiong, et al. (2015). "Active targeting of nano-photosensitizer delivery systems for photodynamic therapy of cancer stem cells." Journal of Biomedical Nanotechnology **11**(4): 531-554.

Lin, M. C. and M. C. Yin (2013). "Preventive effects of ellagic acid against doxorubicin-induced cardio-toxicity in mice." Cardiovascular Toxicology **13**(3): 185-193.

Liu, J. B., M. X. Yu, et al. (2013). "Renal clearable inorganic nanoparticles: a new frontier of bionanotechnology." Materials Today **16**(12): 477-486.

Liu, J. H., L. Cao, et al. (2010). "Fullerene-conjugated doxorubicin in cells." Acs Applied Materials & Interfaces **2**(5): 1384-1389.

Longmire, M., P. L. Choyke, et al. (2008). "Clearance properties of nano-sized particles and molecules as imaging agents: considerations and caveats." Nanomedicine **3**(5): 703-717.

Longmuir, K. J., S. M. Haynes, et al. (2009). "Liposomal delivery of doxorubicin to hepatocytes in vivo by targeting heparan sulfate." International Journal of Pharmaceutics **382**(1-2): 222-233.

Lowengrub, J. S., H. B. Frieboes, et al. (2010). "Nonlinear modelling of cancer: bridging the gap between cells and tumours." Nonlinearity **23**(1): R1-R91.

Lowery, A., H. Onishko, et al. (2011). "Tumor-targeted delivery of liposome-encapsulated doxorubicin by use of a peptide that selectively binds to irradiated tumors." Journal of Controlled Release **150**(1): 117-124.

Lu, P. F., V. M. Weaver, et al. (2012). "The extracellular matrix: A dynamic niche in cancer progression." Journal of Cell Biology **196**(4): 395-406.

Luo, Y., N. J. Bernshaw, et al. (2002). "Targeted delivery of doxorubicin by HPMA copolymer-hyaluronan bioconjugates." Pharmaceutical Research **19**(4): 396-402.

Ma-Ham, A., H. Wu, et al. (2011). "Apoferritin-based nanomedicine platform for drug delivery: equilibrium binding study of daunomycin with DNA." Journal of Materials Chemistry **21**(24): 8700-8708.
Ma, P. and R. J. Mumper (2013). "Anthracycline nano-delivery systems to overcome multiple drug resistance: A comprehensive review." Nano Today **8**(3): 313-331.
Maeda, H. (2012). "Macromolecular therapeutics in cancer treatment: The EPR effect and beyond." Journal of Controlled Release **164**(2): 138-144.
Magan, N., R. J. Isaacs, et al. (2012). "Treatment with the PARP-inhibitor PJ34 causes enhanced doxorubicin-mediated cell death in HeLa cells." Anti-Cancer Drugs **23**(6): 627-637.
Mahnik, S. N., K. Lenz, et al. (2007). "Fate of 5-fluorouracil, doxorubicin, epirubicin, and daunorubicin in hospital wastewater and their elimination by activated sludge and treatment in a membrane-bio-reactor system." Chemosphere **66**(1): 30-37.
Marcucci, F. and F. Lefoulon (2004). "Active targeting with particulate drug carriers in tumor therapy: fundamentals and recent progress." Drug Discovery Today **9**(5): 219-228.
Martin Sabroso, C. and A. I. Torres-Suarez (2014). "Objective: tumor. Strategies of drug targeting at the tumor mass level." Clinical & Translational Oncology **16**(1): 1-10.
Masedunskas, A., O. Milberg, et al. (2012). "Intravital microscopy: a practical guide on imaging intracellular structures in live animals." Bioarchitecture **2**(5): 143-157.
Matouk, A. I., A. Taye, et al. (2013). "Quercetin augments the protective effect of losartan against chronic doxorubicin cardiotoxicity in rats." Environmental Toxicology and Pharmacology **36**(2): 443-450.
May, J. P. and S. D. Li (2013). "Hyperthermia-induced drug targeting." Expert Opinion on Drug Delivery **10**(4): 511-527.
Medeiros, S. F., A. M. Santos, et al. (2011). "Stimuli-responsive magnetic particles for biomedical applications." International Journal of Pharmaceutics **403**(1-2): 139-161.
Mellon, E. A., G. M. Springett, et al. (2014). "Adjuvant radiotherapy and lymph node dissection in pancreatic cancer treated with surgery and chemotherapy." Cancer **120**(8): 1171-1177.
Meng, M. B., N. G. Zaorsky, et al. (2013). "Radiotherapy and chemotherapy are associated with improved outcomes over surgery and chemotherapy in the management of limited-stage small cell esophageal carcinoma." Radiotherapy and Oncology **106**(3): 317-322.
Mielke, D., V. Malinova, et al. (2014). "Comparison of Intraoperative Microscopic and Endoscopic ICG Angiography in Aneurysm Surgery." Neurosurgery **10**: 418-425.
Minotti, G., P. Menna, et al. (2004). "Anthracyclines: Molecular advances and pharmacologic developments in antitumor activity and cardiotoxicity." Pharmacological Reviews **56**(2): 185-229.
Mohammed, S., G. Van Buren, et al. (2014). "Pancreatic cancer: Advances in treatment." World Journal of Gastroenterology **20**(28): 9354-9360.
Moller, P., D. V. Christophersen, et al. (2014). "Role of oxidative stress in carbon nanotube-generated health effects." Archives of Toxicology **88**(11): 1939-1964.
Monti, M., E. Terzuoli, et al. (2013). "The sulphydryl containing ACE inhibitor Zofenoprilat protects coronary endothelium from Doxorubicin-induced apoptosis." Pharmacological Research **76**: 171-181.
Morgensztern, D., M. J. Campo, et al. (2015). "Molecularly Targeted Therapies in Non-Small-Cell Lung Cancer Annual Update 2014." Journal of Thoracic Oncology **10**(1): S1-S63.

Mortell, A., J. Giles, et al. (2003). "Adriamycin effects on the chick embryo." Pediatric Surgery International **19**(5): 359-364.
Moulick, A., I. Blazkova, et al. (2014). "Application of CdTe/ZnSe Quantum Dots in In Vitro Imaging of Chicken Tissue and Embryo." Photochemistry and Photobiology.
Moulin, M., J. Piquereau, et al. (2014). "Sexual dimorphism of doxorubicin-mediated cardiotoxicity in adult rats: potential role of energy metabolism remodeling." European Journal of Heart Failure **16**: 110-110.
Mura, S. and P. Couvreur (2012). "Nanotheranostics for personalized medicine." Advanced Drug Delivery Reviews **64**(13): 1394-1416.
Myers, C. (1998). "The role of iron in doxorubicin-induced cardiomyopathy." Semin. Oncol. **25**(4): 10-14.
Myhr, G. (2008). "Multimodal cancer treatment: Real time monitoring, optimization, and synergistic effects." Technology in Cancer Research & Treatment **7**(5): 409-414.
Mylonopoulou, E., C. D. Arvanitis, et al. (2010). Ultrasonic Activation of Thermally Sensitive Liposomes. 9th International Symposium on Therapeutic Ultrasound. K. Hynynen and J. Souquet. Melville, Amer Inst Physics. **1215:** 83-87.
Narang, A. S. and S. Varia (2011). "Role of tumor vascular architecture in drug delivery." Advanced Drug Delivery Reviews **63**(8): 640-658.
Needham, D. (2013). Reverse engineering of the low temperature-sensitive liposome (LTSL) for treating cancer. Biomaterials for Cancer Therapeutics: Diagnosis, Prevention and Therapy. K. Park. Cambridge, Woodhead Publ Ltd**:** 270-348.
Niedre, M. J., R. H. de Kleine, et al. (2008). "Early photon tomography allows fluorescence detection of lung carcinomas and disease progression in mice in vivo." Proceedings of the National Academy of Sciences of the United States of America **105**(49): 19126-19131.
Nichols, J. W. and Y. H. Bae (2014). "EPR: Evidence and fallacy." Journal of Controlled Release **190**: 451-464.
Nitiss, K. C. and J. L. Nitiss (2014). "Twisting and Ironing: Doxorubicin Cardiotoxicity by Mitochondrial DNA Damage." Clinical Cancer Research **20**(18): 4737-4739.
Novoselov, K. S., V. I. Fal'ko, et al. (2012). "A roadmap for graphene." Nature **490**(7419): 192-200.
Ntziachristos, V., C. Bremer, et al. (2003). "Fluorescence imaging with near-infrared light: new technological advances that enable in vivo molecular imaging." European Radiology **13**(1): 195-208.
Nunney, L. (1999). "Lineage selection and the evolution of multistage carcinogenesis." Proceedings of the Royal Society B-Biological Sciences **266**(1418): 493-498.
Nussbaumer, S., P. Bonnabry, et al. (2011). "Analysis of anticancer drugs: A review." Talanta **85**(5): 2265-2289.
O'Brien, M. E. R., N. Wigler, et al. (2004). "Reduced cardiotoxicity and comparable efficacy in a phase III trial of pegylated liposomal doxorubicin HCl (CAELYX (TM)/Doxil (R)) versus conventional doxorubicin for first-line treatment of metastatic breast cancer." Annals of Oncology **15**(3): 440-449.
Octavia, Y., C. G. Tocchetti, et al. (2012). "Doxorubicin-induced cardiomyopathy: From molecular mechanisms to therapeutic strategies." Journal of Molecular and Cellular Cardiology **52**(6): 1213-1225.
Ohaegbulam, K. C., A. Assal, et al. (2015). "Human cancer immunotherapy with antibodies to the PD-1 and PD-L1 pathway." Trends in Molecular Medicine **21**(1): 24-33.
Osinsky, S., M. Zavelevich, et al. (2009). "Tumor hypoxia and malignant progression." Experimental oncology **31**(2): 80-86.

Osman, A. M. M., S. E. Al-Harthi, et al. (2013). "Chemosensetizing and cardioprotective effects of resveratrol in doxorubicin- treated animals." Cancer Cell International **13**.

Ou, J., F. Wang, et al. (2014). "Fabrication and cyto-compatibility of Fe3O4/SiO2/graphene-CdTe QDs/CS nanocomposites for drug delivery." Colloids and Surfaces B-Biointerfaces **117**: 466-472.

Panchuk, R. R., S. V. Prylutska, et al. (2015). "Application of C-60 Fullerene-Doxorubicin Complex for Tumor Cell Treatment In Vitro and In Vivo." Journal of Biomedical Nanotechnology **11**(7): 1139-1152.

Patel, K. J. and I. F. Tannock (2009). "The influence of P-glycoprotein expression and its inhibitors on the distribution of doxorubicin in breast tumors." Bmc Cancer **9**.

Pathan, R. A., U. Bhandari, et al. (2012). "Anti-apoptotic potential of gymnemic acid phospholipid complex pretreatment in Wistar rats with experimental cardiomyopathy." Indian Journal of Experimental Biology **50**(2): 117-127.

Peer, D., J. M. Karp, et al. (2007). "Nanocarriers as an emerging platform for cancer therapy." Nature Nanotechnology **2**(12): 751-760.

Peng, K., L. He, et al. (2015). "Detection of cervical cancer based on photoacoustic imaging-the in-vitro results." Biomedical Optics Express **6**(1): 135-143.

Petrakova, K., R. Nenutil, et al. (2007). "Mechanizmy rezistence na tamoxifen " Klinicka onkologie **20**(6): 369-376.

Pickhardt, P. J., C. Hassan, et al. (2011). "Colorectal cancer: CT colonography and colonoscopy for detection-systematic review and meta-analysis." Radiology **259**(2): 393-405.

Pissuwan, D., T. Niidome, et al. (2011). "The forthcoming applications of gold nanoparticles in drug and gene delivery systems." Journal of Controlled Release **149**(1): 65-71.

Ploussard, G. and A. de la Taille (2010). "Urine biomarkers in prostate cancer." Nature Reviews Urology **7**(2): 101-109.

Primeau, A. J., A. Rendon, et al. (2005). "The distribution of the anticancer drug doxorubicin in relation to blood vessels in solid tumors." Clinical Cancer Research **11**(24): 8782-8788.

Prylutska, S., I. Grynyuk, et al. (2014). "C60 fullerene as synergistic agent in tumor-inhibitory Doxorubicin treatment." Drugs in R&D **14**(4): 333-340.

Prylutskyy, Y. I., M. P. Evstigneev, et al. (2014). "Characterization of C-60 fullerene complexation with antibiotic doxorubicin." Physical Chemistry Chemical Physics **16**(42): 23164-23172.

Pyrgiotakis, G., C. O. Blattmann, et al. (2013). "Nanoparticle-Nanoparticle Interactions in Biological Media by Atomic Force Microscopy." Langmuir **29**(36): 11385-11395.

Qu, L. Z., D. W. Deng, et al. (2014). "Dox-conjugated high-quality agznins qds for reversal of multidrug resistance." Journal of Innovative Optical Health Sciences **7**(1).

Rajasekaran, M. and C. Kalaimagal (2012). "Cardioprotective Effect of a Medicinal Mushroom, Ganoderma lucidum Against Adriamycin Induced Toxicity." International Journal of Pharmacology **8**(4): 252-258.

Ranganathan, R., S. Madanmohan, et al. (2012). "Nanomedicine: towards development of patient-friendly drug-delivery systems for oncological applications." International Journal of Nanomedicine **7**: 1043-1060.

Rashidi, H. and V. Sottile (2009). "The chick embryo: hatching a model for contemporary biomedical research." Bioessays **31**(4): 459-465.

Ruenraroengsak, P., J. M. Cook, et al. (2010). "Nanosystem drug targeting: Facing up to complex realities." Journal of Controlled Release **141**(3): 265-276.

Ruyra, A., A. Yazdi, et al. (2015). "Synthesis, culture medium stability, and in vitro and in vivo zebrafish embryo toxicity of metal-organic framework nanoparticles." Chemistry (Weinheim an der Bergstrasse, Germany) **21**(6): 2508-2518.

Ryvolova, M., J. Chomoucka, et al. (2011). "Biotin-modified glutathione as a functionalized coating for bioconjugation of CdTe based quantum dots." Electrophoresis **32**(13): 1619-1622.

Saad, M., O. B. Garbuzenko, et al. (2008). "Receptor targeted polymers, dendrimers, liposomes: Which nanocarrier is the most efficient for tumor-specific treatment and imaging?" Journal of Controlled Release **130**(2): 107-114.

Sabroso, C. M. and A. I. Torres-Suarez (2014). "Objective: tumor. Strategies of drug targeting at the tumor mass level." Clinical & Translational Oncology **16**(1): 1-10.

Safra, T., F. Muggia, et al. (2000). "Pegylated liposomal doxorubicin (doxil): Reduced clinical cardiotoxicity in patients reaching or exceeding cumulative doses of 500 mg/m(2)." Annals of Oncology **11**(8): 1029-1033.

Saha, S., C. Burke, et al. (2013). "SPECT-CT: applications in musculoskeletal radiology." British Journal of Radiology **86**(1031).

Sakamoto, J. H., A. L. van de Ven, et al. (2010). "Enabling individualized therapy through nanotechnology." Pharmacological Research **62**(2): 57-89.

Samal, S. K., M. Dash, et al. (2012). "Cationic polymers and their therapeutic potential." Chemical Society Reviews **41**(21): 7147-7194.

Sardi, I., G. la Marca, et al. (2013). "Pharmacological modulation of blood-brain barrier increases permeability of doxorubicin into the rat brain." American Journal of Cancer Research **3**(4): 424-432.

Sartorius, G., S. Spasevska, et al. (2012). "Serum testosterone, dihydrotestosterone and estradiol concentrations in older men self-reporting very good health: the healthy man study." Clinical Endocrinology **77**(5): 755-763.

Sekiya, N. and A. Imamura (2008). "Doxil--pegylated liposomal doxorubicin." Gan to kagaku ryoho. Cancer & chemotherapy **35**(8): 1439-1443.

Seynhaeve, A. L. B., B. M. Dicheva, et al. (2013). "Intact Doxil is taken up intracellularly and released doxorubicin sequesters in the lysosome: Evaluated by in vitro/in vivo live cell imaging." Journal of Controlled Release **172**(1): 330-340.

Shevtsov, M. A., B. P. Nikolaev, et al. (2014). "Magnetic resonance imaging of rat C6 glioma model enhanced by using water-soluble gadolinium fullerene." Applied Magnetic Resonance **45**(4): 303-314.

Shin, K. H., M. Kim, et al. (2014). "Breast cancer-related lymphedema after neoadjuvant chemotherapy, surgery and radiotherapy." European Journal of Cancer **50**: S85-S86.

Schaffer, S. W., C. J. Jong, et al. (2014). "Effect of taurine on ischemia-reperfusion injury." Amino Acids **46**(1): 21-30.

Schaffert, D. and E. Wagner (2008). "Gene therapy progress and prospects: synthetic polymer-based systems." Gene Therapy **15**(16): 1131-1138.

Schenone, A. V., M. J. Culzoni, et al. (2013). "Total synchronous fluorescence spectroscopic data modeled with first- and second-order algorithms for the determination of doxorubicin in human plasma." Analytical and Bioanalytical Chemistry **405**(26): 8515-8523.

Scheuer, W., G. M. van Dam, et al. (2012). "Drug-based optical agents: infiltrating clinics at lower risk." Science Translational Medicine **4**(134).

Schnall, M. and M. Rosen (2006). "Primer on imaging technologies for cancer." Journal of Clinical Oncology **24**(20): 3225-3233.

Schwerdtfeger, P., L. N. Wirz, et al. (2015). "The topology of fullerenes." Wiley Interdisciplinary Reviews-Computational Molecular Science **5**(1): 96-145.

Siegel, R., C. DeSantis, et al. (2012). "Cancer treatment and survivorship statistics, 2012." Ca-a Cancer Journal for Clinicians **62**(4): 220-241.
Siegel, R., J. M. Ma, et al. (2014). "Cancer statistics, 2014." Ca-a Cancer Journal for Clinicians **64**(1): 9-29.
Siegel, R., D. Naishadham, et al. (2012). "Cancer Statistics, 2012." Ca-a Cancer Journal for Clinicians **62**(1): 10-29.
Simsek, E. and M. A. Kilic (2005). "Magic ferritin: A novel chemotherapeutic encapsulation bullet." Journal of Magnetism and Magnetic Materials **293**(1): 509-513.
Simunek, T., M. Sterba, et al. (2009). "Anthracycline-induced cardiotoxicity: Overview of studies examining the roles of oxidative stress and free cellular iron." Pharmacological Reports **61**(1): 154-171.
Singal, P. K., N. Iliskovic, et al. (1997). "Adriamycin cardiomyopathy: pathophysiology and prevention." Faseb Journal **11**(12): 931-936.
Sishi, B. J. N., B. Loos, et al. (2013). "Autophagy upregulation promotes survival and attenuates doxorubicin-induced cardiotoxicity." Biochemical Pharmacology **85**(1): 124-134.
Sobhana, S. S. L., M. V. Devi, et al. (2011). "CdS quantum dots for measurement of the size-dependent optical properties of thiol capping." Journal of Nanoparticle Research **13**(4): 1747-1757.
Sobolev, A. S. (2013). "Modular nanotransporters: A multitarget platform for anticancer drug delivery." Herald of the Russian Academy of Sciences **83**(4): 324-333.
Sobrova, P., I. Blazkova, et al. (2013). "Quantum dots and prion proteins: Is this a new challenge for neurodegenerative diseases imaging?" Prion **7**(5): 349-358.
Song, Y. and C. E. Lunte (1999). "Comparison of calibration by delivery versus no net flux for quantitative in vivo microdialysis sampling." Analytica Chimica Acta **379**(3): 251-262.
Staples, M., Y. Kaneko, et al. (2014). "Bone marrow-derived stem cell therapy for the repair of the blood-brain barrier in metastatic brain cancers." Cell Transplantation **23**(6): 784-784.
Stemmer, N., J. Mehnert, et al. (2012). "Noninvasive fluorescence imaging in animal models of stroke." Current Medicinal Chemistry **19**(28): 4786-4793.
Sterba, M., O. Popelova, et al. (2013). "Oxidative stress, redox signaling, and metal chelation in anthracycline cardiotoxicity and pharmacological cardioprotection." Antioxidants & Redox Signaling **18**(8): 899-929.
Strigun, A., J. Wahrheit, et al. (2012). "Doxorubicin increases oxidative metabolism in hl-1 cardiomyocytes as shown by c-13 metabolic flux analysis." Toxicological Sciences **125**(2): 595-606.
Stuker, F., J. Ripoll, et al. (2011). "Fluorescence molecular tomography: principles and potential for pharmaceutical research." Pharmaceutics **3**: 229-274.
Stuker, F., J. Ripoll, et al. (2011). "Fluorescence molecular tomography: principles and potential for pharmaceutical research." Pharmaceutics **3**(2): 229-274.
Sultana, S., M. R. Khan, et al. (2013). "Nanoparticles-mediated drug delivery approaches for cancer targeting: a review." Journal of Drug Targeting **21**(2): 107-125.
Sun, T. M., Y. S. Zhang, et al. (2014). "Engineered Nanoparticles for Drug Delivery in Cancer Therapy." Angewandte Chemie-International Edition **53**(46): 12320-12364.
Swenson, C. E., W. R. Perkins, et al. (2001). "Liposome technology and the development of Myocet (TM) (liposomal doxorubicin citrate)." Breast **10**: 1-7.
Tacar, O., P. Sriamornsak, et al. (2013). "Doxorubicin: an update on anticancer molecular action, toxicity and novel drug delivery systems." Journal of Pharmacy and Pharmacology **65**(2): 157-170.

Takemura, G. and H. Fujiwara (2007). "Doxorubicin-induccd cardiomyopathy from the cardiotoxic mechanisms to management." Progress in Cardiovascular Diseases **49**(5): 330-352.

Tanada, Y., T. Shioi, et al. (2014). "Branched-chain amino acids prevent heart failure in rats." Cardiology **128**: 382-382.

Tapan, U., M. Ozbayrak, et al. (2014). "MRI in local staging of rectal cancer: an update." Diagnostic and Interventional Radiology **20**(5): 390-398.

Termsarasab, U., I.-S. Yoon, et al. (2014). "Polyethylene glycol-modified arachidyl chitosan-based nanoparticles for prolonged blood circulation of doxorubicin." International Journal of Pharmaceutics **464**(1-2): 127-134.

Theodoulou, M. and C. Hudis (2004). "Cardiac profiles of liposomal anthracyclines - Greater cardiac safety versus conventional doxorubicin?" Cancer **100**(10): 2052-2063.

Thurston, D. E. (2006). Chemistry and pharmacology of anticancer drugs. Boca Raton, CRC Press.

Tmejova, K., D. Hynek, et al. (2013). "Electrochemical behaviour of doxorubicin encapsulated in apoferritin." International Journal of Electrochemical Science **8**(12): 12658-12671.

Tmejova, K., D. Hynek, et al. (2014). "Study of metallothionein-quantum dots interactions." Colloid Surf. B-Biointerfaces **in press**.

Tmejova, K., D. Hynek, et al. (2014). "Study of metallothionein-quantum dots interactions." Colloid Surf. B-Biointerfaces **117**(1): 534-537.

Torchilin, V. (2011). "Tumor delivery of macromolecular drugs based on the EPR effect." Advanced Drug Delivery Reviews **63**(3): 131-135.

Towbin, A. J., A. T. Trout, et al. (2014). "Advances in Oncologic Imaging." European Journal of Pediatric Surgery **24**(6): 474-481.

Tsay, J.-C. J., C. DeCotiis, et al. (2013). "Current readings: blood-based biomarkers for lung cancer." Seminars in thoracic and cardiovascular surgery **25**(4): 328-334.

van 't Veer, L. J. and R. Bernards (2008). "Enabling personalized cancer medicine through analysis of gene-expression patterns." Nature **452**(7187): 564-570.

Vargas, A., M. Zeisser-Labouebe, et al. (2007). "The chick embryo and its chorioallantoic membrane (CAM) for the in vivo evaluation of drug delivery systems." Advanced Drug Delivery Reviews **59**(11): 1162-1176.

Vavrova, A., H. Jansova, et al. (2013). "Catalytic Inhibitors of Topoisomerase II Differently Modulate the Toxicity of Anthracyclines in Cardiac and Cancer Cells." Plos One **8**(10).

Venturoli, D. and B. Rippe (2005). "Ficoll and dextran vs. globular proteins as probes for testing glomerular permselectivity: effects of molecular size, shape, charge, and deformability." American Journal of Physiology-Renal Physiology **288**(4): F605-F613.

Wainstein, A., S. M. Algarra, et al. (2015). "Melanoma early detection and awareness: how countries developing melanoma awareness programs could benefit from melanoma-proficient countries." American Journal of Therapeutics **22**(1): 37-43.

Wang, C., L. A. Cheng, et al. (2011). "Drug delivery with upconversion nanoparticles for multi-functional targeted cancer cell imaging and therapy." Biomaterials **32**(4): 1110-1120.

Wang, C., C. Wu, et al. (2013). "Enhancing cell nucleus accumulation and DNA cleavage activity of anti-cancer drug via graphene quantum dots." Scientific Reports **3**.

Wang, H., Y. Zhao, et al. (2011). "Enhanced anti-tumor efficacy by co-delivery of doxorubicin and paclitaxel with amphiphilic methoxy PEG-PLGA copolymer nanoparticles." Biomaterials **32**(32): 8281-8290.

Wang, R. B., P. S. Billone, et al. (2013). "Nanomedicine in action: An overview of cancer nanomedicine on the market and in clinical trials." Journal of Nanomaterials.

Wang, S. Q., X. Z. Han, et al. (2010). "Flavonoids from Dracocephalum tanguticum and their cardioprotective effects against doxorubicin-induced toxicity in H9c2 cells." Bioorganic & Medicinal Chemistry Letters **20**(22): 6411-6415.

Wang, Y. C., R. Hu, et al. (2013). "Functionalized quantum dots for biosensing and bioimaging and concerns on toxicity." Acs Applied Materials & Interfaces **5**(8): 2786-2799.

Ward, E., C. DeSantis, et al. (2014). "Childhood and adolescent cancer statistics, 2014." Ca-a Cancer Journal for Clinicians **64**(2): 83-103.

Whitaker, G. and C. E. Lunte (2010). "Investigation of microdialysis sampling calibration approaches for lipophilic analytes: Doxorubicin." Journal of Pharmaceutical and Biomedical Analysis **53**(3): 490-496.

Wiench, B., T. Eichhorn, et al. (2012). "Utilizing inherent fluorescence of therapeutics to analyze real-time uptake and multi-parametric effector kinetics." Methods **57**(3): 376-382.

Wilczewska, A. Z., K. Niemirowicz, et al. (2012). "Nanoparticles as drug delivery systems." Pharmacological Reports **64**(5): 1020-1037.

Wilson, M. W., R. K. Kerlan, et al. (2004). "Hepatocellular carcinoma: Regional therapy with a magnetic targeted carrier bound to doxorubicin in a dual MR imaging/conventional angiography suite - Initial experience with four patients." Radiology **230**(1): 287-293.

Wouters, F. S., P. J. Verveer, et al. (2001). "Imaging biochemistry inside cells." Trends in Cell Biology **11**(5): 203-211.

Wrobel, D. and A. Graja (2006). "Modification of electronic structure in supramolecular fullerene-porphyrin systems studied by fluorescence, photoacoustic and photothermal spectroscopy." Journal of Photochemistry and Photobiology a-Chemistry **183**(1-2): 79-88.

Wu, A. G., P. Ou, et al. (2010). "Biomedical applications of magnetic nanoparticles." Nano **5**(5): 245-270.

Wu, J. B., C. Shao, et al. (2014). "Near-infrared fluorescence imaging of cancer mediated by tumor hypoxia and HIFI alpha/OATPs signaling axis." Biomaterials **35**(28): 8175-8185.

Xie, J., S. Lee, et al. (2010). "Nanoparticle-based theranostic agents." Advanced Drug Delivery Reviews **62**(11): 1064-1079.

Xie, J., Z. Zhen, et al. (2013). "Engineering apoferritin nanocages for tumor imaging and therapy." Cancer Research **73**(8).

Xing, R., X. Wang, et al. (2009). "Characterization and cellular uptake of platinum anticancer drugs encapsulated in apoferritin." Journal of Inorganic Biochemistry **103**(7): 1039-1044.

Xu, H. P., Z. Y. Li, et al. (2014). "Nanocarriers in gene therapy: a review." Journal of Biomedical Nanotechnology **10**(12): 3483-3507.

Xu, J. H., Y. Liu, et al. (2012). "Subcellular quantification of doxorubicin and its metabolite in cultured human leukemia cells using liquid chromatography-tandem mass spectrometry." Analytical Letters **45**(14): 1980-1994.

Xu, X. X., H. L. Persson, et al. (2005). "Molecular pharmacology of the interaction of anthracyclines with iron." Molecular Pharmacology **68**(2): 261-271.

Yan, G.-P., L. Robinson, et al. (2007). "Magnetic resonance imaging contrast agents: Overview and perspectives." Radiography **13, Supplement 1**(0): e5-e19.

Yang, F., C. Jin, et al. (2012). "Emerging inorganic nanomaterials for pancreatic cancer diagnosis and treatment." Cancer Treatment Reviews **38**(6): 566-579.

Yang, F., C. J. Kemp, et al. (2013). "Doxorubicin enhances nucleosome turnover around promoters." Current Biology **23**(9): 782-787.
Yang, H., L.-Q. Diao, et al. (2013). "Efficacy of intensity-modulated radiotherapy combined with chemotherapy or surgery in locally advanced squamous cell carcinoma of the head-and-neck." Biologics : targets & therapy **7**: 223-229.
Yang, Z., X. Y. Wang, et al. (2007). "Encapsulation of platinum anticancer drugs by apoferritin." Chemical Communications(33): 3453-3455.
Yankeelov, T. E., R. G. Abramson, et al. (2014). "Quantitative multimodality imaging in cancer research and therapy." Nature Reviews Clinical Oncology **11**(11): 670-680.
Yin, R., M. Wang, et al. (2014). "Photodynamic therapy with decacationic 60 fullerene monoadducts: Effect of a light absorbing electron-donor antenna and micellar formulation." Nanomedicine-Nanotechnology Biology and Medicine **10**(4): 795-808.
Yu, B., H. C. Tai, et al. (2010). "Receptor-targeted nanocarriers for therapeutic delivery to cancer." Molecular Membrane Biology **27**(7): 286-298.
Zaidi, H. A., A. A. Abla, et al. (2014). "Indocyanine Green Angiography in the Surgical Management of Cerebral Arteriovenous Malformations: Lessons Learned in 130 Consecutive Cases." Neurosurgery **10**: 246-251.
Zaloudik, J. (2007). "Onkologicky vyzkum v Ceske republice v souvislostech." Klinicka onkologie(6): 405-407.
Zamboni, W. C. (2008). "Concept and clinical evaluation of carrier-mediated anticancer agents." Oncologist **13**(3): 248-260.
Zhang, P. and J. Kong (2015). "Doxorubicin-tethered fluorescent silica nanoparticles for pH-responsive anticancer drug delivery." Talanta **134**: 501-507.
Zhang, S., X. B. Liu, et al. (2012). "Identification of the molecular basis of doxorubicin-induced cardiotoxicity." Nature Medicine **18**(11): 1639-+.
Zhao, Y., S. Miriyala, et al. (2014). "Redox proteomic identification of HNE-bound mitochondrial proteins in cardiac tissues reveals a systemic effect on energy metabolism after doxorubicin treatment." Free Radical Biology and Medicine **72**: 55-65.
Zhu, G., M. Myint, et al. (2012). "Monofunctional Platinum-DNA adducts are strong inhibitors of transcription and substrates for nucleotide excision repair in live mammalian cells." Cancer Research **72**(3): 790-800.
Zhu, Y., H. Hong, et al. (2013). "Quantum Dot-Based Nanoprobes for In Vivo Targeted Imaging." Curr. Mol. Med. **13**(10): 1549-1567.
Zordoky, B. N. M., A. Anwar-Mohamed, et al. (2010). "Acute doxorubicin cardiotoxicity alters cardiac cytochrome P450 expression and arachidonic acid metabolism in rats." Toxicology and Applied Pharmacology **242**(1): 38-46.
Zordoky, B. N. M., A. Anwar-Mohamed, et al. (2011). "Acute doxorubicin toxicity differentially alters cytochrome P450 expression and arachidonic acid metabolism in rat kidney and liver." Drug Metabolism and Disposition **39**(8): 1440-1450.

8 ABBREVIATIONS

AMP	Adenosine monophosphate
AMPK	AMP-activated protein kinase
BBB	Blood-brain barrier
BSA	Bovine serum albumin
CCD	Charge-coupled device
CE	Capillary electrophoresis
CNPs	Carbon nanoparticles
CNTs	Carbon nanotubes
CT	Computed tomography
DNA	Deoxyribonucleic acid
DOX	Doxorubicin
DOXol	Doxorubicinol
ECM	Extracellular matrix
EPR	Enhanced permeability and retention
FDA	Food and Drug Administration
FMT	Fluorescence-mediated molecular tomography
FRI	Fluorescence reflectance imaging
GFN	Graphene
GO	Graphene oxide
HD	Hydrodynamic diameter
HPLC	High-performance liquid chromatography
ICG	Indocyanine green
IELC	Ion-exchange liquid chromatography
LC	Liquid chromatography
MRI	Magnetic resonance imaging
MWCNTs	Multiwalled carbon nanotubes
NIR	Near infrared region
NMs	Nano-sized molecules
NPs	Nanoparticles
PEG	Polyethylene glycol
PET	Positron emission tomography
PLD	Pegylated liposomal DOX
QDs	Quantum dots
RES	Reticuloendothelial system
RF	Radiofrequency
rGO	Reduced graphene oxide
ROS	Reactive oxygen species
sEH	Soluble epoxide hydrolase
SWCNTs	Single-walled carbon nanotubes
TOP2	Topoisomerase II
US	Ultrasonography